

*Final Report*

DURABILITY OF FIBER-REINFORCED CONCRETE IN FLORIDA  
ENVIRONMENTS

UF Project No.: 00050493

Contract No.: BD545-41

*Submitted to:*

Florida Department of Transportation  
605 Suwannee Street  
Tallahassee, FL 32399



Dr. Reynaldo Roque, P.E.  
Dr. Namho Kim  
Byoungil Kim  
George Lopp

Department of Civil and Coastal Engineering  
College of Engineering  
365 Weil Hall, P.O. Box 116580  
Gainesville, FL 32611-6580  
Tel: (352) 392-9537 extension 1458  
Fax: (352) 392-3394

July 2009

**Technical Report Documentation Page**

1. Report No.		2. Government Accession No.		3. Recipient's Catalog No.	
4. Title and Subtitle Durability of Fiber-Reinforced Concrete in Florida Environments				5. Report Date June 2009	
				6. Performing Organization Code	
7. Author(s) R. Roque, B. Kim, N. Kim, G. Lopp				8. Performing Organization Report No.	
9. Performing Organization Name and Address University of Florida Department of Civil and Coastal Engineering 365 Weil Hall P.O. Box 116580 Gainesville, FL 32611				10. Work Unit No. (TR AIS)	
				11. Contract or Grant No. BD545-41	
12. Sponsoring Agency Name and Address Florida Department of Transportation 605 Suwannee Street, MS 42 Tallahassee, FL 32399				13. Type of Report and Period Covered Final Report September 2004-June 2009	
				14. Sponsoring Agency Code	
15. Supplementary Notes					
16. Abstract An experimental program was performed to evaluate durability of FRC produced with four fiber types (polypropylene/PP, polyvinyl-alcohol/PVA, hooked-end steel/St, and cellulose/Cell). The effect of cellulose could not be evaluated because good fiber distribution was not achieved in laboratory mixing. Transport properties indicated that the addition of fibers to concrete improved the resistance of mass transport of deleterious materials; steel fibers were best. Fibers provided for post-cracking resistance; again, steel fibers were best. FRC beams produced with two concrete classes were subjected to simulated saltwater (immersed and wet/dry) and swamp (acid) environments for 27 months. Effect of fibers on durability could not be assessed reliably based on test results from either average residual strength (ASTM C1399) or flexural performance tests (ASTM C1609) because of non-uniform degradation and stress/strain distributions, as well as development of multiple cracks. Indirect tension testing (IDT) was identified as a more effective approach to achieve a uniformly-degraded cross-section and uniform stress/strain distribution. FRC specimens were subjected to an additional six months of saltwater conditioning, after which cracking and post-cracking behavior was assessed with IDT using testing and data interpretation procedures specifically designed to capture the effects of fibers. Test results indicated that PP fibers had the best resistance to saltwater environments (immersed and wet/dry), while PVA fibers had the worst, and resistance of steel fibers was somewhere between these two. However, steel fibers did not do well in fully immersed environments, but showed little or no degradation in wet/dry environments. The detrimental effect of acetic acid on aggregate and cement overwhelmed the degradation mechanism in swamp water, so the effect of fibers could not be distinguished for this environment. It was concluded that PP has the best durability for non-structural applications in saltwater environments. Steel may be suitable in non-submerged saltwater environments, particularly for structural applications, but should not be used if it will be in direct contact with reinforcing bars because it was found to accelerate corrosion of the bars. PVA should not be used in saltwater environments. Finally, it was concluded that transport properties alone are not necessarily good indicators of resistance to degradation.					
17. Key Word FRC, transport property, conditioning, beam test, post-cracking, toughness, IDT, Resilient deformation ratio				18. Distribution Statement No Restrictions	
19. Security Class if. (of this report) Unclassified		20. Security Class if. (of this page) Unclassified		21. No. of Pages 254	22. Price

**DISCLAIMER**

The opinions, findings and conclusions expressed in this publication are those of the authors and not necessarily those of the State of Florida Department of Transportation.

# SI\* (MODERN METRIC) CONVERSION FACTORS

## APPROXIMATE CONVERSIONS TO SI UNITS

Symbol	When You Know	Multiply By	To Find	Symbol
<b>LENGTH</b>				
in	inches	25.4	millimeters	mm
ft	feet	0.305	meters	m
yd	yards	0.914	meters	m
mi	miles	1.61	kilometers	km
<b>AREA</b>				
in <sup>2</sup>	square inches	645.2	square millimeters	mm <sup>2</sup>
ft <sup>2</sup>	square feet	0.093	square meters	m <sup>2</sup>
yd <sup>2</sup>	square yards	0.836	square meters	m <sup>2</sup>
ac	acres	0.405	hectares	ha
mi <sup>2</sup>	square miles	2.59	square kilometers	km <sup>2</sup>
<b>VOLUME</b>				
fl oz	fluid ounces	29.57	milliliters	ml
gal	gallons	3.785	liters	l
ft <sup>3</sup>	cubic feet	0.028	cubic meters	m <sup>3</sup>
yd <sup>3</sup>	cubic yards	0.765	cubic meters	m <sup>3</sup>
<b>MASS</b>				
oz	ounces	28.35	grams	g
lb	pounds	0.454	kilograms	kg
T	short tons (2000 lb)	0.907	megagrams	Mg
<b>TEMPERATURE (exact)</b>				
°F	Fahrenheit temperature	5(F-32)/9 or (F-32)/1.8	Celsius temperature	°C
<b>ILLUMINATION</b>				
fc	foot-candles	10.76	lux	l
fl	foot-Lamberts	3.426	candela/m <sup>2</sup>	cd/m <sup>2</sup>
<b>FORCE and PRESSURE or STRESS</b>				
lbf	poundforce	4.45	newtons	N
psi	poundforce per square inch	6.89	kilopascals	kPa

NOTE: Volumes greater than 1000 l shall be shown in m<sup>3</sup>.

## APPROXIMATE CONVERSIONS FROM SI UNITS

Symbol	When You Know	Multiply By	To Find	Symbol
<b>LENGTH</b>				
mm	millimeters	0.039	inches	in
m	meters	3.28	feet	ft
m	meters	1.09	yards	yd
km	kilometers	0.621	miles	mi
<b>AREA</b>				
mm <sup>2</sup>	square millimeters	0.0016	square inches	in <sup>2</sup>
m <sup>2</sup>	square meters	10.764	square feet	ft <sup>2</sup>
m <sup>2</sup>	square meters	1.195	square yards	yd <sup>2</sup>
ha	hectares	2.47	acres	ac
km <sup>2</sup>	square kilometers	0.386	square miles	mi <sup>2</sup>
<b>VOLUME</b>				
ml	milliliters	0.034	fluid ounces	fl oz
l	liters	0.264	gallons	gal
m <sup>3</sup>	cubic meters	35.71	cubic feet	ft <sup>3</sup>
m <sup>3</sup>	cubic meters	1.307	cubic yards	yd <sup>3</sup>
<b>MASS</b>				
g	grams	0.035	ounces	oz
kg	kilograms	2.202	pounds	lb
Mg	megagrams	1.103	short tons (2000 lb)	T
<b>TEMPERATURE (exact)</b>				
°C	Celsius temperature	1.8C + 32	Fahrenheit temperature	°F
<b>ILLUMINATION</b>				
lx	lux	0.0929	foot-candles	fc
cd/m <sup>2</sup>	candela/m <sup>2</sup>	0.2919	foot-Lamberts	fl
<b>FORCE and PRESSURE or STRESS</b>				
N	newtons	0.225	poundforce	lbf
kPa	kilopascals	0.145	poundforce per square inch	psi

\* SI is the symbol for the International System of Units. Appropriate rounding should be made to comply with Section 4 of ASTM E380.

## ACKNOWLEDGMENTS

The authors would like to acknowledge and thank the Florida Department of Transportation (FDOT) for providing technical and financial support and materials for this project. Very special thanks to the Florida Department of Transportation personnel Messrs. Mike Bergin, Charles Ishee, Mario Paredes, Chris Ferraro, Richard Delorenzo for their help with the entire process of fabricating test samples and guidance throughout the project. Sincere thanks go to Mr. Younggon Kim and Qiang Li for their help.

## EXECUTIVE SUMMARY

This study was conducted to evaluate durability of FRC produced with four fiber types (polypropylene/PP, polyvinyl-alcohol/PVA, cellulose/Cell, hooked-end steel/St) exposed to simulated Florida environments for 27 months. The addition of fiber affects both ductility and load transfer capacity in cement composites. Stress transfer from the matrix to the fiber resulting from frictional slip of fibers at the interface depends on the mechanical properties and geometry of both matrix and fiber. The unique mechanical properties of the fiber-matrix interface control the fracture toughness and durability of the composite and result in different fracture mechanisms during pull-out from the matrix. An important factor governing the bridging forces is interfacial shear strength between matrix and fibers. Therefore, it is necessary develop relevant accelerated degradation conditioning procedures and appropriate test methods to accurately and reliably determine the failure mechanism of FRC.

An experimental program was performed to examine the effects of fiber type on concrete durability from measurements of both the fresh and hardened concrete properties. Significant reduction in workability resulting from the addition of PP, PVA, and steel fibers to concrete was clearly measured. Both inverted slump cone and Vebe time test methods were more accurate and sensitive to presence of fibers than conventional slump test. However, the inverted slump cone test had the greatest sensitivity to distinguish between workability of different fiber types and involved less expensive equipment than the Vebe test. Peak strengths were affected mainly by the matrix not the fibers. Only the addition of hooked-end steel fibers with high modulus and high tensile strength resulted in a slight improvement in peak strengths. Tests results from the experimental investigation of transport properties indicated that the addition of fibers improved resistance of mass transport of deleterious materials. However, among the fiber types, the

addition of steel fibers had the best ability to resist mass transport of deleterious materials in concrete.

Effect of fibers on cracking resistance could not be assessed based on test results from either average residual strength (ASTM C 1399) or flexural performance (ASTM C 1609) tests. It was determined that the conventional flexural beam approach resulted in non-uniform degradation and stress/strain distributions through the cross-section. Also, beam tests generally resulted in multiple cracks initiating at the bottom of the specimen and instability subsequent to matrix cracking. These critical factors significantly affected the pull-out mechanism of fibers and disturbed the evaluation of failure during post-cracking. Observations and test results from SEM and EDS analysis were probably also affected by problems associated with the flexural beam approach.

Based on findings and observations, the indirect tensile test mode was introduced, which allowed for accelerated transport of deleterious materials and resulted in a uniformly degraded cross-section and uniform stress/strain distributions. Absorption by capillary suction was identified as the most critical transport mechanism for determining an effective damage conditioning method and specimen thickness. A 14-day wetting and drying cyclic conditioning procedure was determined to result in uniform damage throughout the specimen based on absorption test results. A 4×4 inch square specimen one inch thick, which was sliced from beam specimens exposed to lime water immersion, with a hole cored at its center was proposed to most effectively assess the effect of fibers on deterioration of FRC. FEM analysis proved the same stress distribution along vertical plane between circular and square specimens. FRC specimens were subjected to an additional six months of saltwater conditioning.

The effects of fiber type on resistance to chemical degradation were clearly observed from the SuperPave<sup>TM</sup> IDT test methods. The primary advantage of IDT over conventional flexural beam test system is the fact that the failure plane is known a priori so that failure limits can be measured directly on that plane. In addition, the approach resulted in a great reduction of specimen volume, labor, and cost. IDT strength test performed at a slow loading rate was determined to minimize the high energy dissipation and the high rate of deflection subsequent to matrix cracking. Additionally, repeated loading test showed superior advantages to assess deterioration of FRC by evaluating averaged horizontal deformation and increase in horizontal resilient deformation ratio.

The effect of polypropylene fibers at  $V_f = 0.5\%$  provides the best resistance to degradation (best durability) for non-structural application in saltwater environment subjected to submerged and tidal zones. The effect of steel fibers at  $V_f = 1\%$  may be suitable in saltwater environment subjected to tidal zones, but should not be used if it will be in contact with reinforcing bars. The effect of polyvinyl alcohol fibers at  $V_f = 0.75\%$  should not be used in saltwater environment subjected to submerged and tidal zones. The effect of cellulose fibers at  $V_f = 0.1\%$  could not be evaluated because good fiber distribution was not achieved in laboratory mixing. The detrimental effect of acetic acid on aggregate and cement overwhelmed the degradation mechanism in swamp water environments. Therefore, the effect of fibers could not be distinguished for these environments.

Recommendations were made for continued development and validation of testing by considering use of fiber in cement paste only in order to achieve better fiber distribution. The need to evaluate effects of multiple fiber types, fiber volume fractions, fiber aspect ratios, and

fiber configurations with the procedures developed was also emphasized to optimize performance and durability of FRC.

# TABLE OF CONTENTS

	<u>page</u>
EXECUTIVE SUMMARY .....	ii
LIST OF TABLES .....	x
LIST OF FIGURES .....	xi
CHAPTER	
1 INTRODUCTION .....	1
1.1 Background .....	1
1.2 Objectives .....	2
1.3 Scope .....	3
1.4 Hypothesis .....	3
1.5 Research Approach .....	4
2 LITERATURE REVIEW .....	6
2.1 Introduction .....	6
2.2 Microstructure of Fiber-Matrix Interface .....	7
2.3 Mechanical Behavior of Fiber Reinforcement .....	9
2.3.1 Stress Transfer before Matrix Cracking .....	10
2.3.2 Stress Transfer after Matrix Cracking .....	13
2.4 Fracture Mechanics Approach .....	14
2.4.1 Crack Suppression by Fibers .....	15
2.4.2 Crack Stabilization Subsequent to Matrix Crack .....	16
2.4.3 Fiber-Matrix Debonding .....	16
2.5 Fiber Effect on Mechanical Properties .....	17
2.5.1 Compression .....	17
2.5.2 Tension .....	20
2.5.3 Bending .....	21
2.6 Transport Mechanisms .....	23
2.6.1 Permeation .....	24
2.6.2 Absorption .....	25
2.6.3 Diffusion .....	26
2.7 Parameters Affecting Transport Properties .....	27
3 MATERIALS AND EXPERIMENTAL PROGRAM .....	30
3.1 Characterization of Constituent Materials .....	30
3.1.1 Cement .....	30
3.1.2 Coarse Aggregates .....	30
3.1.3 Fine Aggregates .....	31
3.1.4 Chemical Admixtures .....	31

3.1.5	Fibers.....	32
3.2	Mix Proportions .....	34
3.3	Mixing and Curing Procedures .....	35
3.3.1	Mixing Procedure.....	35
3.3.2	Curing Procedure .....	36
3.4	Specimen Preparation.....	37
3.5	Experimental Program .....	39
3.5.1	Fresh Properties.....	39
3.5.1.1	Slump test .....	40
3.5.1.2	Inverted slump cone time.....	40
3.5.1.3	Vebe time.....	42
3.5.1.4	Air content .....	43
3.5.2	Transport Properties.....	43
3.5.2.1	Permeable pore space test.....	44
3.5.2.2	Surface resistivity test.....	44
3.5.2.3	Permeability test .....	46
3.5.2.4	Absorption test.....	47
3.5.2.5	Bulk diffusion test.....	49
3.5.3	Mechanical Properties.....	50
3.5.3.1	Compressive strength testing.....	51
3.5.3.2	Splitting tensile testing .....	52
3.5.3.3	Pressure tension testing.....	53
3.5.3.4	Residual strength testing.....	56
3.5.3.5	Flexural performance testing.....	58
3.5.4	Steel Bar Corrosion.....	60
3.5.5	Ultra Pulse Velocity (UPV) .....	62
3.5.6	Scanning Electron Microscopy (SEM) .....	62
3.5.7	Carbonation.....	63
4	ENVIRONMENTAL EXPOSURE.....	64
4.1	Introduction.....	64
4.2	Deterioration of a Concrete Structure in Seawater .....	64
4.3	Environmental Exposure.....	66
4.4	Deterioration Mechanism.....	74
5	FINDINGS AND ANALYSIS .....	76
5.1	Introduction.....	76
5.2	Fresh Properties Test Results.....	76
5.2.1	Slump Test Results.....	76
5.2.2	Inverted Slump Cone Test Results.....	76
5.2.3	Vebe Test Results.....	78
5.2.4	Air Content Test Results .....	78
5.2.5	Relationships between Workability Tests.....	80
5.3	Transport Property Test Results.....	82
5.3.1	Permeable Pore Space Test Results .....	82

5.3.2	Surface Resistivity Test Results.....	84
5.3.3	Permeability Test Results.....	86
5.3.4	Absorption Test Results.....	88
5.3.5	Bulk Diffusion Test Results.....	93
5.4	Mechanical Property Test Results.....	95
5.4.1	Compressive Strength Test Results.....	95
5.4.2	Splitting Tensile Strength Test Results.....	95
5.4.3	Pressure Tension Test Results.....	95
5.5	Steel Bar Corrosion Test Results.....	97
5.6	Evaluation of Beams Exposed to Conditioning.....	99
5.6.1	Visual and Photographic Inspection.....	99
5.6.2	Ultrasonic Pulse Velocity Inspection.....	102
5.6.3	Permeable Pore Space Change.....	104
5.6.4	Average Residual Strength (ARS) Test Results.....	105
5.6.5	Flexural Performance Test Results.....	107
5.6.6	Carbonation.....	108
5.6.7	Scanning Electron Microscopy.....	111
	5.6.7.1 Fibers subjected to salt and acidic solutions.....	112
	5.6.7.2 Degraded beam.....	113
5.6.8	Distribution Problem for Cellulose Fibers.....	127
5.7	Discussion of Conventional Beam Approach.....	128
5.8	Summary of Conventional Beam Testing.....	134
6	DEVELOPMENT OF CONDITIONING AND TEST METHOD.....	136
6.1	Introduction.....	136
6.2	Determination of Conditioning and Specimen Thickness.....	136
6.3	Proposed Test Method.....	137
6.4	Evaluation of Fiber Resistance to Conditioning.....	140
6.4.1	Experimental Program.....	140
6.4.2	Exposure Conditions.....	141
6.4.3	Testing Procedures.....	141
6.4.4	Evaluation of the Fracture Tests.....	142
	6.4.4.1 Visual examination of fractured specimens.....	143
	6.4.4.2 Examination of strength test results.....	143
	6.4.4.3 Examination of repeated load test results.....	149
	6.4.4.4 Evaluation of failure mechanisms of fibers.....	152
6.5	Summary of Findings.....	157
7	FINDINGS, CONCLUSIONS, AND RECOMMENDATIONS.....	159
7.1	Summary of Findings.....	159
7.2	Conclusions.....	163
7.3	Recommendations.....	163

## APPENDIX

A	FRESH PROPERTY TEST RESULTS.....	171
B	DENSITY, ABSORPTION, VOLUME OF VOIDS TEST RESULTLS.....	172
C	SURFACE RESISTIVITY TEST RESULTS .....	174
D	WATER PERMEABILITY TEST RESULTS.....	177
E	ABSORPTION TEST RESULTS .....	178
F	BULK DIFFUSION TEST RESULTS.....	180
G	MECHANICAL PROPERTIES TEST RESULTS .....	189
H	STEEL CORROSION TEST RESULTS .....	194
I	DEGRADED BEAM TEST RESULTS .....	198
J	INDIRECT TENSILE TEST RESULTS.....	234
	LIST OF REFERENCES.....	164

## LIST OF TABLES

<u>Table</u>	<u>page</u>
3-1	Chemical and mineralogical composition.....30
3-2	Aggregate gradation, coarse aggregates .....31
3-3	Aggregate gradation, fine aggregates .....31
3-4	Properties of fibers used.....33
3-5	Environmental resistance of fibers used .....34
3-6	Material and mix proportions for Classes II/V concrete.....35
3-7	Number of specimens tested for mechanical tests for Classes II/V concrete .....38
3-8	Number of specimens tested for transport property tests for Classes II/V concrete.....38
3-9	Number of specimens prepared for conditioning and testing for Classes II/V concrete ...39
3-10	Surface resistivity-permeability .....46
4-1	Composition of simulated seawater .....67
4-2	Beam specimens exposed to environmental exposure.....68
4-3	Redesigned composition of simulated seawater .....71
5-1	Percent change in UPV test results for Class II concrete.....103
5-2	Averaged UPV test results for Class V concrete .....103
5-3	Averaged permeable pore space before/after conditioning for Classes II/V concrete.....104
5-4	Averaged ARS (psi) test results .....105
5-5	Averaged test results of flexural performance .....107
6-1	Number of specimens tested for IDT for Class II concrete .....141

## LIST OF FIGURES

<u>Figure</u>	<u>page</u>
1-1 Schematic diagram for research approach .....	5
2-1 Schematic description of a fiber deformation and stress fields in the matrix .....	11
2-2 Distribution of interfacial shear stresses and fiber tensile stresses .....	12
2-3 Interfacial shear stress distribution immediately after cracking . .....	14
2-4 Idealized representation of an advancing crack and the stress field .....	16
2.5 ASTM C 1018 techniques of fiber reinforced toughness characterization.....	23
3-1 Fiber types.....	32
3-2 Fiber surfacesl.....	33
3-3 Compulsive pan mixer .....	36
3-4 Concrete blocks for fiber mixtures .....	37
3-5 Steel mold .....	39
3-6 Inverted slump-cone time test setup .....	41
3-7 Vebe time test setup .....	42
3-8 Surface resistivity test set-up. ....	45
3-9 Water permeability test specimens. ....	47
3-10 Absorption test set-up .....	49
3-11 Exposure tank and specimen condition for bulk diffusion .....	50
3-12 Test set-up for compressive strength .....	51
3-13 Test set-up for splitting tensile test .....	52
3-14 Stress state in hollow cylinder under internal or external uniform pressure.....	54
3-15 Nitrogen gas tension test and stress state.....	55
3-16 Pressure tension testing equipments .....	55

3-17	Test setup for measuring residual strength by using deflection gage and yoke.....	56
3-18	Load vs. deflection curve for residual strength measurement .....	57
3-19	Test set-up for measuring flexural performance of FRC with yoke.....	58
3-20	Examples of parameter calculations for different flexural curves .....	59
3-21	Test set-up for steel bar corrosion.....	61
4-1	Schematic diagram for degradation mechanism.....	64
4-2	Flow chart for experimental program .....	68
4-3	Environmental exposure conditioning .....	68
4-4	New wet/dry environmental exposure conditioning .....	71
4-5	Moisture movement with new wet/dry conditioning for limewater wet/dry .....	72
4-6	Moisture movement with new wet/dry conditioning for saltwater wet/dry.....	72
4-7	Moisture movement with new wet/dry conditioning for limewater wet/dry .....	73
4-8	Moisture movement with new wet/dry conditioning for saltwater wet/dry.....	73
4-9	Expected deterioration mechanism.....	75
5-1	Slump test results for Class II concrete.....	77
5-2	Slump test results for Class V concrete .....	77
5-3	Inverted slump cone time test results for Classes II/V concrete.....	78
5-4	Vebe time test results for Classes II/V concrete.....	79
5-5	Air content test results for Class II concrete.....	79
5-6	Air content test results for Class V concrete.....	80
5-7	Inverted slump cone time vs. slump .....	81
5-8	Vebe time vs. slump.....	81
5-9	Inverted slump cone time vs. Vebe time.....	82
5-10	Permeable pore space for Class II concrete without/with fiber .....	83
5-11	Permeable pore space for Class V concrete without/with fiber.....	83

5-12	Permeable pore space for Classes II/V concrete.....	84
5-13	Surface resistivity for Class II concrete.....	85
5-14	Surface resistivity for Class V concrete.....	85
5-15	Coefficient of permeability for Class II concrete with/without fiber .....	86
5-16	Coefficient of permeability for Class V concrete with/without fiber .....	87
5-17	Coefficient of permeability for Classes II/V concrete .....	87
5-18	Absorption vs. time for Classes II/V concrete.....	89
5-19	Absorption rate for Class II concrete with/without fiber.....	90
5-20	Absorption rate for Class V concrete with/without fiber.....	91
5-21	Absorption rate for Class II concrete.....	92
5-22	Absorption rate for Class V concrete.....	92
5-23	Chloride concentration for Classes II concrete.....	93
5-24	Chloride concentration for Classes II/V concrete.....	94
5-25	Coefficient of chloride diffusion for Classes II/V concrete.....	94
5-26	Compressive strength for Classes II/V concrete.....	96
5-27	Splitting tensile strength for Classes II/V concrete.....	96
5-28	Pressure tension strength for Classes II/V concrete.....	97
5-29	Total times for initiation of steel corrosion for Class II concrete.....	98
5-30	Total corrosion rate for Class II concrete .....	99
5-31	Surface degradation comparisons for fiber type.....	100
5-32	Average residual strength results for Classes II concrete.....	106
5-33	Average residual strength results for Class V concrete .....	106
5-34	Flexural performance comparisons for PP fiber mixes for Class II concrete.....	108
5-35	Flexural performance comparisons for PP fiber mixes for Class V concrete.....	109
5-36	Flexural performance comparisons for PVA fiber mixes for Class II concrete .....	109

5-37	Flexural performance comparisons for PVA fiber mixes for Class V concrete .....	110
5-38	Flexural performance comparisons for Steel fiber mixes for Class II concrete .....	110
5-39	Flexural performance comparisons for Steel fiber mixes for Class V concrete .....	111
5-40	Degraded area and carbonated depth for swamp water immersion. ....	111
5-41	Surface properties of PP fibers .....	114
5-42	Surface properties of PVA fibers.....	115
5-43	Surface properties of cellulose fibers.....	116
5-44	Surface properties of steel fibers.....	117
5-45	PP fiber comparisons in limewater and saltwater immersion.....	118
5-46	PVA fiber comparisons in limewater and saltwater immersion.. ....	121
5-47	Steel fiber comparisons in limewater and saltwater immersion. ....	124
5-48	Cellulose fibers distribution.....	127
5-49	Test result for flexural beam testing with third-point loading .....	129
5-50	PP fiber mix for limewater immersion for 27 months .....	130
5-51	PVA fiber mix for limewater immersion for 27 months.....	130
5-52	Steel fiber mix for limewater immersion for 27 months.....	131
5-53	Unstable failure in fiber-reinforced concrete.....	131
5-54	Coefficients for PP fiber beams .....	132
5-55	Coefficients for PVA fiber beams.....	133
5-56	Coefficients for steel fiber beams .....	133
5-57	Overestimated energy effect on determination of toughness.....	134
6-1	Absorption depths vs. time for fiber type and Classes II/V concrete .....	137
6-2	Theoretical stress distribution and gage points spaced at depth/4 .....	138
6-3	Superpave™ IDT specimen setup .....	139
6-4	2-Dimensional FEM analysis for circle and square shapes IDT.....	139

6-5	Proposed test Specimen and stress distribution .....	140
6-6	Flow chart for experimental program .....	142
6-7	Test Setup for IDT .....	142
6-8	Surface degradation and failure plane for saltwater cyclic W/D .....	144
6-9	Fractured surface degradation for Steel fibers .....	145
6-10	Comparison of strength test results at first cracking for PP-II mixes .....	146
6-11	Comparison of strength test results at first cracking for PVA-II mixes .....	147
6-12	Comparison of strength test results at first cracking for steel-II mixes .....	148
6-13	Repeated loading test results for steel fiber mix for Class II concrete . .....	150
6-14	Averaged horizontal permanent deformation vs. number of cycles for steel fiber mix ..	151
6-15	Averaged horizontal permanent deformation vs. number of cycles for PP fiber mix. ....	151
6-16	Averaged horizontal permanent deformation vs. number of cycles for PVA fiber mix..	152
6-17	Schematic diagram for resilient deformation ratio for fiber bridging zone .....	153
6-18	Resilient deformation ratio vs. no. of cycles for fiber bridging zone (steel fibers) .....	155
6-19	Resilient deformation ratio vs. no. of cycles for fiber bridging zone (PP fibers).....	155
6-20	Resilient deformation ratio vs. no of cycles for fiber bridging zone (PVA fibers) .....	156
6-21	Rate of stiffness reduction for resilient deformation ratio .....	156

## CHAPTER 1 INTRODUCTION

### 1.1 Background

Historically, there has been extensive research performed regarding the durability of concrete exposed to the marine environment. However, some mechanisms involved in the deterioration of concrete materials are not fully understood, particularly as related to fiber-reinforced concrete (FRC).

Plain concrete, characterized by low tensile, flexural and residual strength as well as strain tolerance, requires reinforcement for structural usage. Traditionally, continuous reinforcing steel has been used in concrete structures to resist tensile and shear stresses. On the other hand, fiber reinforcement in concrete is comparatively short, discontinuous and randomly distributed throughout the concrete matrix. Currently, design codes do not allow the complete substitution of steel reinforcement with fibers alone as they do not provide sufficient resistance to tensile stresses of structural magnitude (ACI 544.1R, 1996). Therefore, fibers can be most effectively used to resist crack propagation, since they are more uniformly distributed throughout the concrete matrix and more closely spaced than traditional reinforcement. Furthermore, the addition of fibers into a cement matrix enhances fracture toughness by exhibiting much greater post-cracking resistance than plain concrete (Beaudoin and Bentur et al., 1990).

Regourd (1980) indicated that marine structures typically are slowly degraded by chemical and physical mechanisms. Deleterious materials are transported into the concrete through absorption, diffusion, and permeability processes. Deterioration may occur as a result of lime dissolution and formation of ettringite, which is an expansive reaction that may lead to cracking, spalling, and subsequent erosion. For the case of cyclic wetting and drying, both chemical and physical processes are involved in the fundamental mechanisms that attack the marine structure.

Typically, wetting and drying cycles result in leaching of concrete and accelerated ingress of saltwater through repeated adsorption. Ingress of chloride ions results in corrosion of reinforcing steel, which causes expansion that leads to tensile stresses. In addition, mechanical wave action and rapid changes in temperature and wind conditions result in additional tensile stresses of a physical nature.

Almost all durability research performed to date on fiber-reinforced concrete has not considered transport characteristics such as permeability, diffusion, absorption and wicking action which are the fundamental mechanisms involved in the deterioration process of concrete during environmental exposure. Therefore, utilizing concrete materials typically used in Florida, the current state-of-practice, and manufacturer's recommended guidelines, this research is focused on development of a better understanding of the fiber and fiber type effect on transport mechanisms that affect durability and on finding effective test methods to observe and evaluate the chemical and physical changes in the fiber-cement interface.

## **1.2 Objectives**

Although this work originally focused on evaluating the degree of degradation from the measurement of strength and toughness loss with conventional beam specimens, serious problems were encountered in terms of accelerated degradation mechanisms using flexural beam specimen. Therefore, the research was necessarily refocused to investigate and develop alternate advanced evaluation procedures for durability of fiber-reinforced concrete. The focus was to identify a critical transport mechanism for affecting effective degradation conditioning of FRC specimens in the laboratory. A second goal was to identify and/or develop a proper test method that is sensitive to failure mechanism of fibers during post-cracking behavior. Detailed research objectives are as follows:

- To examine the effects of fiber and fiber type on fresh and hardened properties of concrete.

- To evaluate the effect of fiber and fiber type on transport mechanisms that affect concrete durability.
- To identify and develop accelerated degradation conditioning with an effective specimen preparation and testing systems to evaluate the effect of fiber type on the potential of concrete to fail in service.
- To visualize the various interfacial microstructure and morphology changes resulting from chemical attacks by using a scanning electron microscope (SEM).
- To propose recommendations and guidelines for the establishment of an environmental conditioning system and an effective test method for assessing effect of fibers on degradation of FRC for the use of structural and non-structural fibers in Florida.

### **1.3 Scope**

The evaluation performed in this investigation involved the following:

- Ten mixtures involving two concrete mixture types, four kinds of fiber (polypropylene, polyvinyl alcohol, cellulose, and steel) and an unreinforced concrete group were evaluated. Fiber contents and mixture designs were based on current state-of-practice and manufacturer's recommended guidelines.
- Compressive strength, splitting tension, pressure tension, flexural beam and indirect tensile tests were performed to evaluate fiber and fiber type effects on mechanical properties.
- Permeable pore space (voids), water permeability, chloride diffusion, and absorption tests were performed to determine the fiber's effect on transport mechanisms, as well as to establish conditioning and appropriate specimen geometry for effective accelerated deterioration of the FRC.
- Simulated environmental exposure involved three kinds of conditioning systems; 1) salt water immersion; 2) salt water wet/dry cycles; 3) swamp water immersion (acid environment).
- Results of flexural beam and indirect tensile test were compared to identify effective conditioning systems and test methods for evaluation of degraded fiber-reinforced concrete.
- SEM/EDS image analysis was performed to discern the nature of the deterioration mechanism.

### **1.4 Hypothesis**

The hypotheses of this research are:

- The addition of fibers, as well as fiber characteristics, can affect the transport mechanisms of deleterious solutions through concrete, which in turn influence the degradation of physical properties and the durability of FRC subjected to different environments.
- High salt solution, high temperature, pre-cracked beam, and repeated wetting and drying cycles can accelerate degradation mechanisms.

### **1.5 Research Approach**

A schematic diagram for the research approach used is presented in Figure 1-1. The evaluation of the effects of fiber on degradation of concrete was based on a detailed literature review and laboratory investigation. This research not only investigated conventional approaches using the flexural bending test method, but also proposed a new conditioning system and specimen geometry for accelerating deterioration mechanisms, as well as a test method and data interpretation procedure to effectively evaluate the relative durability of FRC subjected to aggressive environments encountered in Florida.

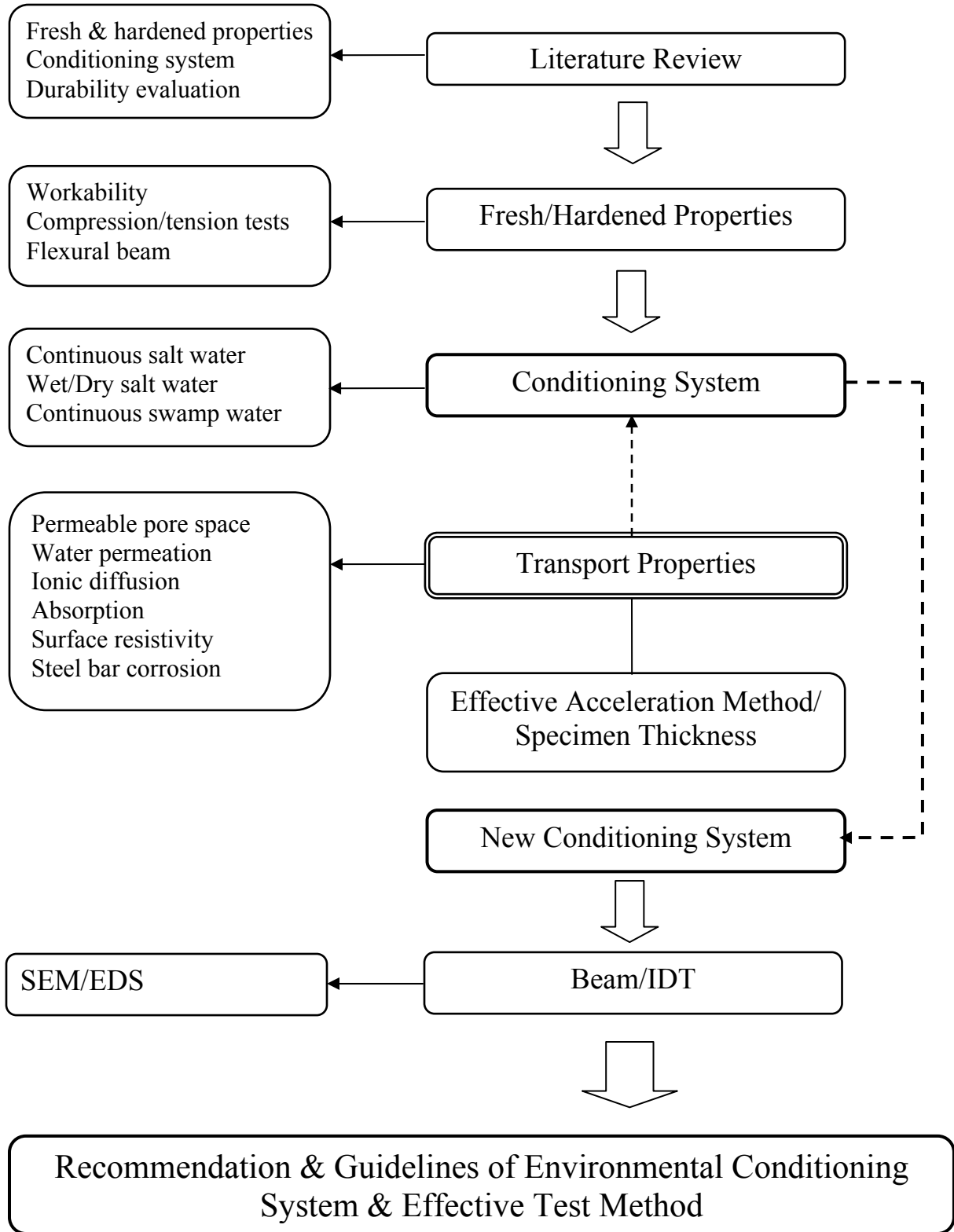


Figure 1-1. Schematic diagram for research approach

## CHAPTER 2 LITERATURE REVIEW

### 2.1 Introduction

A literature review was undertaken to develop a better understanding of the effect of fibers on mechanical and transport properties of concrete. The literature review was also used to identify potentially suitable environmental conditioning procedures and effective test methods to evaluate the effects of chemical and physical changes in the fiber-cement interface. Interfacial microstructure, mechanical behavior of fibers in composites, transport mechanisms, and fracture mechanics for quasi-brittle fracture were reviewed.

Although concrete is generally a durable material, it is vulnerable when exposed to environments that can chemically and physically attack its integrity. Many types and sources of chemical and physical attacks can affect the integrity of concrete. Solutions in the mixing water or adsorbed water may lead to cracking, spalling, and subsequent erosion. Ingress of chloride ions results in corrosion of reinforcing steel, which causes expansion that leads to tensile stresses and potential cracking. Wetting and drying cycles result in leaching and accelerated ingress of solutions. Presence of expansive clays, organics, and salts can also have detrimental effects on durability. Wave action in tidal zones and rapid changes in temperature, wind, and moisture conditions result in mechanically induced tensile stresses that can contribute to cracking. Although one factor may cause the primary distress, other factors may then contribute and accelerate the circumstance (Mindess et al., 2003).

The main motivation for conducting durability studies is to accurately predict material behavior based on short-term testing. By conducting a literature review, a fundamental understanding regarding the development of degradation conditioning systems and effective test

methods for failure mechanism of fibers was created. The reliability and practicality of these approaches for use in fiber-reinforced concrete were examined.

## **2.2 Microstructure of Fiber-Matrix Interface**

It is well known that the aggregate particles in concrete mixture are surrounded by a uniform matrix of hardened cement paste producing an interfacial transition zone (ITZ), which is typically 20-40  $\mu\text{m}$  thick. The structure of ITZ is quite different than that of bulk paste away from the physical interface. The ITZ is characterized as having the following properties: less unhydrated cement, a higher porosity, less C-S-H, large oriented crystals of CH, and a greater concentration of ettringite. Although the ITZ is quite thin, the interfacial region normally makes up 20-40% of the total volume of cementitious matrix which affects transport and mechanical properties of concrete (Mindess et al., 2003 and Mehta et al., 2005).

The process of development of interfacial zone resulting from the addition of fibers into concrete is similar to that between hardened cement paste and coarse aggregate. The discontinuous fiber reinforcement usually results in modification of the microstructure of cementitious composites by reduction of the number and size of mesopores rather than by an increase in number and size of micropores (Beaudoin, 1990). The microstructure of the transition zone in the area of the fiber reinforcement is quite different from that of bulk matrix and is strongly dependent on fiber type, fiber geometry, and the production process. The bonding property of the fiber-matrix interface and the debonding process of the fibers from the matrix affect the failure mechanism of concrete. Stress concentrations may develop at the fiber-matrix interface, which may lower resistance to micro-damage compared with conventional concrete. Conversely, the fibers resistance to pull-out or debonding may help to redistribute stresses over a broader area, which may result in greater resistance to further development of micro-damage, crack initiation, and propagation compared with conventional concrete. The discrete cement

particles vary from 1 to 10  $\mu\text{m}$  in the fresh mix condition reacting with water to form poorly crystallized calcium silicate hydrate (C-S-H), large crystals of calcium hydroxide (CH), and a small amount of ettringite (Mindess, 2003). The nature of cement particles around the discrete fibers results in the development of water-filled spaces during mixing because of water bleeding and entrapment, and inefficient packing of cement grains around the fiber surface (Bentur and Mindess, 1990). Therefore, the microstructure of the transition zone at the interface becomes porous, allowing the crystallization of hydration products.

Al-Khalaf et al. (1979) and Pinchin et al. (1978) studied the microstructure of the interfacial transition zone (ITZ) with steel fibers. They found that the interfacial zone is somewhat porous and abundant in CH, mostly in direct contact with the fiber surface, which differentiates it from the microstructure of the bulk paste matrix. The nucleation of a CH rich zone around the fiber surface results from the CH precipitation at the water-filled spaces in the fresh mix. The CH layer as thin as 1  $\mu\text{m}$  is not necessarily uniform around the fiber and it consists of a duplex film, and needle-like materials (C-S-H, ettringite).

On the other hand, synthetic fibers such as polypropylene fiber with a low modulus of elasticity and polyvinyl alcohol fiber with a high modulus have different microstructure in the transition zone. Rice et al., (1988) and Bentur et al., (1989) found that the interfacial microstructure of fibrillated polypropylene fiber was fairly dense and continuous around the fiber surface and did not contain CH zone at the ITZ because a proprietary surface treatment involving wetting agents and physical roughening of the fiber surface to achieve bonding with the hardened cement paste caused the uniform formation of this dense layer. Hikasa et al. (1986) reported that the interfacial microstructure between cement paste and polyvinyl alcohol with high modulus of elasticity provided a uniform, highly effective reinforcing bond without formation of CH at the

fiber ITZ due to their consistent fiber dispersion in the composites and the high area of fiber surface beneficial for improvement of interfacial bonding.

### 2.3 Mechanical Behavior of Fiber Reinforcement

Short fibers in cement composites are discontinuously dispersed in the matrix during mixing and produce anisotropy and heterogeneity. Krenchel (1975) and Romualdi et al. (1964) suggested that fiber spacing is a geometrical parameter which plays an important role in governing the fiber performance in the composite. The average fiber spacing has been calculated by assuming a uniform fiber distribution within the hardened cement paste matrix. The suggested equation for the spacing of a cylindrical fiber is represented as follows:

$$S = \frac{K \cdot d}{\sqrt{V_f}} \quad (2-1)$$

where

$S$  = fiber spacing

$K$  = constant from 0.8 to 1.12 depending on the fiber orientation

$d$  = fiber diameter

$V_f$  = fiber volume fraction.

Beaudoin (1990) stated that the applied load is transferred from the hardened cement paste matrix to the fiber by shear deformation at the paste / fiber interface. The mechanical properties and geometry of both the fiber and matrix significantly affect the load transfer mechanism during the fiber pull-out process from the hardened cement paste matrix. The role of short and discontinuous fibers is to increase the fracture toughness by arresting cracks and delaying crack propagation.

Bentur and Mindess (1990) determined that the fiber's effectiveness in improving the mechanical properties through fiber-cement paste interactions is governed by both the load transfer process from the matrix to the fiber and the bridging effect across the crack surface. The stress transfer from the matrix to the embedded fiber prior to crack coalescence in concrete is

elastic in nature. Stress due to loading developed between the matrix and fibers is a shear stress which distributes the applied load across the interface, and the strains developed at the concrete matrix ITZ and the fiber are of the same magnitude. After the initiation of cracking, debonding of the fibers from the hardened cement paste matrix is caused by frictional slip, which is an important mechanism during the post-cracking process. Stress transfer from elastic deformation to inelastic frictional slip at the interface happens when the interfacial shear stresses developed at the early stages of loading surpass the shear bond strength or fiber-matrix shear strength at the interface. Therefore, the load transition mechanism of the shear stress along the fiber-matrix interface is primarily important in controlling and evaluating mechanical behavior of fiber reinforced concrete and also valuable to assess effect of fibers in the various environmental exposure conditions.

### 2.3.1 Stress Transfer before Matrix Cracking

During early stages of loading, load is transferred from the hardened cement paste matrix to the fiber in an elastic fashion and is the dominant stress transfer mechanism. The first analytical model for the stress transition in the early stage of loading was developed by Cox (1952). This model is based on the stress analysis surrounding a discontinuous fiber embedded in the matrix. A schematic description showing deformation changes before and after load application is shown in Figure 2-1. Cox (1952) derived the equation below for tensile stress,  $\sigma_f(x)$ , in the fiber, and for interfacial shear stress,  $\tau(x)$ , as a function of the distance  $x$  from the end of fiber:

$$\sigma_f(x) = E_f \varepsilon_m \left[ \frac{1 - \cosh \beta_1 \left( \frac{l}{2} - x \right)}{\cosh \frac{\beta_1 l}{2}} \right] \quad (2.2)$$

$$\tau(x) = E_f \varepsilon_m \left[ \frac{G_m}{2E_f \ln(R/r)} \right]^{1/2} \frac{\sinh \beta_1 (\frac{l}{2} - x)}{\cosh \frac{\beta_1 l}{2}} \quad (2.3)$$

where

$$\beta_1 = \left[ \frac{2G_m}{E_f r^2 \ln(R/r)} \right]^{1/2} \quad (2.4)$$

$R$  = radius of the matrix around the fiber

$r$  = radius of the fiber

$l$  = length of fiber

$E_f$  = modulus of elasticity of the fiber

$G_m$  = shear modulus of the matrix at the interface.

The maximum interfacial shear stress is created at the ends of fiber and gradually decreases and

finally drops to zero toward the center of the fiber as depicted in Figure 2.1c. Note that

interfacial shear stresses are greatest at the end of the fiber and decrease towards the

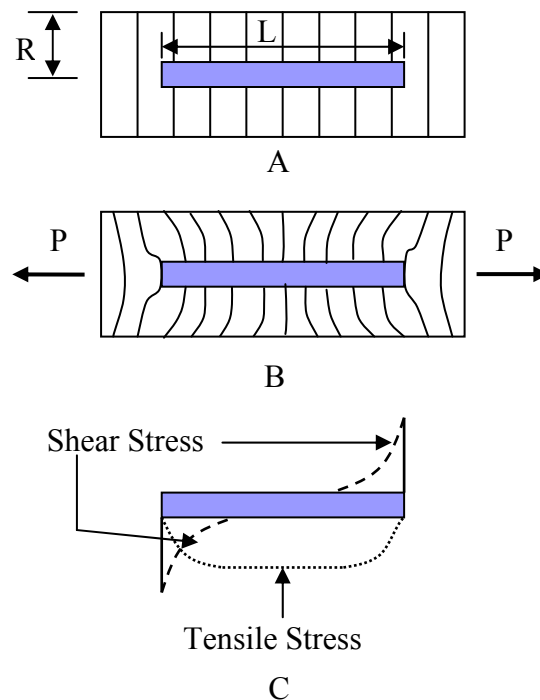


Figure 2-1. Schematic description of a fiber deformation and stress fields in the matrix. A) Before loading. B) After loading. C) Stresses. (after Bentur et al., 1990).

fiber's center. Since the shear stresses act away from the center of the fiber, the maximum tensile stress within the fiber occurs at the fiber's center and goes to zero at the end of the fiber.

If the fiber debonds at the interface before matrix cracking, the interfacial slip resistance mechanism between the fiber and the matrix should be considered for calculation of stress distribution (Bentur and Mindess, 1990). Figure 2.2 is an illustration of the distribution of shear stresses and tensile stresses.

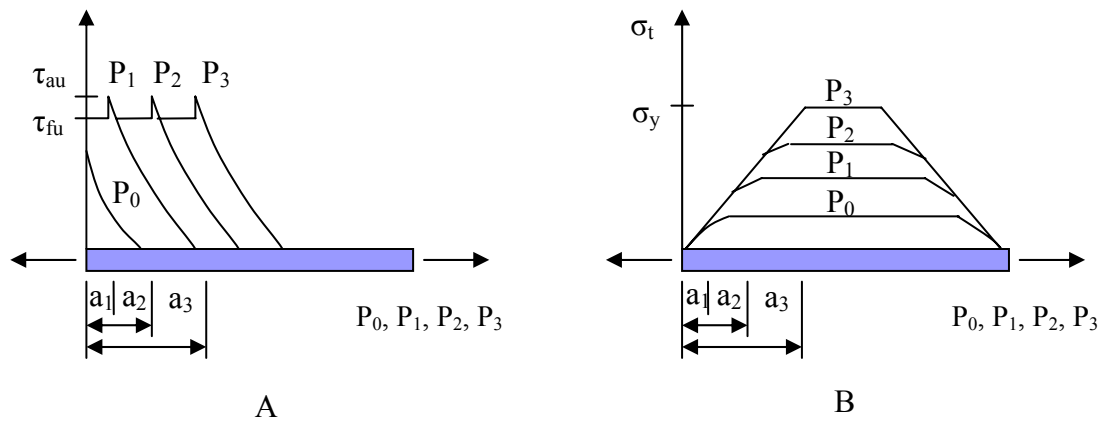


Figure 2-2. Distribution of interfacial shear stresses and fiber tensile stresses. A) Interfacial shear stresses. B) Fiber tensile stresses. (after Bentur et al., 1990).

Figure 2.2a illustrates the stress distribution of the interfacial shear stress. It is assumed that under a given load “ $P_1, P_2, P_3$ ”, the frictional slip in the debonded region “ $a_1, a_2, a_3$ ” produces a uniform frictional shear stress distribution, “ $\tau_{fu}$ ”, at the interface as shown in Figure 2.2a and the tensile stress distribution as shown in Figure 2-2b. Before reaching the adhesional shear bond strength,  $\tau_{au}$ , the shear stress distributions by the applied load ( $P_0$ ) at the interface are as shown in Figure 2-2a. However, when the interfacial shear stress reaches or exceeds the shear bond stress,  $\tau_{au}$ , (at load  $P_1$ ), debonding zone ( $a_1$ ) is created from the end of fiber by distributing uniform interfacial shear stress ( $\tau_{fu}$  in Figure 2-2a) and building up the tensile stress in Figure 2-2b. The interfacial shear stress slowly decreases to zero beyond debonding zone ( $a_1$ ). The length

of debonded zone increases or changes as the applied load increases by following the previous stress transfer mechanisms at the interface.

### **2.3.2 Stress Transfer after Matrix Cracking**

The major benefit of fiber reinforcement in composites is realized in the post-cracking process by arresting crack propagation from the fiber pull-out in the matrix rather than by controlling stress-strain curve prior to matrix cracking. Therefore, the fiber pull-out mechanism representing bridging resistance forces across a crack surface is an important aspect with respect to the effect of fiber type with different mechanical and geometrical properties in the post-cracking zone.

The shear stress transfer mechanisms during fiber pull-out from the matrix have fundamentally the same process as those examined in previous Section 2.3.1. The main difference for post-cracking behavior of fiber reinforced concrete materials is that the maximum interfacial shear stress takes place at the fiber embedment point in the cracked composites (Bentur et al., 1990). When external loading causes the elastic shear stress to exceed the adhesional shear bond strength, debonding occurs and then load transfer mechanism from the cement paste matrix to the fiber at the debonded zone is frictionally slip based at the interface. Subsequent to debonding, the elastic shear stress is redistributed at the end of the debonded zone in the fiber, thus preventing catastrophic failure immediately after the matrix crack.

Figure 2-3 (a) illustrates the combined mode with frictional shear stress distribution at the intersection and elastic shear stress distribution decreasing away from the cracked surface. However, in the absence of debonding prior to matrix cracking, there is no frictional slip at the fiber-crack intersection as shown in Figure 2-3 (b). When the post-cracking mechanism progresses with increased loading, it combines and represents both interfacial shear stress and elastic shear stress distributions between the fiber and the matrix.

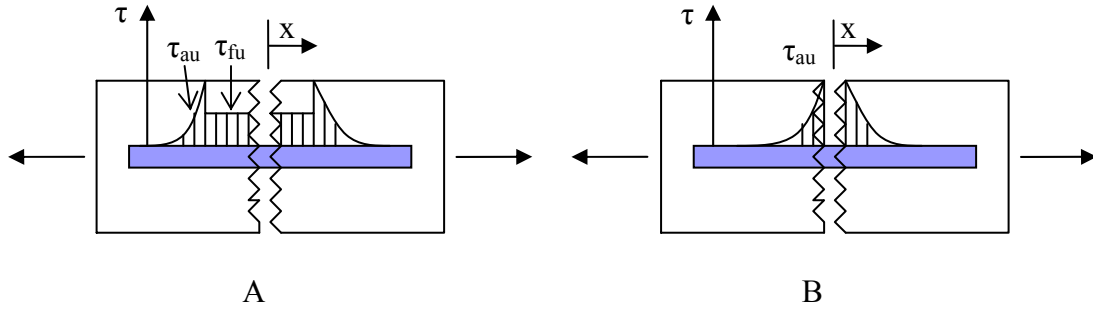


Figure 2-3. Interfacial shear stress distribution immediately after cracking. A) Debonding preceded cracking. B) No debonding prior to cracking. (after Bentur et al., 1990).

An analytical model of fiber pull-out of a single fiber in the matrix has been proposed by Greszczuk (1969):

$$\tau(x) = \frac{P\beta_2}{2\pi r} [\sinh \beta_2 x - \coth(\beta_2 l) \cosh(\beta_2 x)] \quad (2.5)$$

$$\beta_2 = \left[ \frac{2G_m}{b_i r E_f} \right]^{1/2} \quad (2.6)$$

where

$r$  = radius of the fiber

$b_i$  = effective width of the interface

$E_f$  = modulus of elasticity of the fiber

$G_m$  = shear modulus of the matrix at the interface

$l$  = embedded length.

## 2.4 Fracture Mechanics Approach

Linear Elastic Fracture Mechanics (LEFM) calculates stresses near the crack tip for homogeneous, isotropic and linear elastic materials. Crack growth occurs when the stresses near the crack tip exceed the material fracture toughness. The Linear Elastic Fracture Mechanics (LEFM) approach may be an appropriate model to predict the fiber pull-out effect in FRC, but it

is limited to first cracking. The most critical effect of fiber reinforcement in cement composites is to enhance post-cracking behavior. Three important aspects should be considered for the application of fracture mechanics to the fiber-crack interaction of FRC. First, crack suppression which is the increase in stress required for crack initiation due to the addition of fibers. Second, crack stabilization which refers the crack arresting onset of first matrix cracking. Third, fiber-matrix debonding mechanism which refers crack propagation along the interfacial transition zone (Bentur and Mindess, 1990).

#### **2.4.1 Crack Suppression by Fibers**

LEFM applications for the crack suppression, which is the increase of stress needed for crack initiation due to the addition of fibers in fiber cement composites, were studied by Romualdi et al, 1963. The extensions of both the fiber and the matrix prior to crack initiation are the same under tensile loading. However, subsequent to matrix cracking, the behavior between the fiber and matrix is different. The matrix has a tendency of extending further than the fiber due to the stress concentrations just in front of crack tip, but the fibers apply pinching forces through redistribution of interfacial bond stresses subsequent to matrix cracking and decrease the stress intensity factor of the crack. Higher stresses, then, are needed to produce a stress field in front of the crack tip so that the maximum stress surpasses the critical stress intensity factor of the matrix to further crack propagation.

The spacing factor concept relating to the required stress to cause the matrix crack was used to demonstrate its validity for predicting the beneficial effect of fiber on resistance to first crack (Romualdi et al., 1964). However, there are several limitations regarding the application of the spacing factor concept to FRC. The spacing factor must account for fiber length, diameter effects, the fiber orientation, and the characteristics of the fiber-matrix bond, i.e., ‘perfect’ bond.

### 2.4.2 Crack Stabilization Subsequent to Matrix Crack

Fibers tend to arrest cracks within the matrix at the crack surface. There are many analytical models that attempt to explain the complex cracking patterns at the crack tip. The stress transfer mechanism across the crack proposed by Wecharatana and Shah (1983) can be seen in Figure 2-4. They suggested that three distinct zones can be identified at the fracture location: traction free zone where load transfer no longer takes place, fiber bridging zone where stress transfer occurs by frictional slip of fibers, and matrix process zone where continuity and aggregate interlock allow for stress transfer by the matrix itself.

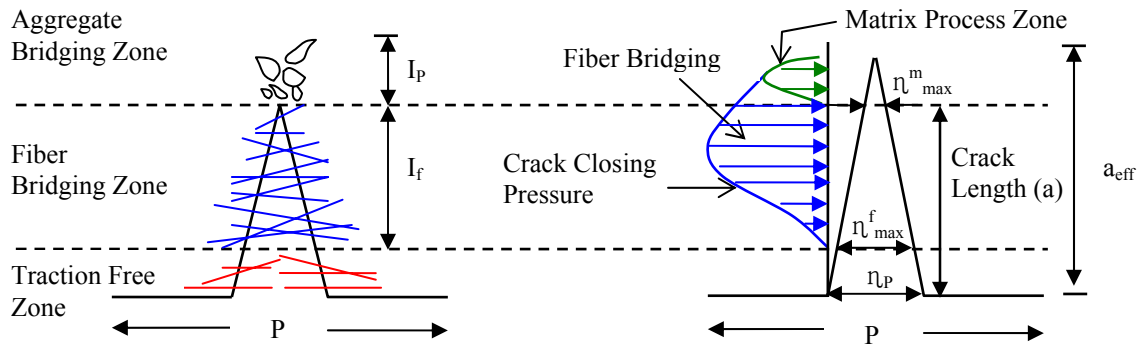


Figure 2-4. Idealized representation of an advancing crack and the stress field. (after Wecharatana and Shah, 1983).

### 2.4.3 Fiber-Matrix Debonding

As discussed in the previous section, the major role of fiber reinforcement is to increase the fracture energy or the toughness required for the crack initiation and propagation. There are two processes that affect the value of fracture energy: 1) fiber debonding; and 2) pull-out mechanisms from the matrix that are related to energy dissipation throughout the fracture process. The interface debonding is defined as the work done in breaking the interfacial shear bond between the fiber and the matrix, and pull-out work is characterized as the work done in extracting the fiber embedded in the matrix after cracking. Fracture mechanics has been used for

the modeling of fiber composites to obtain materials parameters that can explain the debonding mechanism in a more reliable manner, and to experimentally obtain the values of the interfacial shear bond strength (Bentur et al., 1990). The tensile stress required for catastrophic fiber debonding was calculated by Outwater and Murphy (1969) using the classical Griffith theory as:

$$\sigma = \left( \frac{8E_f G_{db}}{d} \right)^{1/2} \quad (2.7)$$

where

$G_{db}$  = the energy required to debond a unit surface area of fiber

$E_f$  = the fiber modulus

$d$  = the fiber diameter.

The above analysis only considers the energy balance of the fiber. Subsequent to the study performed by Outwater et al. (1969), Stang et al. (1986) expanded the solution explaining the compliance of the entire system, including fiber and matrix. Morrison et al. (1988) further enhanced the explanation of the debonding and pull-out behaviors of fibers in composites by determining fracture parameter ( $G_c$ ), which is the average critical strain energy release rate ( $G_c$ ) for fiber debonding at the interface. Swamy (1983) reported that the average value of  $G_c$  for steel fiber was determined to be 2.5 N/m, which is lower than the critical energy release rate of unreinforced mortar determined to be 5.3-12.3 N/m. The crack through the path of least resistance propagates along the fiber/matrix interface rather than through the matrix.

## **2.5 Fiber Effect on Mechanical Properties**

### **2.5.1 Compression**

ACI Committee 544 (1989) reported that the discontinuous distribution of fibers in the hardened concrete matrix changes the failure mode by making the concrete more ductile.

However, fiber reinforcement usually has a relatively small effect in compression compared to

the effect on tensile or bending properties. The effect of fibers in improving the compressive strength in the matrix relies on the properties of concrete having coarse aggregates.

Fanella and Naaman (1985) studied that stress-strain properties of steel fiber reinforced mortar in compression. In their study, three fiber volume contents (1, 2, and 3%) and three aspect ratios (47, 83, and 100) were evaluated in combination with three mortar matrices with smooth and brass-coated steel fibers. The test results showed that the stress-strain curves for the FRC diverged slightly on the ascending portion of the curve and considerable divergence was observed on the descending portion. A higher content of fiber volume resulted in more ductile behavior of the material subsequent to cracking, which resulted in greater toughness. The compressive strength increased from 0 to 15%.

Naaman et al. (1993) reported that the effect of hooked steel fibers of 1.2 in. (30 mm) length, 1% volume content and an aspect ratio of 60 slightly increased the compressive strength of concrete by 17% relative to the control mix. Furthermore the failure strain was considerably increased, which resulted in a much larger area under the stress-strain curve and thus indicating a significant improvement in ductility and energy absorption prior to matrix failure. Naaman et al. (1993) also reported a 30% increase in compressive strength relative to the control mix by increasing the percentage of fibers from 1% to 2% by volume with the same fibers and aspect ratio.

Malhotra et al. (1994) studied the mechanical properties of polypropylene fiber reinforced concrete. In this study, two experimental groups of 1.55 in length fibrillated polypropylene fiber with  $4 \text{ kg/m}^3$  (0.44%) and  $5 \text{ kg/m}^3$  (0.54%) volume contents were used. The introduction of the fibers to the concrete showed no significant effect on the compressive strength. Yao et al. (2000) also observed that there was no significant improvement in the compressive strength using

smooth and straight polypropylene fiber when the fiber content was 0.5% and the length was 15 mm.

In 2003, Choi et al. reported the test results of compressive strength of polypropylene fiber reinforced concrete (PFRC). A monofilament fiber 0.90 mm in diameter and 50 mm in length was used. The fiber contents were 1.0% and 1.5% of the mixed concrete by volume.

Polypropylene fibers with a wavelength shape and collated in small bundles were used for rapid introduction into concrete mixtures. PFRC samples broke with vertical cracks at about 70-85% of the peak load. The average compressive strength showed that the polypropylene fibers did not contribute to the improvement of the compressive strength, although the strains at the peak load increased significantly, as did the toughness.

Naaman et al. (1993) reported that polypropylene fiber mixes containing 1% or 2% by volume with 0.75-in in length showed a significant reduction in the compressive strength. Unlike the steel fiber mix at 1% and 2% volume fraction, the polypropylene mix at 1% and 2% volume fraction showed a significantly lower ductility. They concluded that this lower ductility may be attributed to the low elastic modulus of the polypropylene fibers and their poor bonding properties in comparison with steel fibers. Leung et al. (2005) investigated the addition of 0.5% polypropylene fiber with 15 mm length and 0.5% polyvinyl alcohol fiber with 12 mm length decreased the compressive strength about 10% for PP and 15% for PVA fibers in comparison with plain concrete. They explained that the introduction of small diameter fibers into the mixture makes mix compaction more difficult, and hence, more entrapped air exists in the final mixture. Also, 1% of polyvinyl alcohol fiber with 12 mm length did not alter the compressive strength significantly at 28 day (Schwartzentruber et al., 2004).

Generally, the addition of steel fibers improves the bonding mechanism at the fiber-hardened cement paste matrix interface and might be helpful to obtain the high strength compared with unreinforced concrete, though it strongly depends on fiber length, fiber geometry, fiber volume fraction and aspect ratio of fiber. On the other hand, the addition of synthetic fibers to concrete has not shown improvement in the compressive strength as results of their low elastic modulus and poor bonding properties at the hardened state.

### **2.5.2 Tension**

ACI committee 544 (1999) reported that the use of the splitting tensile strength test (ASTM C 496) for FRC specimens is not recommended for analysis of the behavior of fiber reinforced concrete subsequent to cracking due to unknown stress and strain distributions after the failure. Strain gauge or other sensitive methods of crack detection, such as acoustic emission or laser holography can be used for the identification of the first crack and analysis of stress-strain distribution for post-cracking behavior.

Yao et al. (2003) investigated the mechanical properties of steel fiber-reinforced concrete with 0.5% fiber volume fraction. The steel fibers were hooked end and 30 mm in length. The authors found that the addition of steel fibers increased strength about 9% in comparison with unreinforced concrete. Shaaban and Gesund (1993) carried out splitting tensile tests with 6 x 12 in specimens containing 1 in corrugated steel fibers and fiber contents of 0, 79, 157, 235, and 313 lb/yd<sup>3</sup>. of concrete. Test results showed that steel fiber can significantly enhance the tensile strength of concrete. The load at first visual crack was used for the determination of the tensile strength of SFRC.

Al-Tayyib et al. (1998) reported that little increase in strength has been observed regarding the addition of synthetic fibers to concrete. The tensile strength of PFRC mixes with 0.2% by volume of concrete has been reported to be 2-8% higher than that of ordinary concrete mixes

with the addition of polypropylene fibers with 0.8 in fibrillated bundles. Choi et al. (2005) found that the average splitting tensile strength of PFRC increased by approximately 20-50% using 0.9 mm diameter and 50 mm length PP monofilament fibers at volumes of 1% and 1.5%. Moreover, the addition of polypropylene fibers largely increased the ductility of the concrete. It was noticed that the stress-strain curve was linear up to the proportional limit after which stress capacity sharply decreases, while the strain increased, and then increased again by showing a second peak. This post behavior was repeated several times until the final failure. Yao et al. (2003) reported the mechanical properties of polypropylene fiber at 0.5% fiber volume fraction. The polypropylene fibers were smooth and straight with a 15 mm length. In contrast with the previously cited work, they found that the addition of polypropylene fiber showed no effect on splitting tensile strength in comparison with plain concrete.

### **2.5.3 Bending**

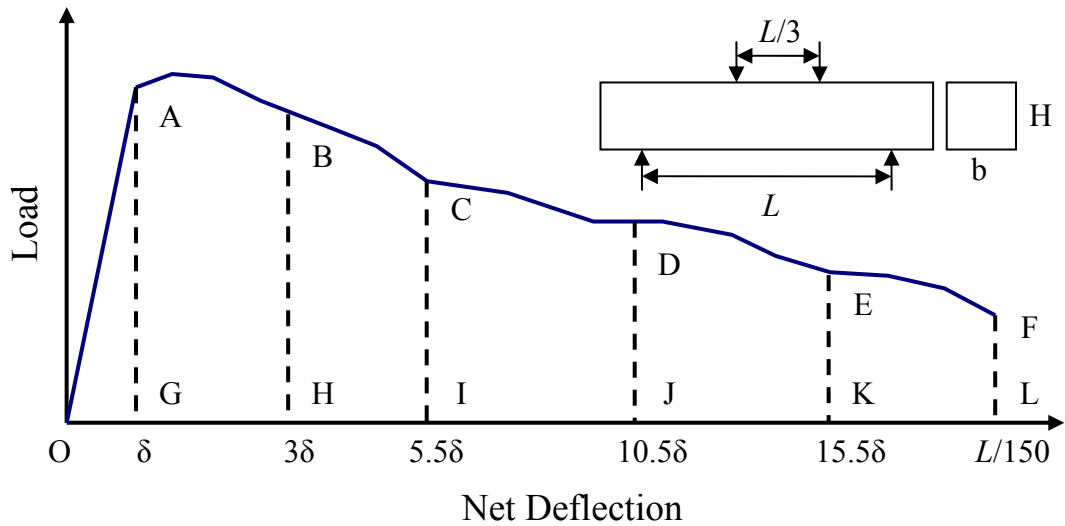
The third point loading test specified in ASTM C 78 (2004), C 1018-97 (2004), and C 1609-06 (2008) is commonly used to measure flexural strength of FRC. Maximum flexural strength is determined at the first peak load as that value of load corresponding to the first point on the load-deflection curve where the slope is zero, that is, the load is a local maximum value. Test procedures of ASTM C 78 from load-controlled testing are different from those of ASTM C 1018 or C1609, which are handled by deflection-controlled procedures.

ACI Committee 544 (1999) reported that an important material property from FRC testing is toughness, which is the energy absorption capacity of a material and can be used to evaluate the effect of fibers or crack propagation. The conventional flexural test approach, which is easy to prepare and simulates practical loading conditions in FRC applications, is normally recommended for measuring toughness in FRC. However, there are some concerns with determination of toughness test procedures specified in ASTM C 1018, representing

serviceability-based toughness indexes and the first-crack strength of FRC as shown in Figure 2-5. Toughness indexes are calculated in terms of energy ratios: the energy absorbed to a certain multiple of first crack deflection to the energy absorbed up to the first crack.

Banthia and Trottier (1995) reported that measuring true specimen deflection at first cracking, which is very important to identify toughness indexes, is difficult due to seating or the downward movement of the specimen. Determination of first cracking point is another issue because the initial ascending part of the curve has considerable nonlinearity before reaching the peak load. Finally, FRC with low fiber volumes or with high-strength matrixes mostly generates instability subsequent to matrix cracking. The sudden high energy dissipation and high rate of deflections at first cracking significantly affect measurement of load-deflection curve during post-cracking behavior of fibers.

ASTM C 1609-06 was recently accepted as a test method to replacement of ASTM C 1018-97. While the proposed new test method maintains the procedures for obtaining the flexural load-deflection curve presently described in C 1018-97, the analysis of the load-deflection curve is completely different. Detailed test procedures are described in Chapter 3.



### Toughness Indexes

$I_5 = \text{Area OABH} / \text{Area OAG}$	$I_{10} = \text{Area OACI} / \text{Area OAG}$
$I_{20} = \text{Area OADJ} / \text{Area OAG}$	$I_{30} = \text{Area OAEK} / \text{Area OAG}$
$\delta = \text{Deflection at first-crack}$	Residual Strength Factors
	$R_{5,10} = 20 (I_{10} - I_5)$
	$R_{10,20} = 10 (I_{20} - I_{10})$

Figure 2-5. ASTM C 1018 techniques of fiber reinforced toughness characterization

## 2.6 Transport Mechanisms

The transport of water, gases and chemical ions into concrete occurs via the pore system or micro-cracks in the hardened cement paste. There are many kinds of chemical or physical mechanisms which control the media transport into the concrete, but the transport mechanism strongly relies on various environmental conditions, pore size distribution or structure, characteristics of the solution, degree of concrete pore saturation, and temperature (Kropp et al., 1995). Therefore, the transport mechanisms may simultaneously operate to convey the transport of media into concrete. In order to derive the transport coefficient for specific conditions, experimental investigations are normally limited to a single transport property. Transport

properties for the use of in theoretical models used for the evaluation of deleterious material transport into concrete are presented in the following sections.

### 2.6.1 Permeation

Permeation is the flow of a fluid under the action of a pressure head. For steady-state flow of a liquid through a saturated porous media material, the flow rate is described by Darcy's law:

$$K_w = \frac{Ql}{tA} \frac{\eta}{\Delta p} \quad (2.7)$$

where

$K_w$  = coefficient of permeability ( $m^2$ )  
 $\eta$  = viscosity of the gas ( $Ns/m^2$ )  
 $Q$  = volume of gas flowing ( $m^3$ )  
 $l$  = thickness of penetrated section (m)  
 $A$  = penetrated area ( $m^2$ )  
 $\Delta p$  = pressure difference ( $N/m^2$ )  
 $t$  = time (s).

The permeation of a gas is defined as the rate of discharge of a gas under laminar flow conditions through a unit cross-sectional area of a porous medium under a unit pressure gradient and standard temperature conditions. The coefficient of permeability for a gas can be described by the following equation (Zagar, 1955):

$$K_g = \eta \frac{Ql}{tA} \frac{2p}{(p_1 - p_2)(p_1 + p_2)} \quad (2.8)$$

where

$K_g$  = coefficient of permeability ( $m^2$ )  
 $\eta$  = viscosity of the gas ( $Ns/m^2$ )  
 $Q$  = volume of gas flowing ( $m^3$ )  
 $l$  = thickness of penetrated section (m)  
 $A$  = penetrated area ( $m^2$ )  
 $P$  = pressure at which volume  $Q$  is measured ( $N/m^2$ )  
 $P_1$  = pressure at entry of gas ( $N/m^2$ )  
 $P_2$  = pressure at exit of gas ( $N/m^2$ )  
 $t$  = time (s).

## 2.6.2 Absorption

Absorption is the material property which characterizes the rate of liquid penetration through a porous material due to capillary action. The standard reference is to a tube in plants but can be seen readily with porous paper. It occurs when the adhesive intermolecular forces between the liquid and a substance are stronger than the cohesive intermolecular forces inside the liquid. The effect causes a concave meniscus to form where the substance is touching a vertical surface. The same effect is what causes porous materials such as sponges to soak up liquids.

In concrete pore system, the liquid containing various deleterious materials is taken up by this capillary action affecting the pressure in the complicated pore system. This transport mechanism depends on the material surface tension, density and viscosity of the liquid, pore structure (such as radius, tortuosity and continuity of capillaries) and on the angle of contact between the liquid and the pore walls (Kropp et al., 1995). The liquid flow for steady-state capillary action is represented by Darcy's law adjusted for non-saturated liquid flow as follows equation:

$$F = -\frac{k_p}{\eta} \frac{dp_w}{dx} \quad (2.9)$$

where

$dp_w/dx$  = gradient of pore water pressure  $p_w$  ( $N/m^2$ )

$\eta$  = viscosity of water ( $Ns/m^2$ )

$k_p$  = coefficient of water permeability ( $kg/m$ ).

Capillary action mechanism in concrete subjected to seawater is very important with regard to the chloride movement process. First, un-saturated concrete in contact with seawater absorbs the salt solution by capillary action, which is several orders of magnitude faster than the penetration of chloride ions by diffusion alone, thereby accelerating the initial progression of

chloride ions into the concrete. Chlorides then diffused into the tortuous pore system by diffusion mechanism and the penetration depth increases at a slower rate (Kropp et al., 1995).

### 2.6.3 Diffusion

Diffusion is the movement of molecules or ions from a region of higher concentration to one of lower concentration by random molecules or ions motion. In a phase with uniform temperature, diffusion processes tend to lead towards even distributions of molecules or ions (Bertolini et al., 2004).

Fick's first law expresses the diffusion phenomenon under stationary conditions:

$$F = -D \frac{dC}{dx} \quad (2.10)$$

where

$F$  = mass flux (kg/m<sup>2</sup>·s)  
 $D$  = diffusion coefficient (m<sup>2</sup>/s)  
 $C$  = concentration (g/m<sup>3</sup>)  
 $x$  = distance (m).

Diffusion coefficient depends on the type of diffusing ion, concrete properties and environmental conditions, which can change as a function of position and time.

When diffusion process reaches stationary conditions, the mass flux relies on time and is controlled by Fick's second law predicting how diffusion causes the concentration field to change with time:

$$\frac{\partial C}{\partial t} = D \frac{\partial^2 C}{\partial x^2} \quad (2.11)$$

where

$D$  = diffusion coefficient (m<sup>2</sup>/s)  
 $C$  = concentration (g/m<sup>3</sup>)  
 $x$  = distance (m)  
 $t$  = time.

This equation is normally integrated by assuming that the surface concentration of the diffusing ions is constant with time and is identical to  $C_s$  ( $C=C_s$  for  $x=0$  and for any  $t$ ) with constant  $D$  through the concrete thickness, and that diffusion coefficient,  $D$ , does not initially include chloride ion ( $C = 0$  for  $x>0$  and  $t = 0$ ). The solution of equation (2.10) is given by:

$$\frac{C(x,t)}{C_s} = 1 - \operatorname{erf}\left(\frac{x}{2\sqrt{Dt}}\right) \quad (2.12)$$

where:

$$\operatorname{erf}(z) = \frac{2}{\sqrt{\pi}} \int_0^z e^{-t^2} dt \quad (2.13)$$

is the error function. The obtained experimental data of  $C$  vs.  $x$  can be used to determine the diffusion coefficient ( $D$ ) from the equation (2.11) using the least squares method.

## 2.7 Parameters Affecting Transport Properties

Tyler et al. (1961) determined that water permeability governs the pressurized water flow rate into concrete, which can induce concrete failure when saturated concrete is frozen. Furthermore, permeability controls the flow rate of chemical solutions, which often contain chloride and sulfate ions that drop the pH of concrete and accelerate steel corrosion rate in concrete structures. Therefore, the permeability of concrete significantly influences long-term durability of concrete structures. Neville (1971, 1981) studied that the water flow into concrete can be fundamentally described as flow in a porous system. However, the porous nature of concrete and the heterogeneous nature of its components make the quantification of the permeability process difficult. Permeability of the hardened cement paste has the greatest influence on permeability of concrete, because coarse aggregates are fully enclosed by the compacted cement paste. The pore structure in the cement paste divide into gel pores occupying about 28% of the paste volume and capillary pores occupying between 0% and 40%, depending

on the ratio of water to cementitious material (w/c) and the degree of hydration. Neville (1981) also reported that concrete with lower w/c ratio produce a lower volume of the capillary voids compared with concrete with higher w/c. Water-cement ratio is one of the important factors influencing permeability of concrete. Powers et al. (1954) concluded that the higher the water-cement ratio, the higher the coefficient of permeability.

The aggregate in concrete also was a significant influence on concrete permeability. Neville (1981) stated that the aggregate decreases the effective area over which water can flow if it has very low permeability. In addition, the effect of aggregate on permeability is considerable because the travel path for solutions increases significantly around the aggregate particles.

Leung et al. (2005) investigated the water permeability of concrete with steel, PP, and PVA fibers at  $V_f = 0.5\%$ . The results showed high variability on the coefficient of permeability among three tested specimens. They concluded that the lower permeability for some fiber specimens may be the fiber effect on reducing internal microcracking (e.g., due to shrinkage) in the concrete so that the presence of fibers in the concrete increases the resistance to water penetration.

The most important factor influencing water absorption rate is the connectivity of capillary pores, which is considerably affected by w/c ratio, aggregate, curing conditioning, age, and compaction. Schonln and Hisdorf (1989) tested the absorption of water by measuring the weight change with time. They concluded that the absorption rate is reduced as the water/cement ratio is reduced. Dhir et al. (1987) also found that the absorption rate is significantly reduced with low water/cement ratio. Additionally, Dhir et al. concluded that the absorption rate of concrete is reduced as the concrete is cured for longer duration time in a saturated condition. The curing conditions of test specimens also influence the absorption rate. Haque (1990) compared the rate

of water absorption of water cured specimens to air stored specimens. The absorption rate was reduced about 40% less for moist cured condition. The compaction effect on absorption has been studied by Hall (1989). Absorption rate is reduced when tamping time is increased for the same concrete composition, as well as longer concrete age, which reduces capillary porosity with the development of hydration reaction.

Martys and Ferraris (1997) examined the effect of boundary conditions on water absorption. Test specimens were either stored in air with sealed sides (top exposed) or in a container at constant humidity without sealing the sides. Specimens placed in air, which were partially saturated at the beginning of the test, decreased in weight for a specified time, indicating that evaporation at the top surface was initially greater than absorption at the bottom. An increase in weight was then observed as rate of evaporation decreased, then weight approached a constant value as the rate of absorption and evaporation became equal. On the other hand, the specimens placed in constant humidity container without sealed sides showed the greatest rate of capillary action due to little and no evaporation of moisture from specimen surface.

CHAPTER 3  
MATERIALS AND EXPERIMENTAL PROGRAM

This chapter is divided into four sections: characterization of constituent materials; mix proportions; mixing and curing procedures; and fresh properties of unreinforced and fiber-reinforced concrete.

**3.1 Characterization of Constituent Materials**

**3.1.1 Cement**

AASHTO cement type II was used to achieve a lower heat of hydration and to resist aggressive media (i.e., sea water and swamp water, etc.). The compounds contained were obtained from the manufacture and described in Table 3-1.

Table 3-1. Chemical and mineralogical composition

Chemical Composition	Value (%)
SiO <sub>2</sub>	20.47
Al <sub>2</sub> O <sub>3</sub>	5.19
Fe <sub>2</sub> O <sub>3</sub>	4.49
CaO	63.49
MgO	1.10
SO <sub>3</sub>	2.55
Na <sub>2</sub> O	0.05
K <sub>2</sub> O	0.28
Mineralogical Composition	Value (%)
C <sub>3</sub> S	54.38
C <sub>2</sub> S	17.98
C <sub>3</sub> A	6.16
C <sub>4</sub> AF	13.66

**3.1.2 Coarse Aggregates**

The coarse aggregate used in this research was crushed limestone with a maximum size of 0.375 in (9.5 mm). The reason for selecting a relatively small-size aggregate was to improve both the uniform distribution of fibers and the effectiveness of fiber reinforcement. The bulk specific gravity of the coarse aggregate was 2.28, the bulk specific gravity at SSD was 2.40, and the apparent specific gravity was 2.59. The absorption of the coarse aggregate was 5.18%. Gradation

results for the coarse aggregates, as obtained from tests performed at the FDOT laboratories according to FM1-T027, are given in Table 3-2.

Table 3-2. Aggregate gradation, coarse aggregates

Sieve Size	Actual Weight Retained (g)	Cumulative Percentage Retained (%)	Cumulative Percentage Passing (%)
1/2 in.	0.00	0	100
3/8 in.	31.00	2	98
No.4	730.20	53	47
No.8	1231.60	90	10
No.16	1314.20	96	4
No.50	1330.20	97	3

### 3.1.3 Fine Aggregates

The fineness modulus for the fine aggregate was 2.39. Following are the specific gravity values: 2.648 BSG<sub>OD</sub>, 2.650 BSG<sub>SSD</sub>, and 2.658 ASG. The absorption of the fine aggregate was 0.18%, which is on the low side of values typically observed in Florida aggregates. Gradation results for the sand, as obtained from tests undertaken in the FDOT laboratories according to FM1-T027, are given in Table 3-3.

Table 3-3. Aggregate gradation, fine aggregates

Sieve Size	Actual Weight Retained (g)	Cumulative Percentage Retained (%)	Cumulative Percentage Passing (%)
No.4	1.10	0	100
No.8	9.80	3	97
No.16	58.70	15	85
No.30	165.80	44	56
No.50	300.50	79	21
No.100	369.50	98	2

### 3.1.4 Chemical Admixtures

Two water reducing admixtures were used in this study to increase the slump without adversely influencing air entrainment or setting times. The first was WRDA<sup>®</sup> 60 by Wr. Grace Construction Products, which produces typically 8-10% water reduction and set retardation. The

amount addition of WRDA<sup>®</sup> 60 added was 195 to 390 ml/100kg (3 to 6 fl oz/100lbs). The second water reducer was WR ADVA<sup>®</sup> 140 superplasticizer by WR Grace Construction Product, which is a high range water-reducing admixture. Addition rates of ADVA<sup>®</sup> 140 superplasticizer can vary with type of application, but will normally range from 390 to 1300 ml/100kg (6 to 20 fl oz/100 lbs) of cement. Dosage rate in this study was 20 fl oz/100 lbs for all mixes.

### 3.1.5 Fibers

Polypropylene (PP), polyvinyl alcohol (PVA), cellulose and steel fibers were used in this study. Photographs and properties of these fibers are presented in Figures 3-1 and Table 3-4. Surface properties magnified 500 times and environmental resistance of fiber type are also presented in Figure 3-2 and Table 3-5. The fibers were selected from four different manufactures i.e., Bekaert, Durafiber, Grace, and Kuraray.

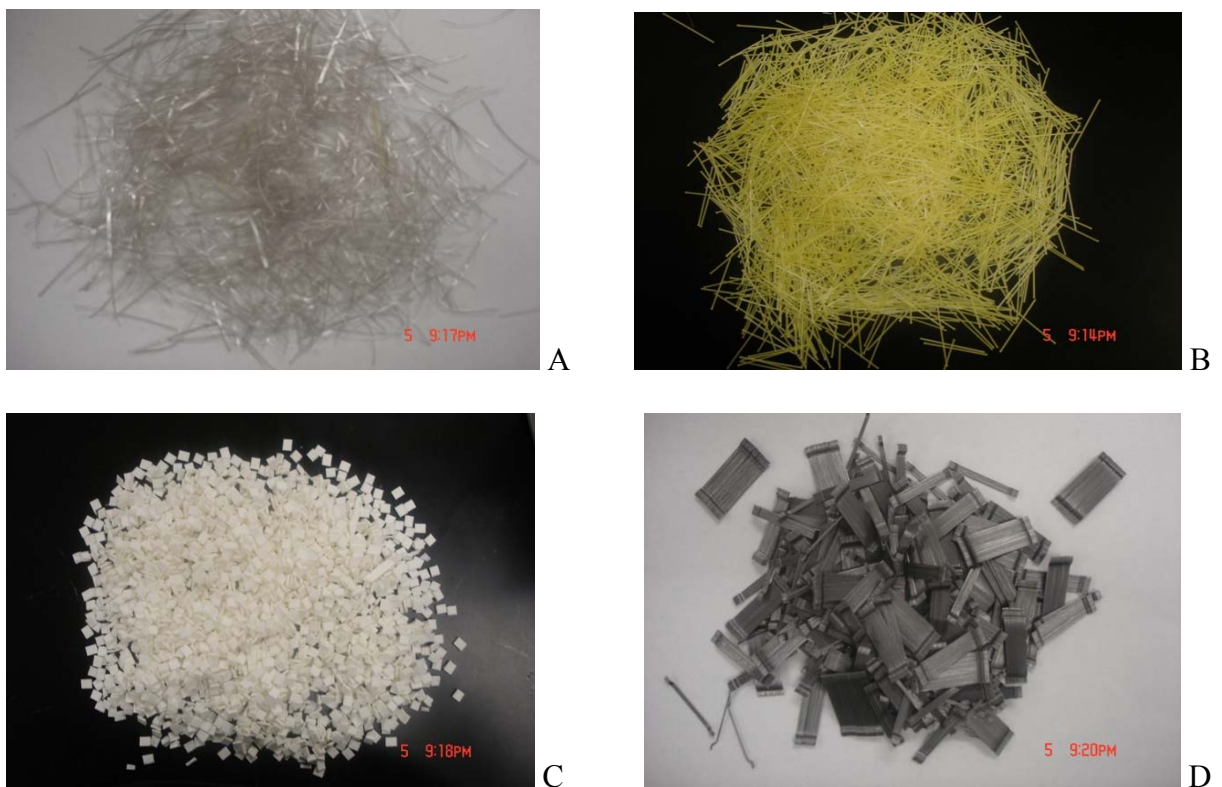


Figure 3-1. Fiber types. A) PP. B) PVA. C) Cellulose. D) Hooked-end steel.

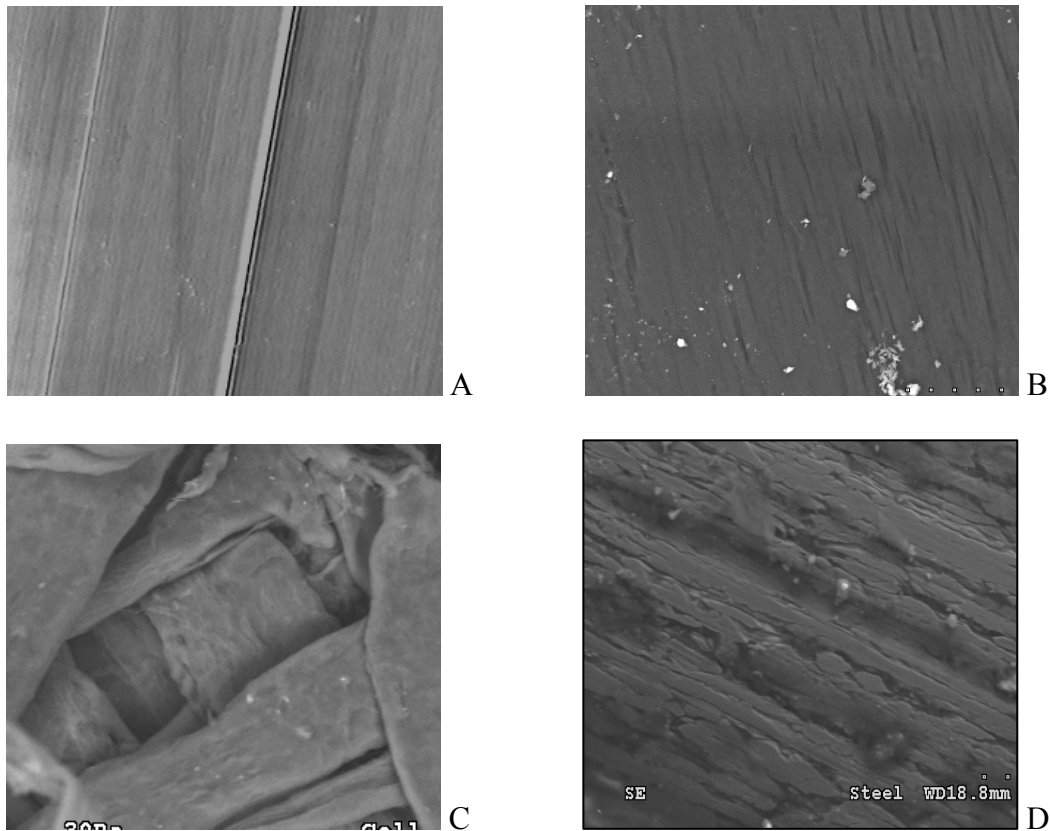


Figure 3-2. Fiber surfaces (x500). A) PP. B) PVA. C) Cellulose. D) Hooked-end steel

Table 3-4. Properties of fibers used

Manufacture	BEKAERT	GRACE	DURAFIBER	KURARAY
Product Name	Dramix ZP 305	STRUX 90/40	Buckeye UltraFiber 500TM	RF 4000x30
Fiber Material	Steel	Polypropylene/ Polyethylene Blend	Virgin Cellulose	Polyvinyl Alcohol
Fiber Type	Hooked-collated	Monofilament	5mm x 6mm Chip	Monofilament
Length (in)	1.2	1.55	0.0826	1.19
Diameter (in)	0.022	0.017	7.08x10 <sup>-4</sup>	0.026
Aspect Ratio(L/D)	55	90	117	45
Modulus(GPa)	200	9.5	.	29
Tensile Strength(MPa)	1104	620	.	800
Specific Gravity	7.85	0.92	1.1	1.3
Absorption	None	None	High	Low
Fracture Strain (%)	3-4	8	.	6-12

Table 3-5. Environmental resistance of fibers used

Fiber Type	PP	PVA	Cellulose	Steel
Surface Texture	smooth	grooved	rough	rough
Absorption	none	low	high	none
Environmental Resistance	acid, alkali, salt	alkali	alkali	poor

### 3.2 Mix Proportions

For synthetic fiber mix dosages above 4 lbs/yd<sup>3</sup>. (2.4 kg/m<sup>3</sup>) AASHTO-AGC-ARTBA Joint Committee (2001) recommends a reduction of coarse aggregate and an increase of the mortar fraction to accommodate the increased surface area due to the synthetic fiber addition. The synthetic fiber mix dosages used in this study were 7.75 lbs/yd<sup>3</sup>. for polypropylene, 16.43 lbs/yd<sup>3</sup>. for polyvinyl alcohol, and 1.5 lbs/yd<sup>3</sup>. for cellulose. Thus, the volume of the coarse aggregate was reduced by adjusting for each of the above synthetic fiber volumes. Also, some adjustment to the mix design is recommended for steel fiber-reinforced concrete (SFRC) from dosage range of at and above 65 lbs/yd<sup>3</sup>. (39 kg/m<sup>3</sup>) in the mixture. The steel fiber mix dosages in this study were 120 lbs/yd<sup>3</sup>. Therefore, the volume of the coarse aggregate was reduced to adjust for the steel fiber volume.

The mix proportions used in this study were applicable to concrete of moderate and high compressive strength of 31 MPa for concrete Class II, designed for bridge deck and 45 MPa for concrete Class V, designed for special case at 28 days specified in the FDOT standard specification for road and bridge construction (2004). A series of ten concrete mixes were prepared with and without fibers. As mentioned earlier, the fiber volume fractions for this study were: 7.75 lbs/yd<sup>3</sup>. for polypropylene fibers, 16.43 lbs/yd<sup>3</sup>. for polyvinyl alcohol fibers, 1.50 lbs/yd<sup>3</sup>. for cellulose fibers, and 120 lbs/yd<sup>3</sup>. for steel fibers corresponding to fiber contents of 0.5%, 0.75%, 0.1%, and 1% by total volume respectively. Table 3-6 summarizes the mix designs for FRC.

Table 3-6. Material and mix proportions for Classes II/V concrete

Mix Types	PC	PP	PVA	Cellulose	Steel
W/C	0.44/0.37	0.44/0.37	0.44/0.37	0.44/0.37	0.44/0.37
Cement (lbs/yd <sup>3</sup> )	611/752	611/752	611/752	611/752	611/752
Water(lbs/yd <sup>3</sup> )	269/278	269/278	269/278	269/278	269/278
CA (lbs/yd <sup>3</sup> )	1444/1430	1424/1410	1414/1400	1439/1425	1407/1393
FA (lbs/yd <sup>3</sup> )	1490/1362	1490/1362	1490/1362	1490/1362	1490/1362
Fiber Content(lbs/yd <sup>3</sup> )	None	7.75	16.43	1.5	120
Air Target (%)	3	3	3	3	3
Set Retarder(oz)	33.8	33.8	33.8	33.8	33.8
High Range WR(oz)	120.3	120.3	120.3	120.3	120.3

Note: CA= coarse aggregate, FA= fine aggregate

### 3.3 Mixing and Curing Procedures

#### 3.3.1 Mixing Procedure

Each batch was mixed in a high shear pan mixer (Figure 3-3) with a maximum capacity of 27 ft<sup>3</sup> at the Florida Department of Transportation (FDOT) State Materials Office (SMO) concrete mixing laboratory. The limestone aggregate was batched at a saturated surface-wet condition. Saturation was achieved by soaking the aggregate in water for 7 days. Cylindrical specimens were prepared for compression, splitting tension, permeability, absorption, and volume of voids testing. Standard 4 x 8 in cylinder molds used to prepare specimen of control mixes. However, fiber-reinforced concrete specimens were prepared by coring 4 x 8 in cylindrical specimens from blocks prepared in 23 x 13 x 8 in wooden molds to ensure proper distribution of the fibers within the concrete. Cylinders were cored from blocks after 14 days of moist curing.

The following mixing procedure was used for all mixes specified in ASTM C 192 except for the procedure of addition of fibers. First, gravel and sand were mixed for approximately 1 minute. Then 50 % of the mixing water was added and the mixture was mixed for 1 minute to allow for water absorption. Next, the cement was added along with the remaining water

containing the set retarder and high-range water reducing admixture. Mixing continued for another 2 minutes. All component materials except for fibers were added to ensure proper and uniform mixing. Finally, fibers were added to the mix. Altogether, the additional mixing time took approximately 3-4 minutes to ensure a uniform fiber distribution and to minimize fiber segregation and balling effects. After completion of the batch, the mix was placed into the appropriate molds, which were then placed on a vibrating table. The vibrating process was continued for approximately 1-2 minutes.



Figure 3-3. High shear pan mixer

### 3.3.2 Curing Procedure

Curing of all specimens was carried out in accordance with ASTM C 192/C M-02 (2004) except for block specimens: after placement, these specimens covered with a plastic sheet and kept in their plastic or wood molds for 24 hours. The specimens were then removed from their molds and moved to the moisture curing room, which was maintained at 100 percent relative humidity and 72 °F (23 °C) until the time of testing. Blocks designated for coring were moved to UF concrete laboratory at 14 days of moist curing and cored. Continuous curing in fresh water was contained for another 2 weeks.

### 3.4 Specimen Preparation

Experimental tests for both mechanical and transport properties were conducted for two types of concrete specified in the FDOT standard specification for road and bridge construction (2004):

- Class II concrete, designed for bridge deck, consisting of 0.44 w/c ratio fiber mixtures containing four types of fibers with different fiber volume fractions (0.5% for PP, 0.75% for PVA, 0.1% for Cellulose, and 1% for Steel).
- Class V concrete, designed for special case requiring high strength, consisting of 0.37 w/c ratio fiber mixtures with the same fiber volume fractions and fiber types as the Concrete Class II.

Standard 4"x8" cylindrical specimens were used for mechanical tests for control mixtures.

Additionally, two 8 × 14 × 23 in. blocks were prepared for fiber mixtures to ensure uniform fiber distribution throughout the blocks as shown in Figure 3-4.



Figure 3-4. Concrete blocks for fiber mixtures

The blocks were cored to make 4 × 8 in. cylinders after 14 days of curing. Three control cylinders were cast before adding fibers to the mix for compression and splitting tension tests to obtain strength properties of the concrete without fibers, as well as absorption, permeability, and volume of voids tests. The cylinder was sliced and prepared for transport property test.

Absorption test specimens were prepared by cutting the top 2 in. of the cylinder. Volume of voids test specimens were prepared by cutting the middle 3 in. of the cylinder. Permeability test

specimens were chosen from bottom 2 in. The number and size of specimens performed for each test is summarized in Tables 3-7 and 3-8.

Individual beam specimens for Plain concrete mixes were cast by using individual steel beam molds ( $4 \times 4 \times 14$  in) as shown in Figure 3-5a. However, for fiber mixes 15 slabs ( $4 \times 20 \times 14$  in.) were prepared to ensure uniform fiber distribution, as shown in Figure 3-5b. The slabs were sliced to make  $4 \times 4 \times 14$  in. individual beams after curing. Then, pre-crack beams for each fiber mixture were produced using the third-point loading apparatus specified in ASTM C 1399 with a steel plate controlling the rate of deflection at the bottom of the specimen. Pre-cracked beams were prepared to induce typical cracking of concrete in the field and accelerate damage mechanism during environmental exposure. However, cellulose fiber mixes were not prepared because they did not show any post-cracking behavior subsequent to first cracking. The number of specimens prepared for conditioning and testing is summarized in Table 3-9.

Table 3-7. Number of specimens tested for mechanical tests for Classes II/V concrete

Mix Type	Fiber Type	Fiber Volume Fraction $V_f$ (%)	Com./ Splitting Tension	Pressure Tension
			Control/Fiber	Control/Fiber
PC	Control	N/A	3/0	3/0
PP	Polypropylene	0.5	3/3	0/3
PVA	Polyvinyl Alcohol	0.75	3/3	0/3
Cell	Cellulose	0.1	3/3	0/3
Steel	Hooked Steel	1	3/3	0/3

Table 3-8. Number of specimens tested for transport property tests for Classes II/V concrete

Mix Type	Fiber Type	Fiber Volume Fraction $V_f$ (%)	Absor./Permea./Voids	Bulk Diffusion
			Control/Fiber	Control/Fiber
PC	Control	N/A	3/0	3/0
PP	Polypropylene	0.5	3/3	0/3
PVA	Polyvinyl Alcohol	0.75	3/3	0/3
Cell	Cellulose	0.1	3/3	0/3
Steel	Hooked Steel	1	3/3	0/3

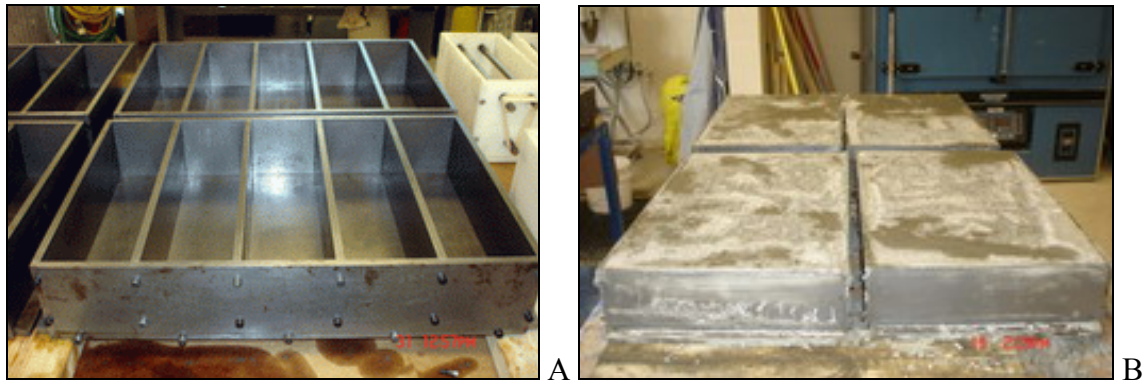


Figure 3-5. Steel mold. A) Individual beam for control mixes. B) Slab for fiber mixes.

Table 3-9 Number of specimens prepared for conditioning and testing for Classes II/V concrete

Mix Type	Fiber Type	Fiber Volume Fraction $V_f$ (%)	ASTM C 1399		ASTM C1609
			Uncracked Beam	Precracked Beam	Uncracked Beam
PC	Control	N/A	25	N/A	25
PP	Polypropylene	0.5	25	25	25
PVA	Polyvinyl Alcohol	0.75	25	25	25
Cell	Cellulose	0.1	25	N/A	25
Steel	Hooked Steel	1	25	25	25

### 3.5 Experimental Program

An experimental program was carried out to obtain a better understanding of the fiber and fiber type on fresh, mechanical, and transport properties of FRC.

#### 3.5.1 Fresh Properties

The measurement of workability of FRC requires a different approach than with conventional concrete mixture, because the slump loss does not necessarily represent a corresponding loss of workability. One disadvantage of using fibers in concrete is a reduction in workability representing an increase of the stiffening effect in the mixture. The Vebe time and inverted slump cone time, which are plastic property tests that measure the energy required to compact the concrete, have been developed specifically to evaluate the fresh properties of FRC. The workability of FRC is affected by fiber aspect ratio and fiber volume fraction. As the fiber

content or aspect ratio increases, the slump decreases. The fresh properties of FRC mixtures were evaluated with slump testing (ASTM C 143/C 143M-00), air content (ASTM C 231-97), inverted slump cone time (ASTM C 995-94), Vebe time (ASTM C 1170-91) and unit weight (ASTM C 231-97).

#### **3.5.1.1 Slump test**

ASTM C 143 for the slump test is a common, convenient, and inexpensive test, but it may not be a good indicator of workability for FRC. However, the slump test was performed with and without fiber during the mixing procedure to compare the fibers effect on workability. A sample of freshly mixed concrete was placed and compacted by rodding in a mold shaped as the frustum of a cone. The mold was raised, and the concrete allowed to subside. The vertical distance between the original and displaced position of the center of the top surface of the concrete is measured and reported as the slump of the concrete.

#### **3.5.1.2 Inverted slump cone time**

ASTM C 995-94 is the standardized test method for inverted slump cone time and has been developed specifically to measure the workability of FRC. It effectively measures the mobility or fluidity of the concrete to flow through a confined space subjected to internal vibration. The test is not suitable for flowable mixtures of FRC, designed to flow freely through a confined space because the concrete tends to run through the cone without vibration. The inverted slump cone test method provides a measure of the consistency and workability of fiber-reinforced concrete. Figure 3-6 is photograph of the inverted slump-cone time test setup. The procedure was carried out according to ASTM C 995-94 as follows: the bucket was dampened and was placed on a level, rigid, horizontal surface free of vibration and other disturbances. The cone was dampened and was placed in the positioning device, where it was level. From the sample obtained, the cone was filled in three layers, each approximately one third of the volume of the cone. Each layer

was lightly leveled with a scoop or trowel to minimize the entrapment of large voids and the surface of the top layer was stroked off by means of a screeding and rolling motion of the tamping rod. Protruding fibers that inhibited screeding were removed by hand. Then, an external vibrator and a stopwatch were started simultaneously. The stopwatch was stopped when the cone became empty, which occurred when an opening became visible at the bottom of the cone. When the cone became plugged during the test, or failed to empty because of an excess of material that has fallen through during filling, the result was disregarded and a new test was performed on another portion of the sample. The time needed for the mix to flow out of the cone was recorded. As shown in Figure 3-6 an external vibration source was utilized for the consolidation of the concrete. The use of an external vibration is a slight deviation from ASTM C 995, which prescribes an internal source. However, the external vibration source was used because it provides more repeatability.



Figure 3-6. Inverted slump-cone time test setup

### 3.5.1.3 Vebe time

ASTM C 1170 is the standardized test method for the Vebe time, which is intended to be used for determining the consistency and density of stiff to relatively dry concrete mixtures as shown in Figure 3-7.



Figure 3-7. Vebe time test setup

The procedure for operating the Vebe time test is as follows. The Vebe's consistometer was installed on an unbending, horizontal and smooth surface, and the cylinder mold was put on the vibrating table and secured using the special screws. The conical mold was moistened, then put into the cylinder mold, and the funnel was positioned over the cylinder mold. The screw of the rotating arm was tightened so that the funnel prevented the mold from lifting. After the concrete was prepared, the conical mold was filled in three steps with 25 strokes of a tamping rod distributed uniformly over the whole surface. The conical mold was lifted vertically, avoiding sideways or torsional movements. The rotating arm was moved so that the transparent disk was

above the concrete surface, and the disk was lowered until it touched the concrete. The transparent disk was left free and the fixing screw on the holding bar was unscrewed so that it moved freely inside the cylinder and touched the concrete, which was then compacted. Then, the vibrating table was operated and the timer was pressed. As soon as the transparent surface was completely covered by the fresh concrete, the timer and the vibrating table were stopped. This resulting time is the Vebe time and represents the workability of concrete.

#### **3.5.1.4 Air content**

The standard test method (ASTM C 231) for air content by the pressure meter was performed to confirm that the addition of fibers did not result in the entrapment of unwanted air voids within the concrete which may be as large as 3 mm and are capable of adversely influencing strength and impermeability (Mehta et al, 2005). Both effects would lead to decreases in durability performance.

#### **3.5.2 Transport Properties**

Degradation of concrete structure is normally due to the movement of aggressive chemical ions (chlorides, sulfates, CO<sub>2</sub>) into concrete. Transport of water, chemical ions or gases into concrete occur through several kinds of transport mechanisms such as diffusion, permeability by pressure head, absorption by capillary suction, adsorption and desorption, and migration by electron field. Laboratory investigation of the transport characteristics for FRC is an important aspect for the understanding of degradation mechanisms for environmental exposure.

In this study, major transport properties including absorption, permeability, and chloride diffusion processes were only performed and evaluated for concrete mixtures containing each fiber type in an effort to investigate their influence on mass transport properties for FRC.

### 3.5.2.1 Permeable pore space test

ASTM C 642 is the standard test method for determination of density, percent absorption, and percent voids in hardened concrete. By using the values for mass determined in oven-dry mass, saturated mass after immersion, saturated mass after boiling, and immersed apparent mass, the total absorbed water into the specimen was calculated as follows to determine “permeable pore space”:

$$p = \frac{(g_2 - g_1)}{g_2} \times 100 \quad (3-1)$$

where

$p$  = permeable pore space (%)  
 $g_1$  = bulk density, dry  
 $g_2$  = apparent density.

This test approach does not include a determination of absolute density. Hence, such pore space as may be present in the specimen that was not emptied during the specified drying or was not filled with water during the specified immersion and boiling, or both, was considered “impermeable” and was not differentiated from the solid portion of the specimen for the calculations, especially those for percent voids.

### 3.5.2.2 Surface resistivity test

This non-destructive laboratory test method (FM 5-578) assesses the electrical resistivity of water-saturated concrete surface and provides an indication of its permeability, but can cause misleading results when embedded electrically conductive materials such as reinforcing steel, conductive fibers, and calcium nitrite, are present (FM 5-578, 2004).

After moist curing, four indelible marks were made on the top circular face of the specimens marking the 0, 90, 180, and 270 degree points along the circumference of the circle. The marks were extended along the longitudinal sides of the specimen serving as visual aids

during the resistivity reading. Small concrete blocks remaining after cores were used to obtain resistivity measurements on fiber specimens. Top and sides of the small block surface were marked and measured. Experimental test set up for surface resistivity is shown as in Figure 3-8.



A



B

Figure 3-8. Surface resistivity test set-up. A) Cylinder specimen. B) Fiber specimen.

A Wenner linear four-probe array with spacing of 1.5 inches was placed longitudinally on the side of the specimen at the 0 degree mark. All the points of the array probe were in contact with the concrete. Resistivity measurements were typically obtained after 3 to 5 seconds or until a stable reading was obtained. This procedure was repeated for 90, 180, and 270 degree marks

and the average resistivity for the set of samples was calculated. Table 3-10 was used to characterize the permeability of the concrete based on surface resistivity per FM 5-578.

Table 3-10 Surface resistivity-permeability

Chloride Ion Permeability	Surface Resistivity Test (kΩ-cm)
High	< 12
Moderate	12-21
Low	21-37
Very Low	37-254
Negligible	> 254

### 3.5.2.3 Permeability test

The water permeability apparatus developed by Soongswang et al. (1988), which measures one dimensional flow into concrete, was used to measure the coefficient of permeability for each of the concrete mixes. A schematic diagram of the water permeability flow apparatus is shown in Figure 3-9. The Plexiglas ring on top of the specimen is a chamber which holds pressurized water. The bottom of the specimen was open to the atmosphere which creates a pressure gradient across the specimen and results in pressurized water flow. A pressure of 275.8 kPa (40 psi) was used for testing. The volume of water flow into the specimen was computed by reading the water level change of the manometer tube. A plot of the cumulative water amount versus time was drawn to determine the steady state flow condition. The coefficient of water permeability was measured from the net rate of inflow using the following expression based on Darcy's law:

$$K_w = \rho \frac{HQ}{PA} \quad (3-2)$$

where

$K_w$  = coefficient of permeability in m/sec

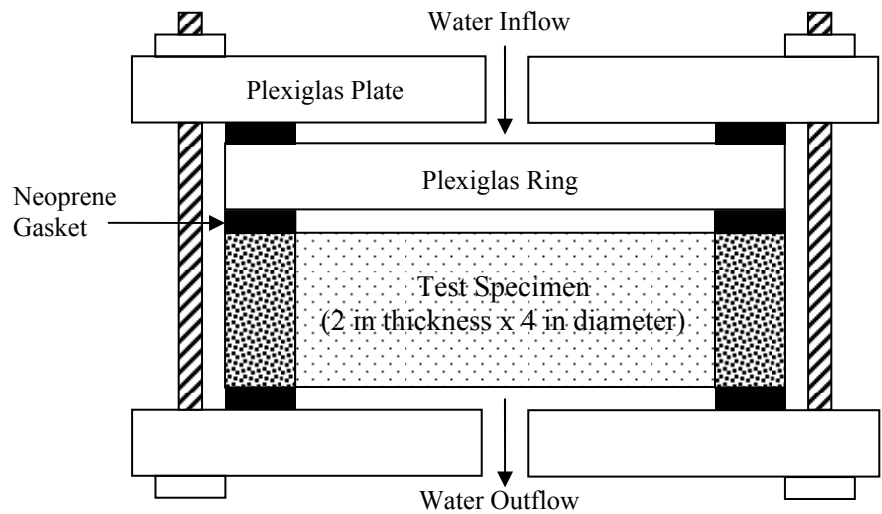
$\rho$  = density of water in Mg/m<sup>3</sup>

$H$  = length of test specimen in m

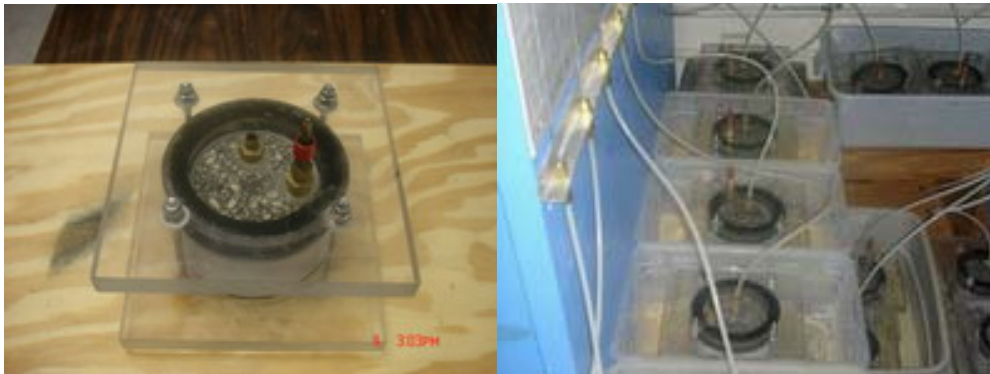
$P$  = water pressure in Pa

$Q$  = net rate of inflow in m<sup>3</sup>/sec

$A$  = cross-sectional area of test specimen in m<sup>2</sup>.



A



B

Figure 3-9. Water permeability test specimens. A) Schematic diagram. B) Test specimen.

#### 3.5.2.4 Absorption test

The ingress of deleterious materials such as chloride and sulfate ions into concrete from the process of diffusion is relatively slow (Martys et al., 1997) in comparison to other transport properties like absorption. Therefore, it may be that mass transport of deleterious materials by capillary action is the main transport mechanism for unsaturated concrete. The fundamental understanding of mass transport in concrete is necessary to evaluate its durability properties and estimate service life. The standard test method for the determination of the rate of water absorption by hydraulic cement concrete in accordance with ASTM C 1585 (2004) is used to

determine the effects of fiber and fiber type. The absorption is determined by the increase in the mass of a specimen resulting from capillary action of water as a function of time when only one surface of the specimen was exposed to water with sealed sides (candle wax) and top surface.

The absorption is the change in mass divided by the product of the cross-sectional area of the test specimen and the density of water. For the purpose of this test, the temperature dependence of the density of water was neglected and a value of 0.001 g/mm<sup>3</sup> was used. The absorption,  $I$ , considering permeable voids in the specimen was calculated as follows:

$$I = m_t \frac{d}{a} \times p \quad (3-3)$$

where

$I$  = the absorption (mm)

$m_t$  = the change in specimen mass in grams, at the time  $t$

$a$  = the exposed area of the specimen, in mm<sup>2</sup>

$d$  = the density of the water in g/mm<sup>3</sup>.

The water transport into concrete by capillarity is controlled by the square root of time relationship. The initial rate of water absorption (mm/s<sup>1/2</sup>) was defined as the slope of the line that is the best fit to  $I$  plotted against the square root of time (s<sup>1/2</sup>). This slope was obtained by using least-squares, linear regression analysis of the plot of  $I$  versus time<sup>1/2</sup>. A schematic setup of the capillary suction test is shown in Figure 3-10. A 100×50 mm cylindrical specimen was placed on the support device at the bottom of the pan, which was filled with tap water so that the water level was maintained at 1 to 3 mm above the top of the support device. The absorbed water quantity was recorded at 1, 5, 10, 20, 30, 60, 120, 180, 240, 300, 360 min and once a day for the first 3 days was recorded, and then 3 measurements at least 24 hours apart during days 4 to 7. The final measurement was recorded at the end of day 7. Any surface water was blotted off with a dampened paper towel for each mass determination.

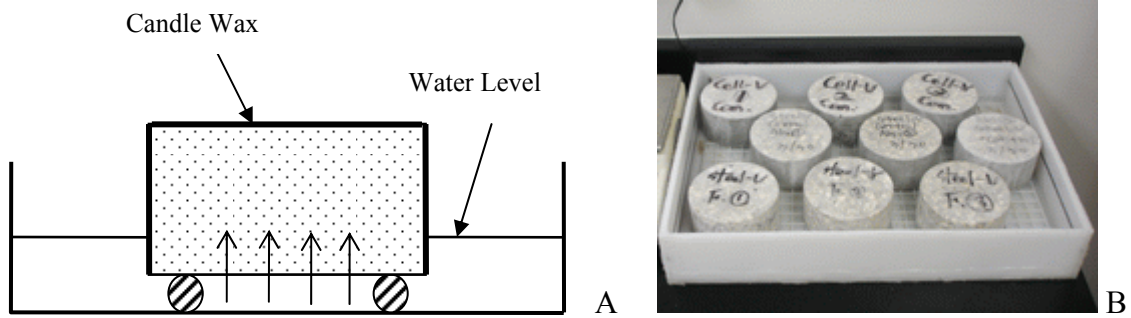


Figure 3-10. Absorption test set-up. A) Schematic diagram. B) Testing specimens.

### 3.5.2.5 Bulk diffusion test

Diffusion process is the primary transport mechanism of chloride ions into concrete when the moisture condition in the pore structure is stable (Song et al, 2008) and differences in chloride concentration induce chloride movement, as opposed to the convective flow of capillary suction or permeation (Kropp, 1995). The chloride diffusion testing was performed in accordance with NT BUILD 443 test method. Upon the completion of 28 days curing, test specimens were taken out of moisture cure and were sliced into two halves. After which, they were immersed in the  $\text{Ca}(\text{OH})_2$  solution until the mass of the concrete stabilized. The specimen immersion for  $\text{Ca}(\text{OH})_2$  solution was repeated after sealing the surfaces of the specimen with Sikadur 32 Hi-Mod epoxy. Subsequent to conditioning, the specimens were immersed in 16.5 percent sodium chloride solution in tanks for 365 days. As part of the exposure process, the solutions were replaced every 5 weeks. Figure 3-11 is a photograph of the exposure tanks located at the FDOT State Material Office.

Upon the removal of the specimens from the exposure tanks, the chloride profile was obtained grinding off material in layers parallel to the exposed surface. The surface chloride concentrations ( $C_s$ ) obtained for each layer which was used to determine coefficients of diffusion ( $D_e$ ). The coefficient of diffusion is calculated by fitting the equation to the measured chloride

contents by means of a non-linear regression analysis in accordance with the method of least squares fit. The solution to Fick's Second Law of Diffusion which is represented as follows:

$$C(x,t) = C_s - (C_s - C_i) \times \operatorname{erf}\left(\frac{0.5x}{\sqrt{D_e t}}\right) \quad (3-4)$$

where

$C(x,t)$  = the chloride concentration, measured at the depth  $x$  at the exposure time  $t$  in mass %

$C_s$  = the boundary condition at the exposed surface in mass %

$C_i$  = the initial chloride concentration in mass %

$x$  = the depth below the exposed surface

$D_e$  = the effective chloride transport coefficient

$t$  = the exposure time

$\operatorname{erf}$  = the error function.

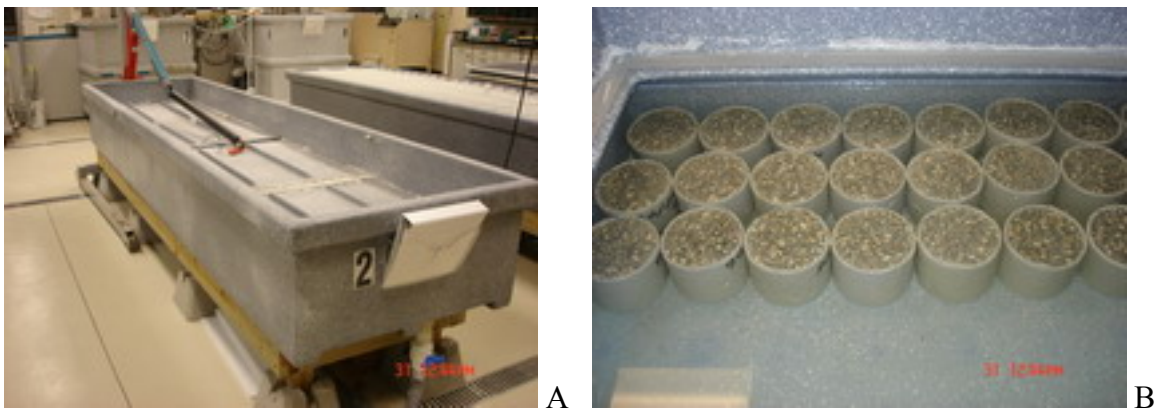


Figure 3-11. Exposure tank and specimen condition for bulk diffusion. A) Exposed tank. B) Testing specimens

### 3.5.3 Mechanical Properties

Unreinforced concrete is a brittle material, but reinforcement of concrete with fibers will create a material with higher compressive, tensile, flexural and shear strength properties. The random distribution of short fibers may contribute to the load transferring mechanism through shear stresses at the fiber-hardened cement paste matrix interface. For a given mixture, the fiber volume fraction, fiber geometry, and fiber distributions have considerable effect on the mechanical properties of FRC (Beaudoin, 1990 and Bentur et al., 1990).

This section describes the mechanical properties of FRC designed to evaluate effects of fiber and fiber type on mechanical properties of FRC. Three different mechanical tests were performed to investigate the physical differences between unreinforced concrete and FRC: compression (ASTM C 39), splitting tension (ASTM C 496), pressure tension, residual strength (ASTM C 1399), and flexural performance of FRC (ASTM C 1609).

### 3.5.3.1 Compressive strength testing

Compressive strength testing in accordance with ASTM C 39 was performed after 28 days of curing time as shown in Figure 3-12. The load was applied at a stress rate of  $35 \pm 7$  psi/s until failure of the specimen. The ultimate compressive strength was calculated by dividing the maximum load by the average cross-sectional area as shown by the following equation:

$$f_c = \frac{4p}{\pi \cdot D^2} \quad (3-5)$$

where

$f_c$  = ultimate compressive strength of cylinder, in psi

$p$  = ultimate compressive axial load applied to cylinder, in lbs

$D$  = diameter of cylinder specimen, in inches.

The average values of compressive strength from three cylinders were taken as the compressive strength of the concrete.



Figure 3-12. Test set-up for compressive strength

### 3.5.3.2 Splitting tensile testing

Three standard cylindrical 4 x 8 in test specimens were prepared to determine the splitting strengths (ASTM C 496-01) at 28 days. This was obtained directly from the load recorded by using a 600 kip capacity FORNEY testing machine. The setup for the splitting tensile tests is shown in Figure 3-13.

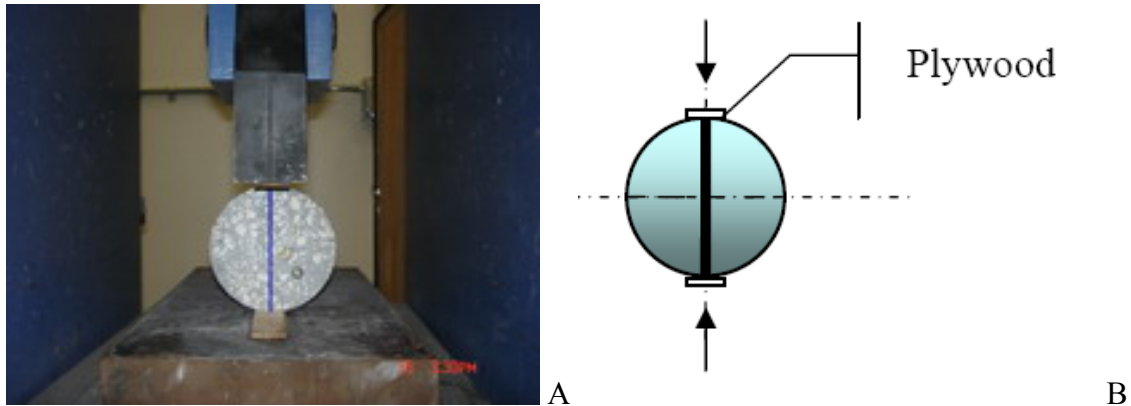


Figure 3-13. Test set-up for splitting tensile test. A) Test set-up. B) Loading condition.

Before testing, the diameter and length of the each test specimen were determined to nearest 0.01 in. (0.25 mm) by averaging three diameters measured near the ends and the middle of the specimen and two lengths of the specimen on the two ends. The splitting tensile testing was performed in accordance with the ASTM C 496-01. Diametral lines were drawn on each end of the specimen using a suitable device to ensure that they were in the same axial plane, and then two pieces of hard wood measuring  $0.25 \times 0.75 \times 8$  in. were placed  $180^\circ$  apart along the longitudinal axis of each cylinder, as shown in Fig. 3-13b. This was done to avoid any stress concentrations that might result along the line of application of the load. The load was applied continuously and without shock, at a constant rate within a range 100 to 200 lbs/sec until failure of the specimen. The maximum applied load indicated by the testing machine at failure was recorded. The splitting tensile strength was computed as follows:

$$f_{st} = \frac{2P}{\pi l D} \quad (3-6)$$

where

$f_{st}$  = splitting tensile strength, in psi  
 $P$  = maximum applied load, in lbf  
 $l$  = length of cylinder, in inches  
 $D$  = diameter of cylinder, in inches.

### 3.5.3.3 Pressure tension testing

Elastic behavior of hollow cylinder specimens based on the theory of elasticity helps to understand the stress states of pressure tension test. Timoshenko and Goodier (2004) represented the stress states in cylinder specimens with the radius  $R$  as shown in Figure 3-14 by following equation:

$$\sigma_R = \frac{P_0 b^3 (R^3 - a^3)}{R^3 (a^3 - b^3)} + \frac{P_i a^3 (b^3 - R^3)}{R^3 (a^3 - b^3)} \quad (3-7)$$

$$\sigma_t = \frac{P_0 b^3 (2R^3 + a^3)}{2R^3 (a^3 - b^3)} - \frac{P_i a^3 (2R^3 + b^3)}{2R^3 (a^3 - b^3)} \quad (3-8)$$

where

$\sigma_R$  = radius stress  
 $\sigma_t$  = tangential stress  
 $b$  = outer diameter  
 $a$  = inner diameter  
 $P_0$  = outer pressure  
 $P_i$  = inner pressure.

The radius and tangential stresses in the hollow container depend on a function of Radius ( $R$ ). If  $P_i = 0$ , then

$$\sigma_R = \sigma_t = P_0 \quad (3-9)$$

The pressure tension test was developed by the British Research Establishments in the UK (Clayton et al, 1979) as shown in Figures 3-15 and 3-16 pressurizes the concrete specimen

cylinder or core by means of an externally applied gas pressure with a rubber ring between steel jacket and end ring to prevent leakage of pressurized nitrogen gas. This applied pressure acts only upon the curved surface of the specimen, which is positioned within a pressure sleeve, since the ends of the cylinder project outside the pressurized area. As long as the specimen is saturated an internal pore pressure develops in response to this applied pressure, acting equally in all directions. It is generally agreed that the maximum pressure of nitrogen gas is fundamentally equal to the tensile strength (Mindess et al., 2005; Clayton et al., 1979; Clayton, 1978; Boyd et al., 2001), though the failure mechanism is not perfectly understood.

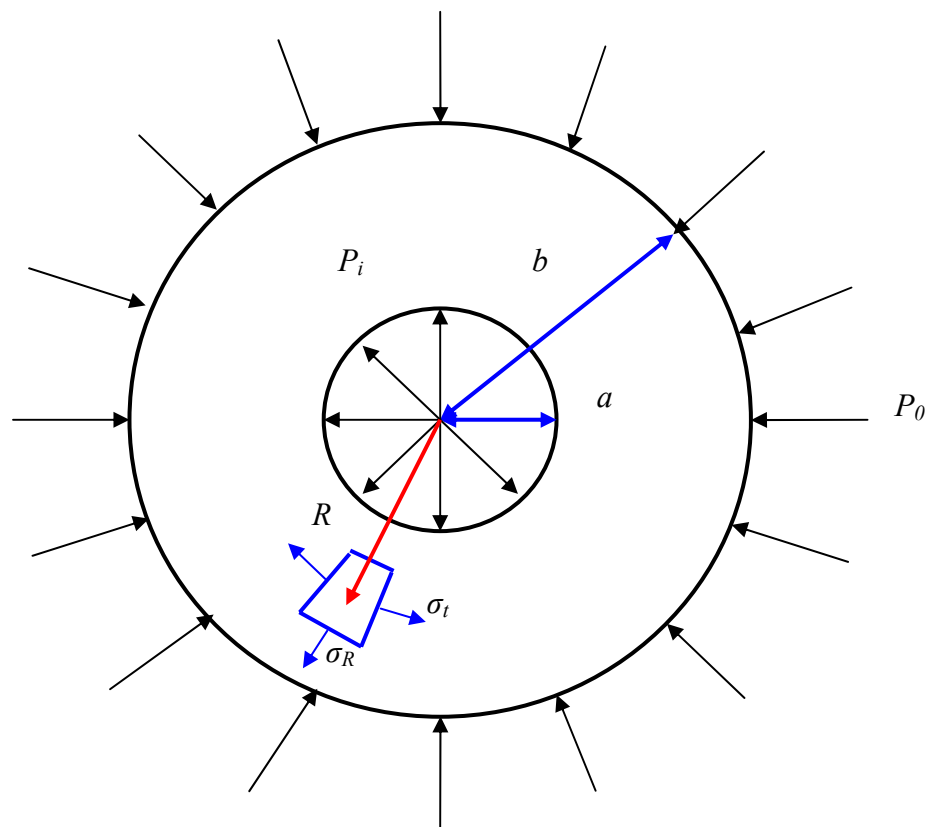


Figure 3-14. Stress state in hollow cylinder under internal or external uniform pressure

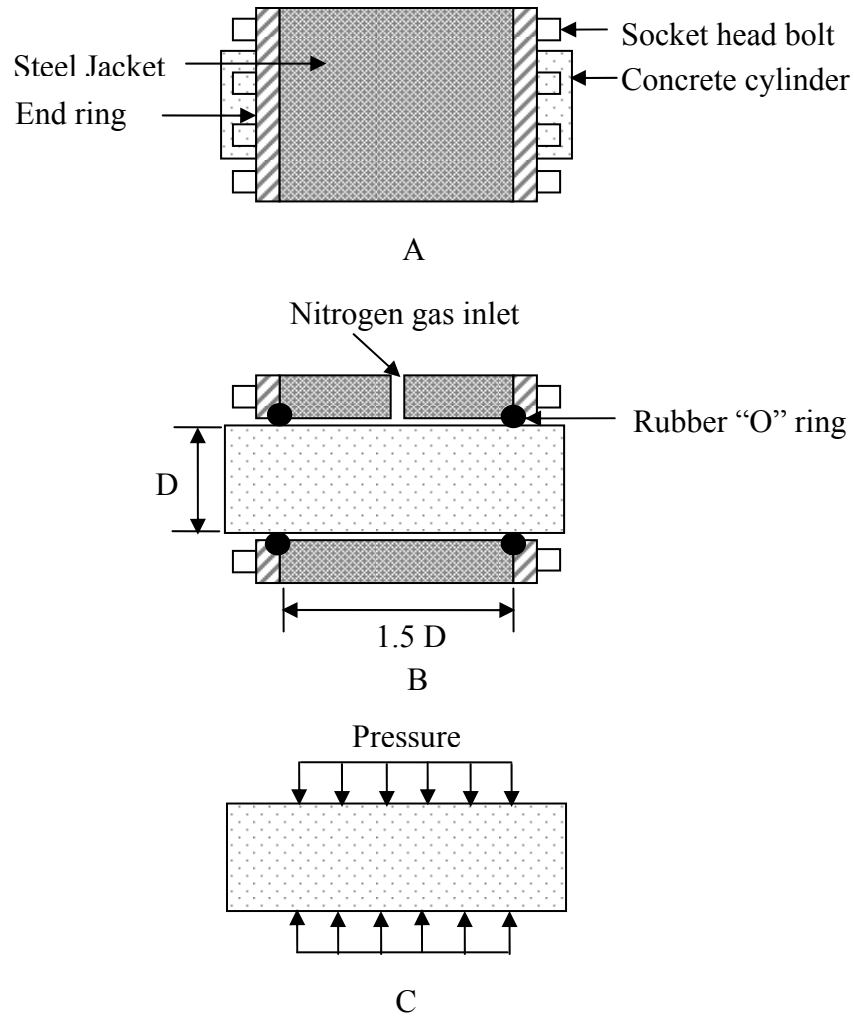


Figure 3-15. Nitrogen gas tension test and stress state. A) Overview. B) Second view. C) Stress state. (after Mindess et al., 2005).

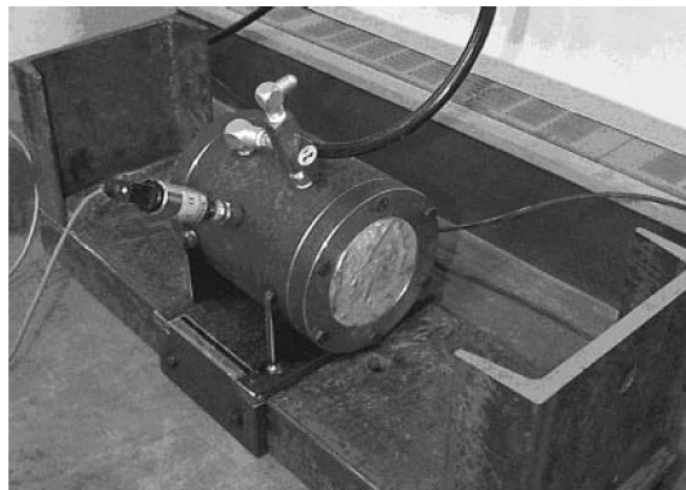


Figure 3-16. Pressure tension testing equipments

### 3.5.3.4 Residual strength testing

Average residual-strength (ARS) measurement for fiber-reinforced concrete as specified in ASTM C 1399 was performed for the beam specimens subsequent to pre-cracking with the steel plate at the bottom of the beam to control the rate of deflection as shown in Figure 3-17.

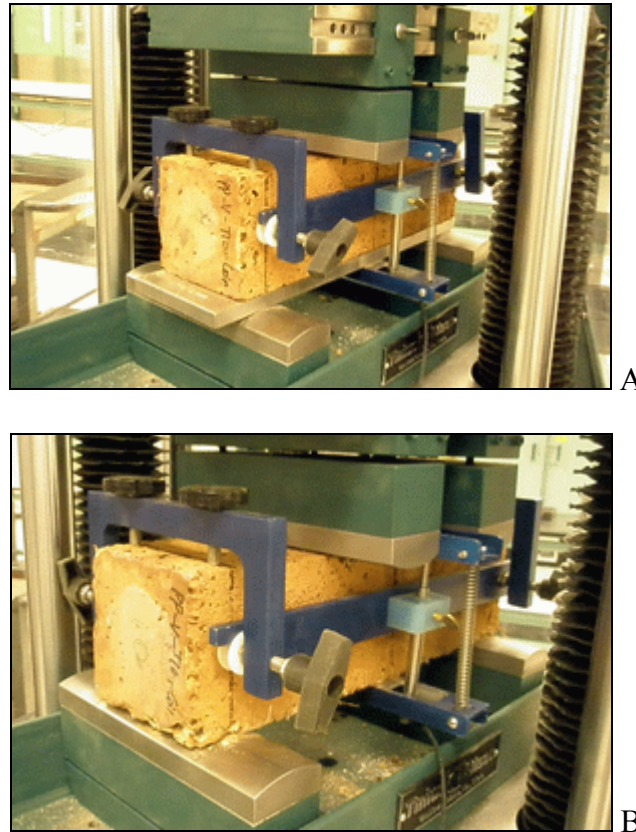


Figure 3-17. Test setup for measuring residual strength by using deflection gage and yoke. A) Before inducing crack with steel plate. B) After crack.

As specified, the rate of cross-head movement was set at  $0.65 \pm 0.15$  mm/in ( $0.025 \pm 0.005$  in/min). Then, the degraded beams were turned to their sides with respect to their position as molded and were placed on top of the steel plate to be loaded. The reason for the steel plate is to aid the beam specimen during the initial loading period to limit the expected high rate of deflection of the beam upon cracking. The beam specimen was placed on the steel plate with support yoke and the steel plate was centered on the lower bearing blocks. The deflection gage

was adjusted and loading was applied until a deflection of 0.5 mm (0.02 in.) was reached in combination with the steel plate. If cracking had not occurred after the beam reached a specified deflection, the test was considered invalid. After removal of the steel plate, the crack induced beam and deflect in gages were adjusted on the lower bearing blocks. Loading was applied to cracked beam at the specified rate used for the initial loading and the test was stopped at a deflection of 1.25 mm (0.05 in.). The average residual strength was calculated using the measured loading at reloading deflections of 0.5, 0.75, 1, and 1.25 mm (0.02, 0.03, 0.04, and 0.05 in.) as follows (Figure 3-18):

$$ARS = ((P_A + P_B + P_C + P_D) / 4) \times k \quad (3-10)$$

where

$$k = L/bd^2, \text{ mm}^{-2} \text{ (in}^{-2}\text{)}$$

$ARS$  = average residual strength, MPa (psi)

$P_A + P_B + P_C + P_D$  = sum of recorded loads at specified deflection, N (lbf)

$L$  = span length, mm (in.)

$b$  = average width of beam, mm (in.)

$d$  = average depth of beam, mm (in.).

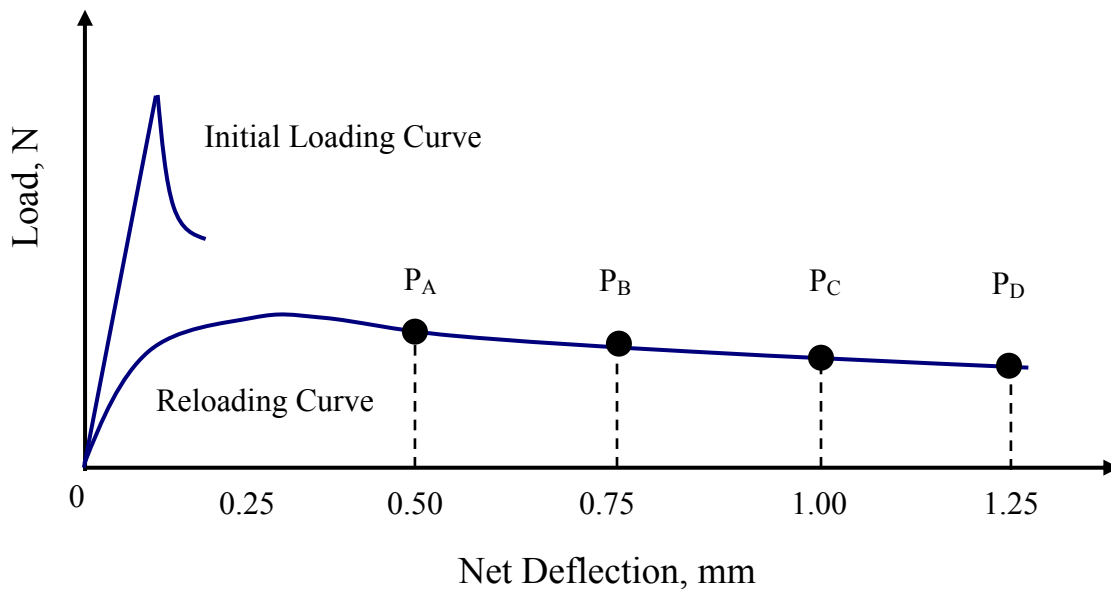


Figure 3-18. Load vs. deflection curve for residual strength measurement

### 3.5.3.5 Flexural performance testing

The test method specified in ASTM C 1609 evaluated the flexural performance of fiber-reinforced concrete using parameters derived from the load-deflection curve obtained by testing a simply supported beam under third-point loading as shown in Figure 3-19.

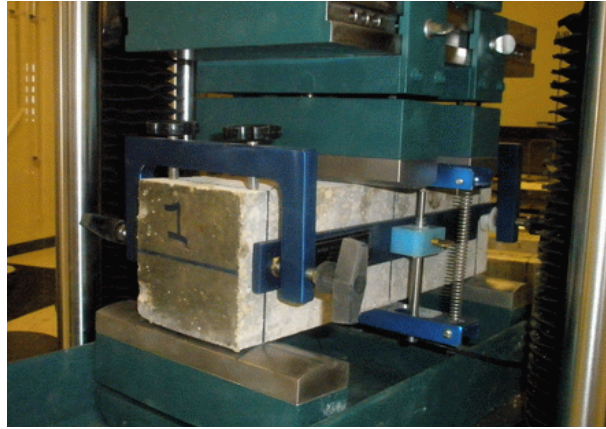


Figure 3-19. Test set-up for measuring flexural performance of FRC with yoke.

The test specimens after environmental conditioning were turned on their side with respect to the position as cast when placing on the support system. Then, support yoke and deflection gage were arranged to obtain net deflection. The load was applied at the rate of increase of net deflection within the range 0.05 to 0.1 mm/min (0.002 to 0.004 in./min) until a net deflection of  $L/600$  was reached. After that, the rate of increase of net deflection was within the range 0.05 to 0.2 mm/min (0.002 to 0.008 in./min) until reaching net deflection of  $L/150$ . Test results were discarded when the crack initiated outside of the middle third of the span. The first-peak load was that value of load corresponding to the first points on the load-deflection curve where the slope is zero was determined as well the corresponding deflection value at that point. The first-peak strength ( $f_1$ ) using the first-peak load ( $P_1$ ) was calculated by following formula for modulus of rupture:

$$f_1 = \frac{PL}{BD^2} \quad (3-11)$$

where

$f_l$  = the strength, MPa (psi)

$P$  = the load, N (lbf)

$L$  = the span length, mm (in.)

$B$  = the average width of the specimen, mm (in.)

$D$  = the average depth of the specimen, mm (in.).

The peak load was that value of load corresponding to the point on the load-deflection curve that corresponds to the greatest value of load ( $P_p$ ) obtained prior to reaching the end-point deflection, which was determined as the corresponding deflection ( $\delta_p$ ) value at that point. Then, the peak strength was calculated. The residual loads ( $P_{4, 0.02}$  and  $P_{4, 0.08}$ ) at span/600 and span/150, as well the corresponding residual strengths were calculated. Finally, the total area ( $T_{4, 0.08}$ ) under the load-deflection curve up to a net deflection of span/150 was calculated. Examples for parameter calculations for different Flexural curves are represented in Figure 3-20.

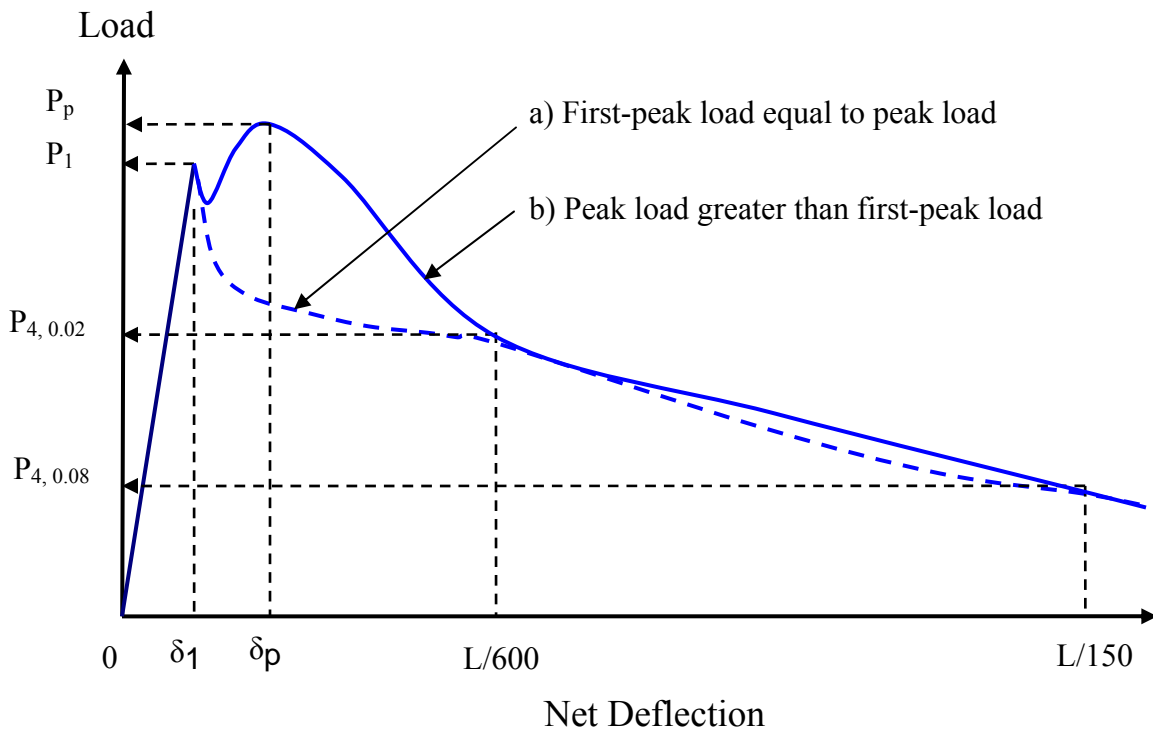


Figure 3-20. Examples of parameter calculations for different flexural curves

### 3.5.4 Steel Bar Corrosion

The steel bar corrosion testing in accordance with ASTM G 109 was used to evaluate the effect of fibers on resistance to corrosion of steel bars embedded in fiber reinforced concrete. The fibers used in this test were cut into 0.5 in. in length by considering the size of steel bar in concrete structure. Two specimens were prepared and cast for control and each fiber type for concrete classes II and V. The steel bars were sand blasted to near white metal. One end of each bar was drilled/tapped and a stainless steel screw and two nuts were attached. Each end of the steel bar was taped with electroplater's tape so that a 200 mm (8 in.) portion in the middle of the bar was left exposed. A 90 mm (3.5 in.) length of neoprene tubing was placed over the electroplater's tape at each end of the bar. The steel bars and titanium bar representing corrosion potential of the bars were placed in the mold (11 × 6 × 4.5 in.) as shown in Figure 3-20b and then concrete was placed and consolidated. Upon removal from the moist room after 28 days curing, the top surface of the concrete specimens was hand-wire brushed and dried for two weeks in a 50% relative humidity room before applying a plastic dam with an epoxy sealer. The plastic dam, 75 mm (3 in.) wide and 150 mm (6 in.) long, with a height of 50 mm (2 in.) was placed on the top surface with the outside of the plastic dam sealed with silicone caulk and epoxy sealer. The sealed specimens were stored in a 50% relative humidity (RH) environment for an additional two weeks and then testing was started. The plastic dam was filled with 16.5% NaCl solution and the specimens were stored at 90°F in a temperature controlled room. After two weeks, the solution was vacuumed off and allowed to dry for two weeks. This cyclic wetting and drying was repeated until significant steel corrosion was detected. The current and corrosion potential of the bars were monitored once every day. The test set-up for corrosion is shown in Figure 3-21. The

ratio of total integrated current of the damaged specimens to that of the control and time the test ended was calculated. The total integrated current is:

$$TC_j = TC_{j-1} + [(t_j - t_{j-1}) \times (i_j + i_{j-1}) / 2] \quad (3-12)$$

where

$TC$  = total corrosion (coulombs)

$t_j$  = time (seconds) at which measurement of the macrocell current is carried out

$i_j$  = macrocell current (amps) at time,  $t_j$ .

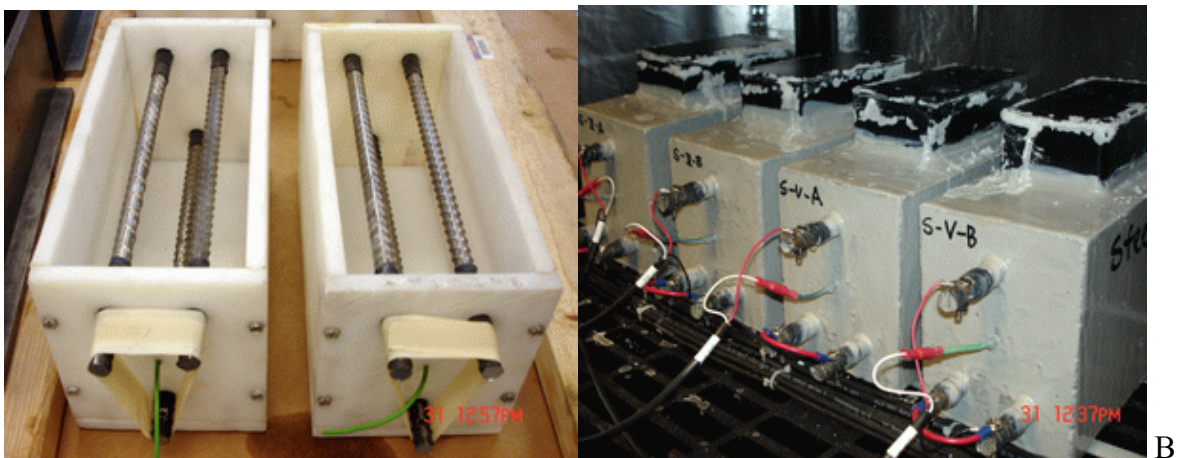
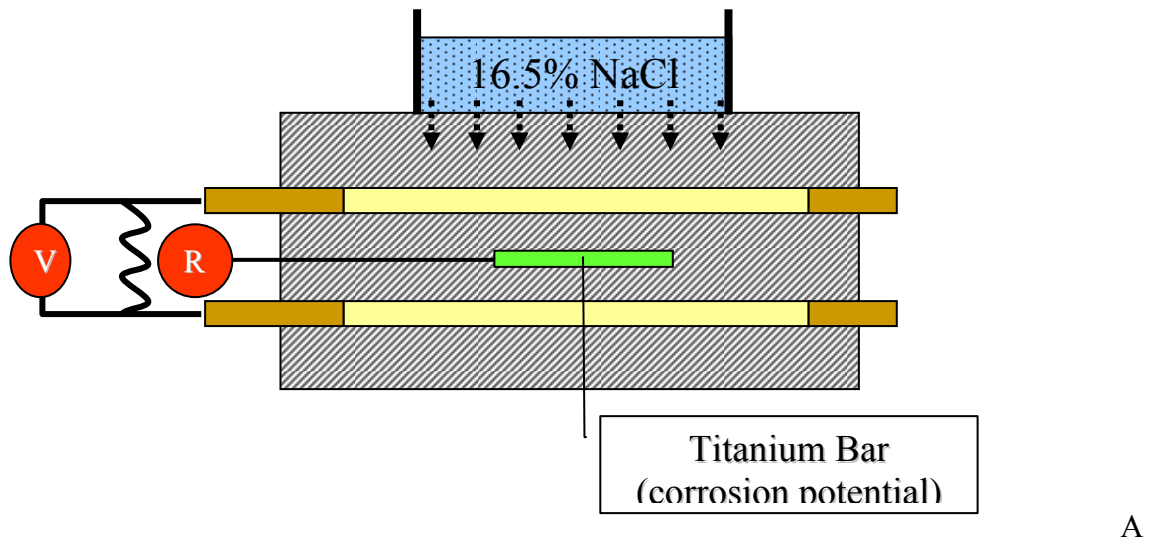


Figure 3-21. Test set-up for steel bar corrosion. A) Schematic diagram. B) Mold and test set-up.

### 3.5.5 Ultra Pulse Velocity (UPV)

Ultra Pulse Velocity (UPV) specified in ASTM C 597 was performed to indicate any changes of the properties in FRC to estimate the severity of deterioration of beams subsequent to environmental exposure. Pulses of longitudinal stress wave are produced by an electro-acoustical transducer that is held in contact with one surface of the beam. After traversing through the beam, the pulses were received and converted into electrical energy by a second transducer located a distance from the transmitting transducer. The degree of saturation of the concrete affects the pulse velocity. The pulse velocity in saturated concrete may be up to 5% higher than in dry concrete (Bungey, 1989). The pulse velocity,  $V$ , of longitudinal stress waves in concrete mass is related to its elastic properties and density according to the following relationship:

$$V = \sqrt{\frac{E(1-\mu)}{\rho(1+\mu)(1-2\mu)}} \quad (3-13)$$

where

$E$  = dynamic modulus of elasticity

$\mu$  = dynamic Poisson's ratio

$\rho$  = density.

The pulse velocity was calculated as follows:

$$V = L/T \quad (3-14)$$

where

$V$  = pulse velocity, m/s

$L$  = distance between centers of transducer faces, m

$T$  = transit time, s.

### 3.5.6 Scanning Electron Microscopy (SEM)

Semi-quantitative chemical analysis for Scanning Electron Microscopy (SEM) with Energy Dispersive Spectrometer (EDS) were performed to observe microstructure changes in the interfacial zone between the fiber and the hardened cement paste matrix as a result of chemical

reaction during environmental exposure. Two Class II concrete specimens per fiber type subjected to limewater and saltwater immersion were chosen and analyzed. The specimen sliced from the fractured beam was in a saturated condition due to long term exposure. Unpolished surfaces were prepared by using a diamond bladed saw because epoxy-impregnated sawn polished surfaces general used to prepare concrete samples can cause damage in the form of cracking patterns or crystals (Stella, 1995). Before examination, specimens were coated with a thin carbon film by sputtering with low deposition rate. Secondary Electron (SE) images, which are capable of displaying the morphology of the microstructure were obtained, as well as X-ray element analysis providing elemental compositions marked on a chart, where specifically selected elements are recognized on a continuous spectrum according to the position of its peak. Finally, a dot map indicating the distribution of a particular element was created.

### **3.5.7 Carbonation**

The depth of the carbonation was determined by fracturing or chipping the beam specimens after flexural beam testing. After splitting one face of the specimen, the specimen was cleared of dust and loose particles and then phenolphthalein indicator solution was sprayed on the fractured surface. The phenolphthalein indicator changes color at a pH of 9.0 to 9.5. The depth of carbonation was determined by measuring the area of the broken surface which does not turn purple after spraying.

## CHAPTER 4 ENVIRONMENTAL EXPOSURE

### 4.1 Introduction

This chapter is divided into three sections: degradation mechanism of concrete structure in seawater; environmental exposure; and expected deterioration mechanism during conditioning.

### 4.2 Deterioration of a Concrete Structure in Seawater

Mehta (1980) determined that the type and severity of degradation is not consistent through concrete structural elements based on the environmental exposure conditions. The portion of the concrete structure exposed to seawater is typically separated into three kinds of zones, which are represented in Figure 4-1.

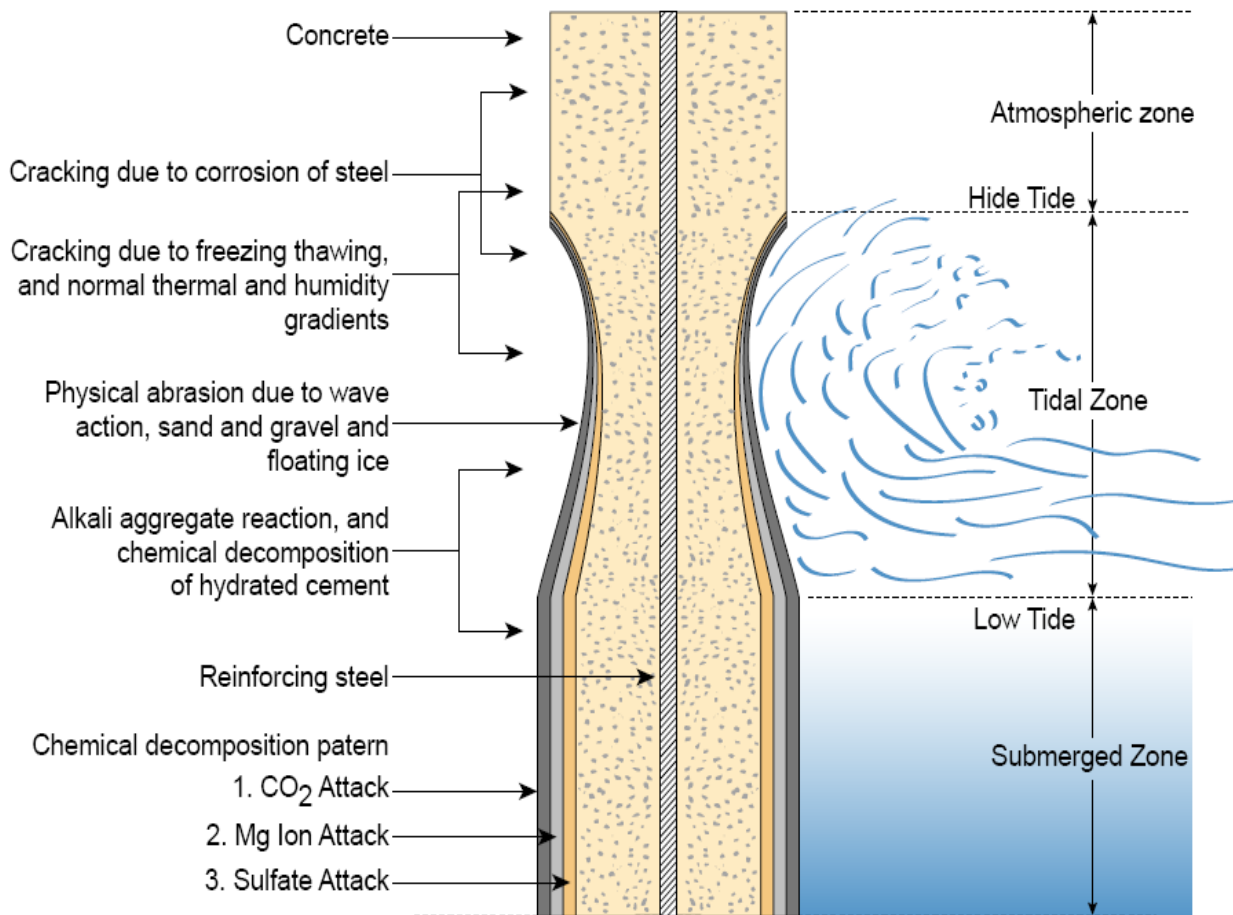
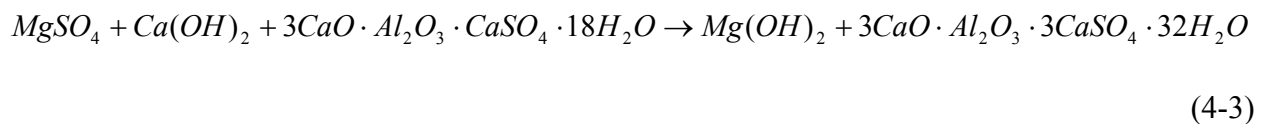
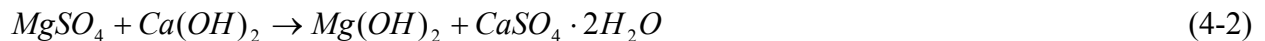
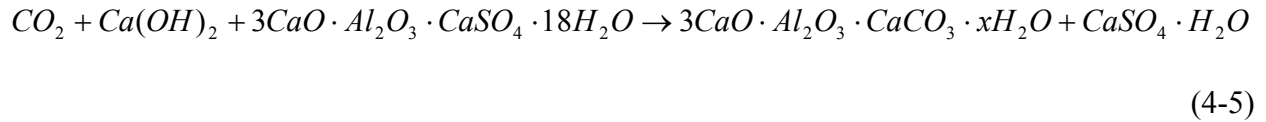


Figure 4-1. Schematic diagram for degradation mechanism of a concrete structure exposed to seawater. (From P. K. Mehta, 1980 and Mehta et al., 2005).

The first part, which is above the high-tide line, is directly exposed to atmospheric air, winds containing sea salts and will be more vulnerable to cracking due to steel bar corrosion or spalling from freezing/thawing damage action in northern climates. The second part, in the tidal zone, is susceptible to cracking and spalling from the cyclic wetting and drying action, steel corrosion, and frost action. The concrete in the tidal zone is also subject to materials degradation or loss due to chemical decomposition of cement paste, and erosion due to impact of wave action. The lower part, which is the submerged zone under low tide line, is vulnerable to strength or material loss resulting from the reaction of chemical ions ( $\text{CO}_2$ , sulfate, chloride,  $\text{Mg}^{2+}$ ) between sea water and cement paste. The chemical reactions between magnesium salts, typically contained 3200 ppm  $\text{MgCl}_2$  and 2200 ppm  $\text{MgSO}_4$  and  $\text{Ca}(\text{OH})_2$  produce  $\text{CaCl}_2$  and gypsum ( $\text{CaSO}_4 \cdot 2\text{H}_2\text{O}$ ), soluble in sea water, lead to materials loss or weakening. The formation of ettringite ( $3\text{CaO} \cdot \text{Al}_2\text{O}_3 \cdot 3\text{CaSO}_4 \cdot 32\text{H}_2\text{O}$ ) by  $\text{MgSO}_4$  also causes the expansion and cracking of concrete:



Carbon dioxide dissolved in sea water contributes to the chemical decomposition of hardened cement paste. Small quantities of carbon dioxide are normally dissolved from absorption of atmospheric  $\text{CO}_2$ , but highly carbonated sea water due to decaying organic matter drops the pH of sea water less than 7 or less and the chemical reactions produce bicarbonate of calcium or gypsum. Both chemical products are soluble in sea water and cause loss of material or weakening of cement paste:



The dominant transport mechanism of solutions into partially saturated condition is capillary suction. The chemical ions within the solutions, deposit into pore spaces by the evaporation of as it undergoes cyclic wetting and drying. Hong and Hooton (1999) studied the penetration of chloride ions into cover concrete to evaluate the effects of wet-dry cycles with NaCl solution. The research found that the rate of chloride movement into concrete was increased as drying time increases. A relationship was developed between the depth of chloride penetration and the square root of the number of cycles for the outer 10 mm of concrete cover where absorption is the primary transport mechanism.

### 4.3 Environmental Exposure

Previous studies (Al-Tayyib et al.; 1988, Balaguru et al.; 1986, Mangat et al., 1985) exposed undamaged concrete blocks to environmental conditioning, thus limited fiber exposure. However, this study examined the resistance of FRC exposed to both a virgin un-cracked condition and a pre-cracked condition as explained per ASTM C 1399 testing.

Three exposure conditions were created for the evaluation of concrete specimens in this research. The first exposure condition completely immersed fiber reinforced concrete in simulated sea water with 5 % chlorides and 1 % sulfate ions at 90°F water temperature for 21 month exposure period. High salt concentration in pores accelerated transport of chemical ions into concrete and also potential damage due to the hygroscopic effect of the salt in the pore system (Kropp et al., 1995). The composition of simulated sea water is summarized in Table 4-1.

A second exposure condition provided cyclic wetting and drying where the beam specimens were immersed six hours in seawater and dried at room temperature for another six hours for duration of 21 months. Water was pumped automatically from one tank to another tank after wetting periods. While the specimens were immersed, the water was circulated through the bath. Wet/dry cycling tends to accelerate accumulation of deleterious materials in the pore system such as chloride and also may induce cracking in concrete. Absorbed chloride ions during wetting period remain in the pore system when water evaporates upon drying. Therefore, increased salt concentration near-surface of concrete accelerates mass transport of chloride ions and salt crystallization in the pore system might cause micro-cracking. Repeated wetting and drying accelerates sulfate attack and salt crystallization in the pore during drying periods causing expansive forces in the intertidal zone where additional damage action can take place (Mindess et al., 2003).

Table 4-1. Composition of simulated seawater

Constituent	Ocean Salinity (35g/1000g)		Simulated Salinity (115g/1000g)	
	Percentage	PPM	Percentage	PPM
Chloride	55.04	19,350	43.58	50056
Sodium	30.61	10760	27.47	31556
Sulfate	7.68	2710	8.41	9661
Magnesium	3.69	1290	2.16	2482
Calcium	1.16	410	0.16	184
Potassium	1.10	400	0.15	176
Total	99.28	34920	81.93	94117

The third conditioning solution exposed beam specimens to swamp water. The swamp water solution had a pH 4.5 controlled by the addition of vinegar in an effort to simulate the swamp environment typical to the state of Florida. The flow chart for experimental program and numbers of specimens in the environment conditioning are summarized in Table 4-2 and Figures 4-2 and 4-3.

Table 4-2 Beam specimens exposed to environmental exposure

Mix Type	Lime water	Lime water	Salt water	Salt water	Swamp water
	Immersion	Wet/Dry	Immersion	Wet/Dry	Immersion
PC-II (V)	10 (10)	10 (10)	10 (10)	10 (10)	10 (10)
PP-II (V)	15 (15)	15 (15)	15 (15)	15 (15)	15 (15)
PVA-II (V)	15 (15)	15 (15)	15 (15)	15 (15)	15 (15)
Cell-II (V)	10 (10)	10 (10)	10 (10)	10 (10)	10 (10)
Steel-II (V)	15 (15)	15 (15)	15 (15)	15 (15)	15 (15)

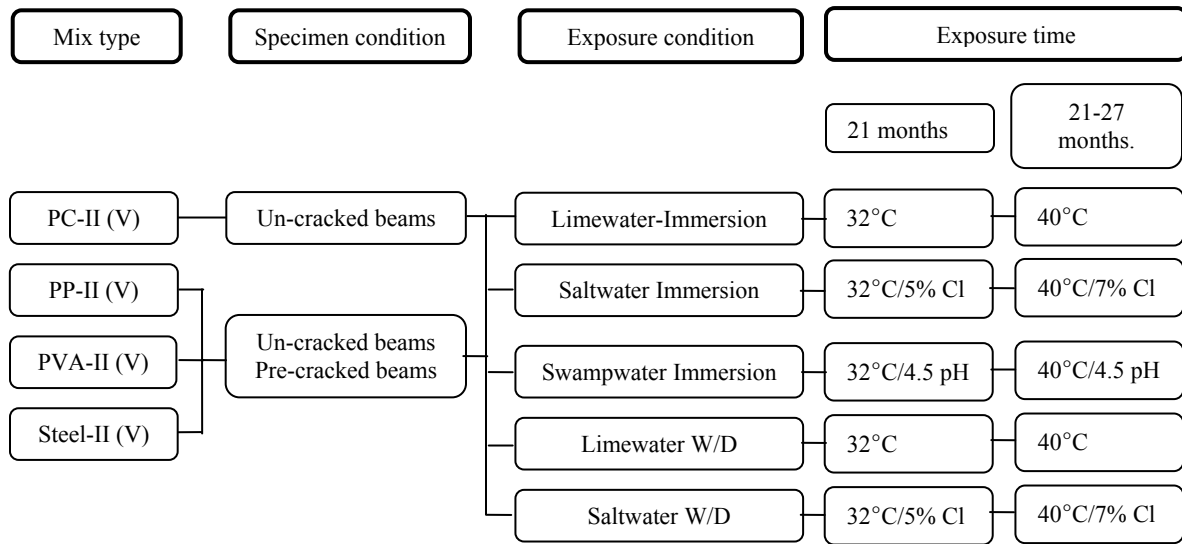


Figure 4-2. Flow chart for experimental program

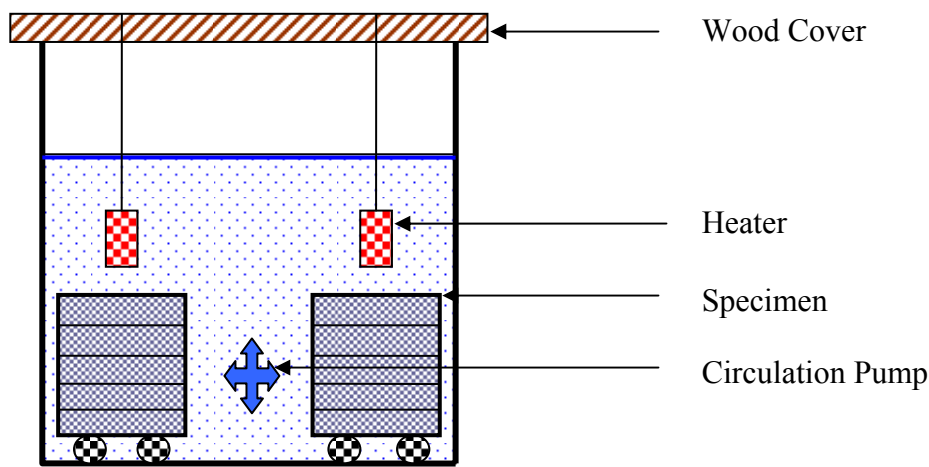


Figure 4-3. Environmental exposure conditioning. A) Schematic diagram for beam condition in tank. B) Exposure Tanks. C) Beam Arrangement. D) Swamp water immersion.



B



C



D

(b) Exposure tanks and beam arrangement

Figure 4-3. Continued

Development of New Wet/Dry Condition System: Water transfer into beam specimens subjected to field conditions was determined to be between 30 g in March and 50 g in August based on preliminary test results. However, the relatively high humidity in the laboratory resulted in very little amount of moisture movement of about 1 to 3 g in the beam specimens. This was not enough to promote certain types of degradation such as corrosion or to accelerate cracking by increasing the salt concentration in the pore network from the surface layers during 12 hours cyclic wetting and drying period. Thus the experiment was redesigned to reconcile the problem.

An extensive amount of work was done to identify and design a system that would result in significant drying of specimens when not submerged, thereby more closely simulating wet/dry

conditions in the field, which cause much greater concentration and penetration of ions and potential for corrosion. After several trials involving dehumidifiers and different types of heating systems, an appropriate system was identified and installed as shown in Figure 4-4. The system involves the use of specially designed heater/blowers combined with a reduced volume tank. The hotter air from the heater/blowers force much greater amounts of moisture from the tank, which results in much drier specimens in less time. However, 6 hours for wetting (90°F) and 6 hours for drying (100~135°F) conditioning, even with the heater/blowers, were still not enough to induce significant damage area on the fracture surface to evaluate fiber resistance on post-cracking failure.

Therefore, the wetting and drying cycle times were increased to 7 days for wetting and 7 days for drying to maximize moisture gain and loss with minimizing micro-damage and also minimize carbonation rather than oven conditioning. The final depth of absorbed water for 7 days wetting was determined to be 12.5mm (0.5in.) from the concrete surface, which corresponds to approximately 50% of the beam volume. As a result of the redesign of the drying system and the increase of the cycle time, the total amount of water transferred was 100 to 150g. Another change in the experiment per the new wet/dry conditioning was the increase of the chloride concentration of the solutions to 7% and the water temperature was increased to 105°F. The redesigned composition of simulated seawater is summarized in Table 4-3. The moisture transfer test results with increased wetting and drying time with new conditioning system is shown in Figures 4-5, 4-6, 4-7, and 4-8. Additional environmental exposure for all specimens was continued from 21 months to 27 months.

Table 4-3. Redesigned composition of simulated seawater

Constituent	Ocean Salinity (35g/1000g)		Simulated Salinity (115g/1000g)	
	Percentage	PPM	Percentage	PPM
Chloride	55.04	19,350	46.22	70525
Sodium	30.61	10760	29.13	44460
Sulfate	7.68	2710	6.55	9990
Magnesium	3.69	1290	1.70	2592
Calcium	1.16	410	0.17	260
Potassium	1.10	400	0.16	247
Total	99.28	34920	83.93	128074

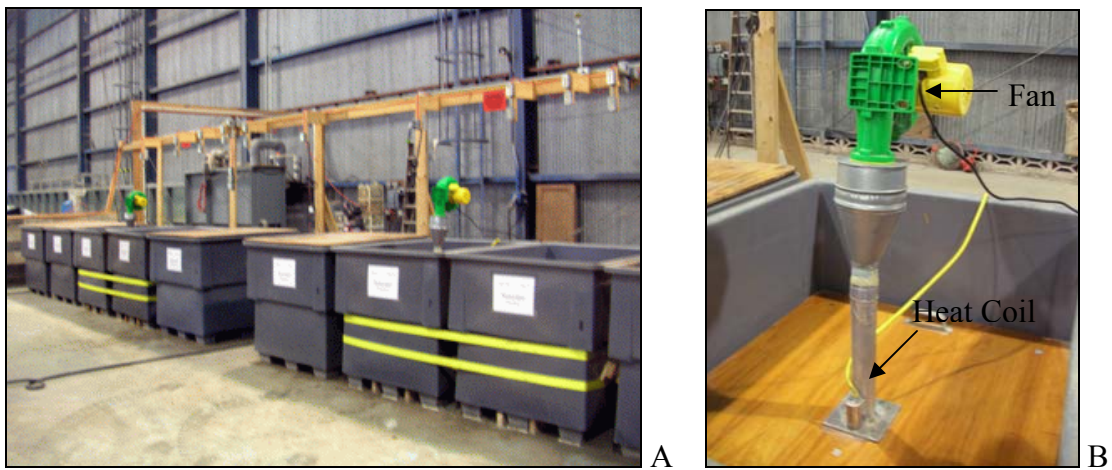


Figure 4-4. New wet/dry environmental exposure conditioning. A) Exposure Tanks. B) Air blower/heater. C) Schematic diagram for new wet/dry system.

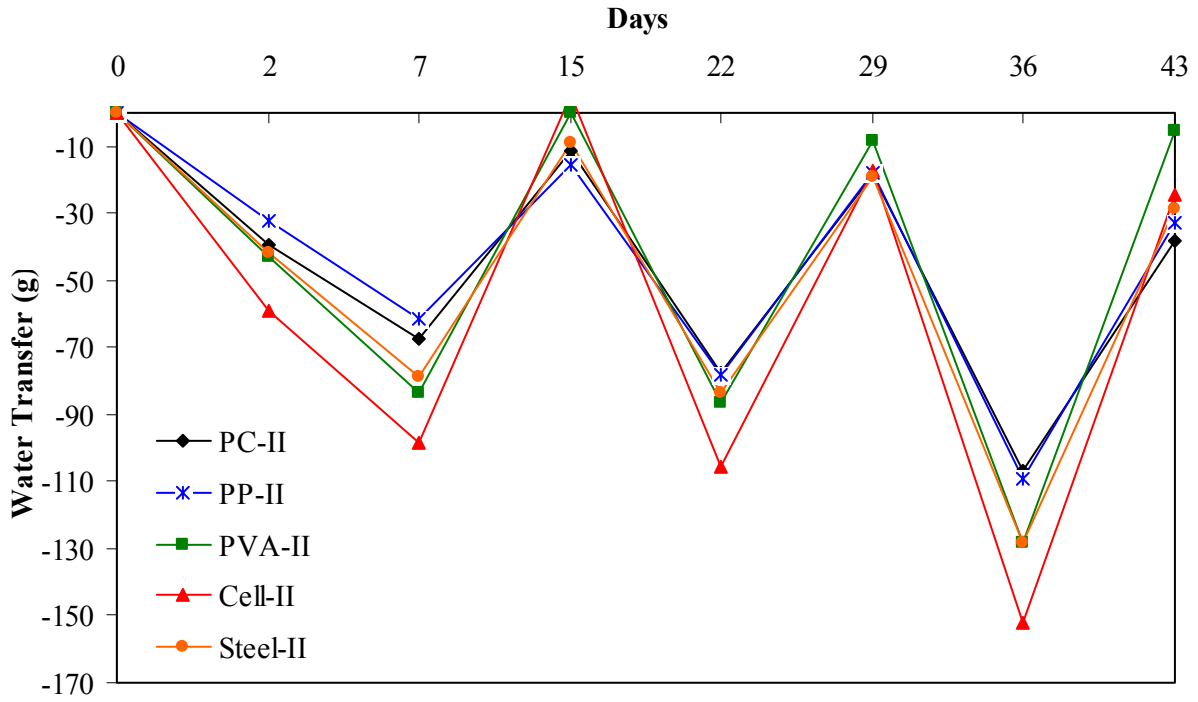


Figure 4-5. Moisture movement with new wet/dry conditioning for limewater wet/dry for Class II concrete

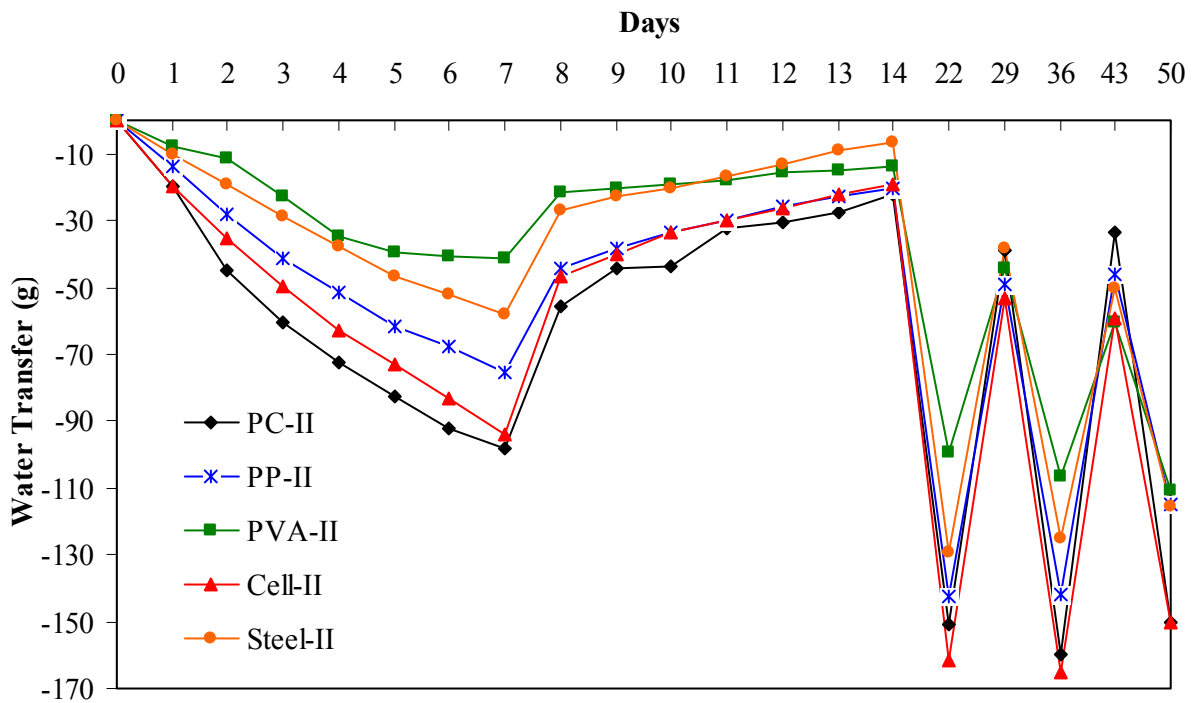


Figure 4-6. Moisture movement with new wet/dry conditioning for saltwater wet/dry for Class II concrete

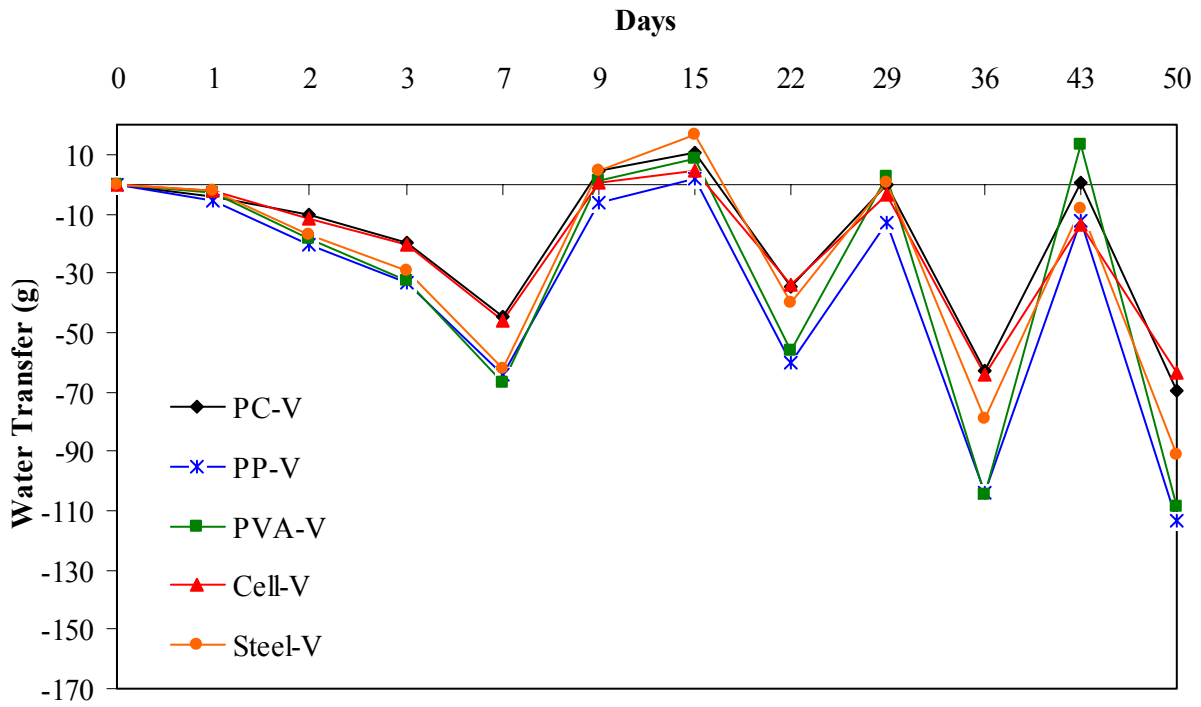


Figure 4-7. Moisture movement with new wet/dry conditioning for limewater wet/dry for Class V concrete

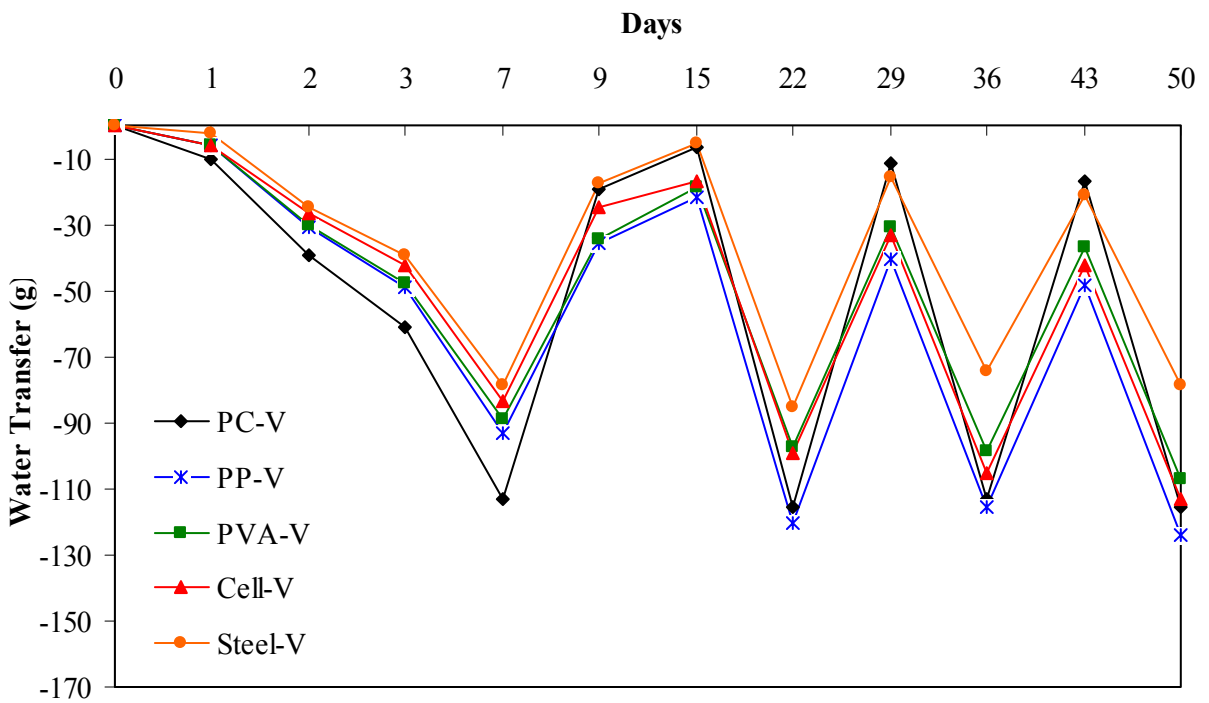
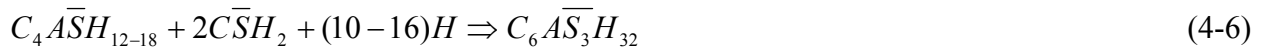


Figure 4-8. Moisture movement with new wet/dry conditioning for saltwater wet/dry for Class V concrete

#### 4.4 Deterioration Mechanism

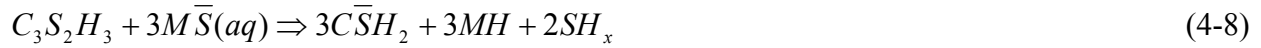
The expected deterioration mechanisms for salt water immersion, cyclic wetting and drying, and acidic solutions are summarized in Figure 4-9. Sulfate ions in salt water can attack the hydration products of cement paste, resulting in the degradation of the paste itself (Mindess et al., 2003). When the amount of  $C_3A$  is equal to or less than 5% in Portland cement, and the gypsum is approximately 5%, the hydration reaction converts all of the  $C_3A$  to ettringite ( $C_3\overline{AS}_3H_{32}$ ). However, the AASHTO cement type II used in this study contains 6.16%  $C_3A$  so that monosulfate hydrate ( $C_3\overline{ASH}_{12-18}$ ) can be produced as the additional hydration product. The chemical reactions with  $C_3A$  and monosulfate hydrate ( $C_3\overline{ASH}_{12-18}$ ) when the cement paste comes in contact with  $SO_4^{2-}$  convert to ettringite ( $C_3\overline{AS}_3H_{32}$ ) in the presence of  $CH$  (Cohen et al, 1993; Tian, 1998):



The formation of ettringite related to the needle-like formation of the crystal can produce expansion forces and cracks in concrete. The formation of cracks influences transport characteristics, by essentially providing large pathways resulting in the acceleration of chemical ions into concrete.

Sulfate attack also generates progressive damage resulting in the loss of strength and loss of mass due to degradation of the cement hydration products. The most commonly available hydration products of cement paste,  $CH$  and  $C-S-H$  gel, may be transformed to gypsum as a result of sulfate attack (Cohen, 1993). The dissolution of  $CH$  happens when the pH decreases to below 12.5 whereas the dissolution of  $C-S-H$  gel begins at below pH 8.8 (Metha, 2005). The

sulfate attack resulting from Magnesium sulfates is typically a more aggressive attack due to the destruction of the *C-S-H* and the calcium sulfoaluminates (Mindess et al, 2003):



The steel fibers distributed in concrete are naturally protected by the protective oxide film on the fiber surface due to the presence of alkalinity of the concrete in pore water. However, chlorides in pore space cause a local breakdown of the passivation film on the steel fibers, so that the localized corrosion can subsequently occur and increased volume from active corrosion leads to expansion forces or microrcracking in the concrete (Mindess et al., 2003). The degradation of FRC by acidic solutions will result in a different deterioration process. The hydrogen ions in solutions will accelerate the leaching of calcium hydroxide by causing efflorescence and increasing permeability (Mehta et al., 2005). The *C-S-H* gel, naturally weak due to its micro-porosity structure may also be dissolved by acid attack when the hydrogen ions are highly accumulated. In addition, the hydration products of cement paste, limestone, and fibers exposed to acidic solutions will be expected to have dissolution or loss of mass.

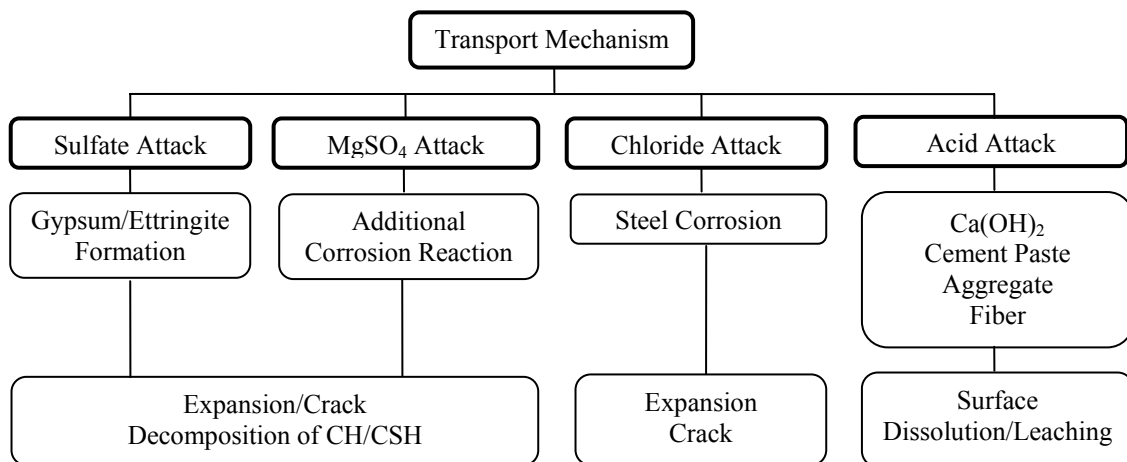


Figure 4-9. Expected deterioration mechanism

## CHAPTER 5 FINDINGS AND ANALYSIS

### 5.1 Introduction

This chapter describes and discusses test results of laboratory investigations of fresh properties, transport properties, mechanical properties, and evaluation of degraded specimens on beam tests based on visual inspection, permeable pore space change, carbonation, and SEM analysis.

### 5.2 Fresh Properties Test Results

A comprehensive summary of test results can be found in appendix A (Tables A-1 and A-2). A more succinct summary of findings is presented in the sections below.

#### 5.2.1 Slump Test Results

The test results for both concrete Classes are shown in Figures 5-1 and 5-2. These figures demonstrate the reduction of fresh mix workability due to the introduction of fibers. The reduction range for each fiber was 7.0-4.5 in. for PP, 5.50-4.25 in. for PVA, 3.50-1.25 in. for cellulose, and 4.75-2.50 in. for steel fibers. It was noted that the introduction of cellulose fiber for concrete Class II resulted in the lowest slump loss (reduction in slump relative to the control mix) implying non-uniform fiber distribution or fiber balling in the mixture.

#### 5.2.2 Inverted Slump Cone Test Results

The results of inverted slump cone time are shown in Figure 5-3. The addition of fibers definitely requires more time to make the stiffer fiber mixtures flow. The cellulose fibers indicated the lowest time, one again indicating the fiber's non-uniform distribution within the mixture. It is noted that the higher the slump loss, the longer the time to make the fiber mixes flow, which is consistent with the greater amount of energy required.

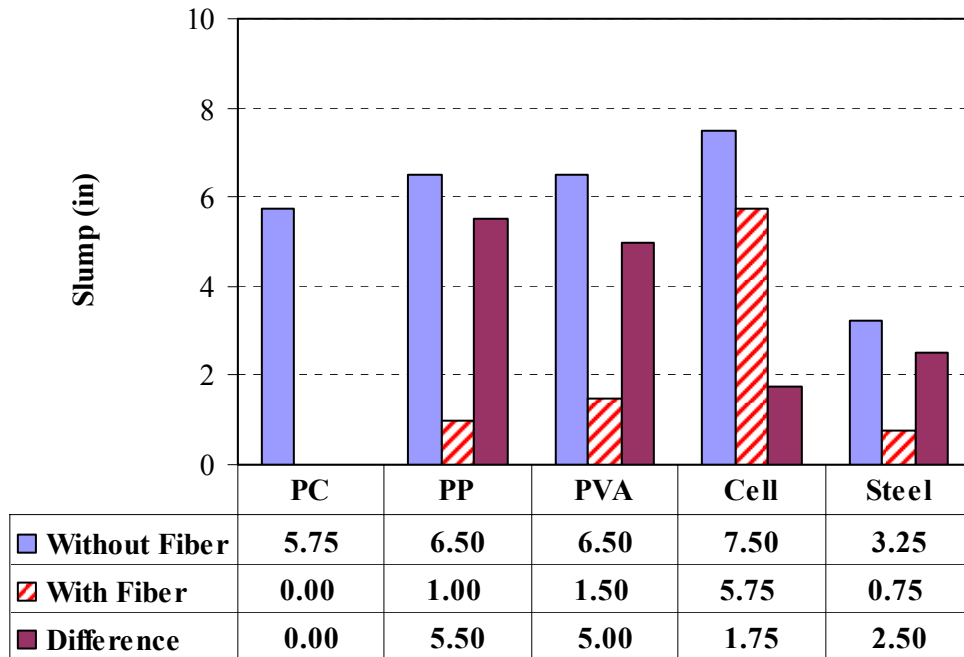


Figure 5-1. Slump test results for Class II concrete

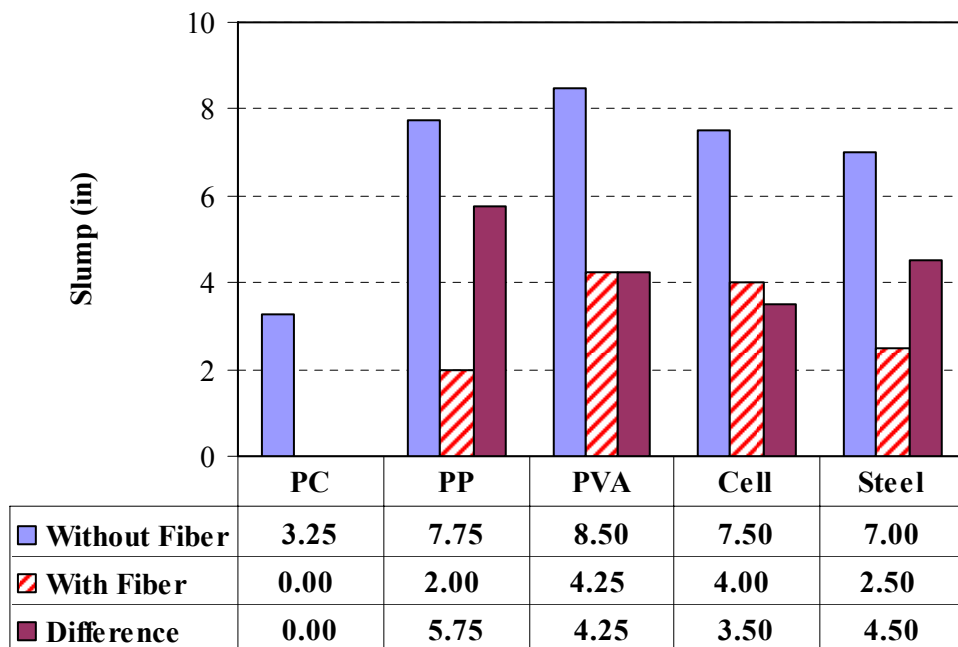


Figure 5-2. Slump test results for Class V concrete

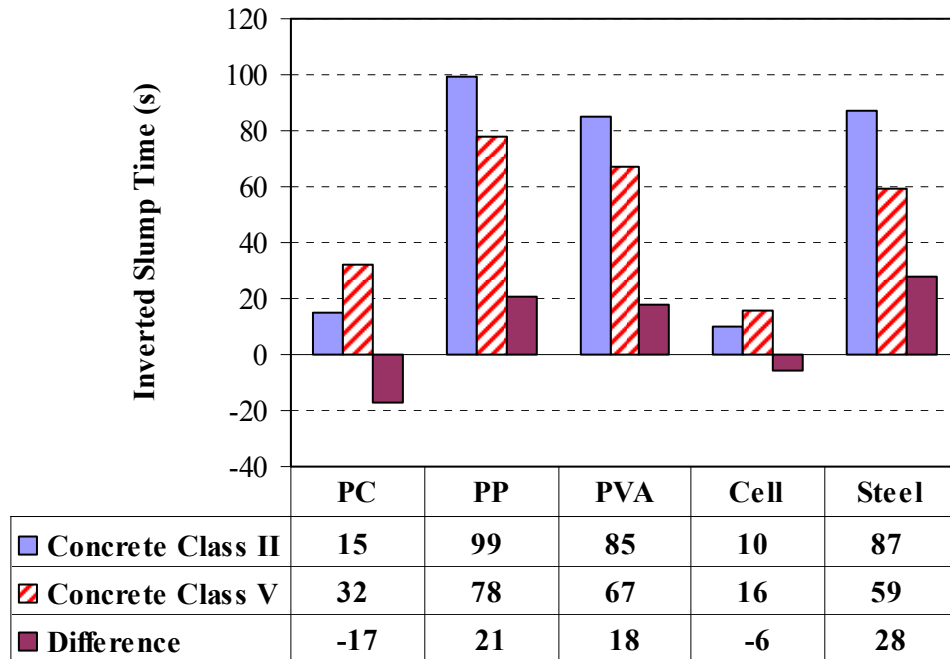


Figure 5-3. Inverted slump cone time test results for Classes II/V concrete

### 5.2.3 Vebe Test Results

The test results of Vebe time are shown in Figure 5-4. Although it requires less time than the inverted slump cone test, the test results are very similar to that of inverted slump cone time (Figure 5-3). It was observed that there was significant decrease of workability of the concrete upon the addition of PP, PVA, and hooked Steel fibers.

### 5.2.4 Air Content Test Results

Figures 5-5 and 5-6 indicate that there were slight differences in the air content resulting from the addition of PP, PVA, cellulose and steel fibers. However, these small differences are likely within measurement error and do not appear to be sufficient to justify any observed differences in concrete performance.

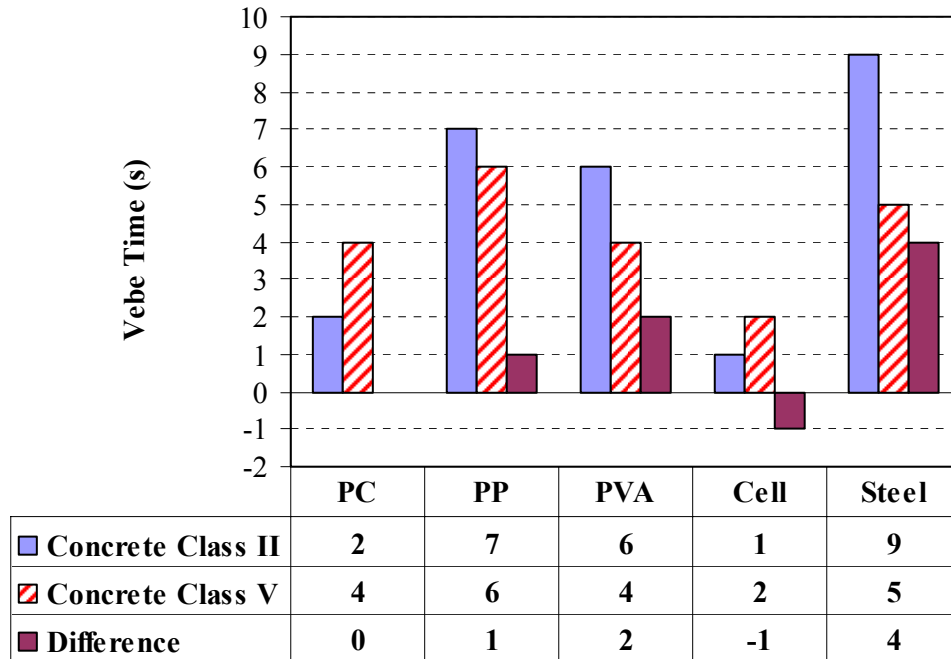


Figure 5-4. Vebe time test results for Classes II/V concrete

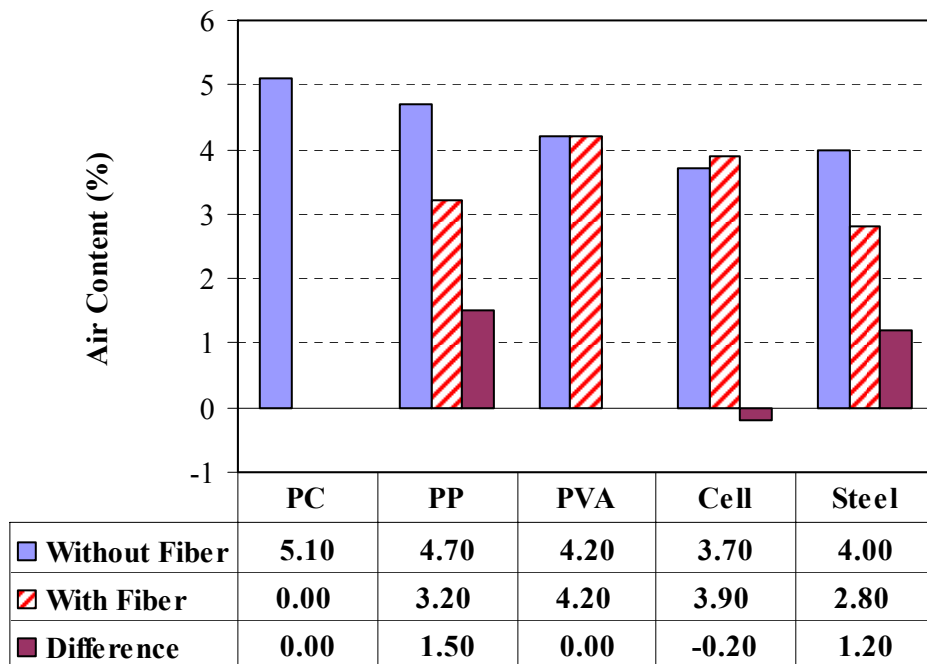


Figure 5-5. Air content test results for Class II concrete

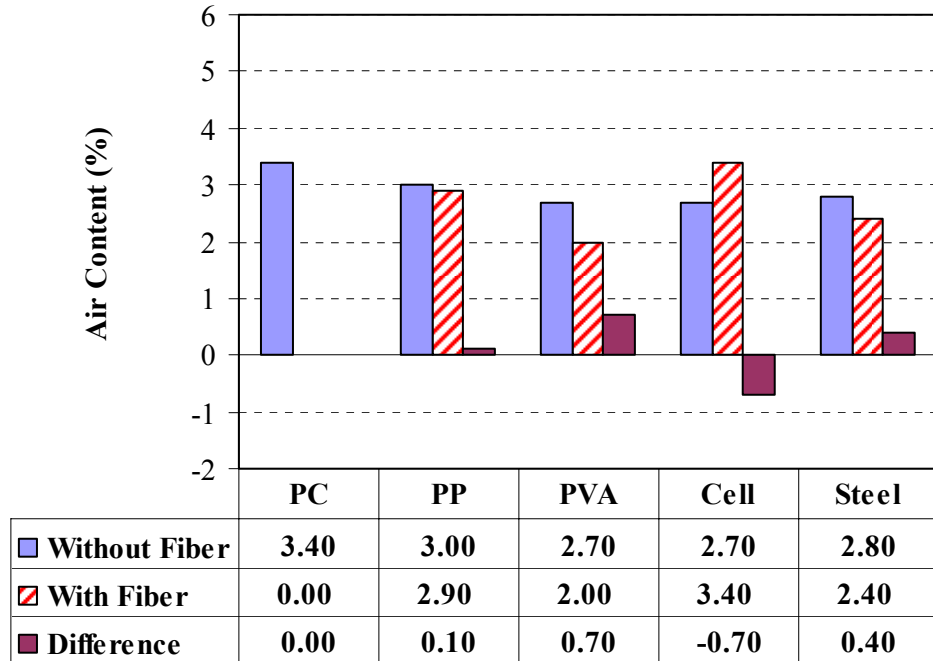


Figure 5-6. Air content test results for Class V concrete

### 5.2.5 Relationships between Workability Tests

The relationship between conventional slump values and inverted slump cone time is presented in Figure 5-7. As expected, the slump was inversely proportional to the inverted slump cone time and the fibers with lowest slump require longer times. Similar test results for Vebe time versus slump are shown in Figure 5-8. The relationship illustrating direct proportionality between the inverted slump cone and Vebe time is presented in Figure 5-9. These results are completely consistent with fresh property test results reported by ACI committee 544.

Both inverted slump cone and Vebe time test methods are more accurate for measuring workability of FRC than the conventional slump test, but the inverted cone test exhibited the greatest sensitivity between workability of different fiber types and involves less expensive equipment. Therefore, the inverted slump cone test is recommended for measurement of workability of FRC.

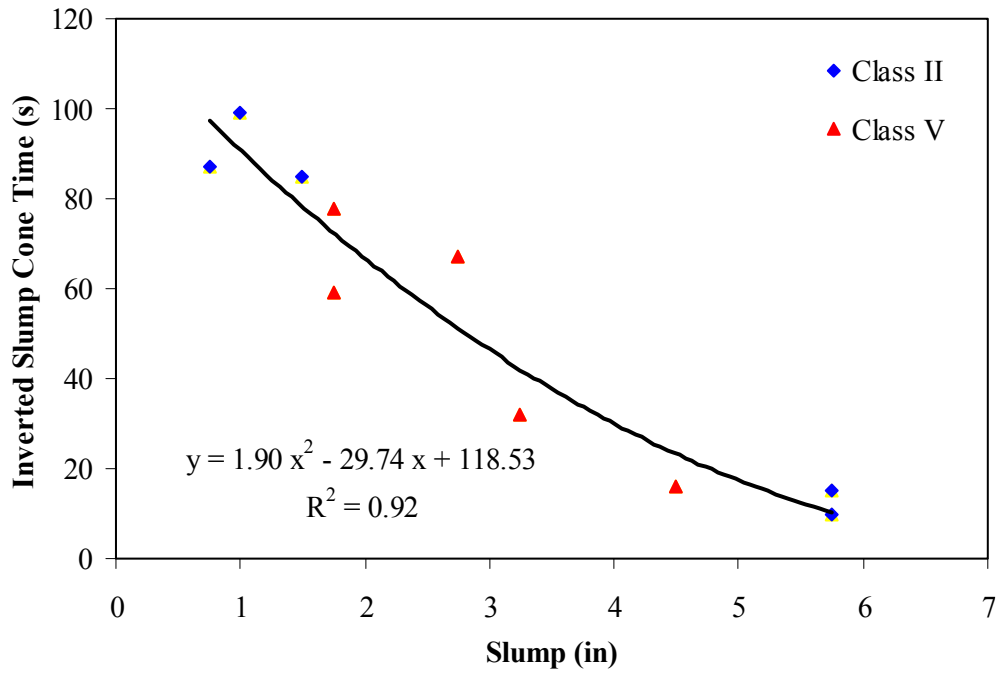


Figure 5-7. Inverted slump cone time vs. slump

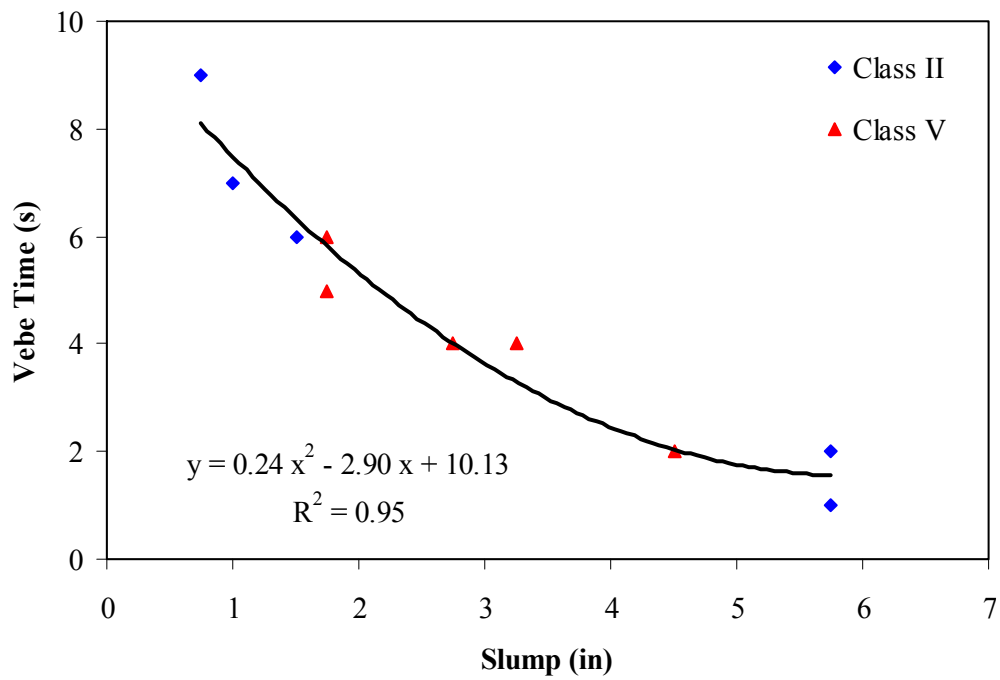


Figure 5-8. Vebe time vs. slump

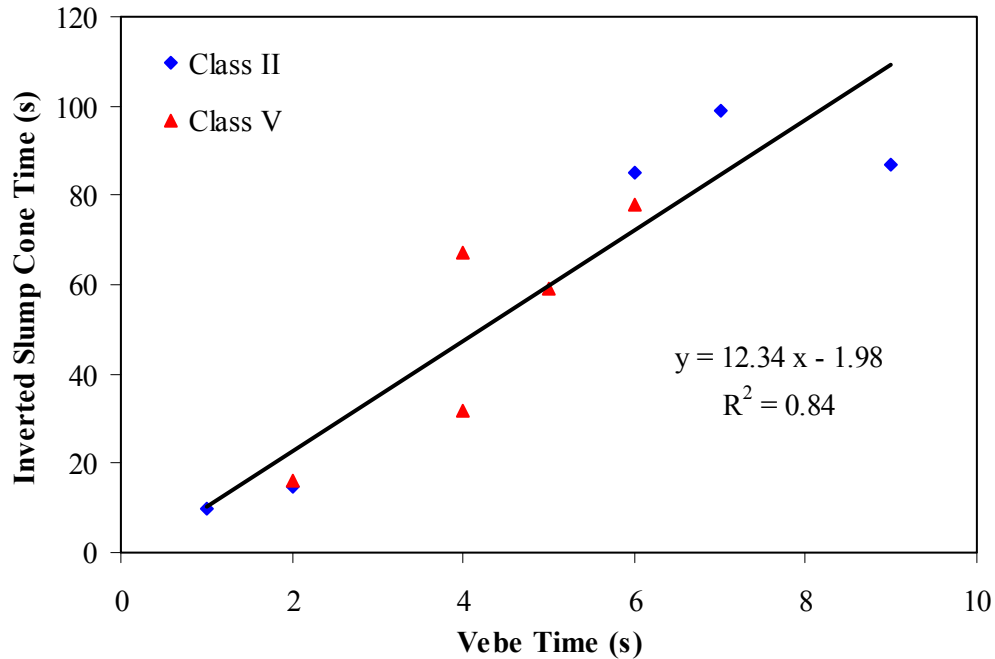


Figure 5-9. Inverted slump cone time vs. Vebe time

### 5.3 Transport Property Test Results

An experimental program was performed examining the effects of fiber and fiber type on transport characteristics of hardened concrete. Permeable pore space, permeability, absorption and chloride diffusion tests were used as representatives of the hardened physical transport properties. A comprehensive summary of test results can be found in the Appendixes B through F. A more succinct summary of findings is presented in the sections below.

#### 5.3.1 Permeable Pore Space Test Results

The permeable pore space changes due to the addition of different types of fibers to concrete were tested at 28 days. Test results for permeable pore space from the addition of fibers are shown in Figures 5-10, 5-11, and 5-12. The addition of PP and PVA fibers for both concrete Classes slightly increased permeable pores in concrete compared with both control mixes and control specimens cast before adding fibers. On the other hand, steel fiber mixes showed reduced

permeable pores for Class II concrete, but no effect or a slight increase in permeable pores for Class V concrete. However, cellulose fibers showed no significant effect on permeable pores in the hardened cement paste concrete. Generally, the addition of fibers in concrete had a small effect on an increase of permeable pore space.

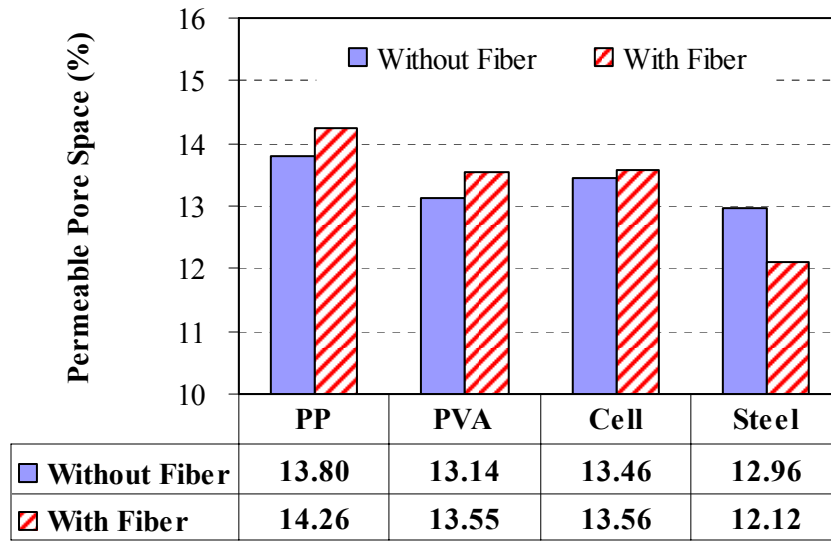


Figure 5-10. Permeable pore space for Class II concrete without/with fiber

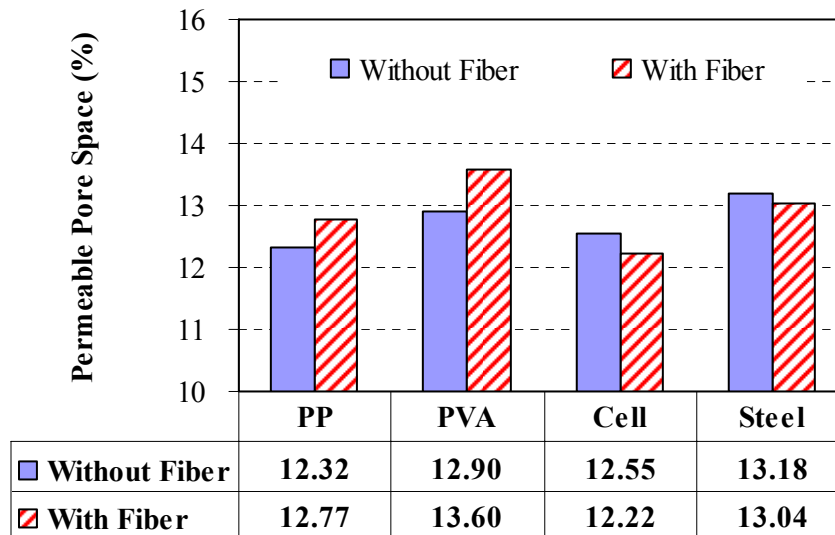


Figure 5-11. Permeable pore space for Class V concrete without/with fiber

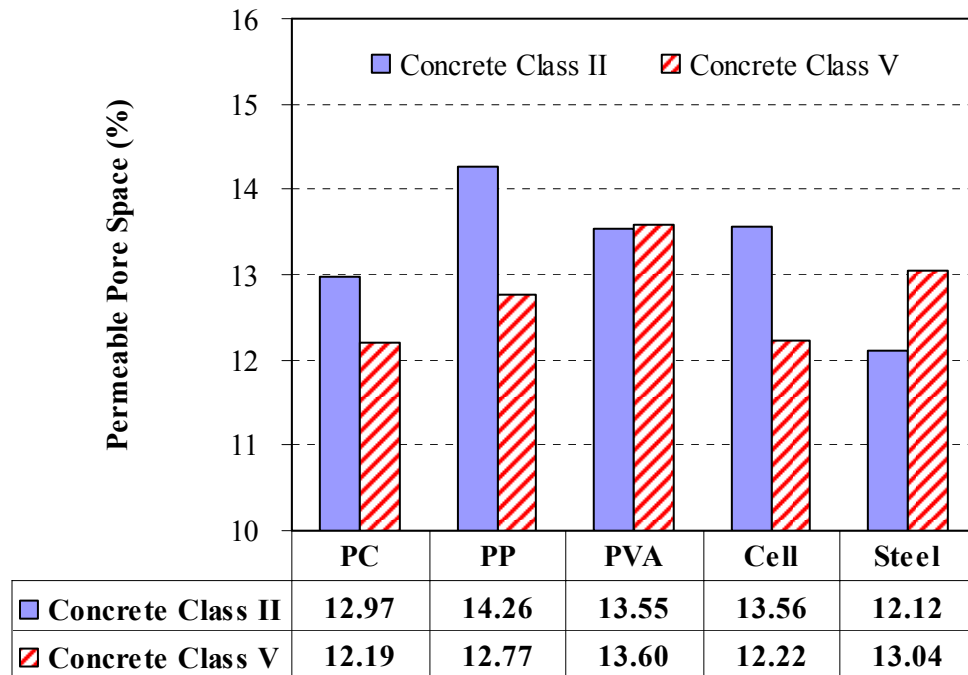


Figure 5-12. Permeable pore space for Classes II/V concrete

### 5.3.2 Surface Resistivity Test Results

Surface resistivity tests were performed for mixes with different types of fibers at the following times: 28, 56, 91, 182, 364, 540 and 730 days of 100% humidity curing. The effects of fiber and fiber type on penetration of chloride ions based on resistivity results are summarized as follows:

- Figure 5-13 shows surface resistivity measurements for Class II concrete. The surface resistivity of PP, PVA and cellulose fiber mixtures sharply increased after 91 days curing period and peaked at 1 year. After 1 year, the resistivity for permeability decreased and appeared to level out after 540 days. Among the fiber types, steel fibers, which are electrically conductive, had the lowest surface resistivity.
- Figure 5-14 shows surface resistivity measurements for Class V concrete. There were no sharp increases in the surface resistivity of PP and PVA. Resistivity of cellulose fibers peaked at 1 year. Once again, steel fibers showed the lowest surface resistivity.
- All fiber mixtures including both concrete Classes showed high possibility for chloride ion permeability from concrete surface according to the criterion indicated in Table 3-10.

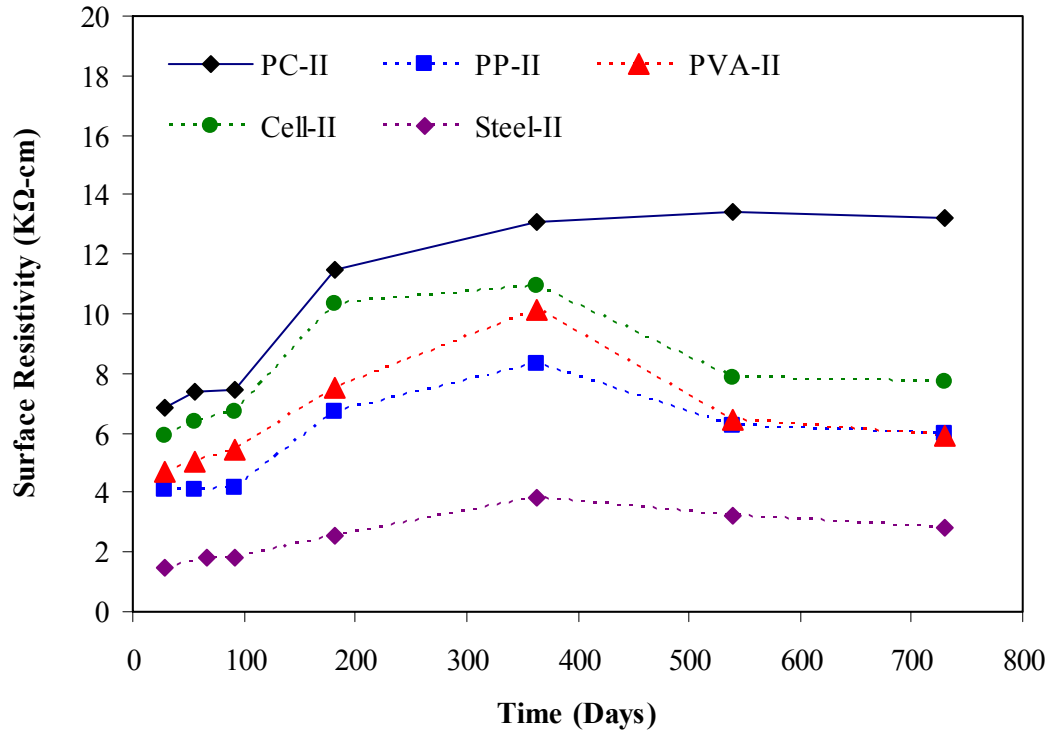


Figure 5-13. Surface resistivity for Class II concrete

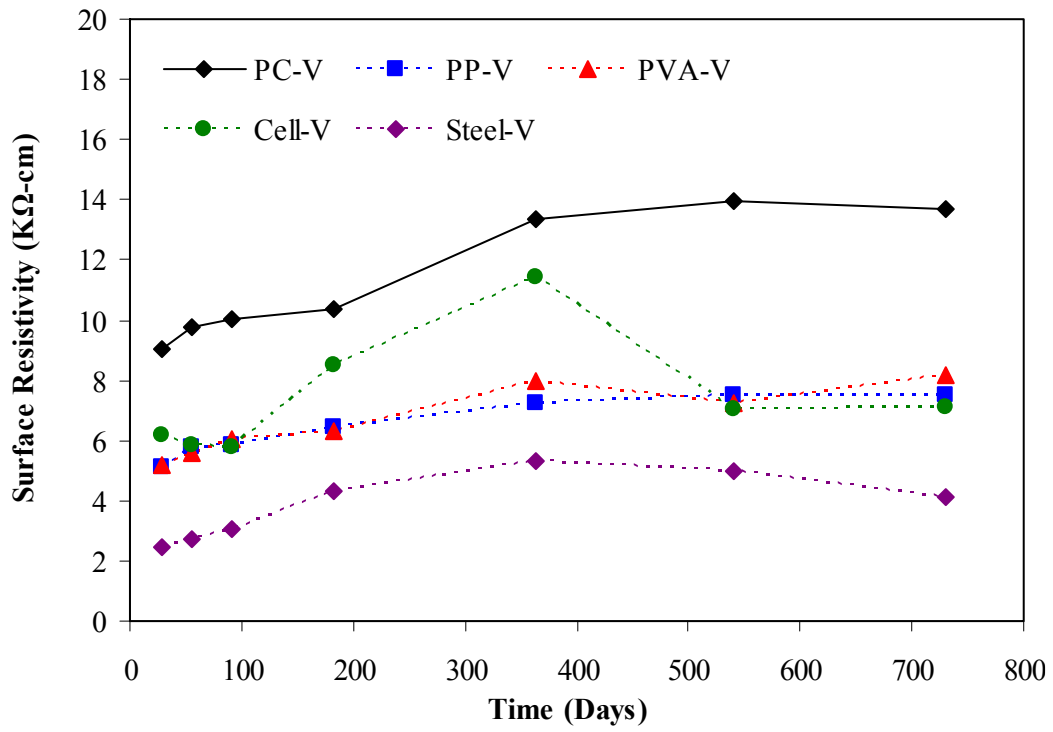


Figure 5-14. Surface resistivity for Class V concrete

### 5.3.3 Permeability Test Results

The calculated water permeability coefficients of each kind of FRC mixture on hardened concrete at 28 days of age were examined to determine the effects of fiber and fiber type on the permeability characteristics of FRC. Test results are summarized as follows:

- Figures 5-15 and 5-16 indicate the effects of water permeability for with/without fiber in the same mixture. The addition of PP and PVA fibers for both concrete Classes showed no significant effect on coefficient of permeability. Among the fiber types, the steel fibers showed the highest reduction in water permeability for Class II concrete.
- Figure 5-17 shows the effect of fiber type on permeability for each concrete Class. The addition of polypropylene fibers showed no significant effect on coefficient of water permeability for both concrete Classes. The incorporation of polyvinyl alcohol fibers into the mixture showed no effect on water permeability for Class II concrete, but exhibited some reduction for Class V concrete. Among the fiber types, introduction of hooked-end steel fibers resulted in the greatest reduction for both concrete Classes.
- Among the fiber types, the use of hooked-end steel fibers showed the most consistent results in comparison with control mixes and control specimens prepared before adding fiber and has the highest resistance to water permeability in concrete. The addition of cellulose fiber generally showed higher permeability, which implies non-uniform distribution of fibers in concrete.

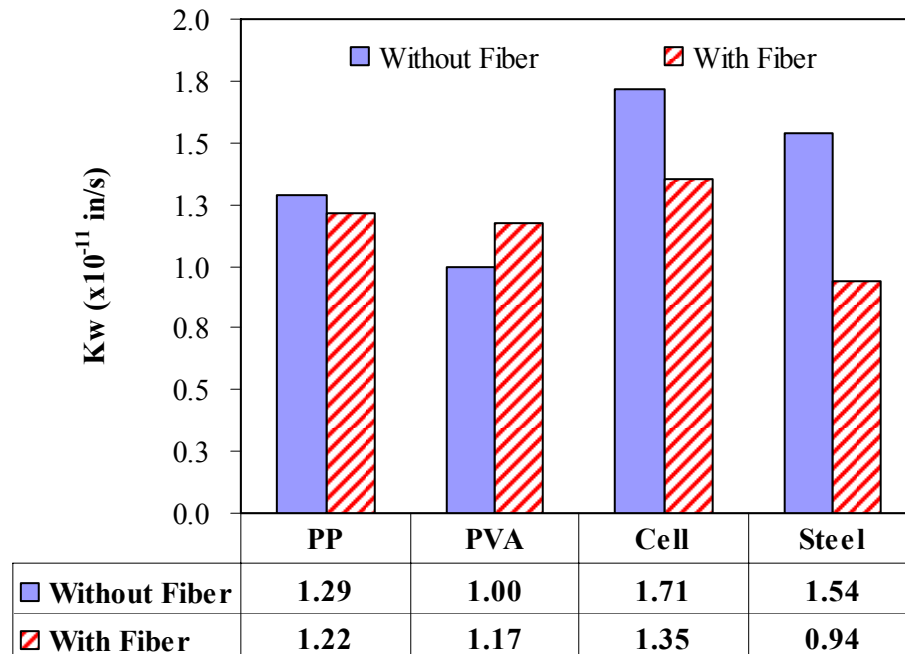


Figure 5-15. Coefficient of permeability for Class II concrete with/without fiber

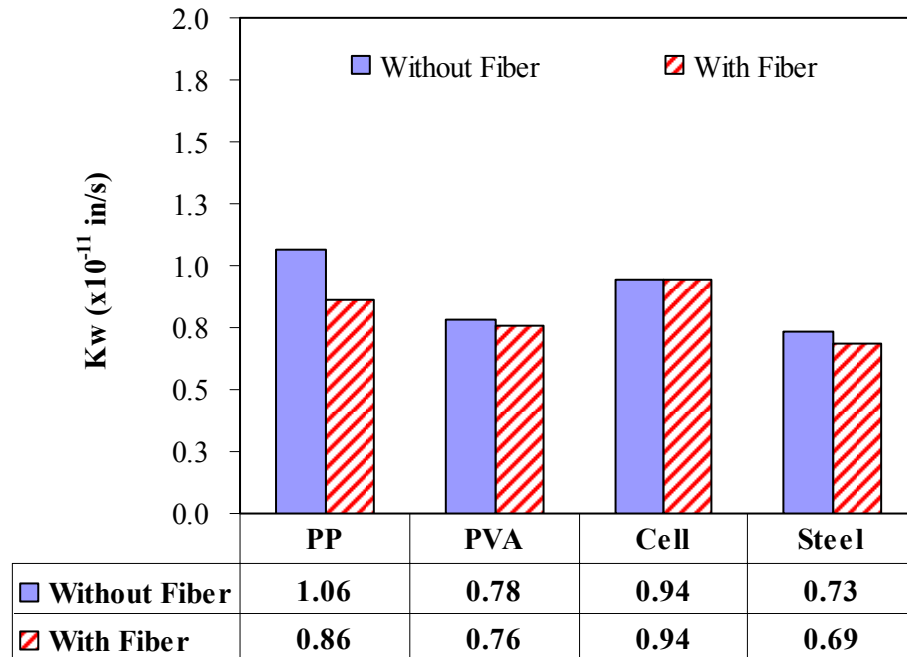


Figure 5-16. Coefficient of permeability for Class V concrete with/without fiber

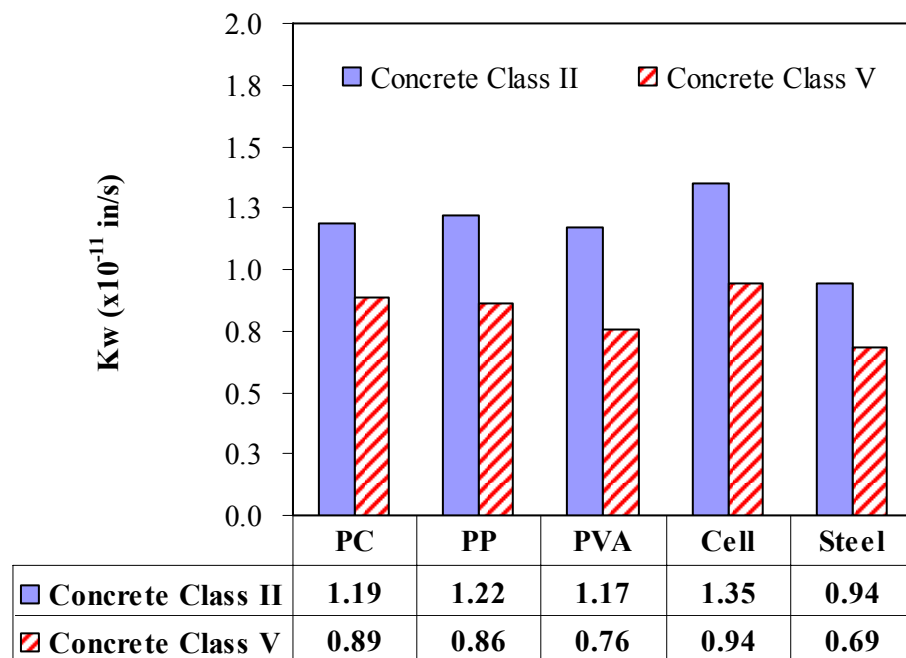
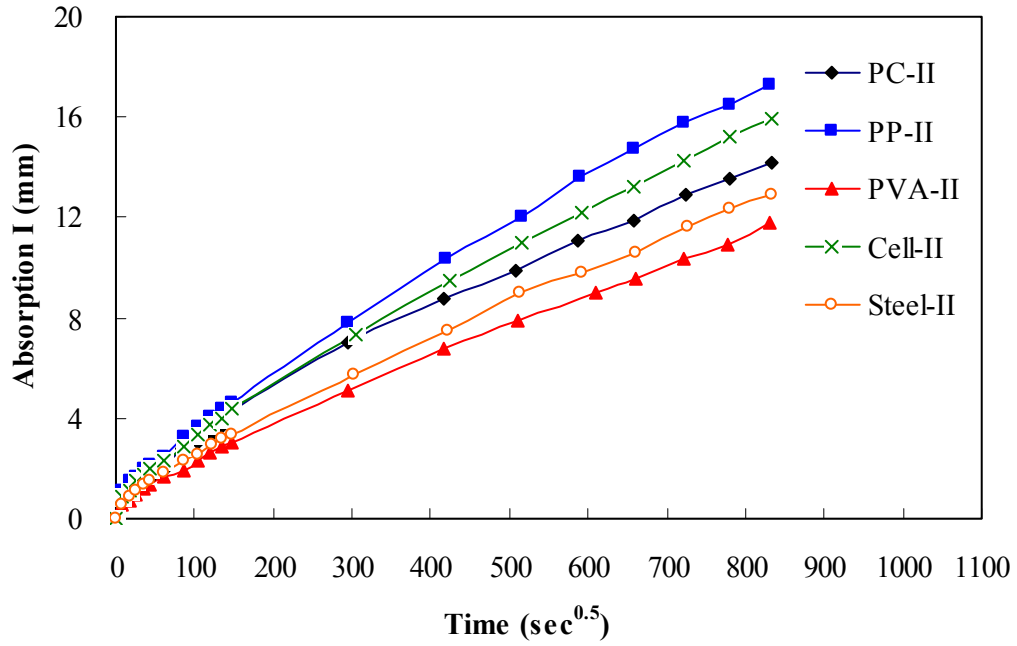


Figure 5-17. Coefficient of permeability for Classes II/V concrete

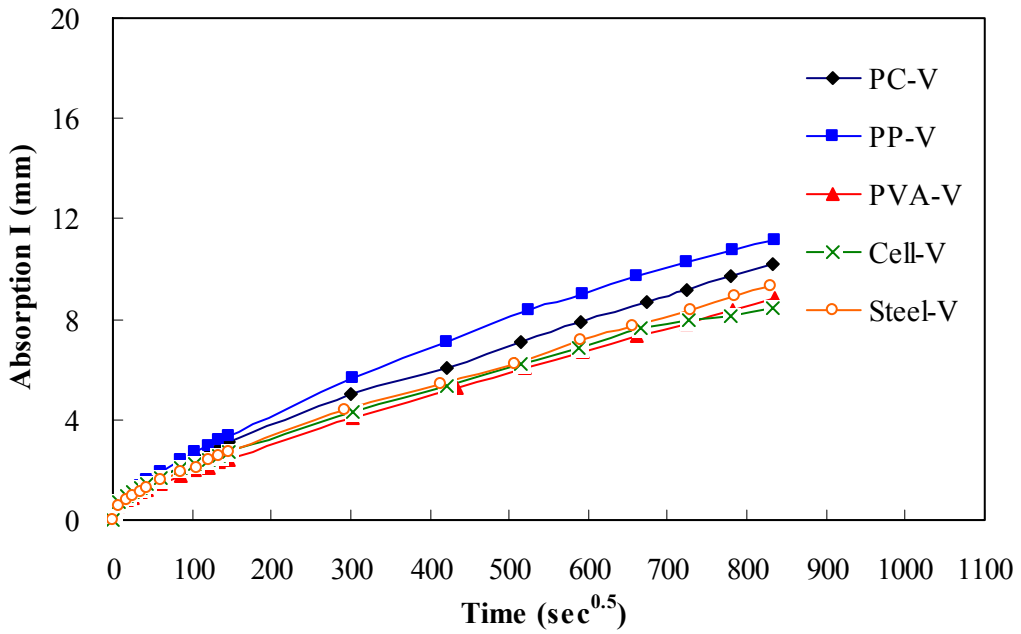
### 5.3.4 Absorption Test Results

The absorption rate changes due to the addition of fiber and fiber type were examined at 28 days curing. Test results are summarized as follows:

- Figure 5-18 presents typical examples of absorbed water versus square root of time for each mixture. The absorption rates for each Class of concrete were linearly proportional to square root of time. Among the fibers, PVA and hooked-end steel fibers showed the best resistance to capillary action for each concrete Class. However, PP fibers for both concrete Classes indicated the fastest rate of absorption for both initial and secondary time periods compared to the control and other fibers.
- Figures 5-19 and 5-20 compare absorption rate changes between mixtures with and without fiber. The addition of PP fibers showed significant increase in absorption rate for both concrete Classes. The addition of PVA fibers slightly increased the absorption rate for Class II concrete, but showed no significant change for Class V concrete. The use of cellulose fiber slightly increased capillary action rate for both concrete Classes. The addition of steel fibers showed no significant effect on Class II concrete, but indicated a higher absorption rate for Class V concrete.
- Figures 5-21 and 22 show the effect of fiber type on absorption for each concrete Class. The addition of PP fibers showed a significant increase in absorption rate for both concrete Classes, but the incorporation of PVA and steel fibers reduced the absorption rate for both concrete Classes.
- The addition of PP fibers, which showed greater absorption than other fibers, significantly accelerated mass transport of water into concrete. The elongated interfacial transition zone from the addition of PP fibers, which are relatively thin and long and hydrophobic in nature, might act as a route of ingress for mass transport of water between the fiber and the hardened cement paste matrix. However, the addition of PVA and steel fibers generally showed higher resistance to mass transport of water than control specimens, implying relatively strong bonding which blocks water travel between the fiber and the hardened cement paste matrix. However, the effect of cellulose fibers in absorption was not clear because of inconsistent test results.

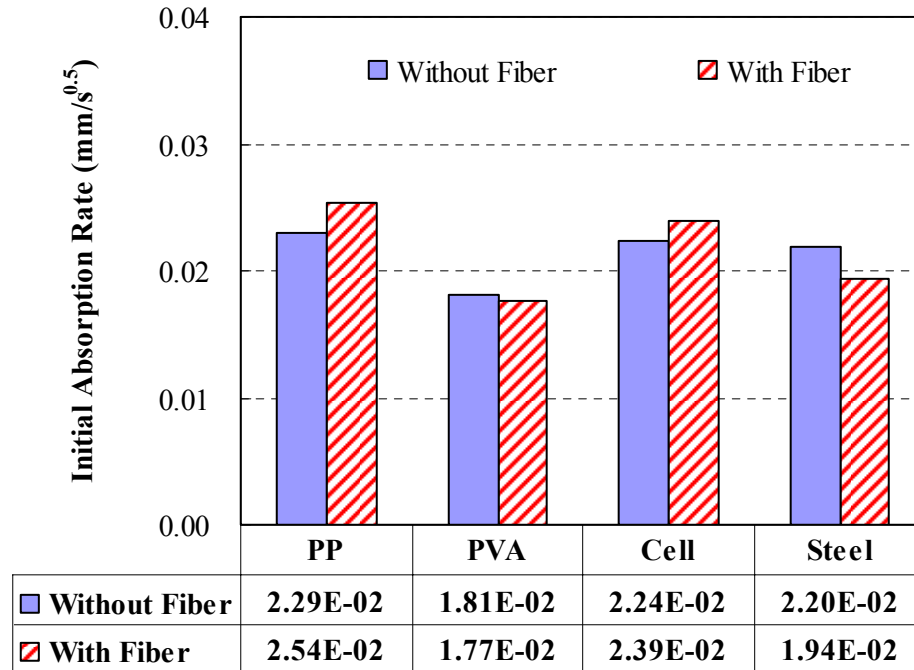


A

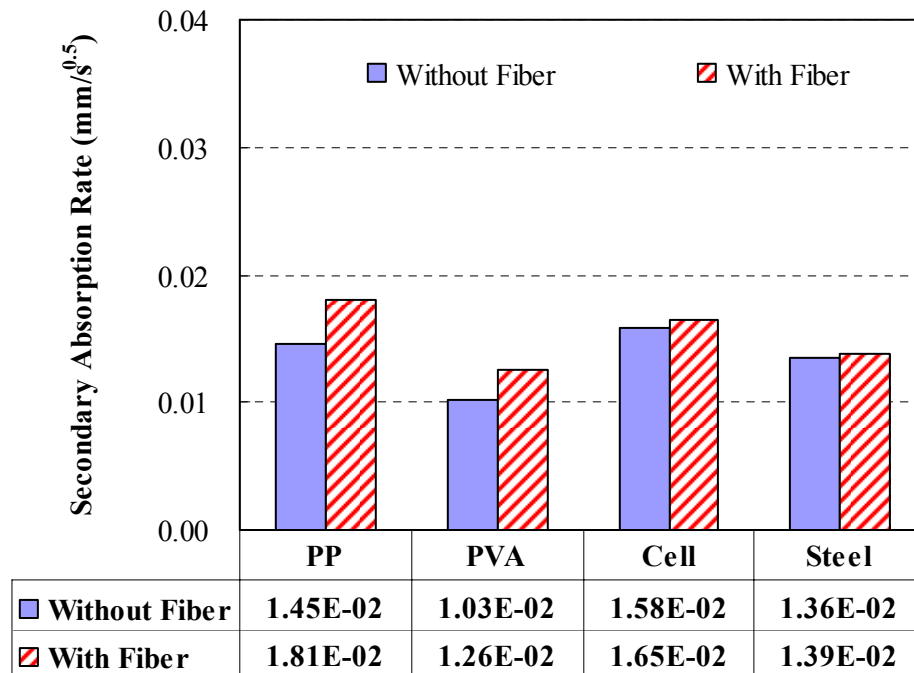


B

Figure 5-18. Absorption vs. time for Classes II/V concrete. A) Class II concrete. B) Class V concrete.

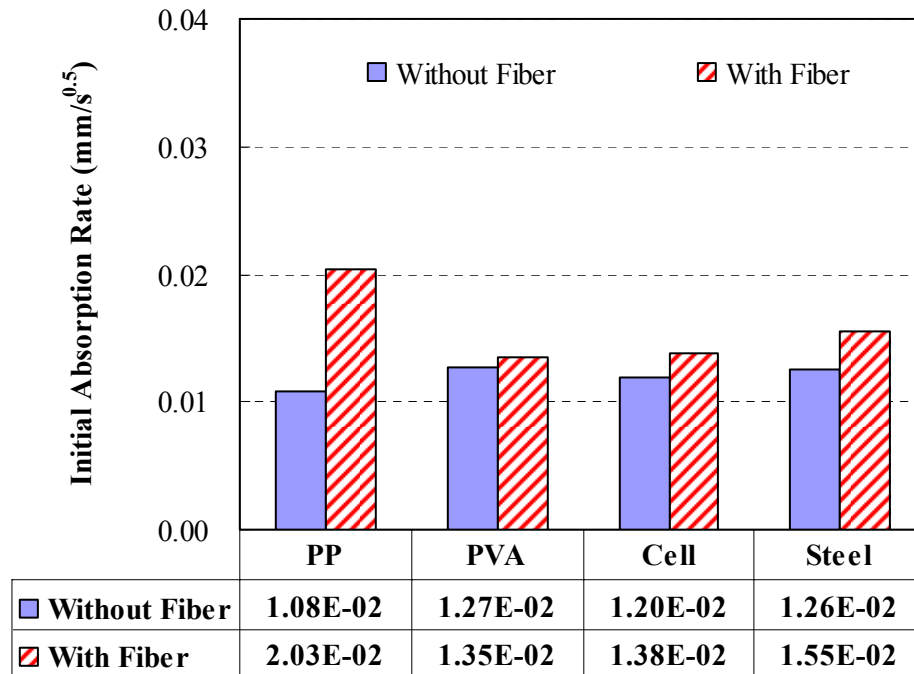


A

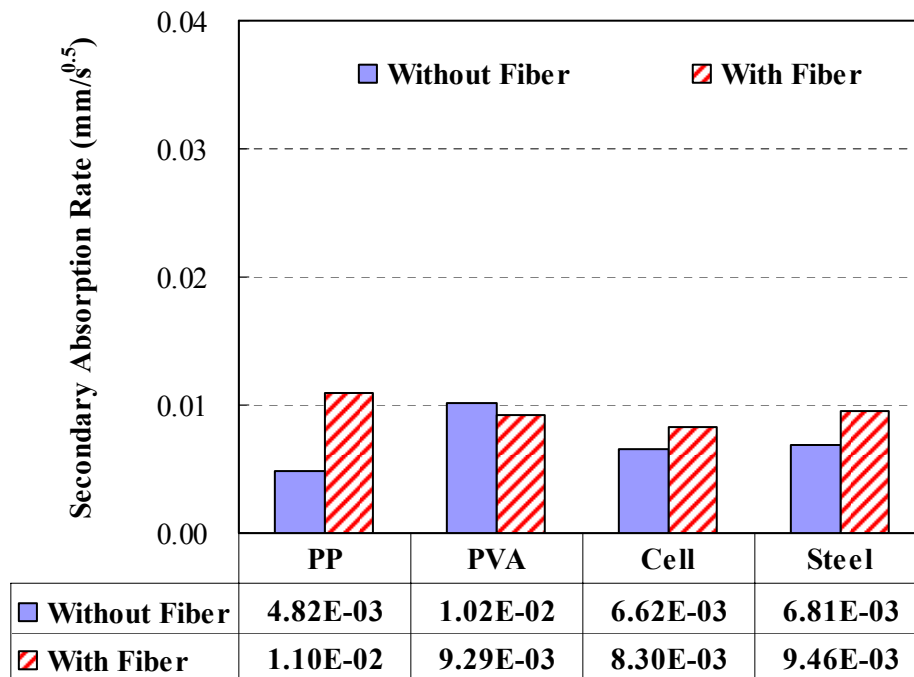


B

Figure 5-19. Absorption rate for Class II concrete with/without fiber. A) Initial absorption rate. B) Secondary absorption rate.



A



B

Figure 5-20. Absorption rate for Class V concrete with/without fiber. A) Initial absorption rate. B) Secondary absorption rate.

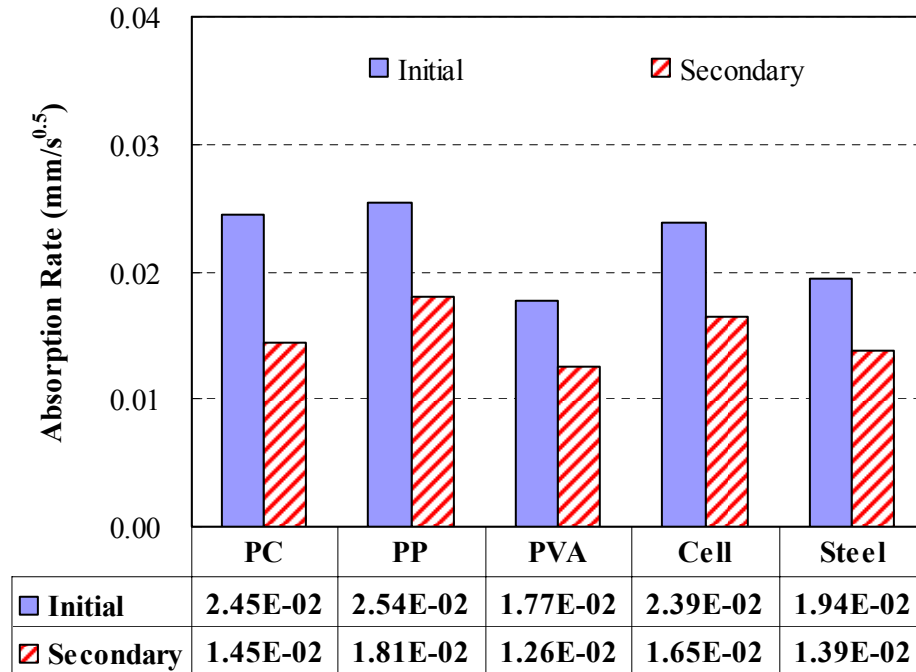


Figure 5-21. Absorption rate for Class II concrete

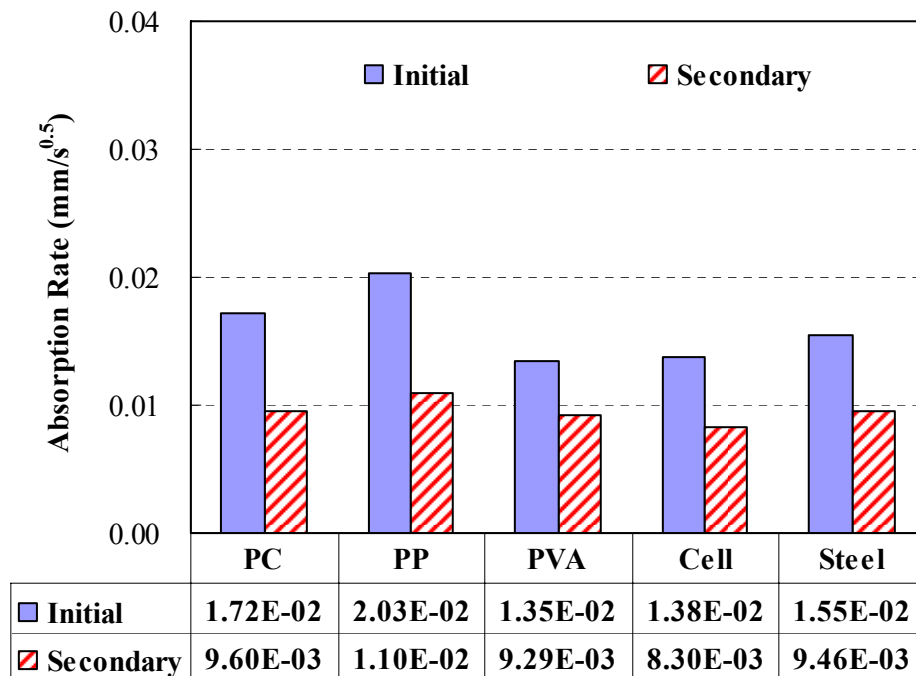


Figure 5-22. Absorption rate for Class V concrete

### 5.3.5 Bulk Diffusion Test Results

The coefficients of chloride diffusion on hardened concrete at 365 days were examined.

Test results are summarized as follows:

- Figure 5-23 and 5-24 show typical examples of the chloride concentration profiles in pounds per cubic yard for Class II and V concrete. This figure illustrates that concrete mixture containing fibers had lower rates of the chloride diffusion when compared to concrete without fiber. Considerable reductions of chloride concentration for both concrete Classes were observed beyond the first layer. The hooked-end steel fiber exhibited the lowest chloride content in the fiber composite.
- Test results for the bulk diffusion were analyzed to get the best fit curve for the chloride coefficients by using Crank's solution to Fick's second law. Figure 5-25 shows the coefficients of chloride diffusion for each fiber type. The addition of PP fibers slightly increased the coefficient of chloride diffusion for concrete Class II. The PVA fibers decreased the coefficient of chloride diffusion for Class II concrete, but not for Class V concrete. The use of cellulose fiber showed no effect on Class II concrete, but significantly increased the coefficient of chloride diffusion for Class V concrete. The steel fibers exhibited the greatest reduction of chloride diffusion for both concrete Classes.
- Generally, the addition of PVA and steel fibers reduced the chloride coefficient and had a positive effect on resistance to chloride diffusion in concrete. Among the fiber types, steel fibers had the greatest resistance to chloride diffusion through the pore structure.

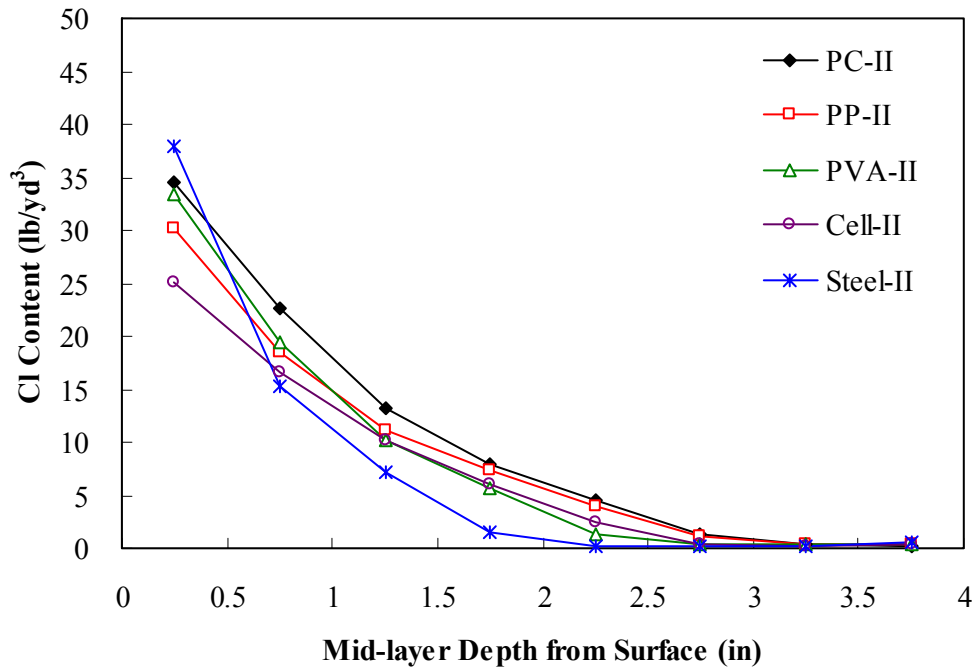


Figure 5-23. Chloride concentration for Classes II concrete

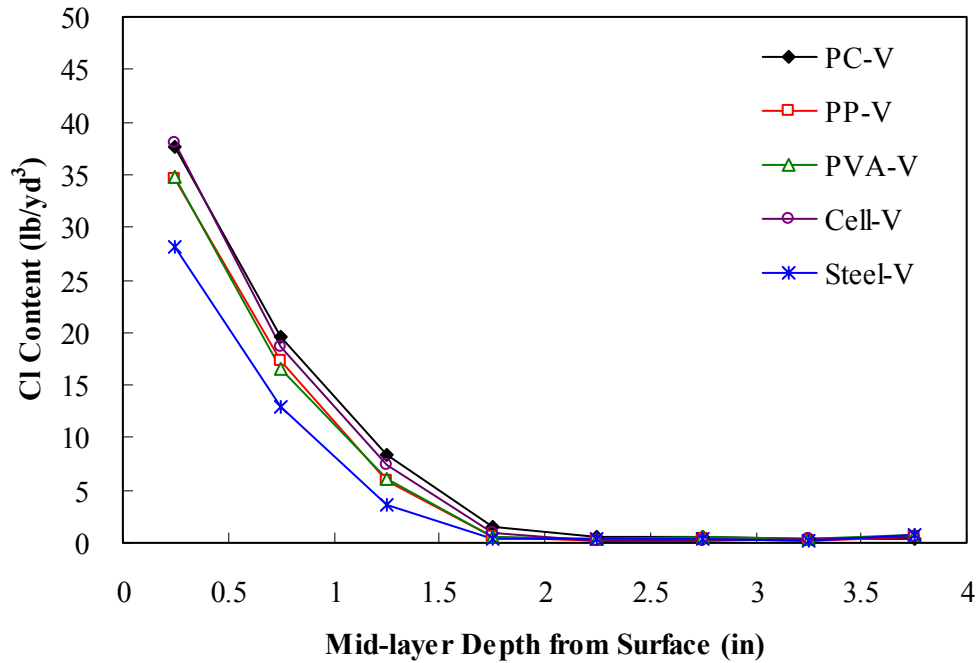


Figure 5-24. Chloride concentration for Classes II/V concrete

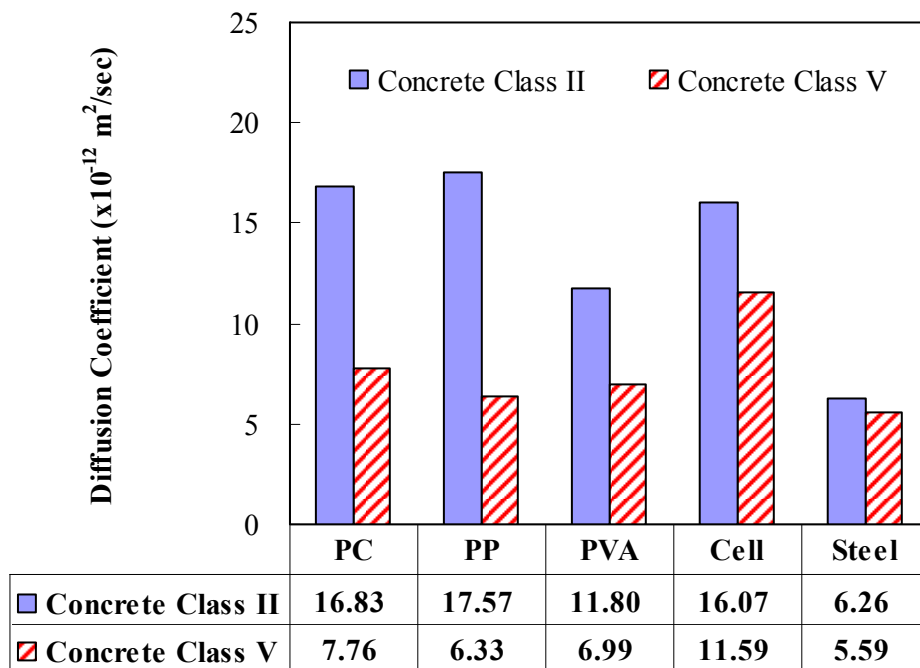


Figure 5-25. Coefficient of chloride diffusion for Classes II/V concrete

## **5.4 Mechanical Property Test Results**

An experimental program was performed to examine the effects of fiber and fiber type on mechanical properties of hardened concrete. Compression, splitting tension, and pressure tensile strength testing results were used to evaluate physical and mechanical properties of hardened concrete. A comprehensive summary of test results can be found in the appendix G. A more succinct summary of findings is presented in the following section.

### **5.4.1 Compressive Strength Test Results**

The experimental investigation for compressive strength tests is shown in Figure 5-26. The addition of PVA and steel fibers showed a small increase in the compressive strength for both concrete Classes. As expected, the addition of fibers did not affect peak strength.

### **5.4.2 Splitting Tensile Strength Test Results**

The splitting tensile test results for fiber and fiber type are shown in Figure 5-27. The addition of steel fibers showed a slight effect on the improvement of tensile strength for both concrete Classes.

### **5.4.3 Pressure Tension Test Results**

The experimental test results for pressure tension test are shown in Figure 5-28. Although the pressure tension test results have a similar trend in comparison with the splitting tensile strength test results, the reduction in strength of fiber mixes compared to plain concrete from pressurized gas was greater than for splitting tensile approach. However, these effects are almost certainly a result of the difference in specimen preparation. Plain concrete specimens were cast in cylinders, while FRC specimens were cored from slabs. The smoother, less permeable surface of the cast specimens required greater external pressure to achieve the same internal pressure as in the more open cored surfaces. This was the primary reason for the apparent difference in strength.

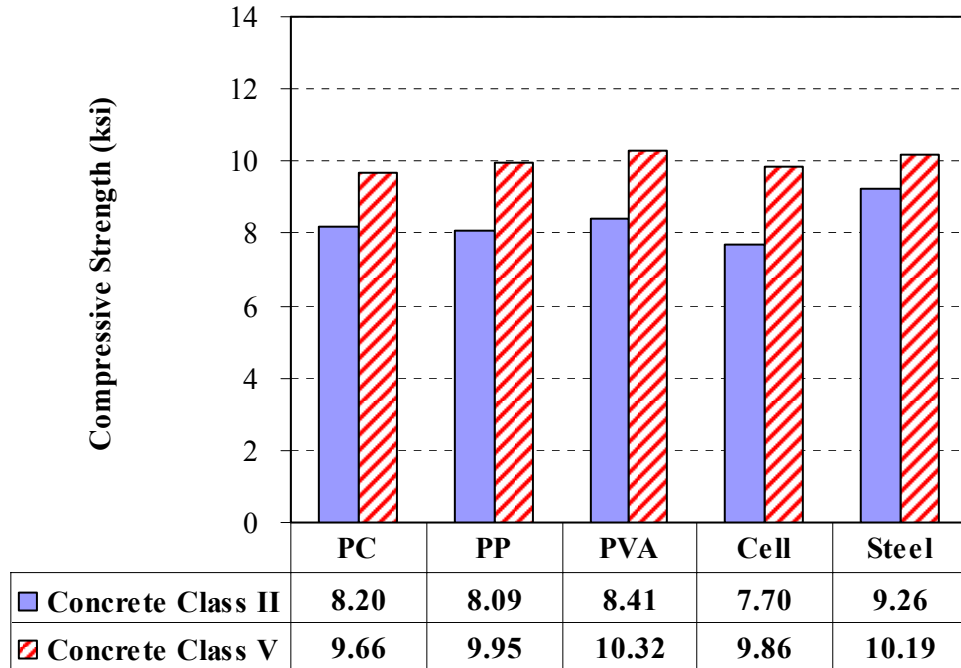


Figure 5-26. Compressive strength for Classes II/V concrete

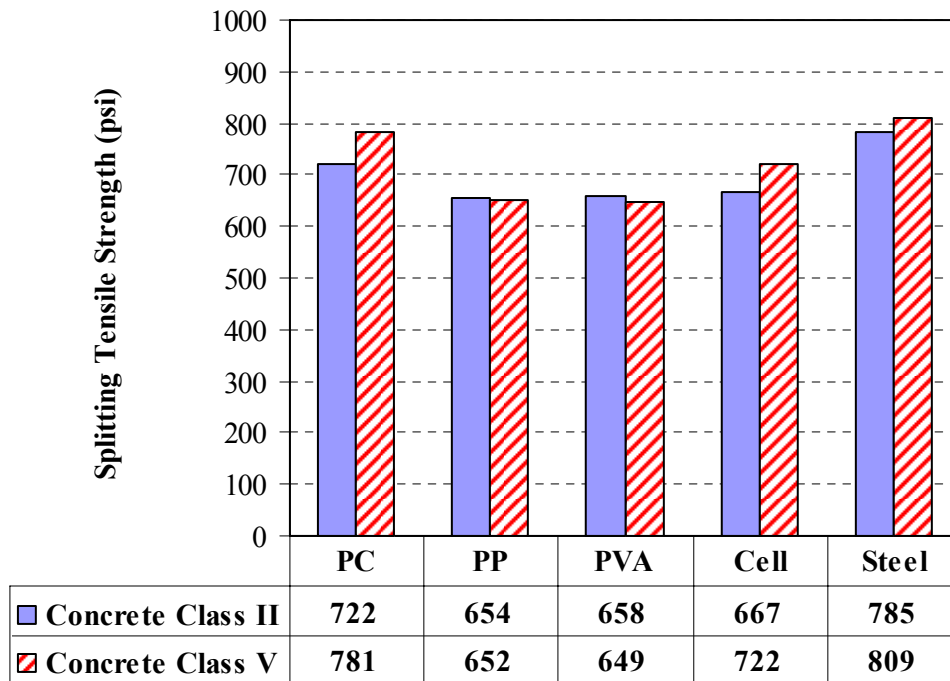


Figure 5-27. Splitting tensile strength for Classes II/V concrete

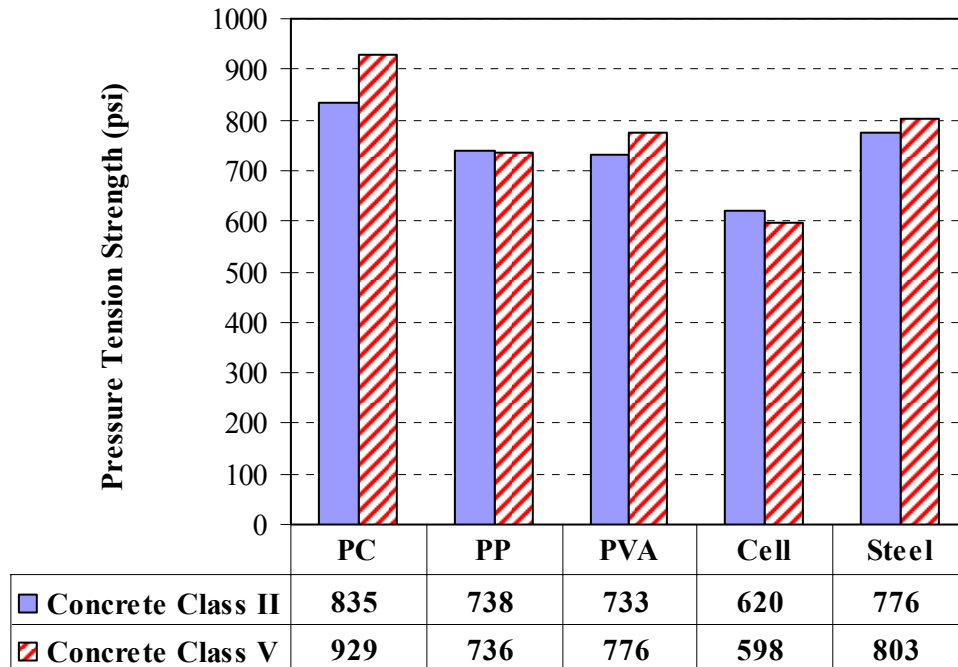


Figure 5-28. Pressure tension strength for Classes II/V concrete

### 5.5 Steel Bar Corrosion Test Results

This section summarizes the results for Class II concrete obtained from the steel bar corrosion test. Corrosion in the Class V concrete and one PVA fiber specimen for Class II concrete has not been detected as of publication of this report but continue to be monitored. The corrosion potential of the titanium bar and current as a function of time had been recorded for a total of 693 days (25 cycles) for PC, PP, PVA, and cellulose fiber mixes, and a total 617 days (22 cycles) for steel fiber mix. Details on the values and photographs of the effects of fiber and fiber type on steel corrosion can be found in the Appendix H.

Test results for time at the initiation of steel corrosion and total corrosion are shown in Figures 5-29 and 5-30. Only the addition of PVA fiber appears to better resist mass transport of chloride ions into concrete. PVA fiber in the hardened cement paste matrix showed relatively high resistivity in terms of both time to initiation and corrosion rate from cyclic wetting and

drying. The addition of steel fiber, which showed the greatest resistance to mass transport of deleterious materials, showed the earliest failure time and relatively high corrosion rate. This result may have been caused by localized steel fiber corrosion near the steel bar, which transferred higher current from the steel fibers to the steel bar, thereby accelerating the corrosion rate from cyclic wetting and drying. PP fiber showed relatively good resistance to initiation time, but high corrosion rate after initiation of steel bar corrosion. PP fiber, which is relatively low modulus and tensile strength, does not resist stresses occurring from an increase in volume of steel bar. On the other hand, cellulose fiber mix showed relatively similar results in both initiation time and corrosion rate in comparison with plain concrete mix, implying fiber balling in the matrix.

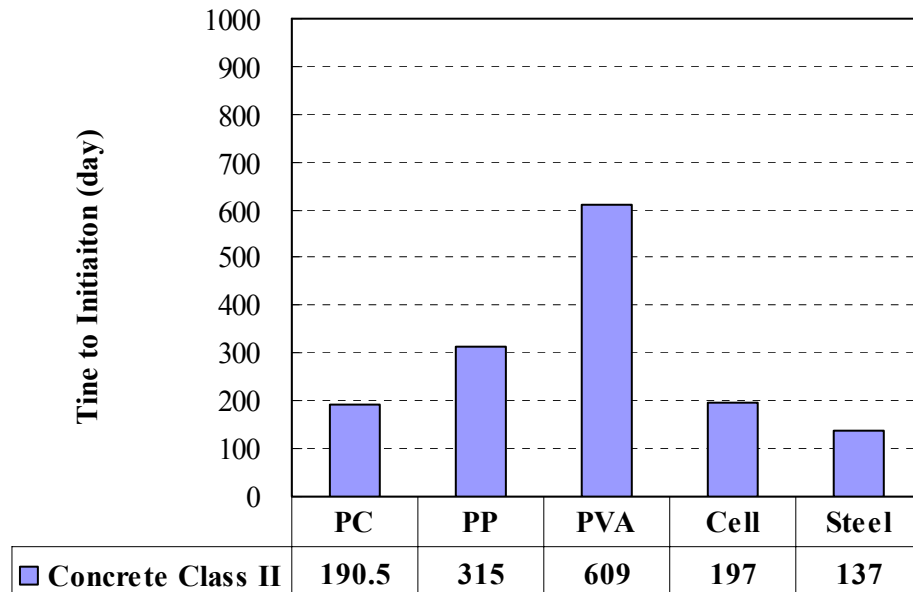


Figure 5-29. Total times for initiation of steel corrosion for Class II concrete

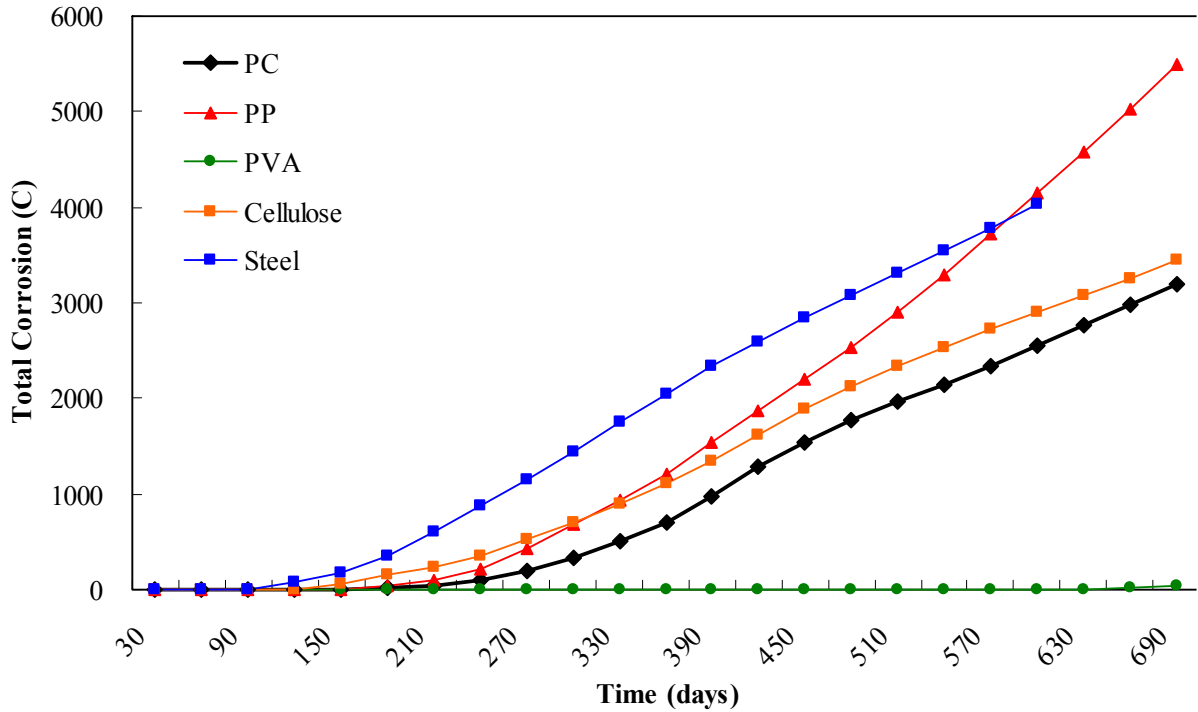


Figure 5-30. Total corrosion rate for Class II concrete

## 5.6 Evaluation of Beams Exposed to Conditioning

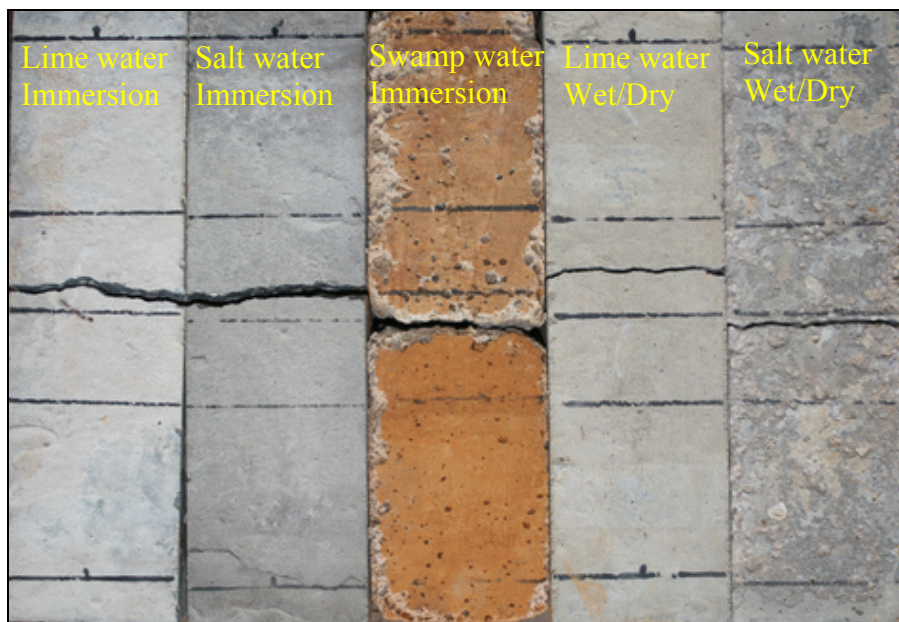
Determination of FRC beam specimens exposed to 27 months environmental conditioning were evaluated using visual or photographic inspection, non-destructive (Ultrasonic Pulse Velocity) and destructive beam testing, permeable pore space change, carbonation depth, and Scanning Electron Microscopy (SEM)/ Energy Dispersive Spectrometer (EDS) analysis. Results are presented in the sections that follow.

### 5.6.1 Visual and Photographic Inspection

The appearance of beam surfaces was generally quite similar between control and fiber specimens. Figure 5-31 shows surface appearance for control and fiber specimens. The following observations were made:

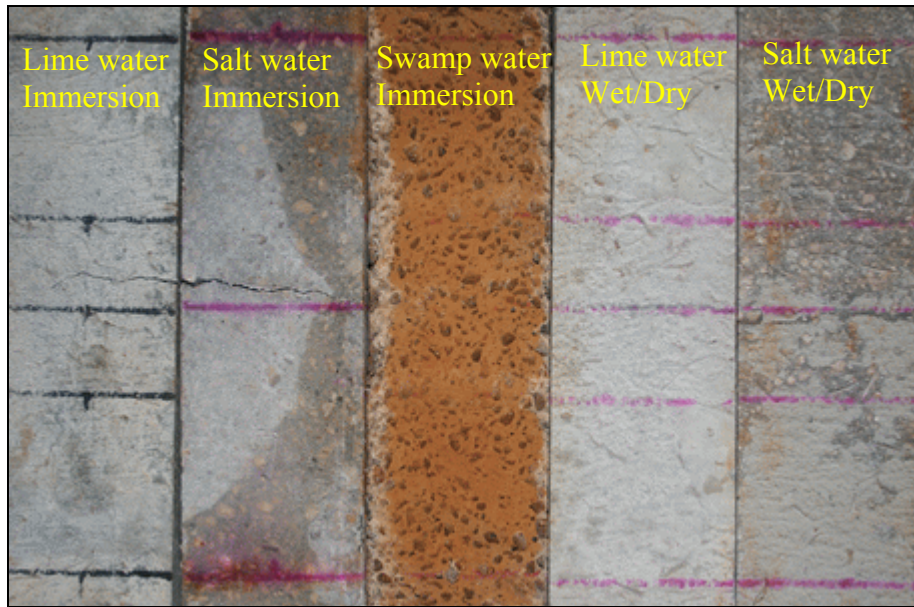
- Salt water immersion: beam specimens exposed to salt water immersion exhibited a thin layer of salt crystals attached to the sides of the beam surface. Surface rusting for steel fibers was not observed for salt water immersion (Figure 5-31d).

- Swamp water immersion: swamp water conditioning with acidic solution showed severe degradation of beam surface for each mix. Acetic acid solutions containing vinegar attacked the concrete surface and resulted in degradation or dissolution of the components for the cement paste, aggregate (limestone), fibers and hydration products of cement paste. The surface of fiber specimens (PP, PVA, and steel fiber mixes) sliced from the slabs showed more distinct surface degradation, specifically limestone, due to its direct contact with acetic acid.
- Salt water W/D: beam specimens subjected to salt water wetting and drying cycles resulted in spalling failure on the surface of the specimens. Dissolved salt ions during wetting periods migrated into the concrete and then crystallized inside of the concrete near the surface as the water evaporated. As the salt crystals expanded, shear stresses accumulated, which resulted in spalling from the concrete surface (Kropp et al., 1995). The finished surface of the control concrete mix was covered by a dense cement paste. Sliced surfaces exposed aggregate or fiber showed and exhibited more pronounced spalling failure. The severe corrosion of steel fibers on the surface was only observed for salt water cyclic wetting and drying and swamp water solutions (Figure 5-31d).
- Specimens pre-cracked before saltwater conditioning re-adhered or healed due to dissolved materials (salt or lime) in solutions and sometimes cracks were initiated away from the pre-cracked plane resulting from conventional flexural beam testing.

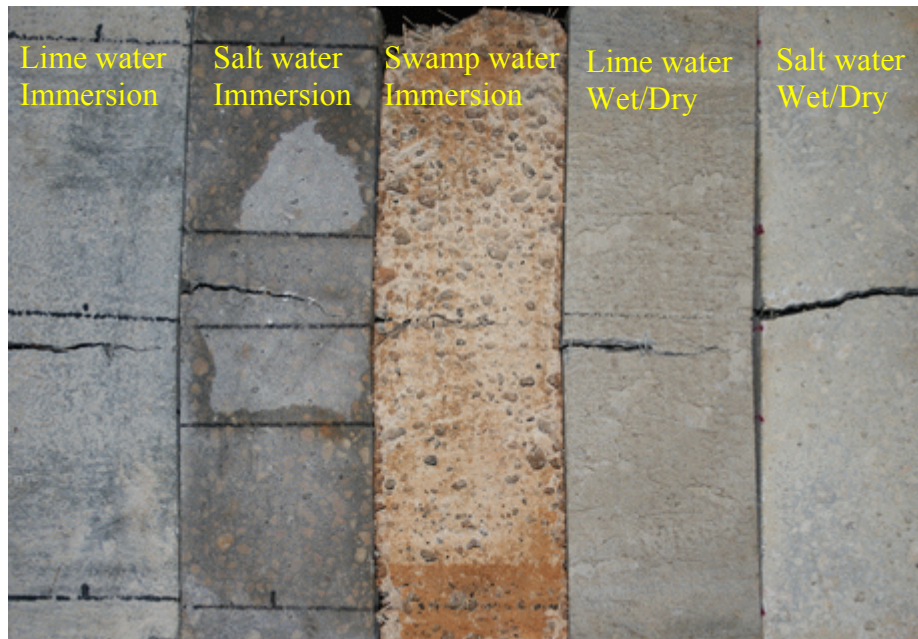


A

Figure 5-31. Surface degradation comparisons for fiber type. A) Plain Concrete beams. B) PP fiber beams. C) PVA fiber beams. D) Steel fiber beams.

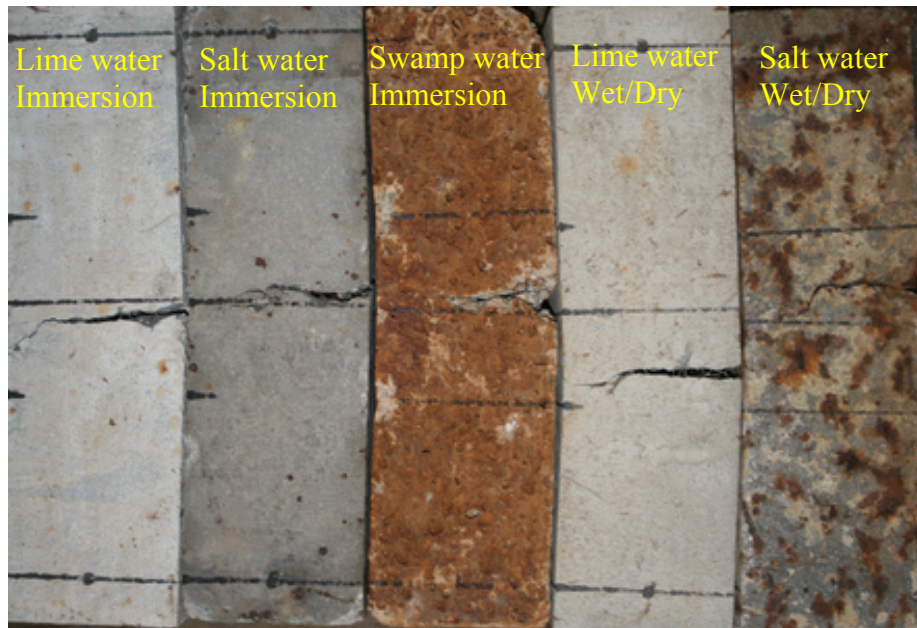


B



C

Figure 5-31. Continued



D

Figure 5-31. Continued

### 5.6.2 Ultrasonic Pulse Velocity Inspection

Ultrasonic Pulse Velocity tests, which are nondestructive, were performed before flexural beam testing to quantitatively evaluate the degree of degradation of FRC resulting from environmental conditioning. Percent changes in UPV compared with lime water immersion are shown in Tables 5-1 and 5-2. Detailed values of test results can be found in the Appendix I (Tables I-1 and I-2).

Only swamp water immersion resulted in significant reduction in UPV for all fiber types and for both concrete Classes. As a result of relatively fast process of dissolution of limestone or fibers in acetic acid solutions, degraded volume and degree of degradation in beam specimens was larger or worse than in specimens submerged in salt water. Both effects from an increase of specimen's density during exposure periods and relatively fast degradation process resulted in slower pulse wave velocities and the reduction was more for swamp water conditioning.

Wetting and drying conditioning resulted in slightly lower pulse velocity for FRC mixes compared to control mixes. However, there was no difference between lime water w/d and salt water w/d conditioning. It appears that the effect of salt crystallization or spalling from repeated wetting and drying only affected the outer surface of the beam and did not affect a large internal portion of the beam. It is noted that the effect from cyclic wetting and drying definitely created a non-uniformly damaged beam specimen.

Table 5-1 Percent change in UPV test results for Class II concrete

UPV	Percent Change (%)					
	Environmental Exposure	Lime-imm.	Salt-imm.	Swamp-imm.	Lime-w/d	Salt-w/d
ASTM C 1399 Specimens	PP-II-Pre-cracked	-	-6	-25	-4	-7
	PP-II-Un-cracked	-	-5	-25	-4	-7
	PVA-II-Pre-cracked	-	-6	-24	-5	-9
	PVA-II-Un-cracked	-	-5	-23	-5	-7
	Steel-II-Pre-cracked	-	-4	-19	-5	-5
	Steel-II-Un-cracked	-	-6	-20	-6	-6
ASTM C 1609 Specimens	PC-II-Un-cracked	-	-5	-22	-6	-9
	PP-II-Un-cracked	-	-6	-25	-4	-6
	PVA-II-Un-cracked	-	-5	-21	-5	-8
	Steel-II-Un-cracked	-	-5	-18	-5	-6

Table 5-2 Averaged UPV test results for Class V concrete

UPV	Percent Change (%)					
	Environmental Exposure	Lime-imm.	Salt-imm.	Swamp-con	Lime-w/d	Salt-w/d
ASTM C 1399 Specimens	PP-V-Pre-cracked	-	-2	-18	-1	0
	PP-V-Un-cracked	-	-5	-20	-5	-3
	PVA-V-Pre-cracked	-	-7	-21	-5	-5
	PVA-V-Un-cracked	-	-5	-22	-4	-4
	Steel-V-Pre-cracked	-	-7	-17	-9	-8
	Steel-V-Un-cracked	-	-7	-12	-9	-8
ASTM C 1609 Specimens	PC-V-Un-cracked	-	-1	-13	2	4
	PP-V-Un-cracked	-	-6	-16	-3	-2
	PVA-V-Un-cracked	-	-6	-23	-3	-4
	Steel-V-Un-cracked	-	-6	-14	-5	-4

There was no difference in pulse velocity between pre-cracked beam and un-cracked beam. It appears that the dissolved salt or lime in solutions was attached to cracked surface and blocked penetration of deleterious materials into concrete along the crack path.

### 5.6.3 Permeable Pore Space Change

Permeable pore space of tested beam specimens was determined at different times using the test method specified in ASTM C 642 to observe the change of voids resulting from ingress of chemical ions into concrete and associated chemical reactions. Permeable pore space was compared to initial values measured before conditioning. Averaged test results are shown in Table 5-3. Salt water conditioning for both immersion and wet/dry showed more pronounced reduction in permeable pores in comparison with lime water conditioning. The change in voids was caused by the intrusion and chemical reaction ions (chloride, sodium, sulfate, magnesium, calcium, potassium) into pore spaces. High concentration of NaCl solution effected the greatest reduction in pore space as a result of salt crystallization, while additional reduction in pore space was caused by other ions binding in the pore system.

Table 5-3 Averaged permeable pore space before/after conditioning for Classes II/V concrete

Concrete Class	Permeable Pore Space (%)					
	Environmental Exposure	Before Exposure	Limewater Immersion	Saltwater Immersion	Limewater W/D	Saltwater W/D
II	PC-II	12.97	12.34	10.55	12.05	8.83
	PP-II	14.26	13.37	11.12	13.14	11.93
	PVA-II	13.55	13.32	11.37	13.24	12.56
	Steel-II	12.12	12.48	10.30	12.26	10.79
V	PC-V	12.19	10.60	9.11	10.68	8.44
	PP-V	12.77	11.46	9.85	11.88	9.16
	PVA-V	13.60	12.35	10.00	11.76	10.20
	Steel-V	13.04	12.06	9.90	11.82	9.14

#### 5.6.4 Average Residual Strength (ARS) Test Results

This section summarizes residual strength test results for beams subjected to different environmental conditioning for 27 months. Detailed test results for individual beams can be found in Appendix I (Tables I-3 to I-8). Typical examples of residual load-deflection curves for each fiber type and conditioning method are also presented in Appendix I (Figures I-1 to I-6). Three beam test results from five tested beams were averaged after removing maximum and minimum test results. Test results are summarized in Table 5-4. Averaged residual strength for each conditioning method and fiber type are presented in Figures 5-32 and 5-33 for Class II and Class V concrete, respectively. PP and PVA fibers had similar averaged residual strength, which was significantly lower than that of steel fibers. ARS was about the same for pre-cracked and uncracked beams, indicating that pre-cracking did not accelerate fiber degradation. Formation of salt crystals in the pre-cracked area prevented further penetration of mass transport of chemical ions. Acidic solutions resulted in significant reduction of averaged residual strength for all fiber types, because of limestone's susceptibility to acetic acid. Similar trends of averaged residual strength were observed for both Class II and Class V concrete.

Table 5-4 Averaged ARS (psi) test results

Mix Type	Specimen Type	Limewater Immersion	Saltwater Immersion	Swampwater Immersion	Limewater W/D	Saltwater W/D
PP-II	Precracked beams	311	284	131	273	248
	Uncracked beams	248	210	148	331	238
PVA-II	Precracked beams	362	277	107	422	388
	Uncracked beams	395	323	118	263	317
Steel-II	Precracked beams	769	760	342	671	518
	Uncracked beams	674	679	381	613	732
PP-V	Precracked beams	347	411	164	200	358
	Uncracked beams	251	385	167	239	310
PVA-V	Precracked beams	322	343	228	342	358
	Uncracked beams	266	328	186	334	328
Steel-V	Precracked beams	847	785	374	665	636
	Uncracked beams	827	806	561	681	588

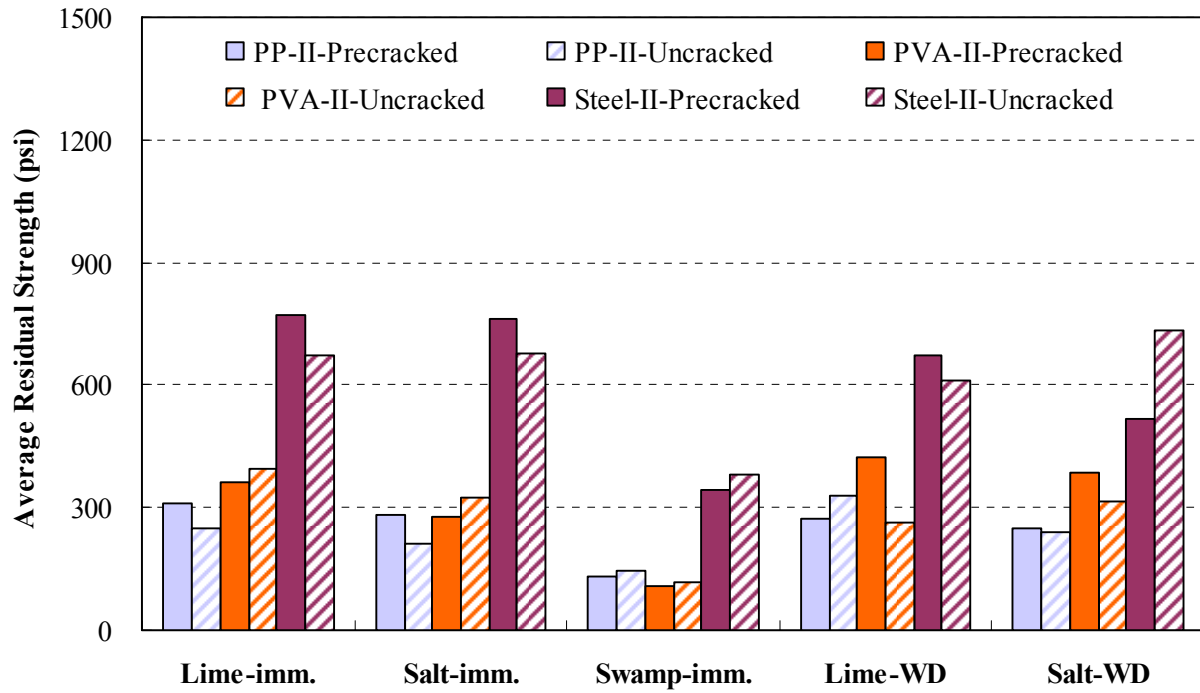


Figure 5-32. Average residual strength results for Classes II concrete

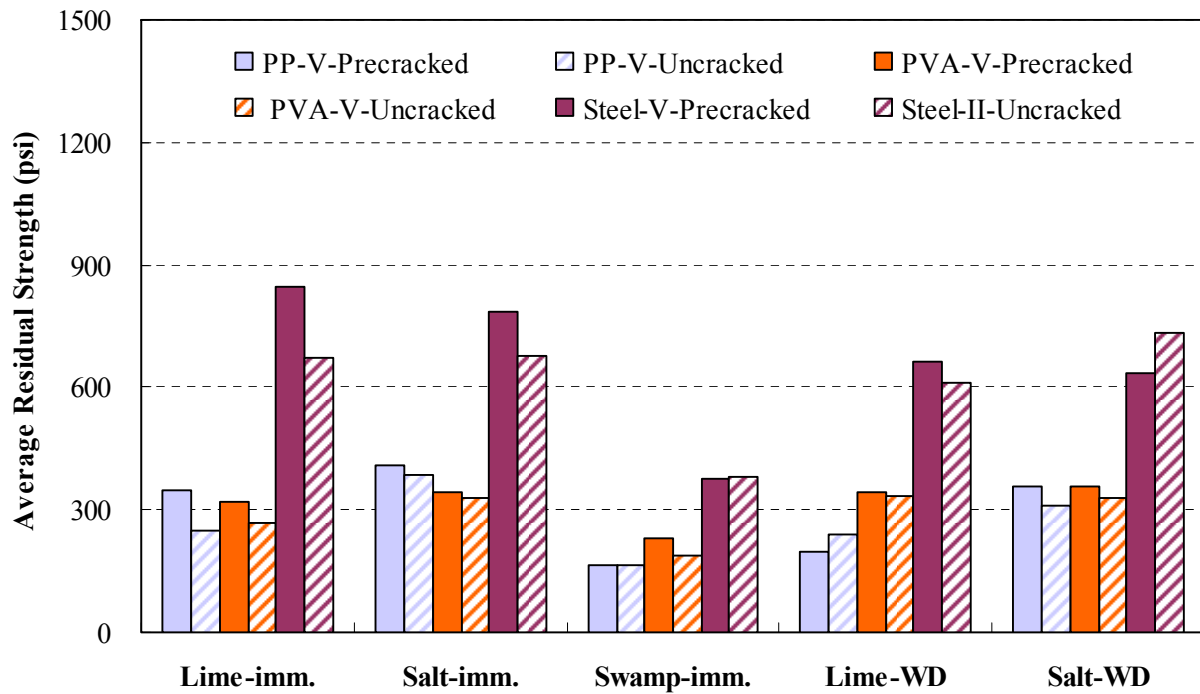


Figure 5-33. Average residual strength results for Class V concrete

### 5.6.5 Flexural Performance Test Results

This section summarizes flexural performance test results for degraded beams subjected to different environmental conditioning for 27 months. Detailed test results for individual beams can be found in Appendix I (Tables I-9 to I-14). Typical examples for residual load-deflection curves for each fiber type and conditioning method are also presented in Appendix I (Figures I-7 to I-11). Three beam test results from five tested beams were averaged after removing maximum and minimum test results. Test results are summarized in Table 5-5.

Table 5-5 Averaged test results of flexural performance

PP	Class II concrete					Class V concrete				
	$f_1^1$	$f_p^2$	$f_{600}^3$	$f_{150}^4$	$T_{150}^5$	$f_1^1$	$f_p^2$	$f_{600}^3$	$f_{150}^4$	$T_{150}^5$
Limewater immersion	962	962	376	393	195	1079	1079	301	304	177
Saltwater immersion	906	906	231	243	143	1277	1277	300	302	210
Swampwater immersion	358	358	141	160	74	495	495	160	203	94
Limewater W/D	935	935	237	257	147	1189	1189	399	395	210
Saltwater W/D	967	967	339	364	179	1247	1247	x	306	203
PVA	$f_1^1$	$f_p^2$	$f_{600}^3$	$f_{150}^4$	$T_{150}^5$	$f_1^1$	$f_p^2$	$f_{600}^3$	$f_{150}^4$	$T_{150}^5$
Limewater immersion	915	915	387	260	192	972	972	213	164	150
Saltwater immersion	964	964	390	225	184	1272	1272	315	233	211
Swampwater immersion	403	403	159	176	89	457	457	198	218	111
Limewater W/D	1053	1053	324	293	181	1249	1249	397	220	193
Saltwater W/D	1105	1105	329	218	181	1360	1360	406	285	221
Steel	$f_1^1$	$f_p^2$	$f_{600}^3$	$f_{150}^4$	$T_{150}^5$	$f_1^1$	$f_p^2$	$f_{600}^3$	$f_{150}^4$	$T_{150}^5$
Limewater immersion	1092	1124	1002	589	363	1143	1149	981	681	392
Saltwater immersion	1061	1061	731	414	274	1319	1319	998	641	385
Swampwater immersion	477	477	448	376	175	589	589	493	434	205
Limewater W/D	1114	1114	806	361	274	1245	1245	801	249	248
Saltwater W/D	1234	1234	870	416	298	1282	1377	1272	545	419

$f_1^1$  is first peak strength, psi.

$f_p^2$  is peak strength after cracking, psi.

$f_{600}^3$  is residual strength at net deflection of span/600, psi.

$f_{150}^4$  is residual strength at net deflection of span/150, psi.

$T_{150}^5$  is area under the load vs. net deflection curve to 0 to span/150, lb-in.

Figures 5-34 through 5-39 show the percent change of several flexural performance measurements for specimens subjected to different conditioning methods relative to control specimens immersed in lime water for PP, PVA, and steel fibers, respectively. Once again,

because of limestone's susceptibility to acetic acid, large reductions in all performance measurements were generally observed for specimens immersed in swamp water. Salt water immersion reduced residual strength and toughness of PP and steel fiber specimens in Class II concrete, where a smaller or no reduction was observed for the PVA specimens. Conversely, for Class V concrete salt water immersion resulted in 30-40% increase in performance measurements for PVA fiber specimens and more modest improvements for PP and steel fiber specimens. However, test results may not be reliable as expected in section 5.7.

### 5.6.6 Carbonation

Figure 5-36 shows the damaged and undamaged area for both salt water W/D and swamp water immersion. The damaged area for specimens exposed to salt water cyclic wetting and drying is shown in Figure 5-36a. Carbonation was only observed for swamp water conditioning in Figure 5-36b. Swamp water immersion with pH 4.5 appeared to have a severe extent of damage and carbonation on the fracture surface each of the fiber types and mixtures. It can be noted that fiber type for both concrete Classes had no effect on the resistance to carbonation as a result of the overwhelming effect of reaction with acidic solutions.

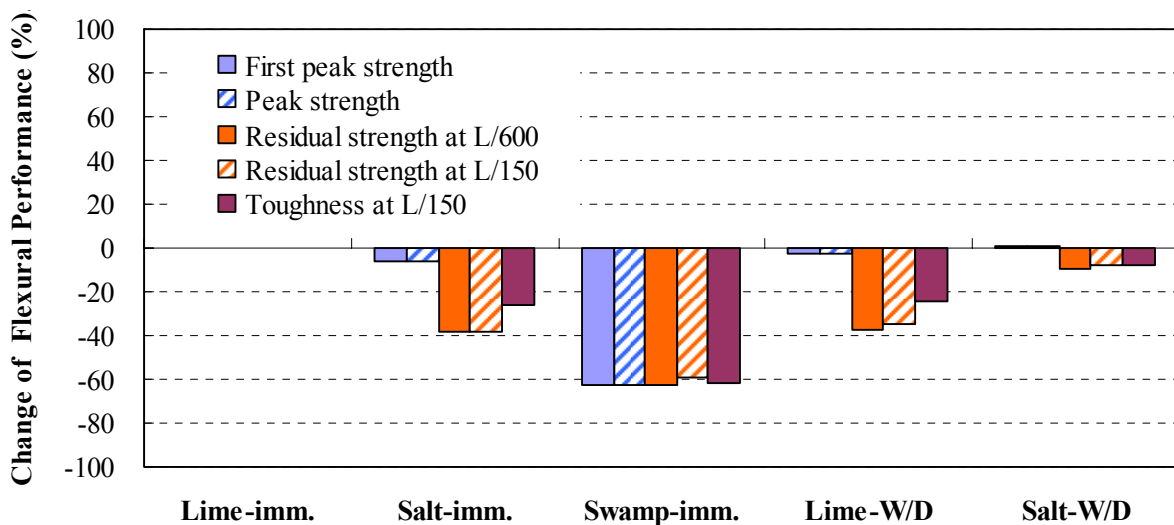


Figure 5-34. Flexural performance comparisons for PP fiber mixes for Class II concrete

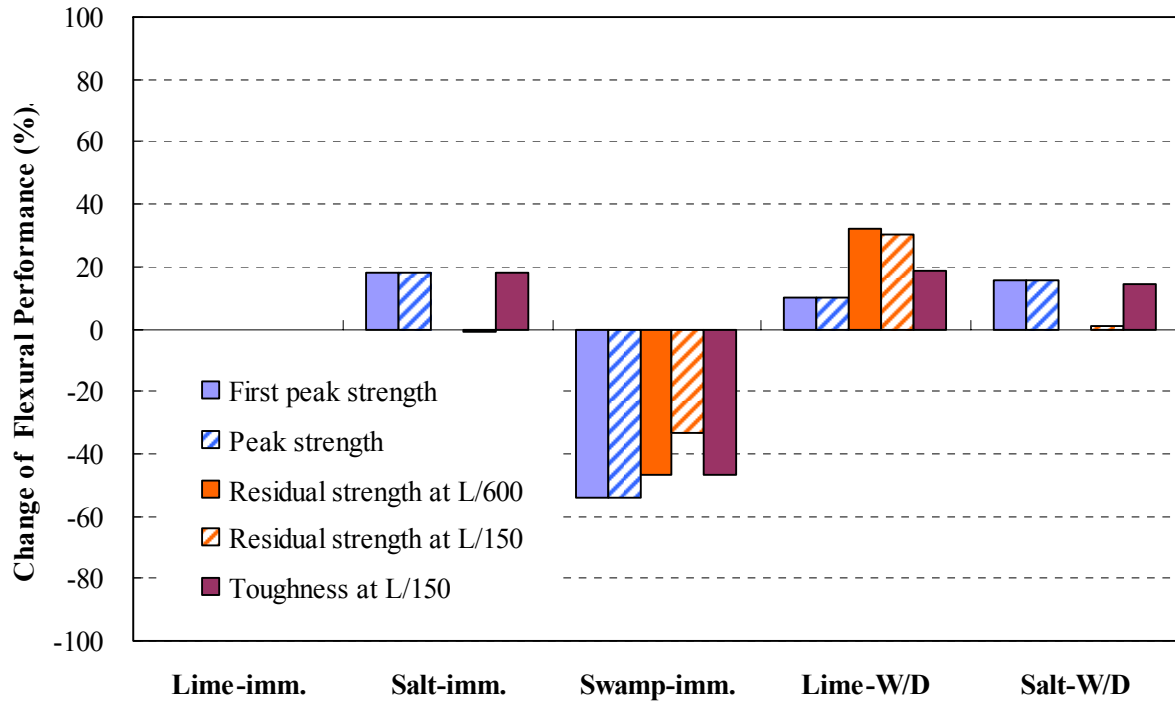


Figure 5-35. Flexural performance comparisons for PP fiber mixes for Class V concrete

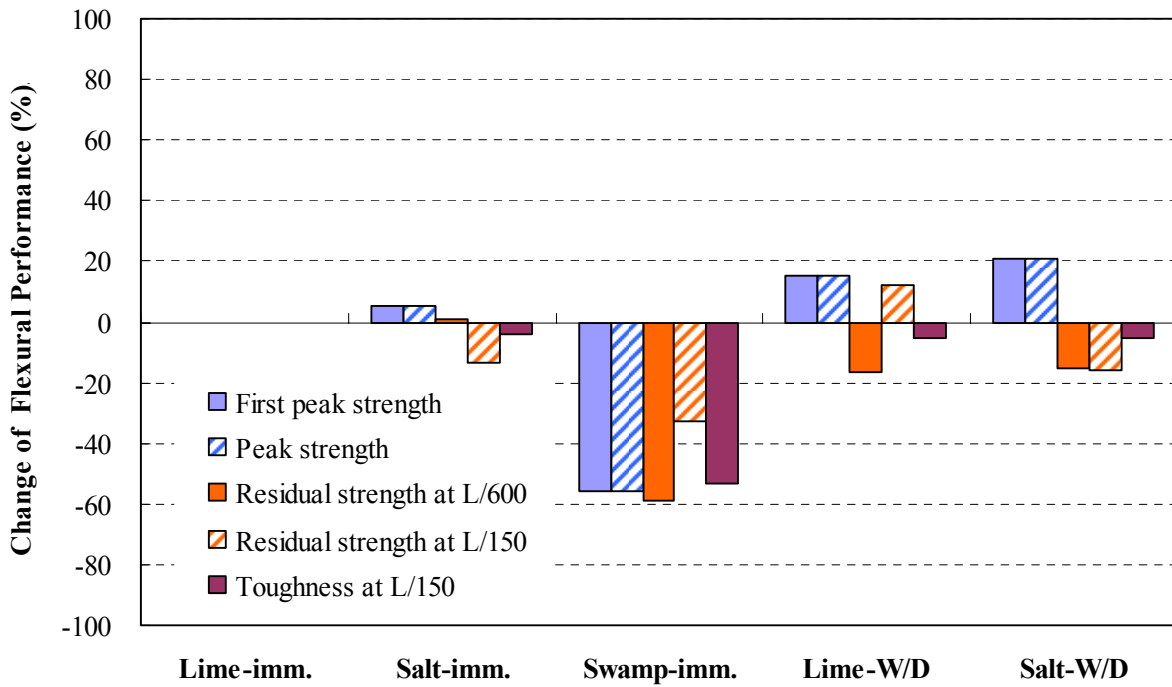


Figure 5-36. Flexural performance comparisons for PVA fiber mixes for Class II Concrete

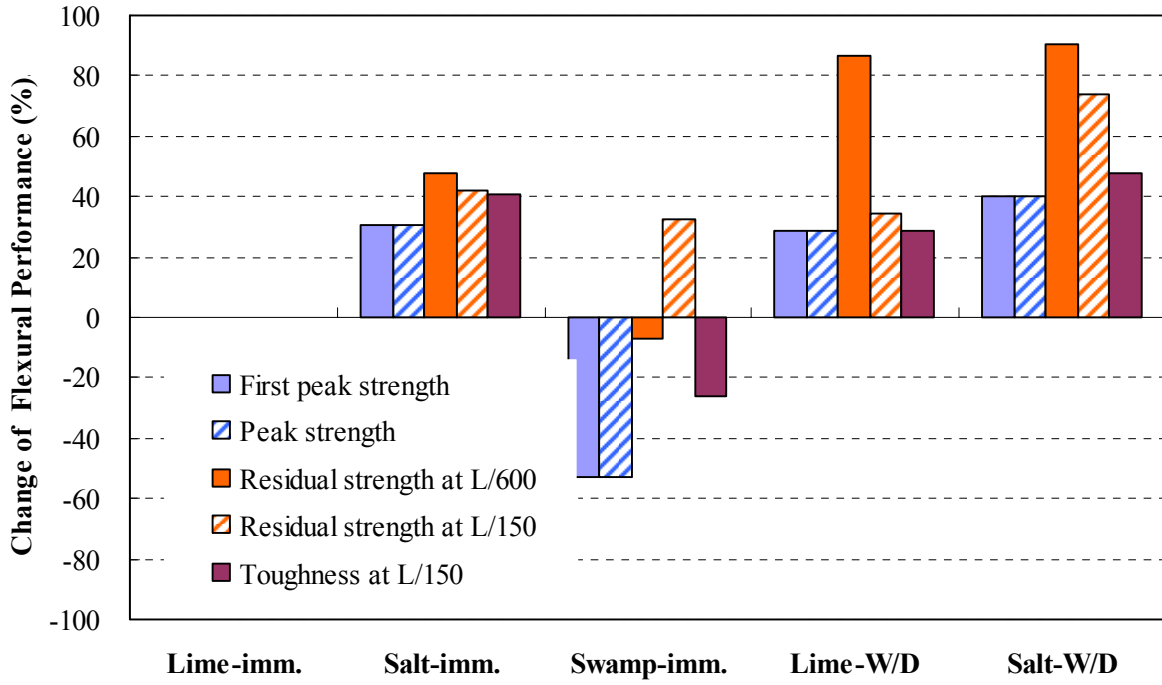


Figure 5-37. Flexural performance comparisons for PVA fiber mixes for Class V concrete

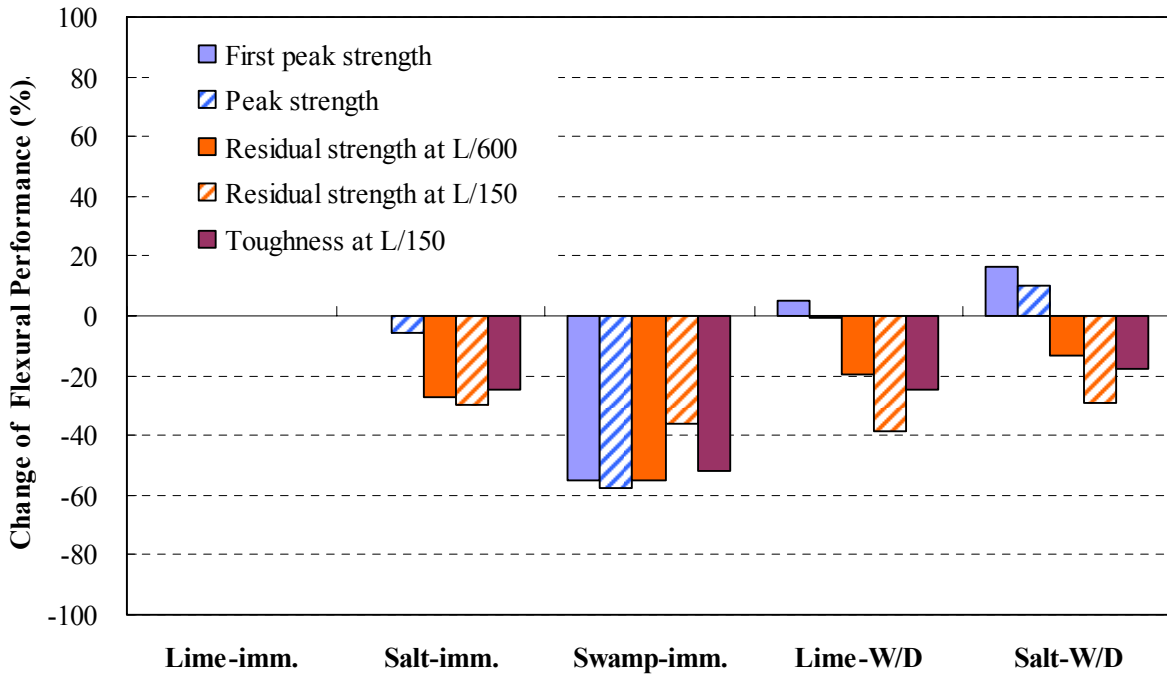


Figure 5-38. Flexural performance comparisons for Steel fiber mixes for Class II concrete

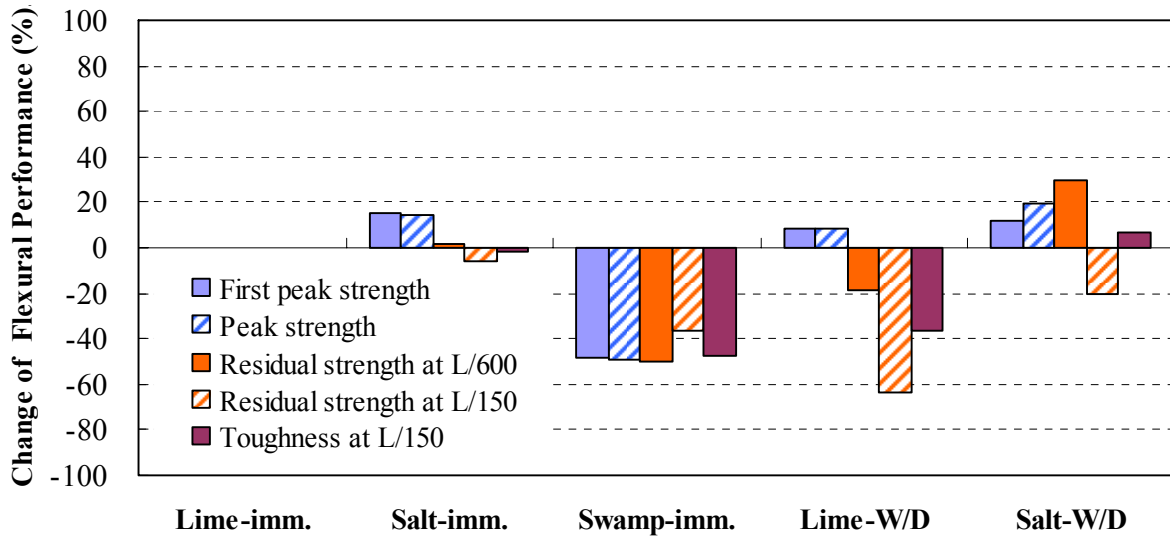


Figure 5-39. Flexural performance comparisons for Steel fiber mixes for Class V concrete

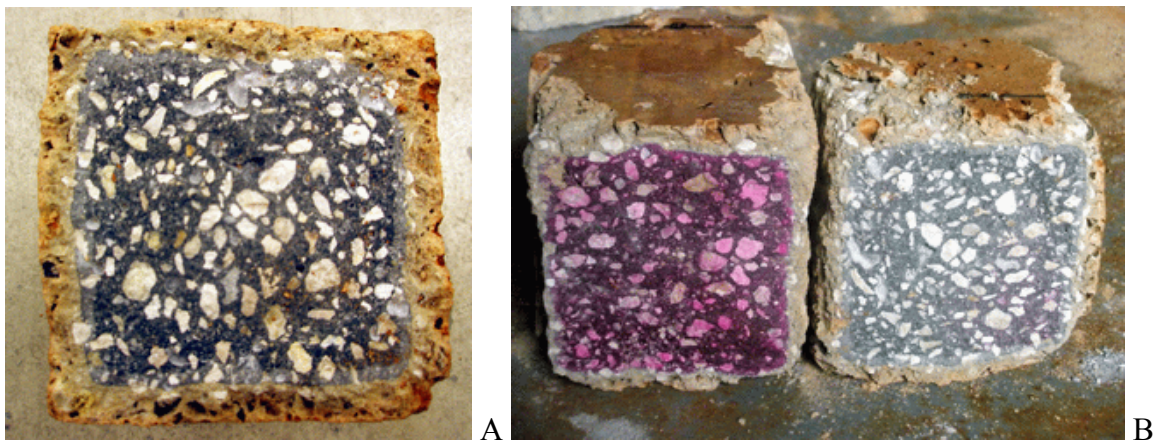


Figure 5-40. Degraded area and carbonated depth on fracture surface for swamp water immersion. A) Damaged area. B) Carbonated depth.

### 5.6.7 Scanning Electron Microscopy

Semi-quantitative chemical analysis for Scanning Electron Microscopy (SEM) and Energy Dispersive Spectrometer (EDS) were performed on fibers and beam specimens to observe microstructure changes in fiber surface and interfacial zone between the fiber and the matrix as a result of chemical reaction during environmental exposure. Two specimens for each fiber type, including limewater and saltwater immersion for Class II concrete, were chosen and analyzed. Specimens were sliced from the fractured beams, which were in a saturated condition due to long

term exposure. Small unpolished specimens were then obtained using a diamond blade saw. This method was employed because the epoxy-impregnated saw polishing approach, generally used in sample preparation for concrete, can cause damage in the form of cracking patterns or crystals (Stella, 1995). Before examination, specimens were coated with a thin carbon film by sputtering using a low deposition rate. Secondary Electron (SE) images, which are capable of displaying the morphology of the microstructure, were obtained as well as X-ray element analysis providing elemental compositions. Results are presented on a chart, where selected elements are recognized on a continuous spectrum according to the position of their peaks. Finally, a dot map indicating the distribution of a particular element was created.

#### **5.6.7.1 Fibers subjected to salt and acidic solutions**

The results were used to study the nature of PP, PVA, cellulose, and steel fibers, as well as to evaluate the resistance to salt and swamp water solutions. Higher SEM magnification of fibers exposed to saltwater with 5% chloride and swamp water with pH 4.5 solutions directly for 45 days showed the following characteristics:

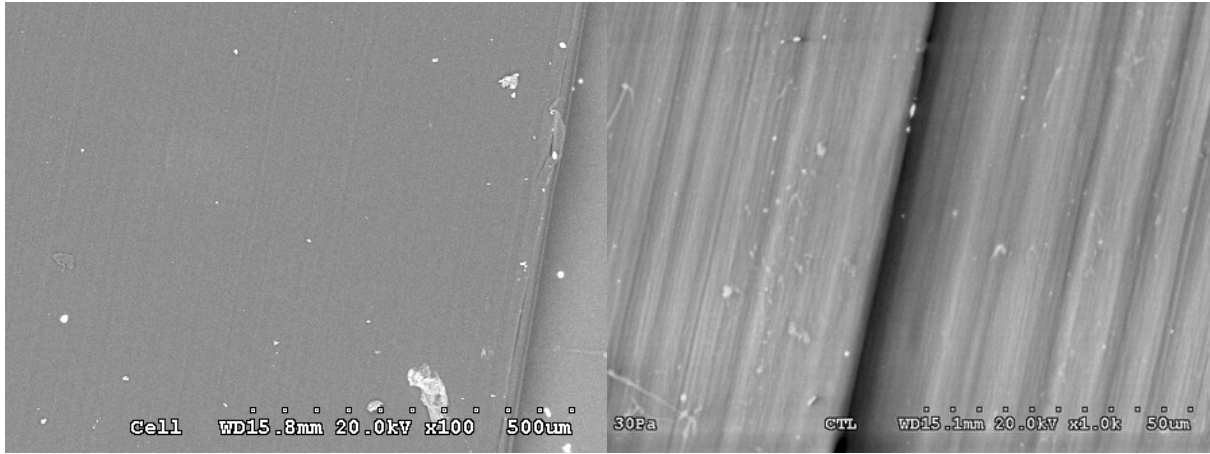
- The surface of the undamaged PP fiber was smooth and had long striations through the fibers but at high magnification (1000 ×), the image showed fracture planes in the fiber (Figure 5-41a). Many fracture planes in the fiber were created by salt water reaction, where the salt crystals caused expansion of the fibers (Figure 5-41b). On the other hand, the smooth surface of PP fibers was transformed to a wrinkled shape and some thin fibrils appeared due to acidic attack (Figure 5-41c).
- The high magnification (1000 ×) image of the surface of undamaged PVA fiber indicated the presence of many small split gaps, which provide a larger surface area, potentially improving the bonding of the fiber with cement paste (Figure 5-42a). However, the split gaps were filled with salt crystals, which caused expansion within the fibers, and a small amount of degradation was also found (Figure 5-42b). The sponge surface of PVA fibers indicated a little degradation from exposure to acidic solution. (Figure 5-42c).
- Numerous bunches of micro-fibers were packed for the original surface of cellulose fiber that were inter-twined (Figure 5-43a). An abundance of salt crystals were deposited (Figure 5-43b) and degradation was found on the fiber surface (Figure 5-43c).

- The surface of the original steel fiber was uneven, providing greater surface area that might have the potential effect of improving the bonding with cement paste (Figure 5-44a). A severe extent of rusting and iron was found on the surface of the fiber in both salt water and swamp water solutions (Figures 5-44b and 5-44c).

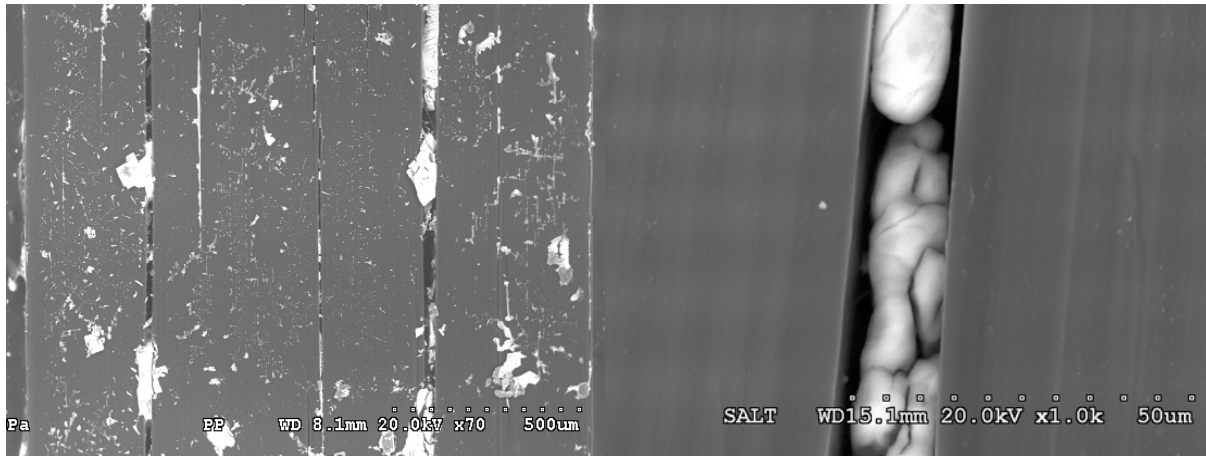
#### 5.6.7.2 Degraded beam

It was very difficult to detect property changes or reaction products from the chemical reaction with seawater solutions due to the limitations of the SEM/EDS analysis, which are qualitative in nature. Another reason for difficulty to discern the nature of the deterioration mechanism of fibers was that SEM analysis required very small, completely dry specimen, which tended to induce cracking or damage of the microstructure. In addition, sputter coating was required to induce conductivity. The properties of PP, PVA and steel fibers in the hardened cement paste matrix are summarized as follows:

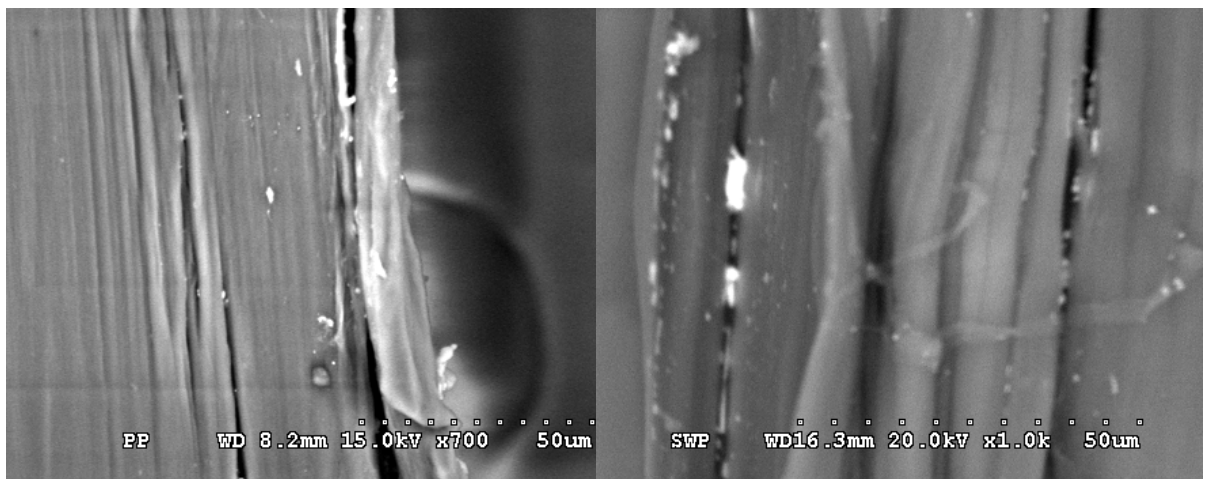
- The SE image for PP fiber exposed to lime water immersion is shown in Figure 5-45a and X-ray spectrum for the whole area shown in Figure 5-45e indicated several kinds of peak elements (C, Ca, Mg, Si, Al, S, Fe, O). The dot map presented in Figure 5-45c shows distributions of peak elements using white dots. Distributions of carbon (C) and silica (Si) represent PP fibers and lime stone (coarse aggregate) respectively. Calcium (Ca) indicates hydrated cement paste such as calcium hydroxide ( $\text{CaOH}_2$ ), C-S-H, and ettringite.
- Although different in SEM images between control and saltwater immersion for PP fibers was not clear in Figures 5-45a and 5-45b, the dot map study in Figures 5-45c and 5-45d and X-ray element analysis in Figures 5-45e and 5-45f showed more pronounced changes as a result of degradation of specimen to salt water solution. Sodium (Na), magnesium (Mg), chloride (Cl), potassium (K) and sulfate (S) contained in salt water were detected.
- The test results of SEM and X-ray elemental analysis for PVA and steel fibers shown in Figures 5-46 and 5-47 showed similar characteristics in comparison with those of PP fibers.



A Undamaged PP fibers: a) 100x, b) 1000x

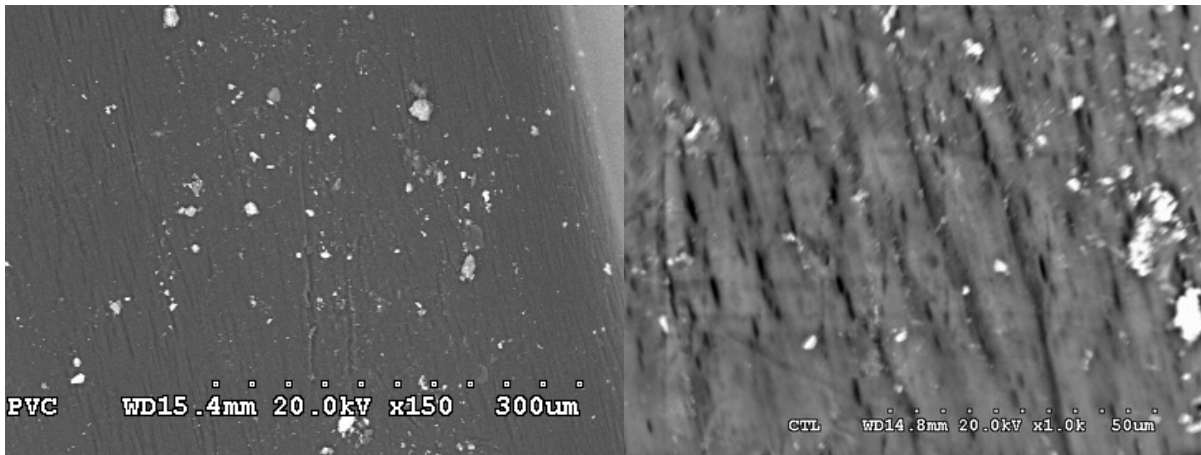


B Damaged PP fibers in saltwater solution (45 days): a) 70x, b) 1000x

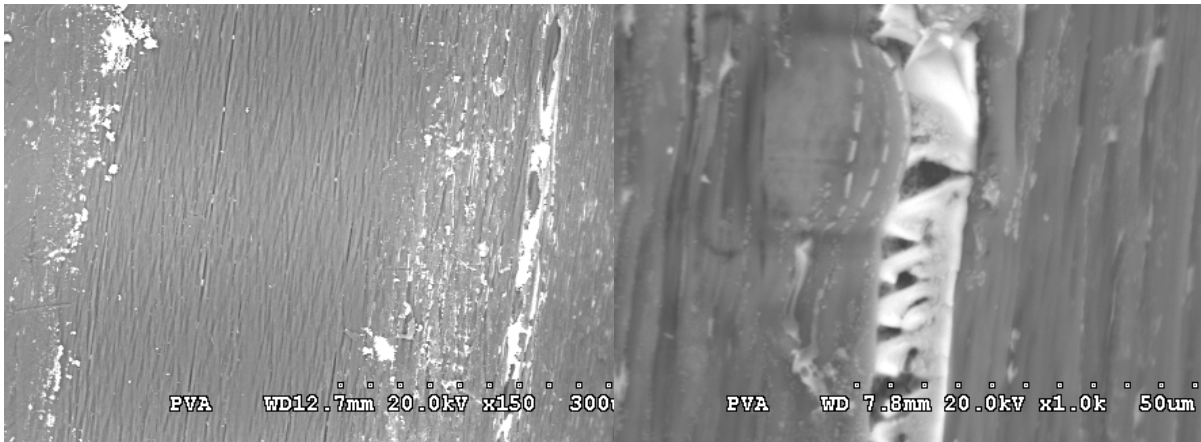


C Damaged PP fibers in swamp water solution (45 days): a) 700x, b) 1000x

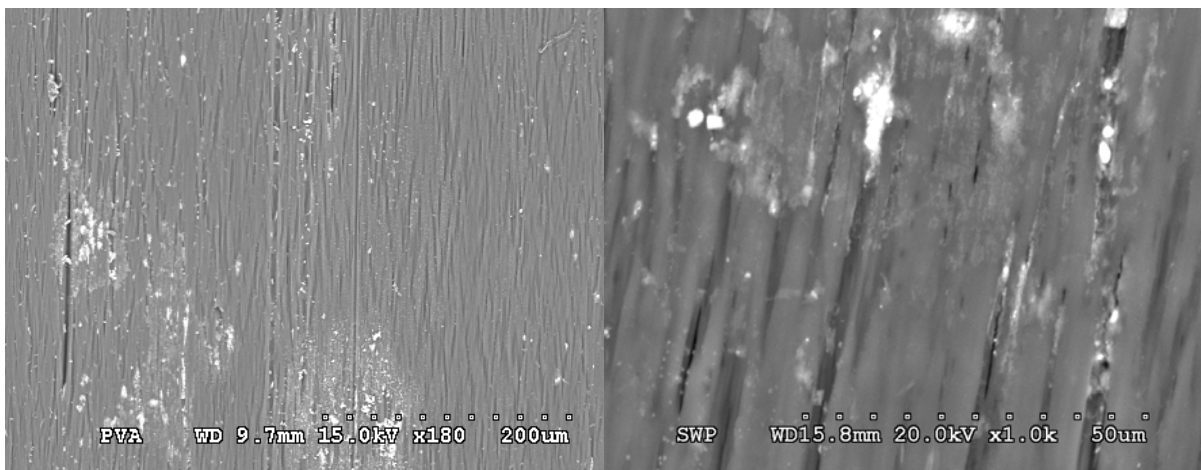
Figure 5-41. Surface properties of PP fibers



A Undamaged PVA fibers: a) 150x, b) 1000x

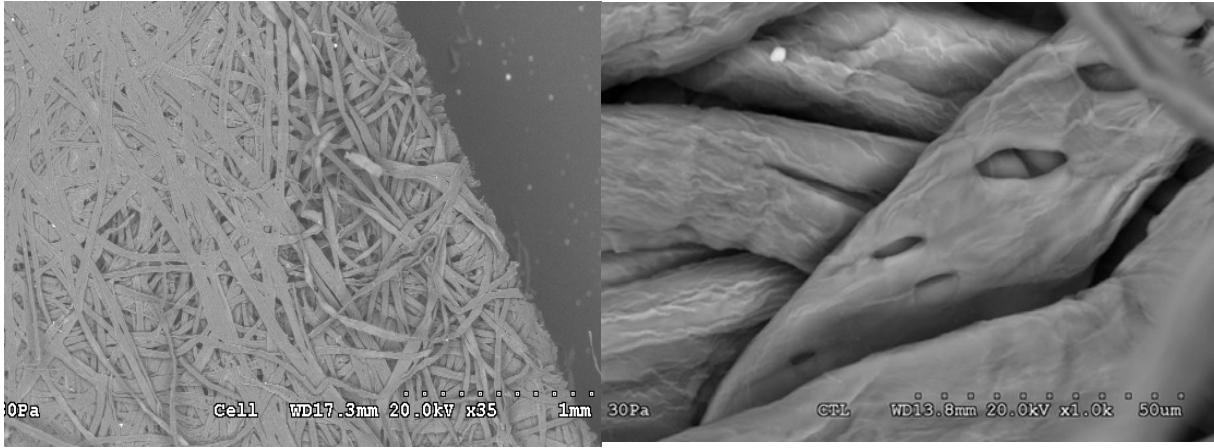


B Damaged PVA fibers in saltwater solution (45 days): a) 150x, b) 1000x

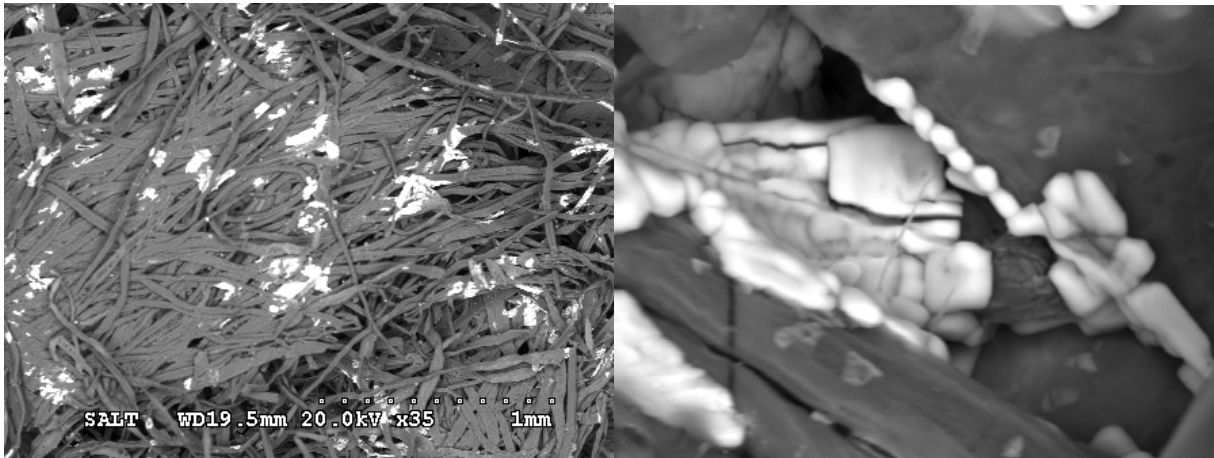


C Damaged PVA fibers in swamp water solution (45 days): a) 180x, b) 1000x

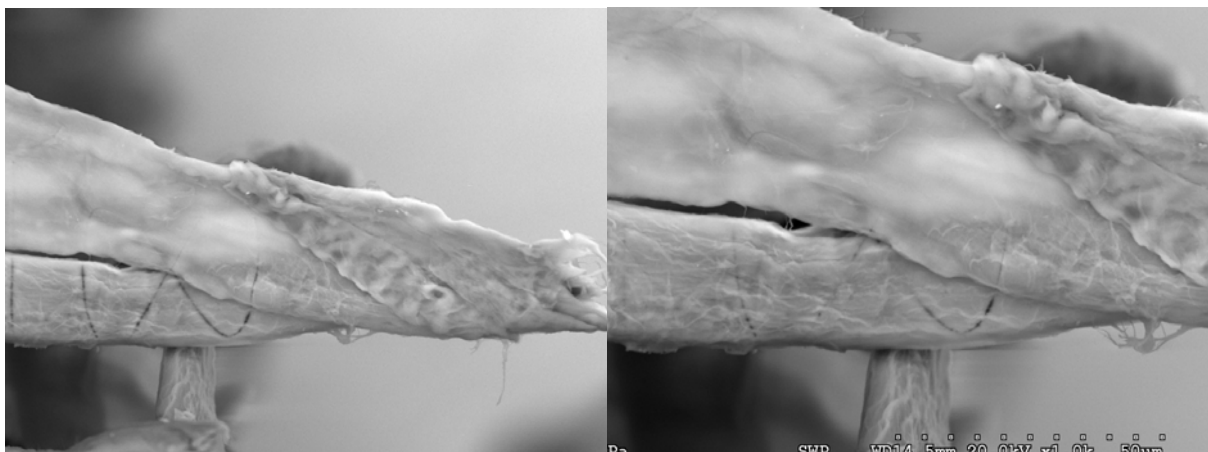
Figure 5-42. Surface properties of PVA fibers



A Undamaged cellulose fibers: a) 35x, b) 1000x

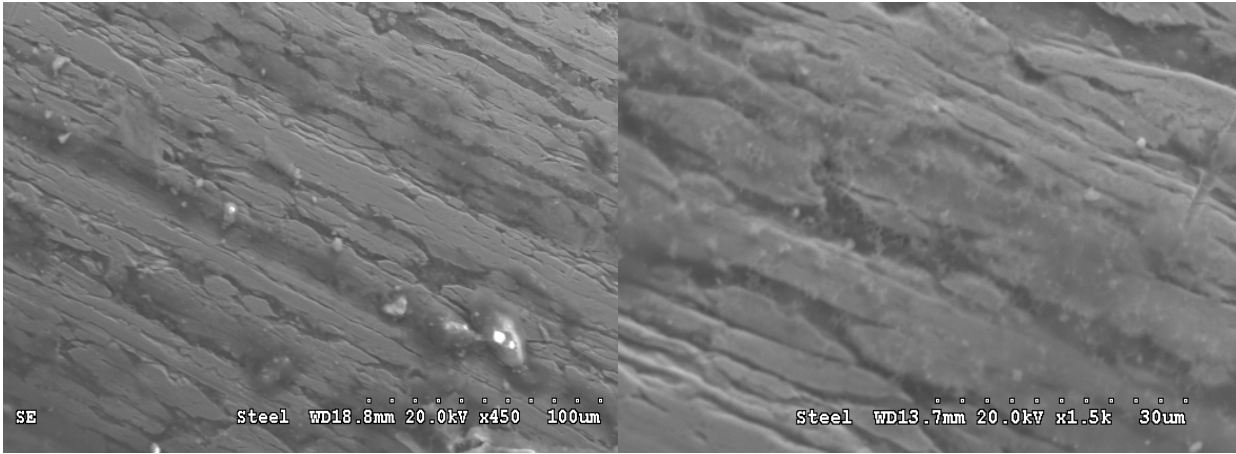


B Damaged cellulose fibers in saltwater solution (45 days): a) 35x, b) 1000x

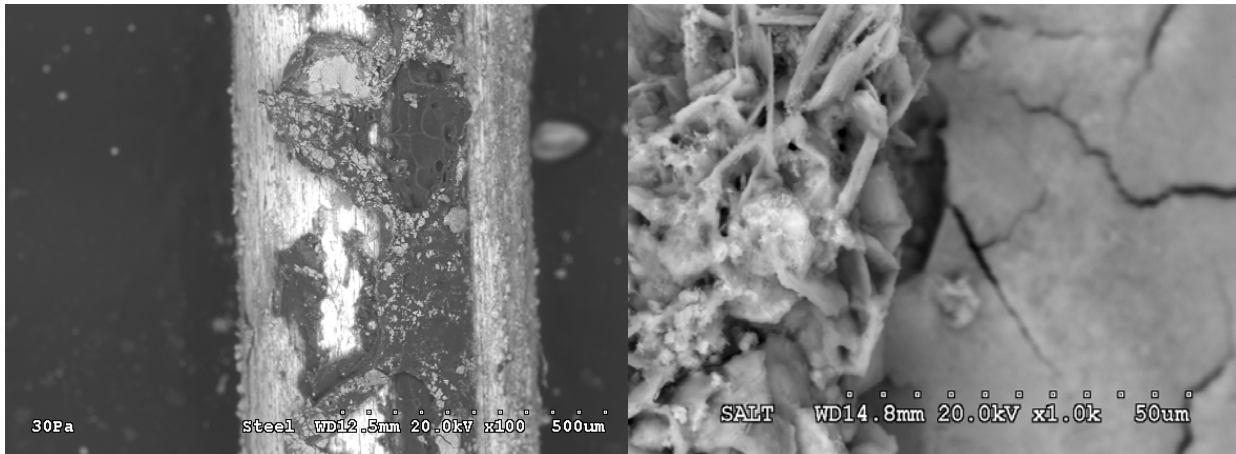


C Damaged cellulose fibers in swamp water solution: a) 500x, b) 1000x

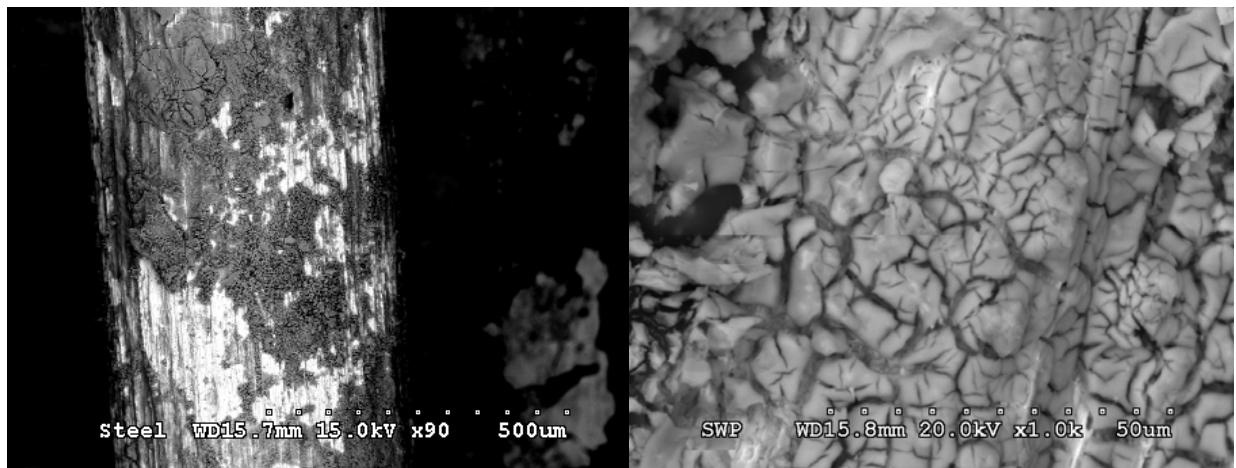
Figure 5-43. Surface properties of cellulose fibers



A Undamaged steel fibers: a) 450x, b) 1000x

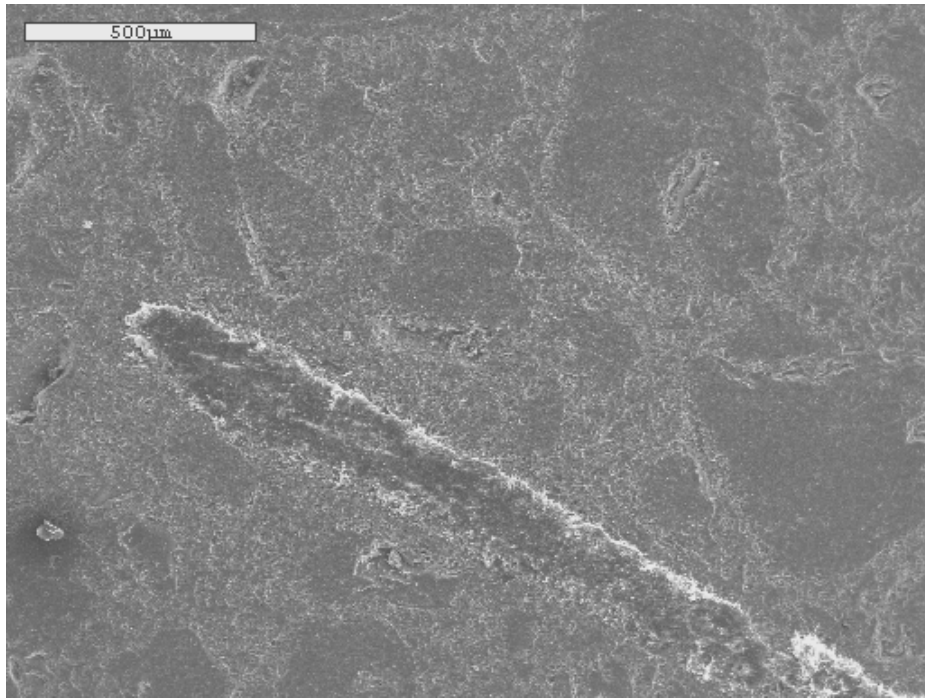


B Damaged steel fibers in saltwater solution (45 days): a) 100x, b) 1000x

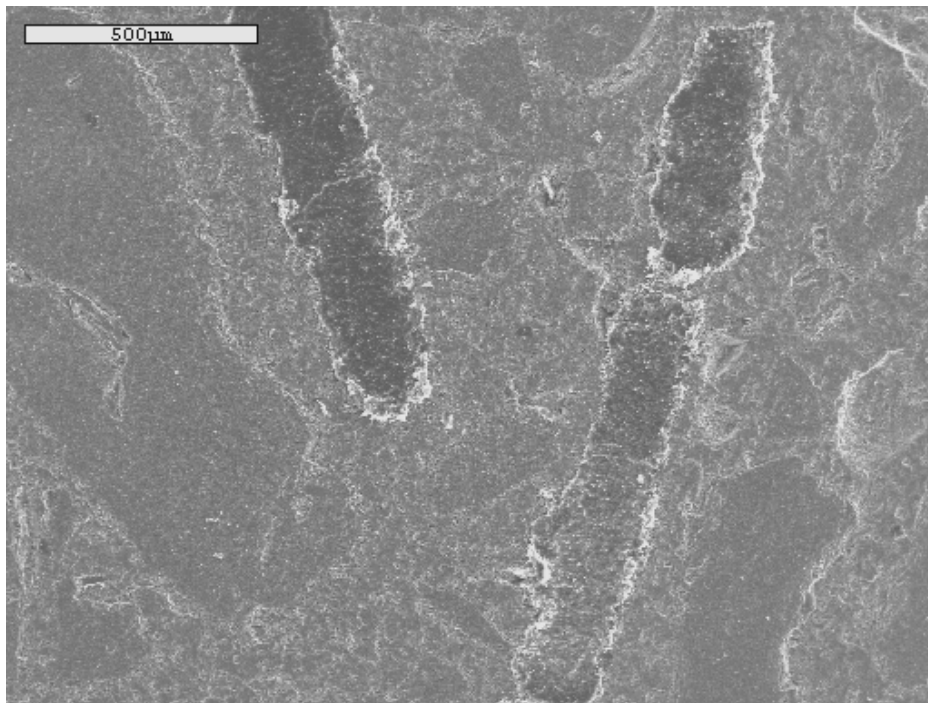


C Damaged steel fibers in swamp water solution (45 days): a) 90x, b) 1000x

Figure 5-44. Surface properties of steel fibers

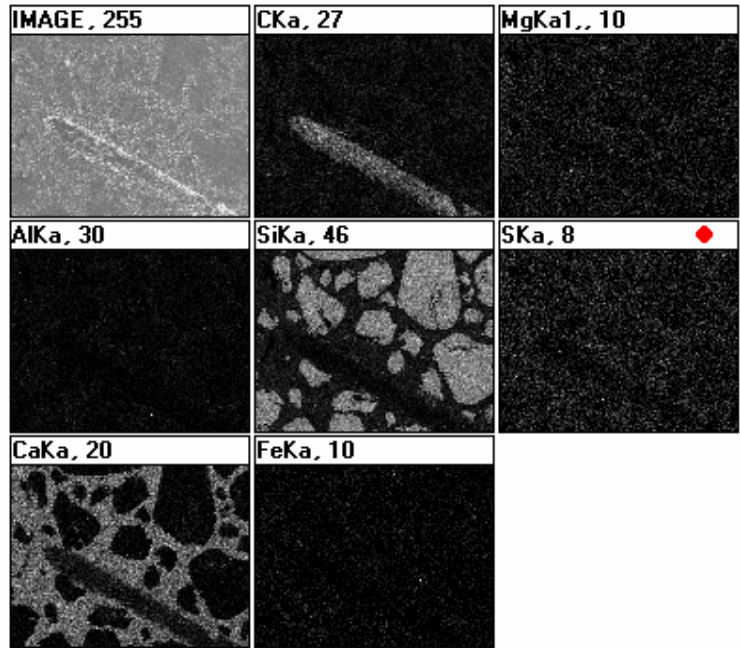


A

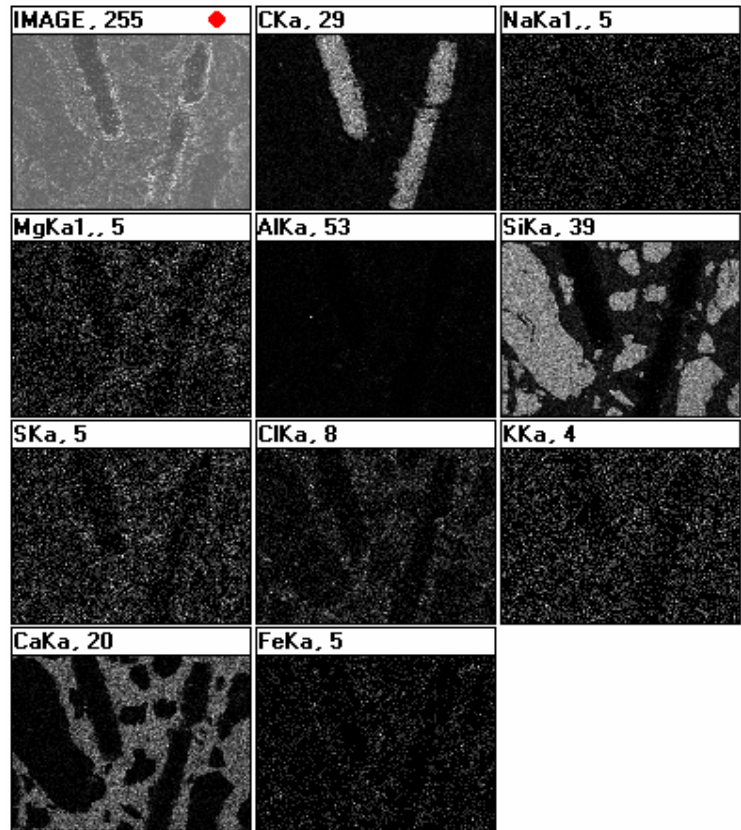


B

Figure 5-45. PP fiber comparisons in limewater and saltwater immersion. A) SE image (60x) for limewater immersion. B) SE image (60x) for saltwater immersion.

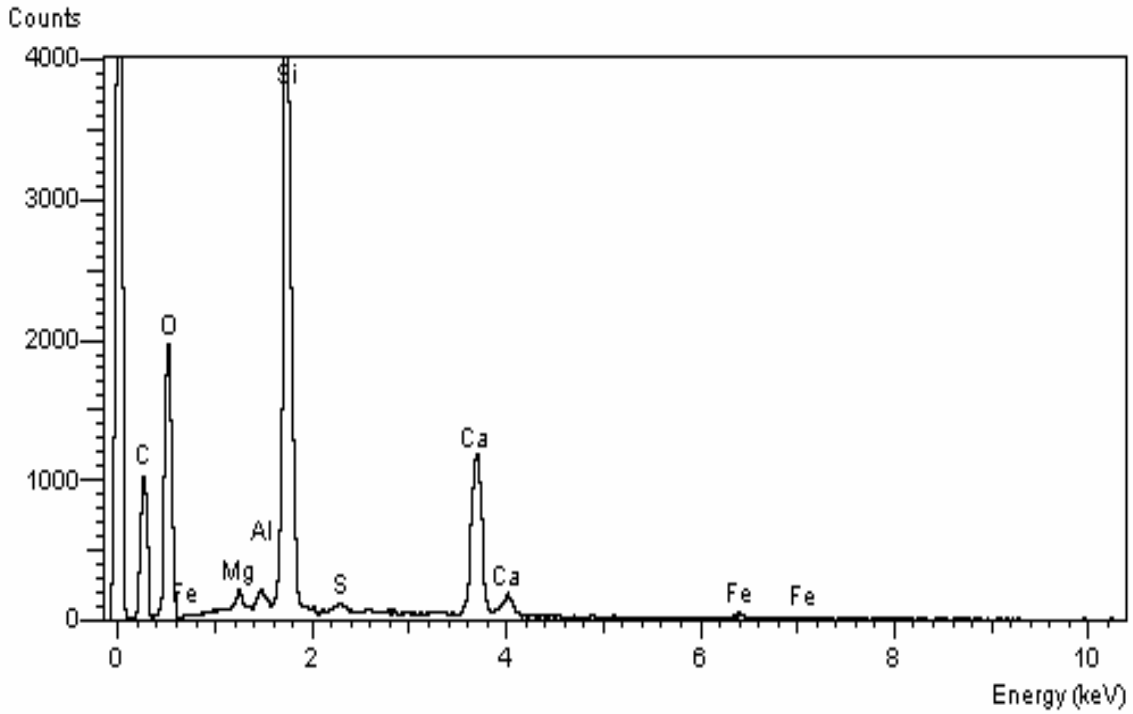


C

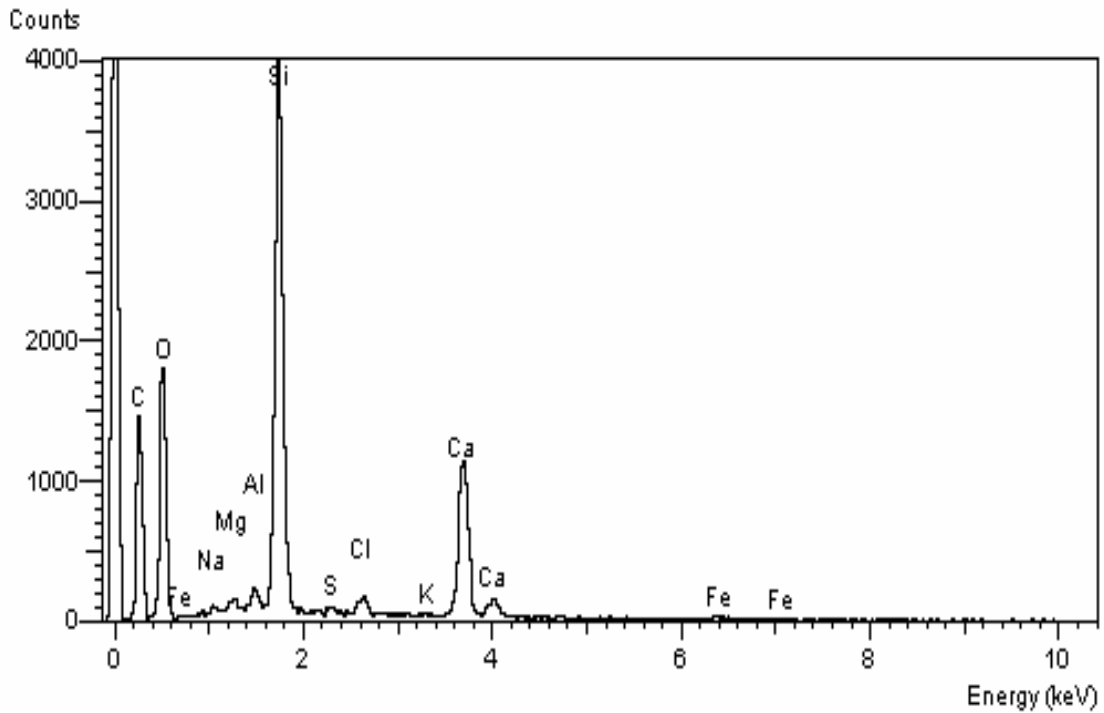


D

Figure 5-45. Continued. C) Dot mapping for limewater immersion. D) Dot mapping for saltwater immersion.

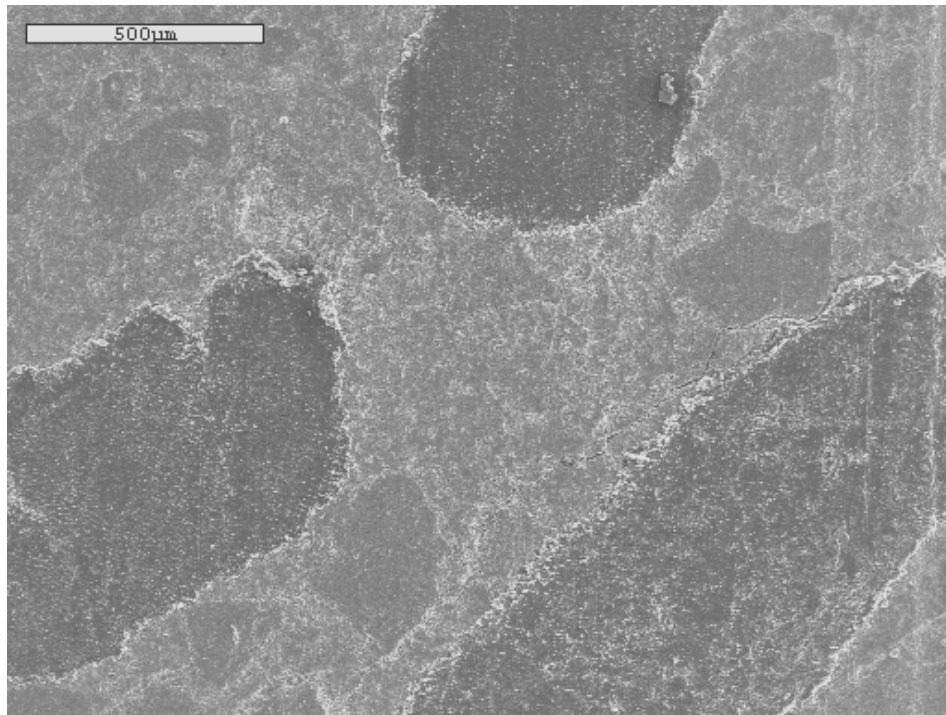


E

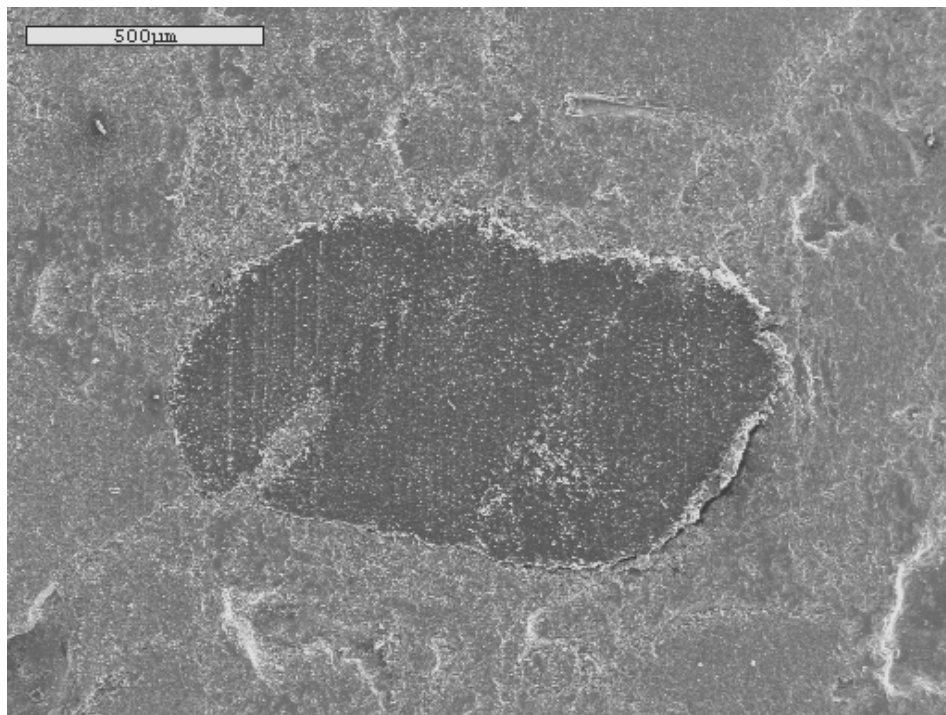


F

Figure 5-45. Continued. E) EDS Spectrum for limewater immersion. F) EDS Spectrum for saltwater immersion.

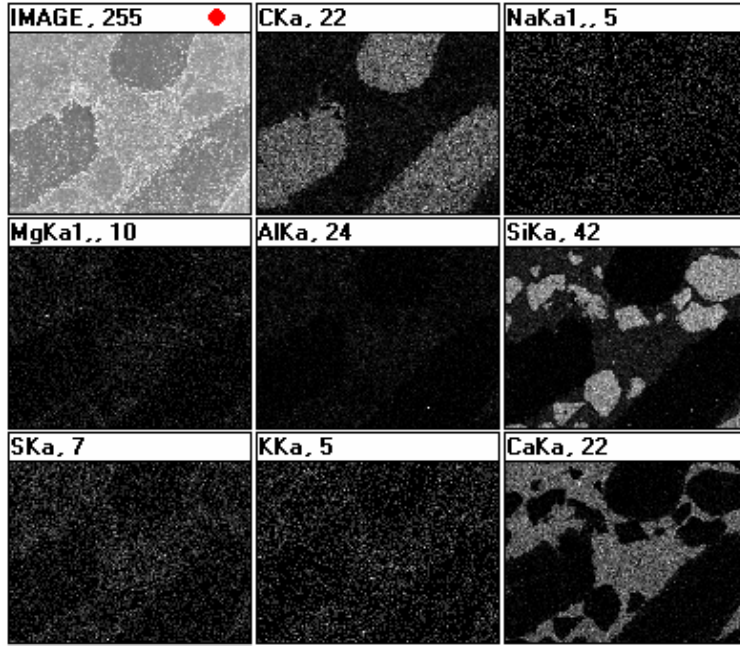


A

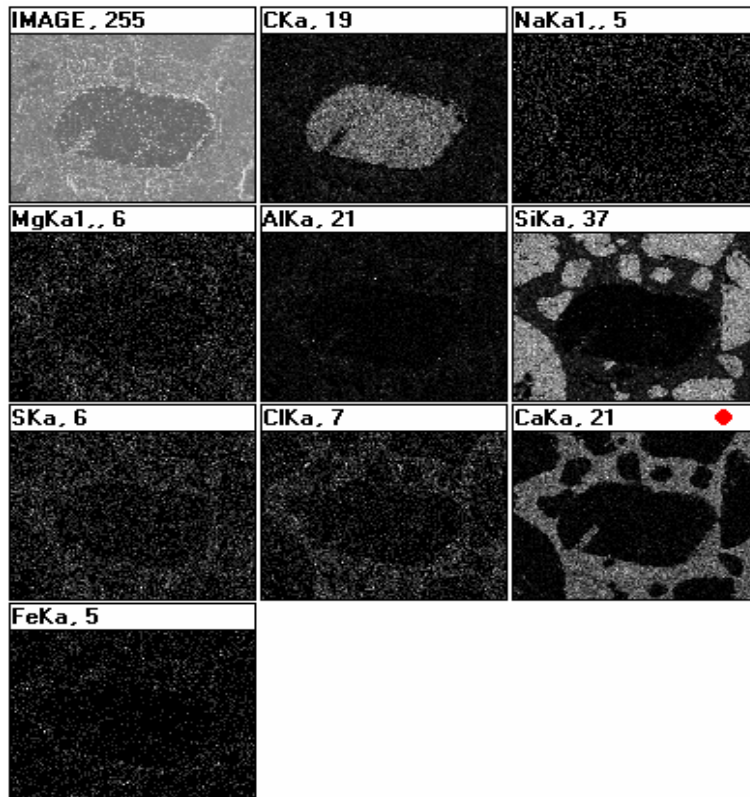


B

Figure 5-46. PVA fiber comparisons in limewater and saltwater immersion. A) SE image (60x) for limewater immersion. B) SE image (60x) for saltwater immersion.

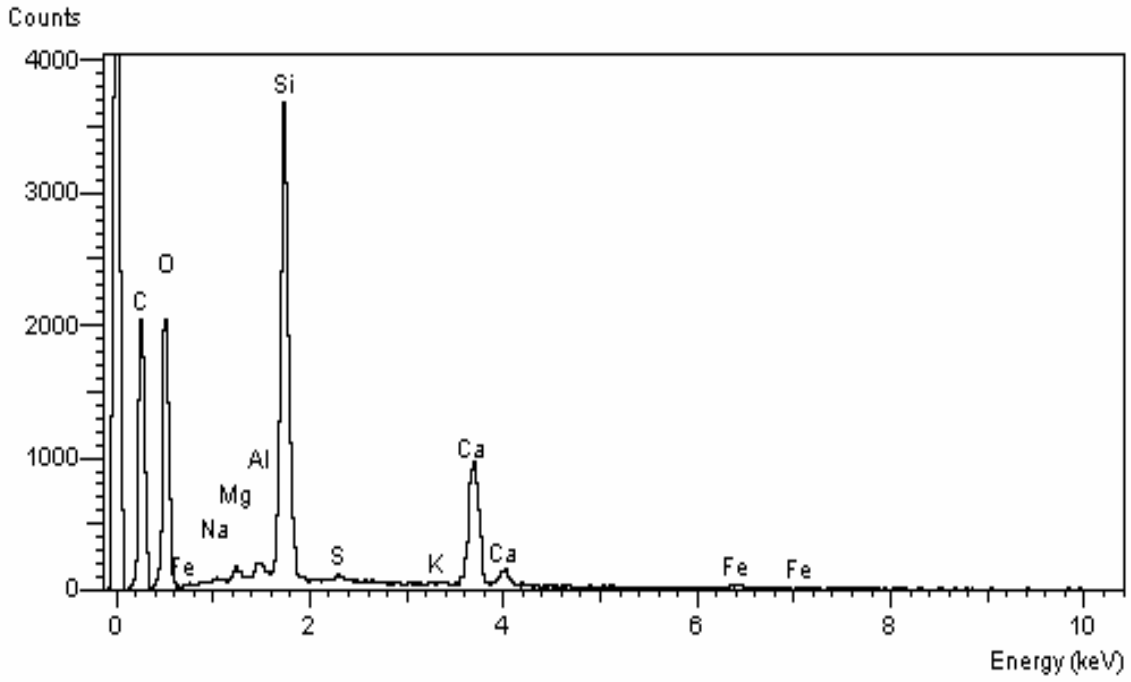


C

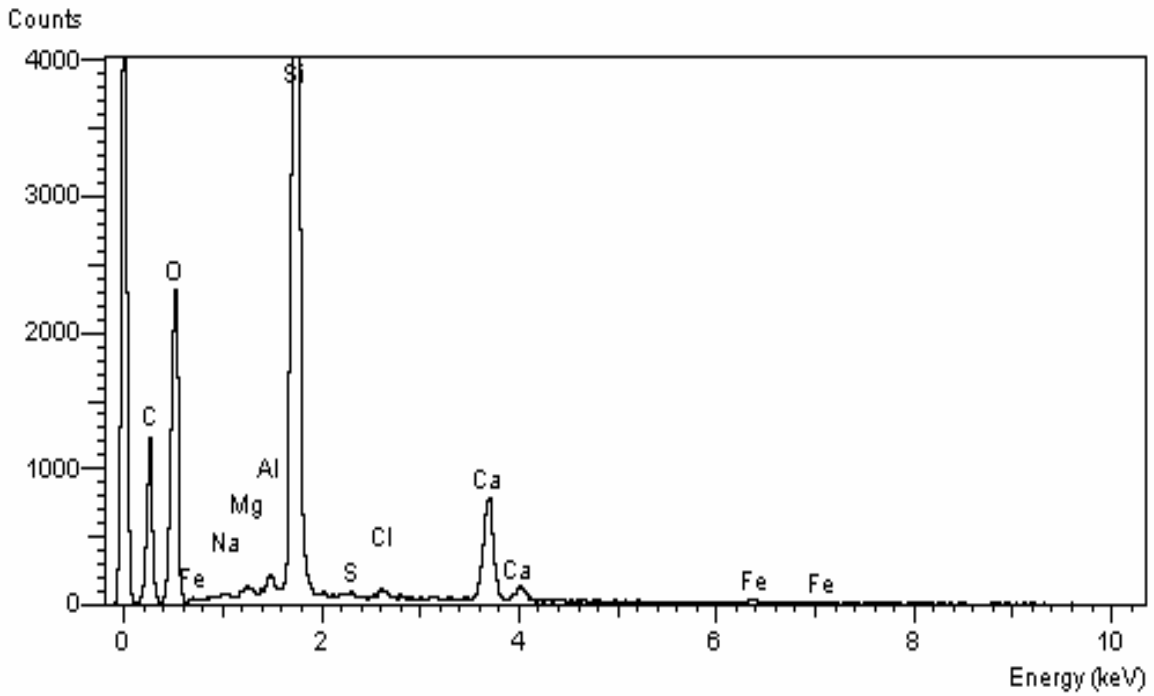


D

Figure 5-46. Continued. C) Dot mapping for limewater immersion. D) Dot mapping for saltwater immersion

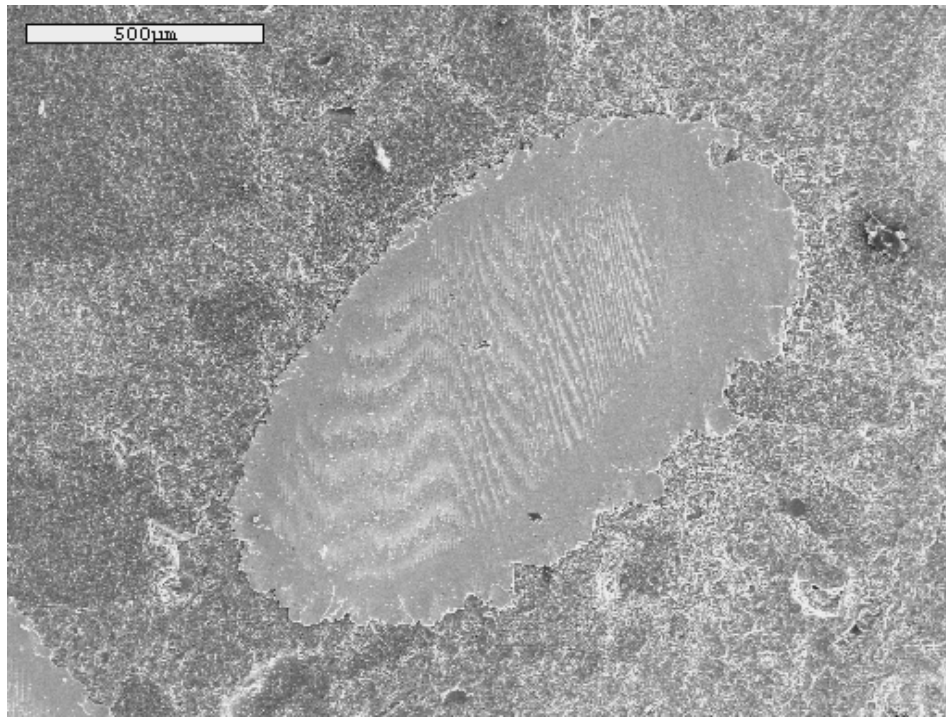


E

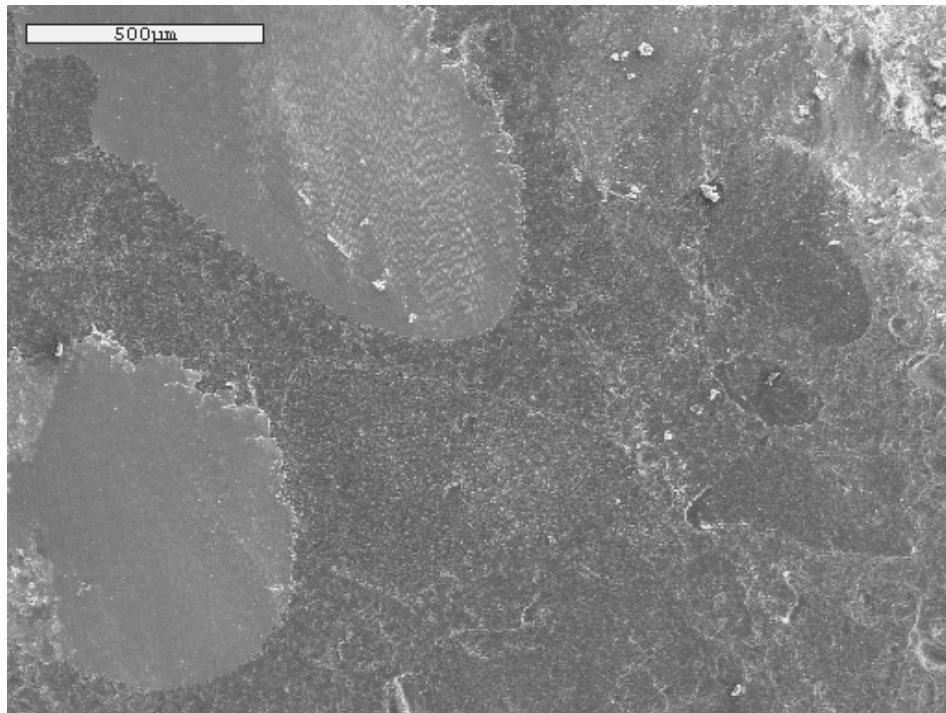


F

Figure 5-46. Continued. E) EDS spectrum for limewater immersion. F) EDS spectrum for saltwater immersion.

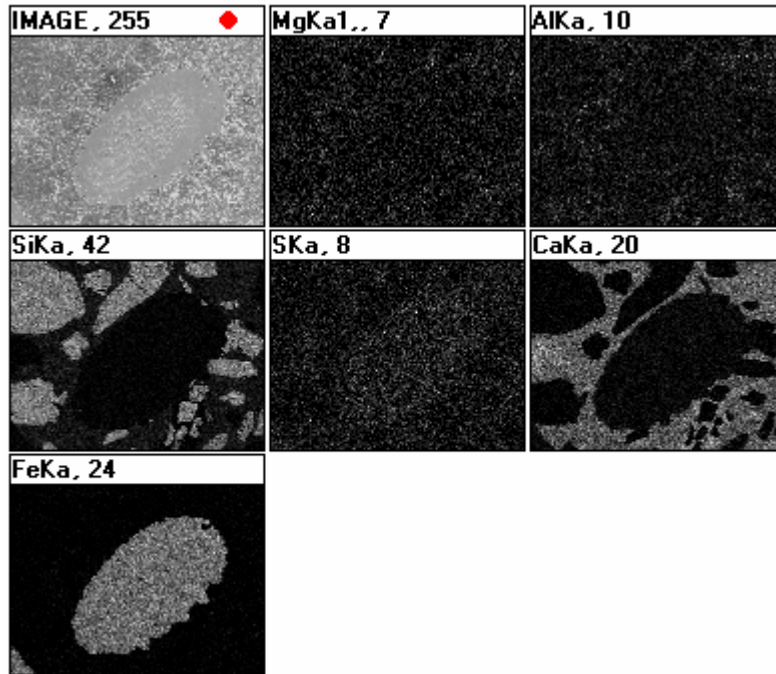


A

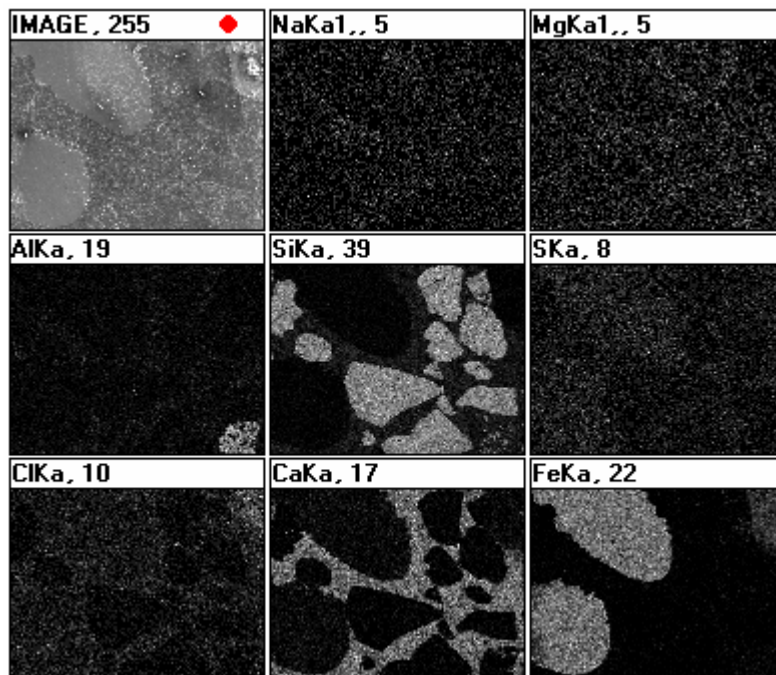


B

Figure 5-47. Steel fiber comparisons in limewater and saltwater immersion. A) SE image (60x) for limewater immersion. B) SE image (60x) for saltwater immersion.

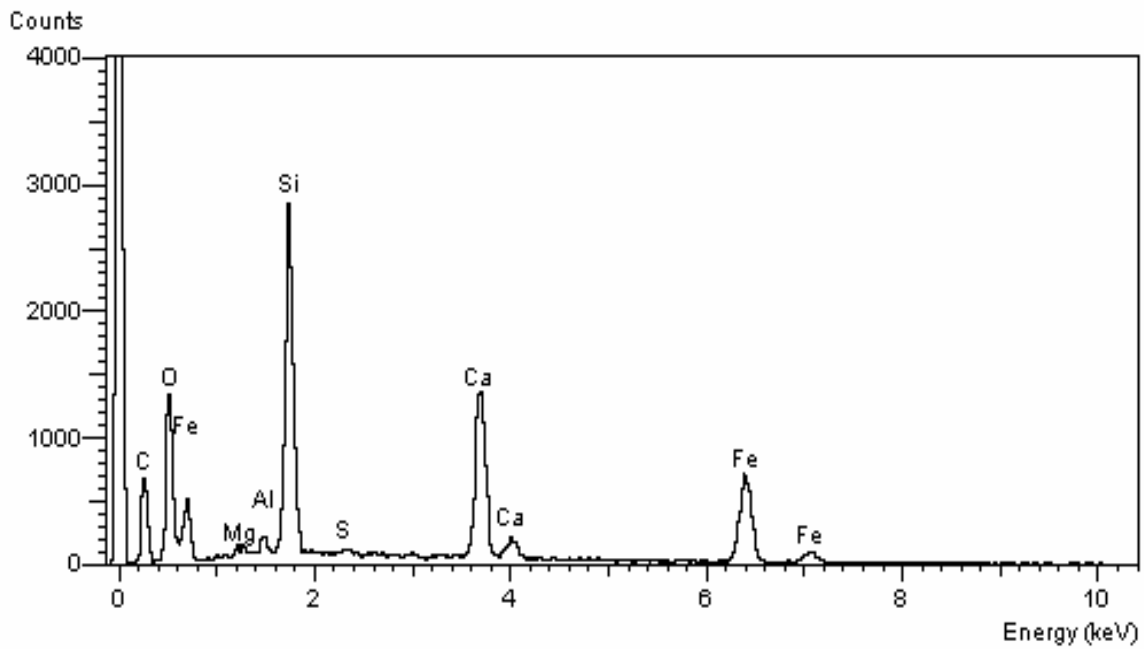


C

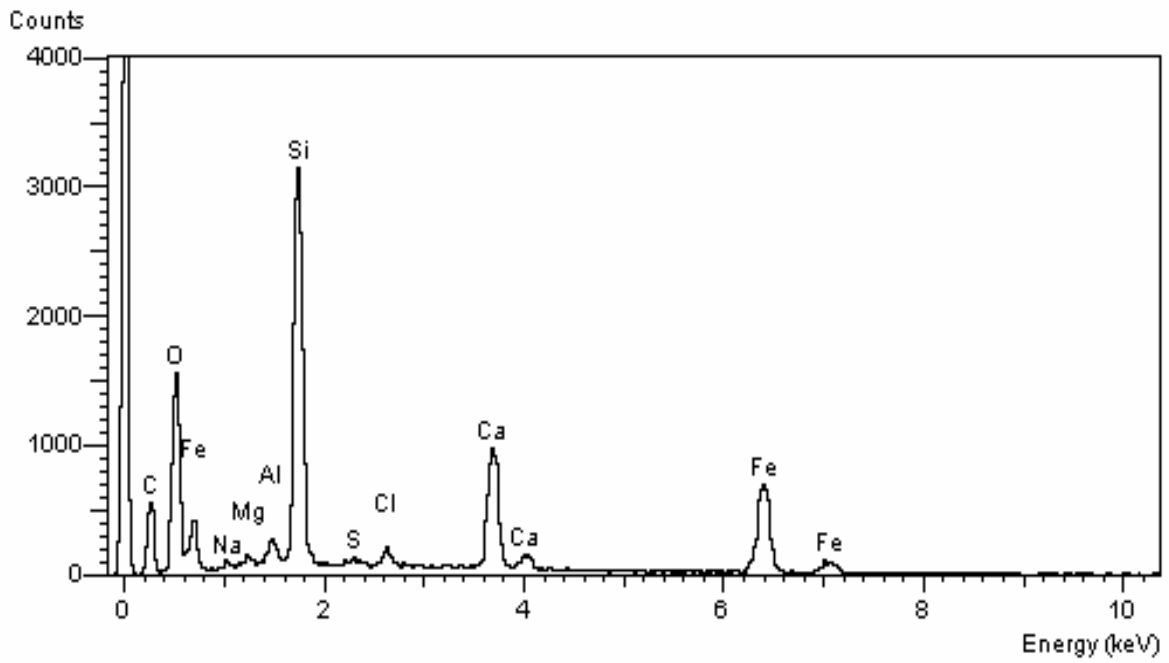


D

Figure 5-47. Continued. C) Dot mapping for limewater immersion. D) Dot mapping for saltwater immersion.



E



F

Figure 5-47. Continued. E) EDS spectrum for limewater immersion. F) EDS spectrum for saltwater immersion.

### 5.6.8 Distribution Problem for Cellulose Fibers

Buckeye UltraFiber500™ is 100% virgin specialty cellulose fiber designed to provide an improved level of secondary reinforcement with high fiber surface area, close fiber spacing, excellent bonding with the cement matrix, high tensile strength, as well as to improve concrete durability by reducing the transport of deleterious materials. The manufacturer indicates that the addition of UltraFiber500™ reinforcing fibers at a normal dosage rate in the form of 5 x 6 mm chips containing over 33,000 fibers does not require any mix design changes. They also indicate that fibers disperse best when added at the beginning of the batching sequence following normal mixing time and speed, as recommended by ASTM C 94 (Buckeye Technologies Inc.).

However, cellulose fibers did not disperse properly in this project, and fiber balling was observed in the mixes. Test results for mechanical properties (compression, splitting tension, pressure tension strength) showed no improvement in strength or transport properties (absorption, permeability, diffusion), clearly indicating no improvement in resistance to mass transport of deleterious materials into concrete. Therefore, the number of beams for degraded specimens was reduced to two specimens for each environmental condition. Beam test results showed no post-cracking behavior and undistributed fibers were found as shown in Figure 5-48.

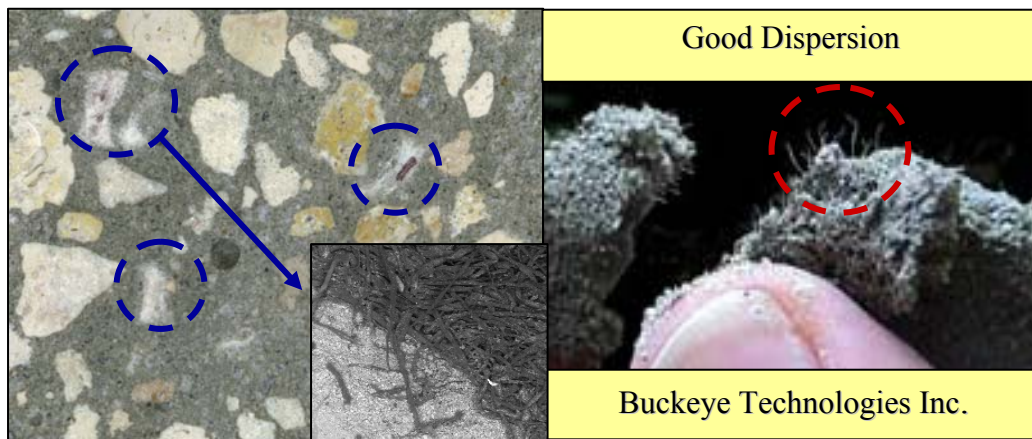


Figure 5-48. Cellulose fibers distribution: undistributed fibers (left) at this project; good distribution (right) in cement paste from manufacture

## 5.7 Discussion of Conventional Beam Approach

For fiber reinforced concrete, the flexural beam test with third-point loading is most commonly used to evaluate the effect of fiber degradation on the flexural strength and toughness due to bridging effect subsequent to matrix cracking (Kosa et al., 1991). Previous researchers (Morse et al., 1977; Mangat et al., 1985) have used beams subjected to the wet/dry cycles to evaluate the durability of fiber reinforced concrete. To accelerate the deterioration mechanism, specimens were exposed to intermittent wetting and drying in simulated solutions over specific time periods. The durability performance of the specified beams representing structural elements such as columns or bridge decks was evaluated by determining the rate of reduction in strength or pullout resistance throughout the cracking process.

Although the flexural beam test is easy to prepare and perform, its cross-sectional stress and strain distributions are non-uniform and crack initiates at the bottom of the specimen, sometimes outside the middle third of the span for third-point loading. Also, beam specimens subjected to salt water conditioning for 6 months with the new wet/dry conditioning system developed in this study, created highly non-uniform degradation in the beam cross-section and variable crack initiation at failure as shown in Figure 5-49, making test data is difficult to interpret.

Typical examples of load versus deflection curves for PP, PVA, and Steel fibers exposed to limewater solution for 27 months are shown in Figures 50, 5-51, and 5-52. Beam specimens for each fiber type showed almost the same values in modulus of rupture due to uniformly distributed maximum moment at the bottom of the beam, and then the applied load dropped significantly subsequent to matrix cracking, when matrix stresses were transferred to the fiber and the fiber-matrix interface. A schematic diagram for unstable failures in fiber reinforced concrete is presented in Figure 5-53. The instability at first cracking from non-uniform stress

distribution in the cross-section and variable cracking away from the specimen's center resulted in highly unstable behavior of fibers during the post-cracking process.

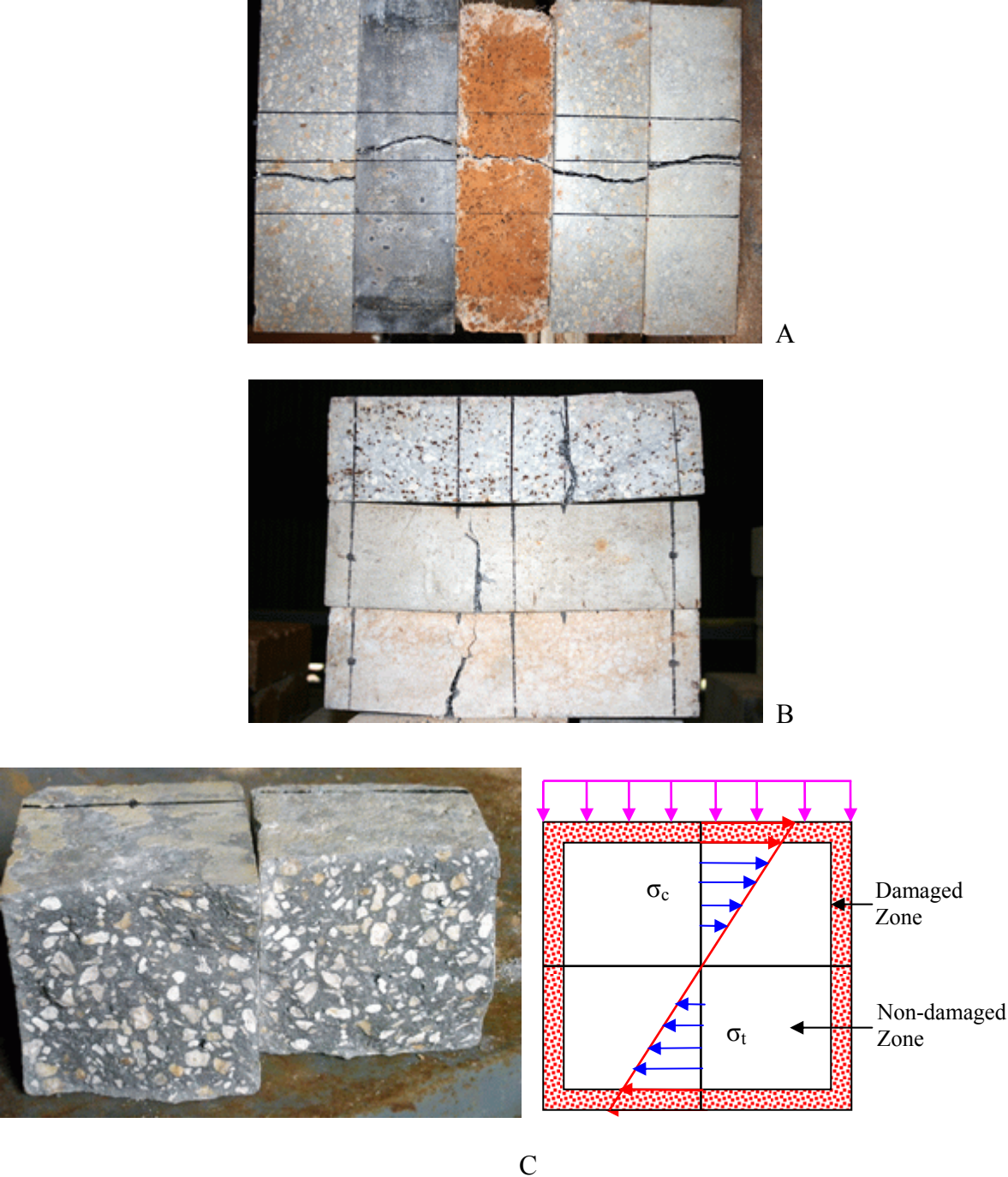


Figure 5-49. Test result for flexural beam testing with third-point loading. A) Multiple cracking for PVA fibers. B) Multiple cracking for Steel fibers. C) Non-uniformly damaged specimen and stress distribution.

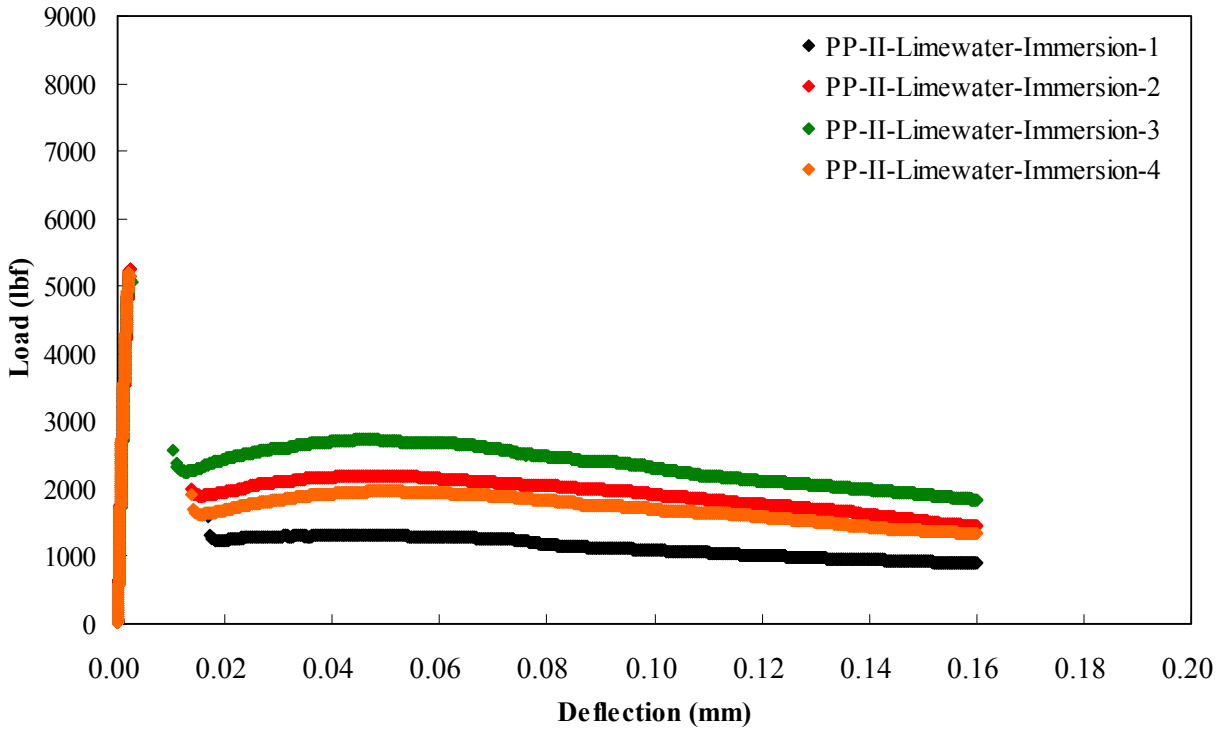


Figure 5-50. PP fiber mix for limewater immersion for 27 months

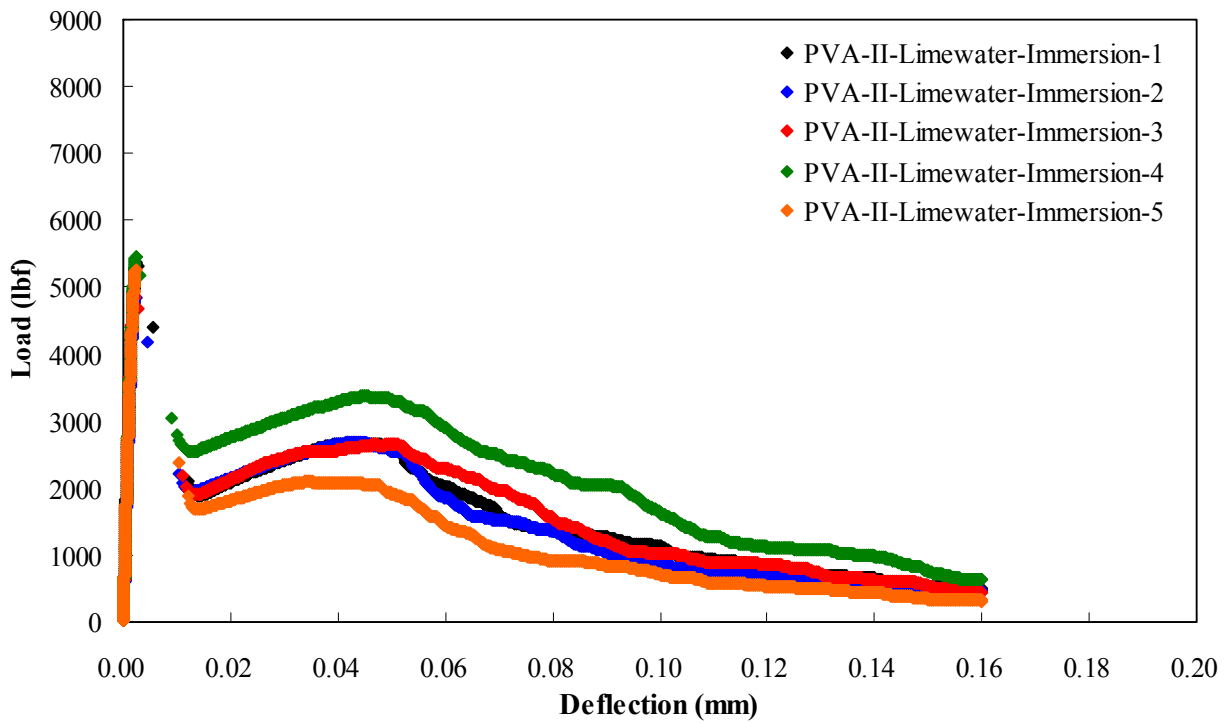


Figure 5-51. PVA fiber mix for limewater immersion for 27 months

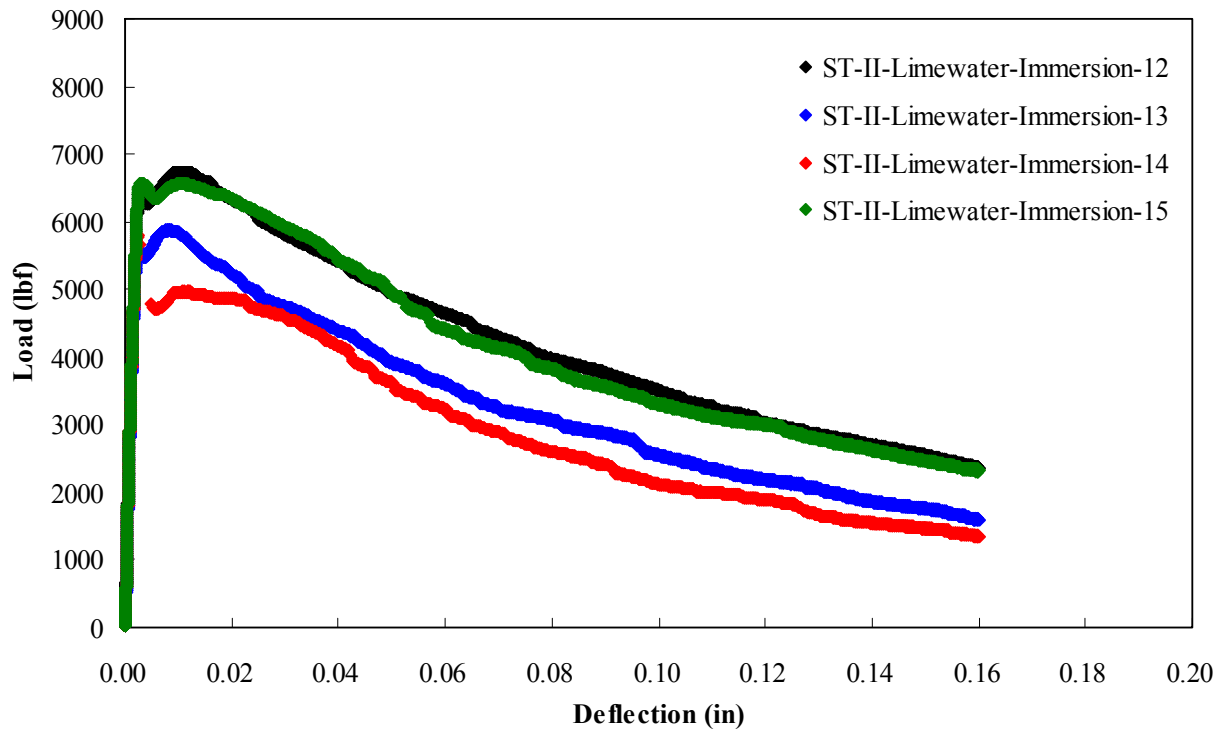


Figure 5-52. Steel fiber mix for limewater immersion for 27 months

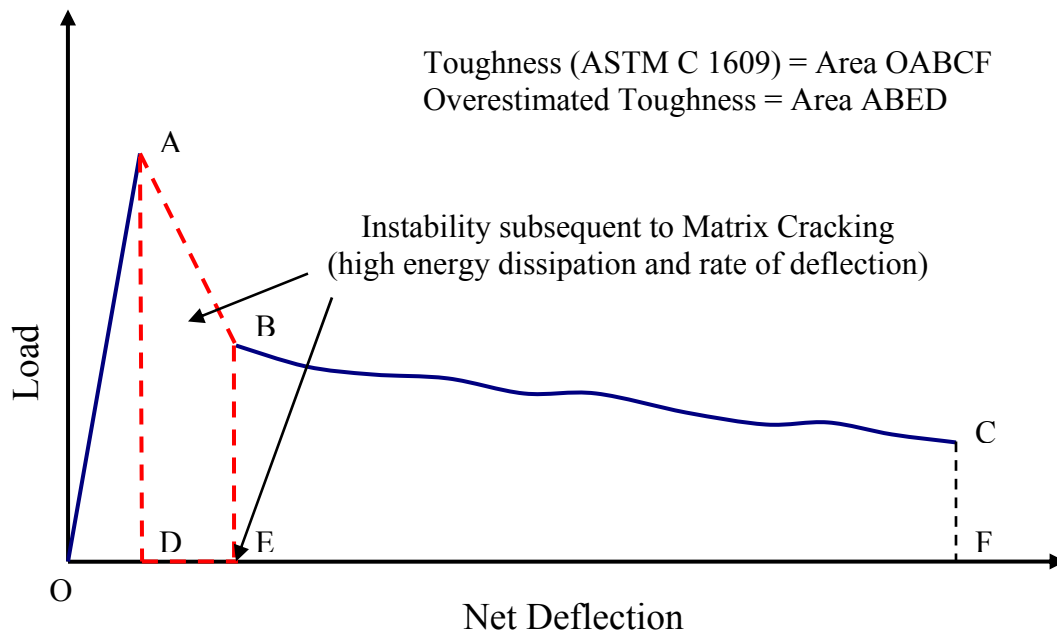


Figure 5-53. Unstable failure in fiber-reinforced concrete

Coefficients of variation for flexural performance test results are shown for each fiber type and conditioning method in Figures 5-54, 5-55, and 5-56. Significant increase in coefficient of variation was found subsequent to matrix cracking for all fiber types and conditioning methods. Non-uniform stress distributions in the cross-section, unstable crack initiation, and high energy dissipation (overestimated toughness) at first cracking appeared to affect the failure mechanism of fibers during post-cracking. The effects of overestimated energy to toughness measurement from instability subsequent to matrix cracking are shown in Figure 5-57. It is noted that PP and PVA fibers were significantly affected. Consequently, the flexural test was found to have serious limitations for durability evaluation. Therefore, another approach is needed for specimen preparation, conditioning, and testing.

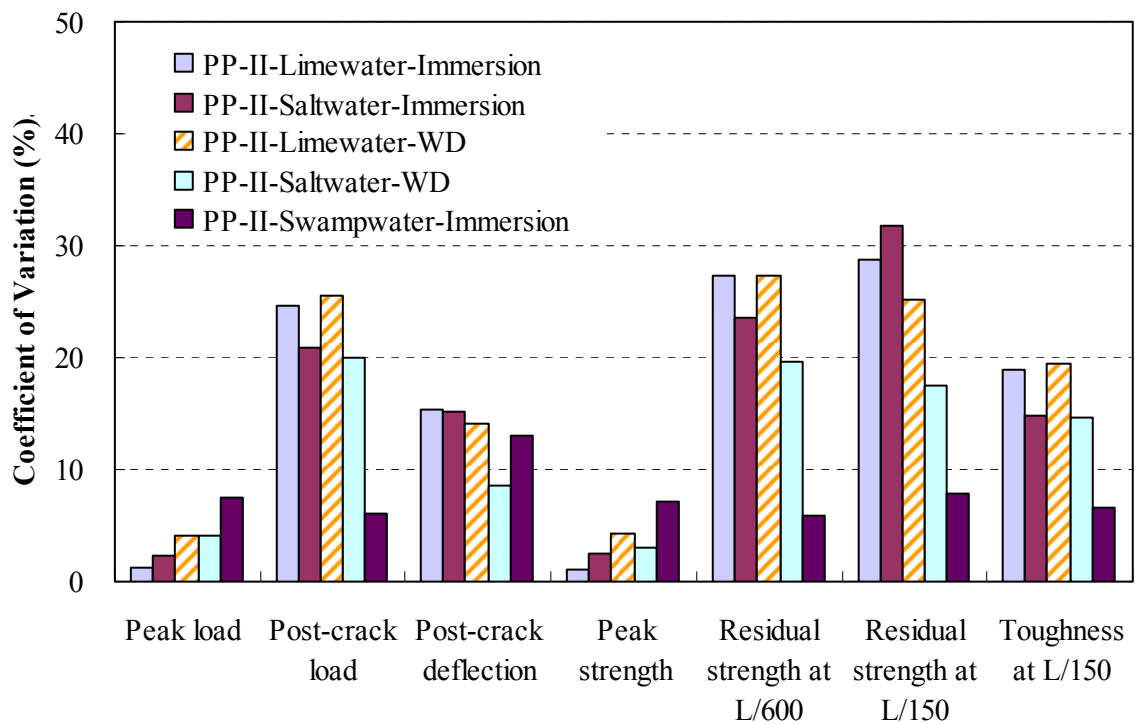


Figure 5-54. Coefficients for PP fiber beams

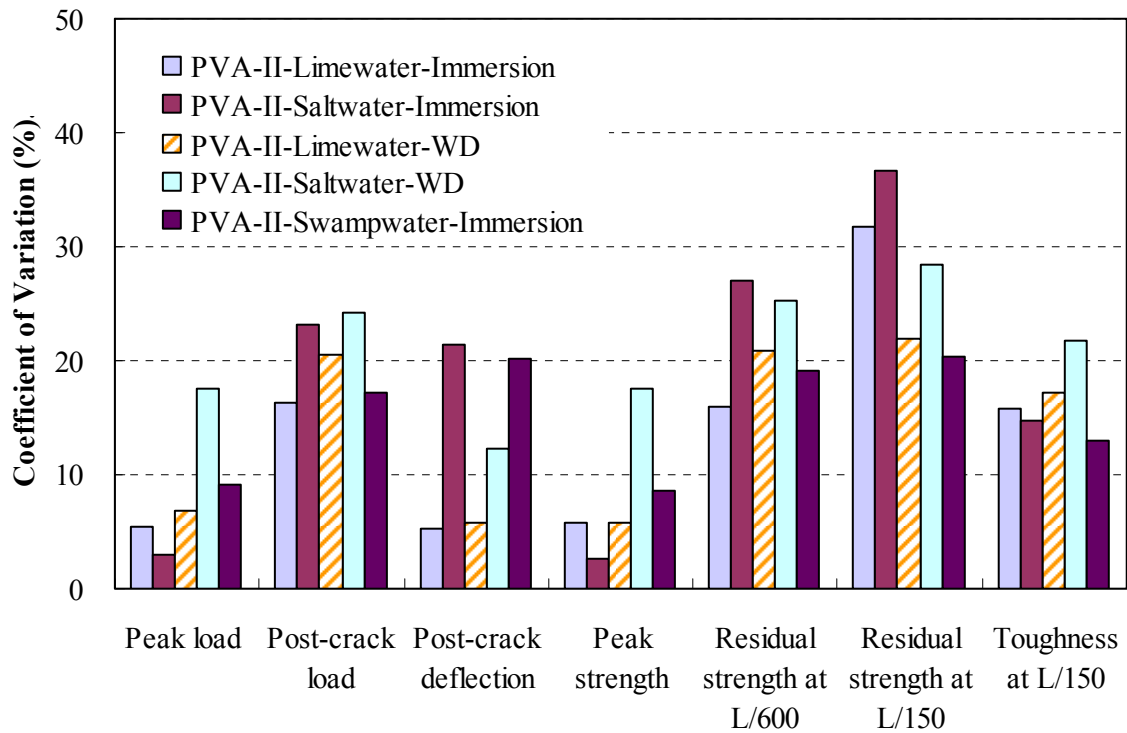


Figure 5-55. Coefficients for PVA fiber beams

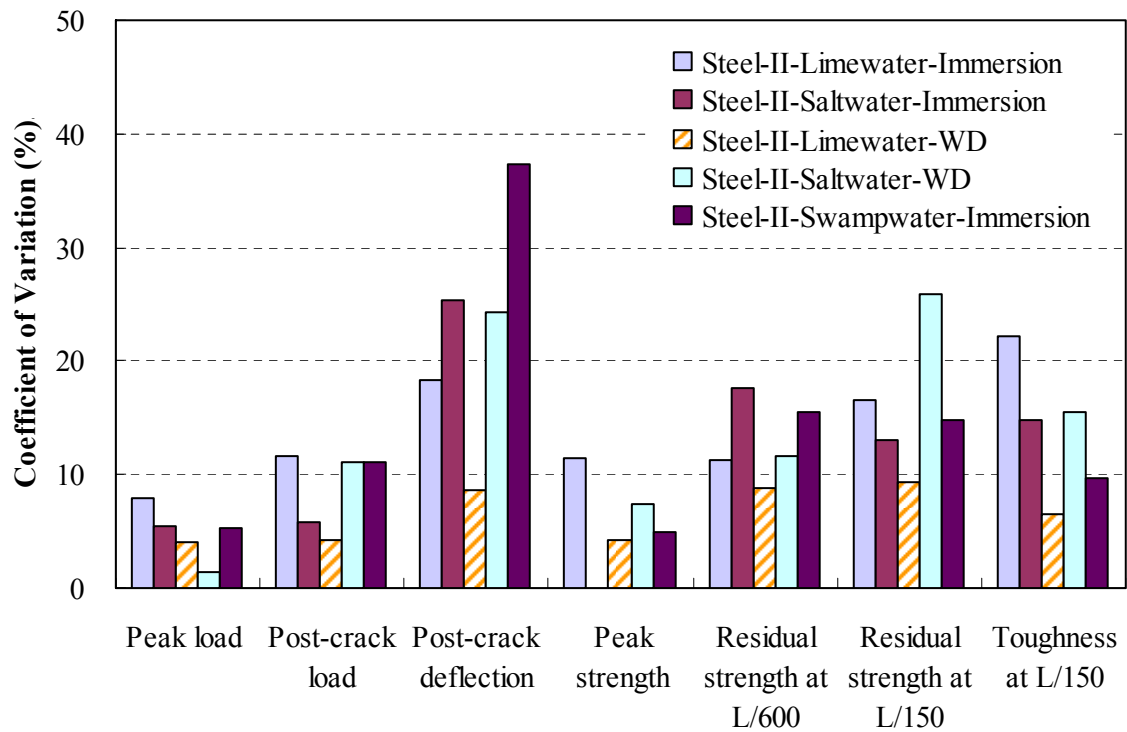


Figure 5-56. Coefficients for steel fiber beams

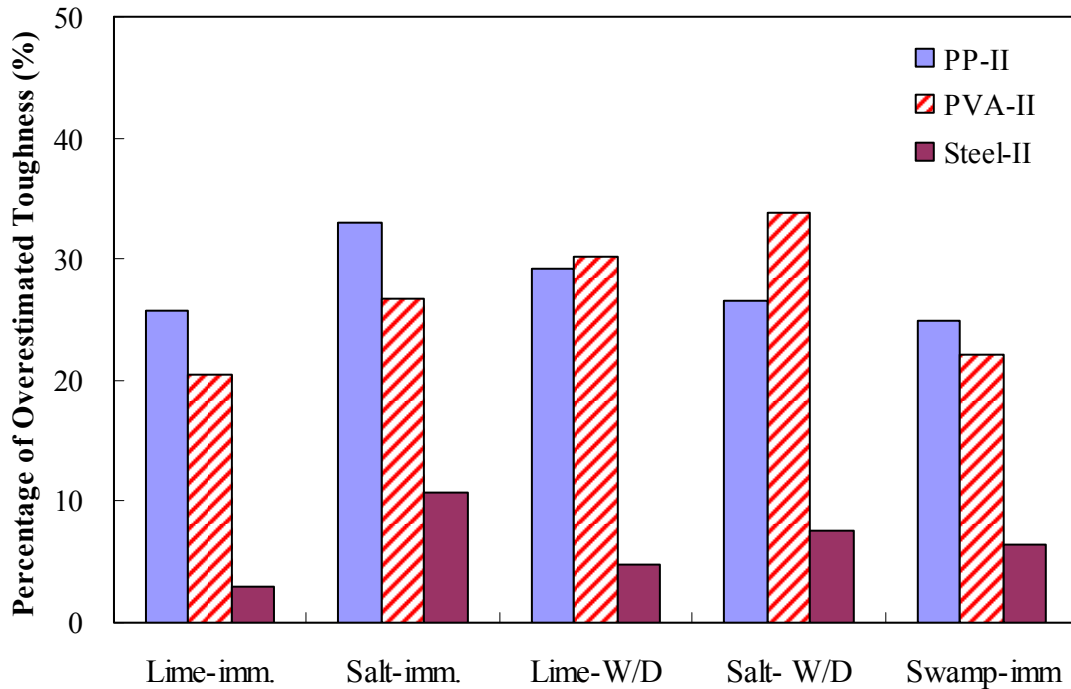


Figure 5-57. Overestimated energy effect on determination of toughness

### 5.8 Summary of Conventional Beam Testing

This section summarizes the environmental resistance of FRC exposed to various conditioning methods based on test results from residual strength (ASTM C 1399) and flexural performance (ASTM C 1609). The results may be summarized as follows:

- Test results from both average residual strength (ASTM C 1399) and flexural performance (ASTM C 1609) tests were not effective to evaluate deterioration of FRC exposed to various conditions. Specimens exposed to acidic solutions showed significant degradation in both ARS and flexural performance for all fiber types. However, it was not possible to clearly assess fiber resistance to crack propagation with the conventional beam approach because of non-uniform stress distributions, multiple cracking, and instability, which affect the pull-out mechanism of fibers. Observation and test methods from SEM and EDS analysis were probably also affected by problems associated with the flexural beam approach.
- Beam specimens also can be problematic in terms of achieving proper conditioning using cyclic wetting and drying. It was found that cyclic wetting and drying only degrades the outer half inch shell of beam, which results in non-uniformly damaged cross-sections.

- These results clearly indicated the need to develop effective conditioning to achieve uniformly damaged specimen. Also, proper test methods are required to clearly evaluate failure mechanisms from the pull-out of fibers as a result of chemical deterioration.

## CHAPTER 6 DEVELOPMENT OF CONDITIONING AND TEST METHOD

### 6.1 Introduction

A conditioning system that effectively accelerates damage and results in a uniformly damaged specimen is required for proper evaluation of the effects of degradation on physical properties. Furthermore, an effective testing system that is sensitive to the effects of fibers is also needed to evaluate differences in fiber pull-out resistance caused by deterioration.

Conceptually, uniform stress distribution at the failure surface can be obtained in the direct tension test. However, the test specimen must be perfectly glued to the loading heads or held between grips. Mechanical grips are generally a problem in direct tensile testing since a biaxial tensile stress condition will be induced in the specimen's end through the lateral confinement (Mier, 1997). A similar effect develops when loading heads are epoxied to the specimen, which is also time consuming. The indirect tensile test mode has unique advantages for transporting deleterious material into the specimen and for obtaining a uniformly degraded cross-section, as well as uniform stress and strain distributions.

### 6.2 Determination of Conditioning and Specimen Thickness

Figure 6-1 indicates that absorption depths by capillarity for different fiber types and concrete classes clearly depend on time. A seven day wetting cycle is needed to penetrate Class II concrete by capillary action to a depth of one inch. Additional time is required to penetrate Class V concrete, which had less depth of penetration than Class II concrete at seven days. A 9.5-mm diameter hole was introduced at the center to concentrate stress and further accelerate ingress of deleterious materials around the hole. Based on absorption test results, a one inch thickness with the circular hole in the center of the specimen, obtained by seven days of wet

conditioning by capillary action from both sides, appears to be appropriate to obtain a uniformly damaged FRC specimen for the indirect tensile testing.

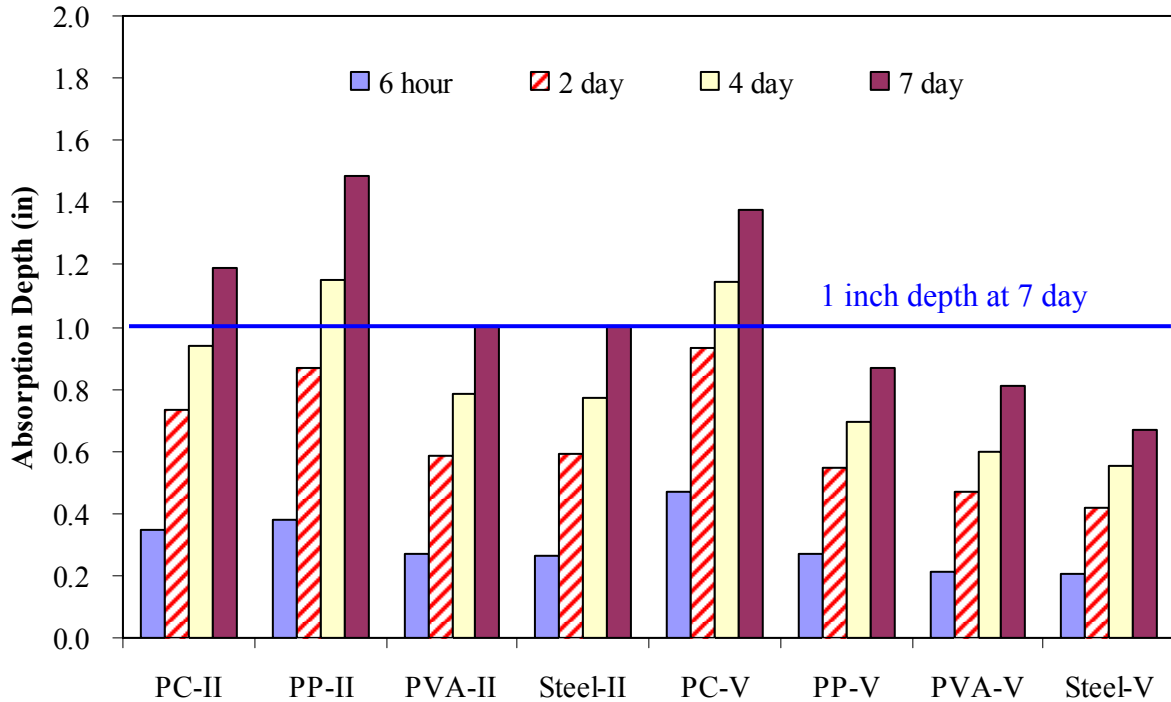


Figure 6-1. Absorption depths vs. time for fiber type and Classes II/V concrete

### 6.3 Proposed Test Method

The indirect tensile test has been developed and used extensively to determine stiffness and fracture properties of asphalt materials. A 3-dimensional finite element model with 100 mm diameter and variable thicknesses was used to evaluate and analyze indirect tension specimens (Roque et al., 1992). The theoretical stress distribution on the vertical diametral plane is fairly uniform near the center of the specimen as shown in Figure 6-2. However, there are significant differences between the theoretical plane stress analysis and the 3-dimensional specimen behavior. Uniformly distributed horizontal tensile stress was found to exist for specimen thickness of less than one inch. On the other hand, for specimen thickness of 2.5 inches and greater, the difference in horizontal stresses between the specimen face and center is about 30%.

In addition, non-uniform specimen bulging on the specimen face and edges occurs, which affects deflection measurements obtained at the surface by producing sensor rotating during the test. Therefore, one inch thickness is not only most appropriate for evaluating FRC with Indirect Tensile Test (IDT) based on the absorption test results, but also from the standpoint of stress uniformity. The sensor mounting system shown in Figure 6-2, having a gage length of one inch was recommended for 4 inches diameter specimens (Roque et al., 1992). A key advantage of IDT is that the fracture plane is known before testing. Therefore, fracture limits can be determined exactly on the fracture plane.

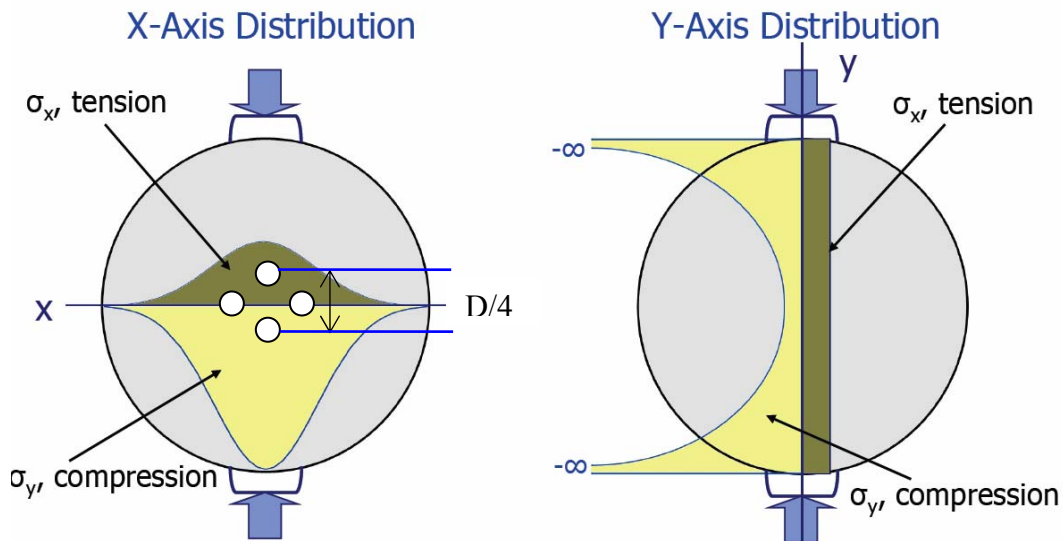


Figure 6-2. Theoretical stress distribution and gage points spaced at depth/4

The schematic test setup for Superpave™ indirect tensile mode is shown in Figure 6-3. The one deviation from standard Superpave™ IDT testing is the use of a 100×100 mm (4×4 inches) square shape specimen with 25.4 mm (one inch) thickness as opposed to a circular specimen. The rectangular specimens can be obtained more easily from beam specimens. Finite element analysis was performed to compare stress distributions between circular and square shapes. The results presented in Figure 6-4 show that the same stress distribution along vertical

plane was observed between the square and the circular specimen. As mention earlier, to accelerate transport mechanisms and concentrate stress, a 9.5 mm size circular hole as shown in Figure 6-5 was cored in the center of the specimen.

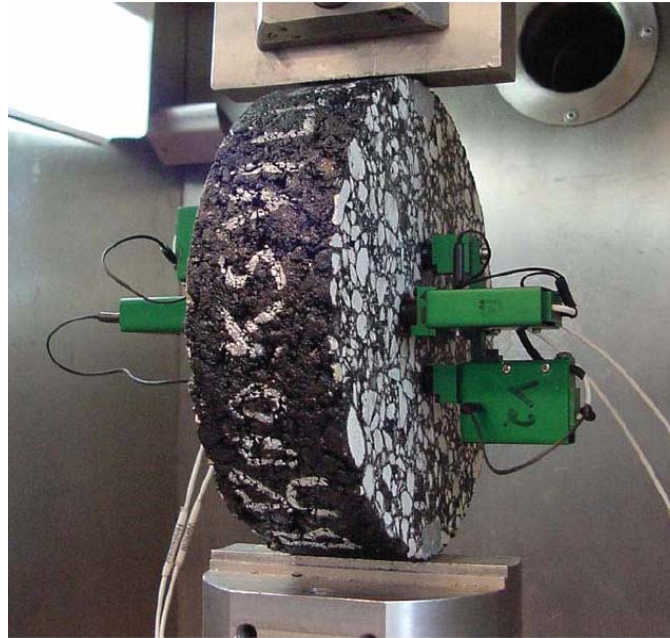


Figure 6-3. Superpave™ IDT specimen setup

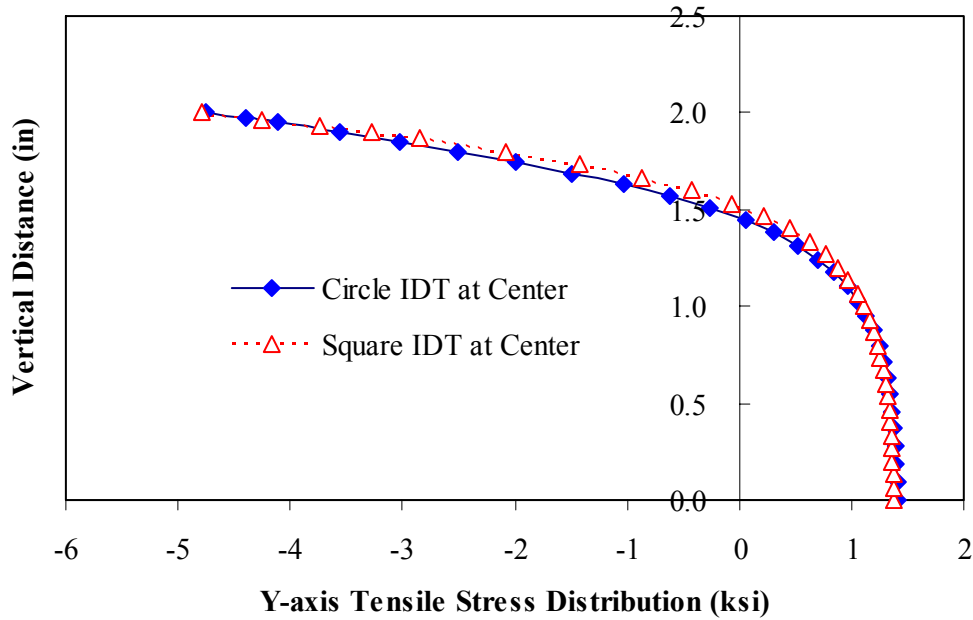


Figure 6-4. 2-Dimensional FEM analysis for circle and square shapes IDT

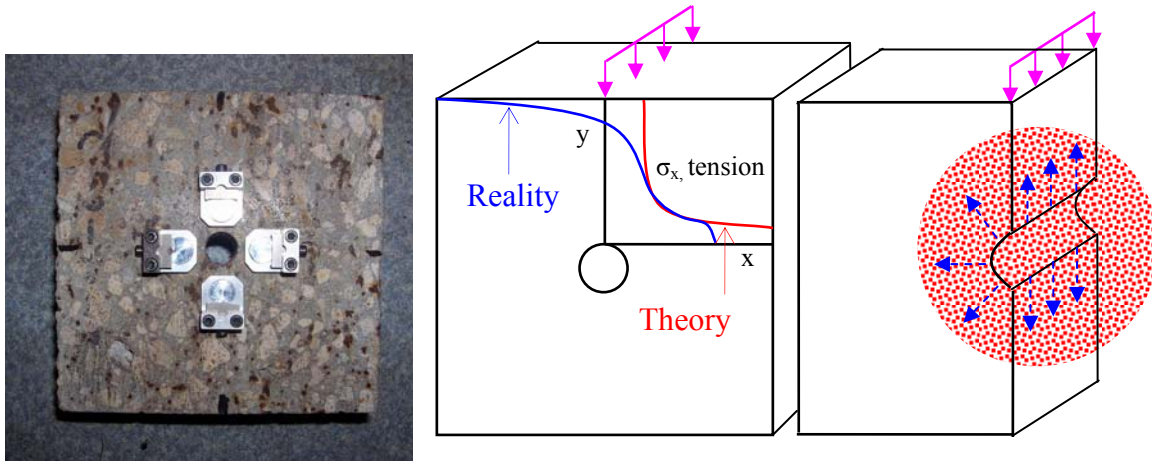


Figure 6-5. Proposed test specimen and stress distribution

## 6.4 Evaluation of Fiber Resistance to Conditioning

### 6.4.1 Experimental Program

An experimental program was carried out to evaluate the resistance of fibers to crack propagation in concrete subjected to different conditioning methods. The experimental program included the following components:

#### (1) Specimen Preparation

- One inch IDT specimens were sliced from beam specimens conditioned in lime water at 21 months. Class II concrete for PP, PVA, and Steel fibers was used. Tests were not performed for control and cellulose fiber mixes because they did not exhibit post-cracking behavior. Table 6-1 summarizes fiber type and number of specimens used for testing.

#### (2) Strength Testing

- Strength testing was performed at a constant rate of net displacement of 0.005 in/min until a crack was initiated in the specimen.

#### (3) Repeated Load Testing

- Repeated load testing was performed after crack initiation with a constant repeated haversine load of 0.1 second followed by a rest period of 0.9 second.
- Two horizontal deformation measurements, applied load, and the corresponding time were recorded at a rate of 500 points per seconds for 6 seconds at intermittent times until the maximum horizontal deformation was reached.

Table 6-1. Number of specimens tested for IDT for Class II concrete

Mix Type	Fiber Type	Fiber Volume Fraction $V_f(\%)$	Environmental Exposure			
			Limewater Immersion	Saltwater Immersion	Limewater WD	Saltwater WD
PP	Polypropylene	0.5	3	3	3	3
PVA	Polyvinyl Alcohol	0.75	3	3	3	3
Steel	Hooked Steel	1	3	3	3	3

### 6.4.2 Exposure Conditions

IDT specimens were exposed to limewater immersion, saltwater immersion, limewater W/D, and saltwater W/D for an additional 6 months. Water temperature and simulated seawater solutions were identical to those used for beam conditioning. The new wet/dry conditioning system proposed for beam conditioning with heater/blower was applied with a reduced tank volume. Seven days for wetting and seven days for drying time were repeated to maximize chemical ions gain and loss with minimal micro-damage. A flow chart showing the experimental program and numbers of specimens for environmental conditioning is summarized in Figure 6-6.

### 6.4.3 Testing Procedures

Indirect tensile test with low loading rate (0.005 in/min) was first carried out to initiate cracking in the hardened cement paste matrix. Slow loading rate of cross-head movement minimized the energy dissipation and the high rate of deflection of the specimen subsequent to first cracking. Once first cracking was initiated, repeated loading was performed for each fiber type using 90% of the averaged maximum load required to initiate cracking. Total horizontal deformation, resilient horizontal deformation, applied load and the corresponding times were measured. The test setup for IDT is shown in Figure 6-7.

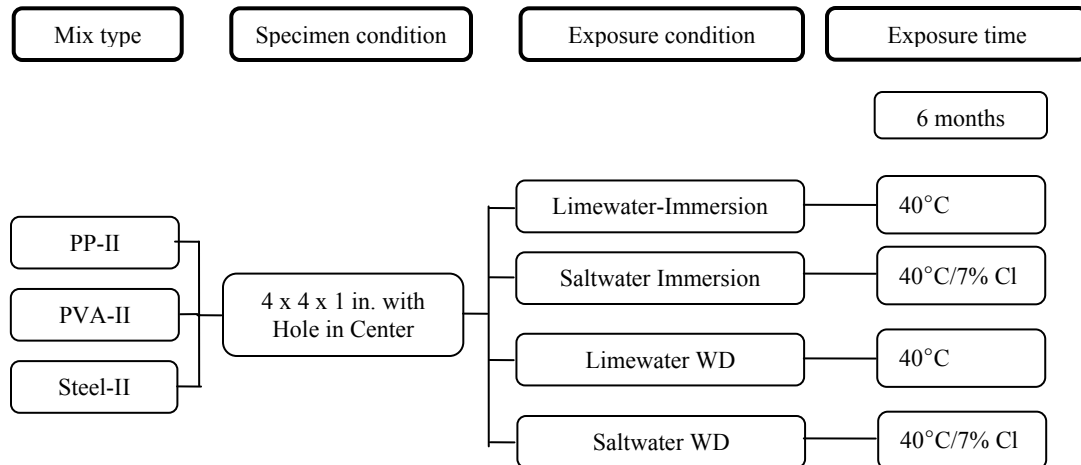


Figure 6-6. Flow chart for experimental program



Figure 6-7. Test setup for IDT

#### 6.4.4 Evaluation of the Fracture Tests

This section summarizes the fracture test results obtained from strength and repeated load tests for each fiber type after 6 months of accelerated environmental conditioning. Evaluation of the fracture test results presented in this section includes: (1) visual examination of fractured specimens; (2) strength test results; (3) evaluation of horizontal deformation; (4) evaluation of horizontal resilient deformation ratio.

#### **6.4.4.1 Visual examination of fractured specimens**

Fracture subsequent to matrix cracking for each fiber type was exactly initiated at the center of the hole, which generated the maximum tensile stresses, as shown in Figure 6-8. Significant degradation of the matrix and the fiber on the surface for each fiber type was observed for cyclic wetting and drying in saltwater. Among fiber types, considerable steel fiber corrosion was found in both surface and internal specimens for salt water immersion and salt water cyclic wetting and drying as indicated in Figure 6-9, as well as that of the cored hole surface showing significant steel fiber rusting. It appeared that the new conditioning system from specially designed heater/blowers completely saturated IDT specimens and generated uniformly damaged specimens. In addition, the fractured planes subsequent to matrix cracking were uniform regardless of fiber type.

#### **6.4.4.2 Examination of strength test results**

Figures 6-10, 6-11, and 6-12 show strength test results with loading rate of 0.005 in/min compared with the flexural beam test results subsequent to crack initiation in the hardened cement paste matrix. Indirect tensile mode for PP, PVA, and Steel fiber mixes instantly transferred the load from the matrix to the fiber without the high energy dissipation and the high rate of deflection, which was commonly observed in beam testing at the moment of matrix failure. It was noted that strength tests performed at slower loading rates minimize the instability subsequent to matrix cracking which can significantly affect post-cracking behavior of fibers embedded in the hardened cement paste matrix.



A



B



C

Figure 6-8. Surface degradation and failure plane for saltwater cyclic W/D. A) PP fiber specimen. B) PVA fiber specimen. C) Steel fiber specimen.

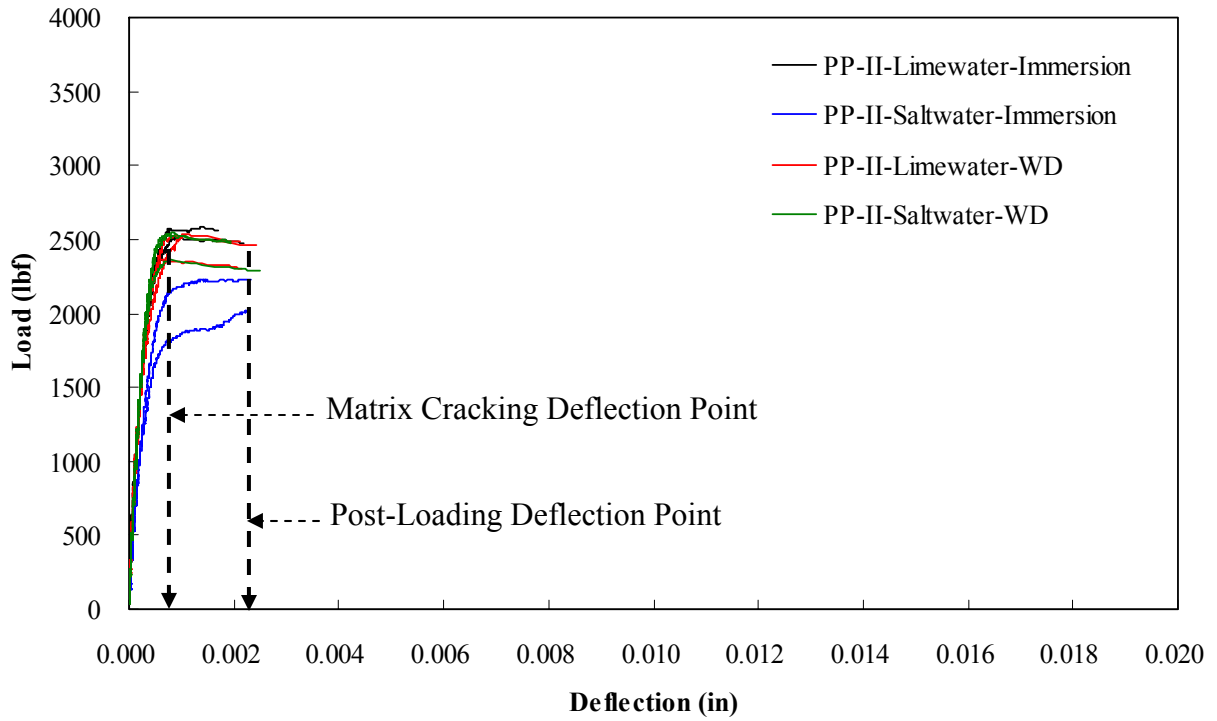


A

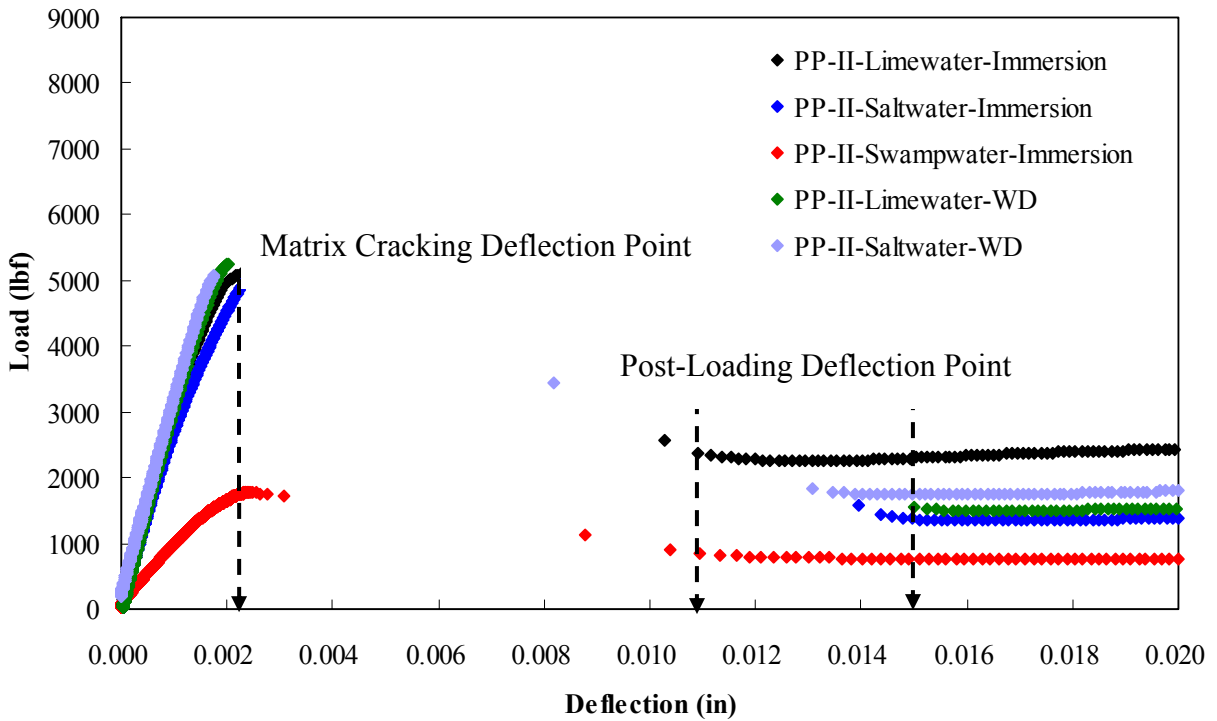


B

Figure 6-9. Fractured surface degradation for Steel fibers. A) Comparison with lime water immersion and w/d. B) Comparison with salt water immersion and w/d.

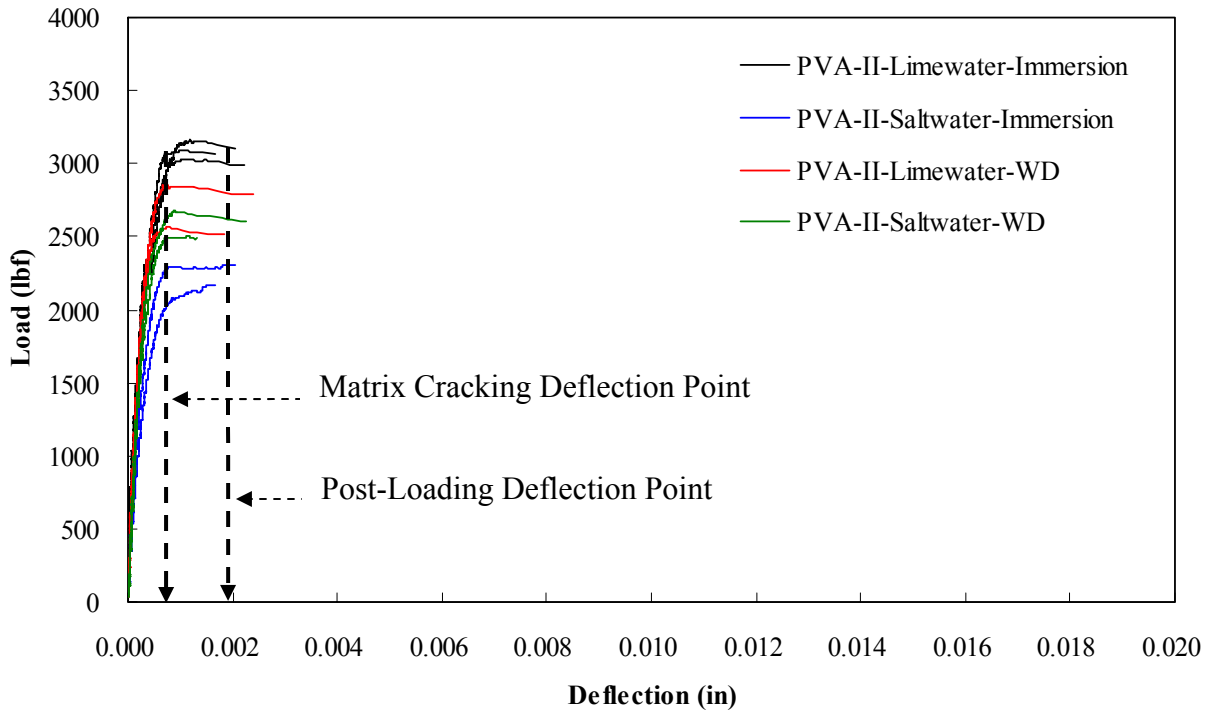


A

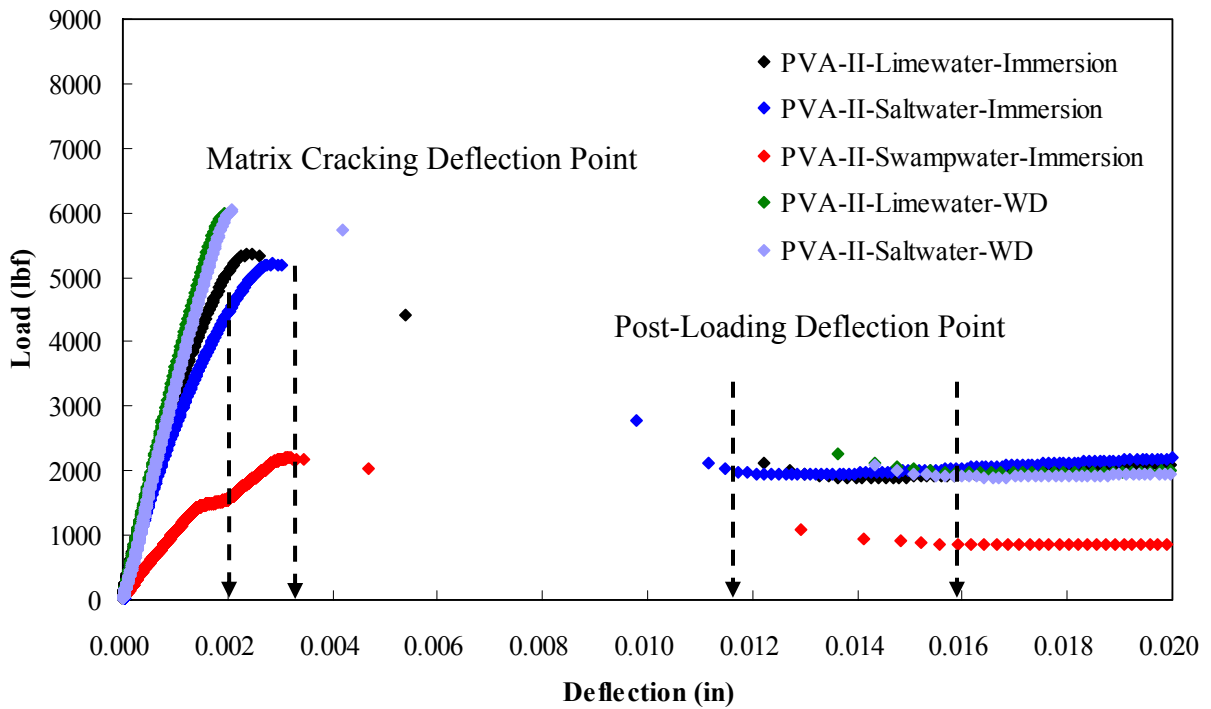


B

Figure 6-10. Comparison of strength test results at first cracking for PP-II mixes. A) IDT. B) Beam test.

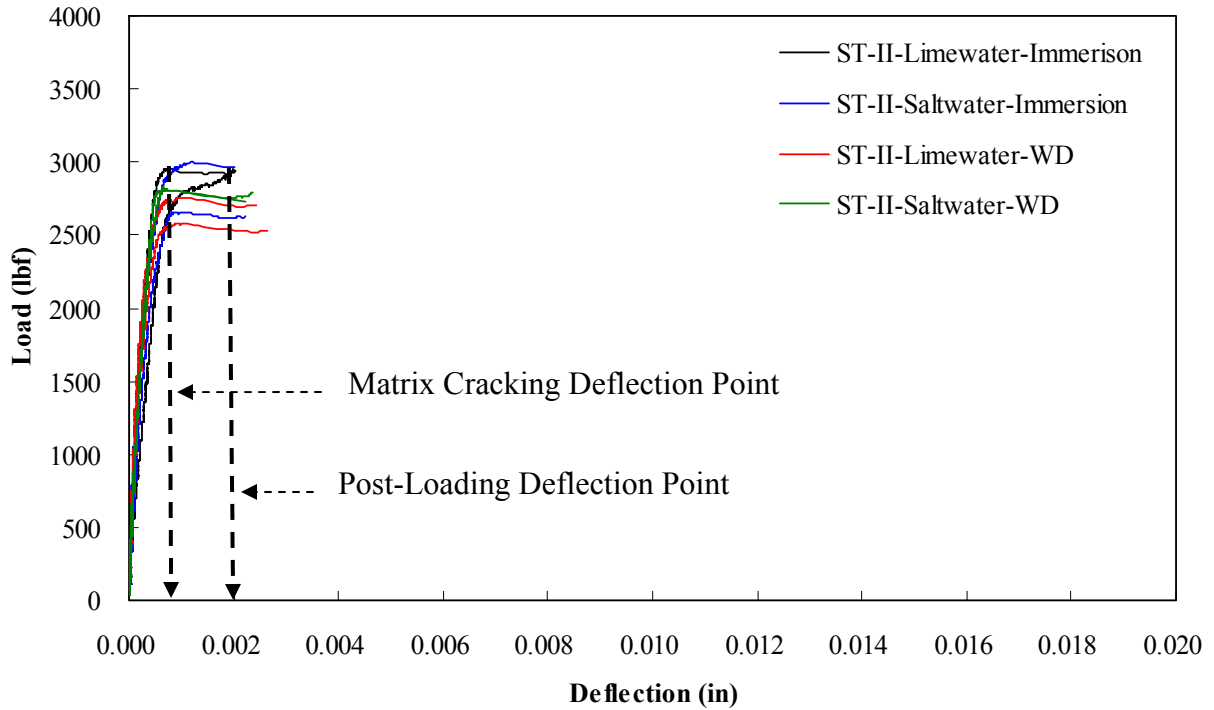


A

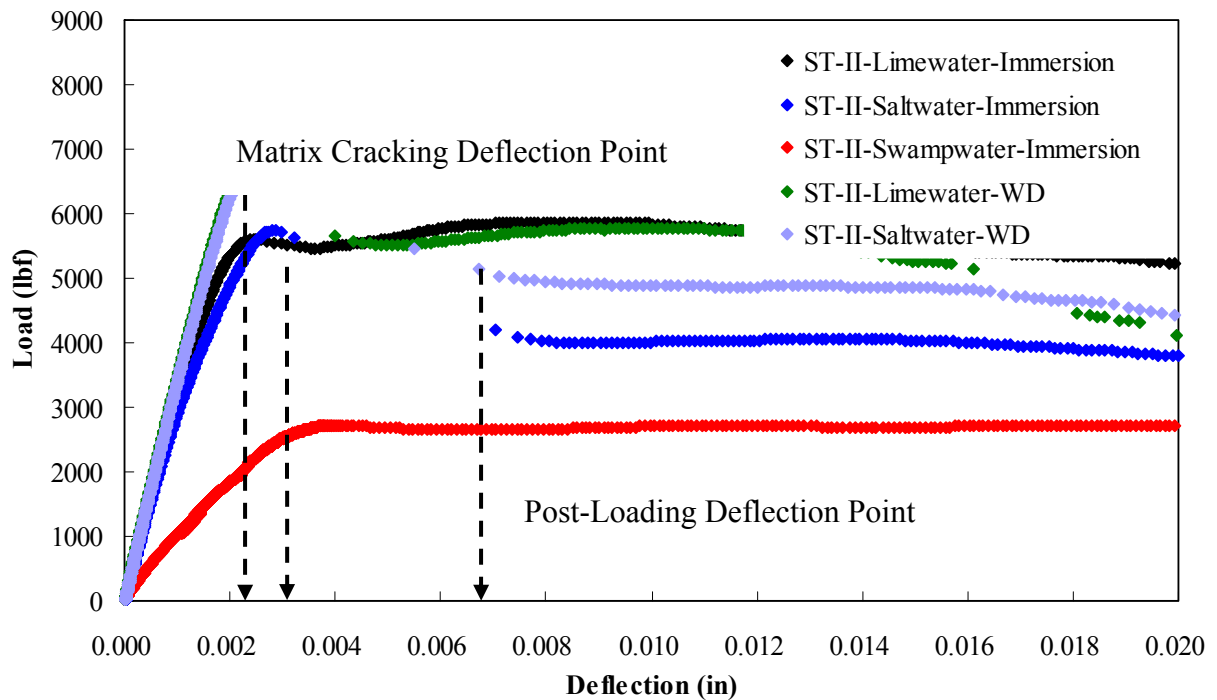


B

Figure 6-11. Comparison of strength test results at first cracking for PVA-II mixes. A) IDT. B) Beam test.



A



B

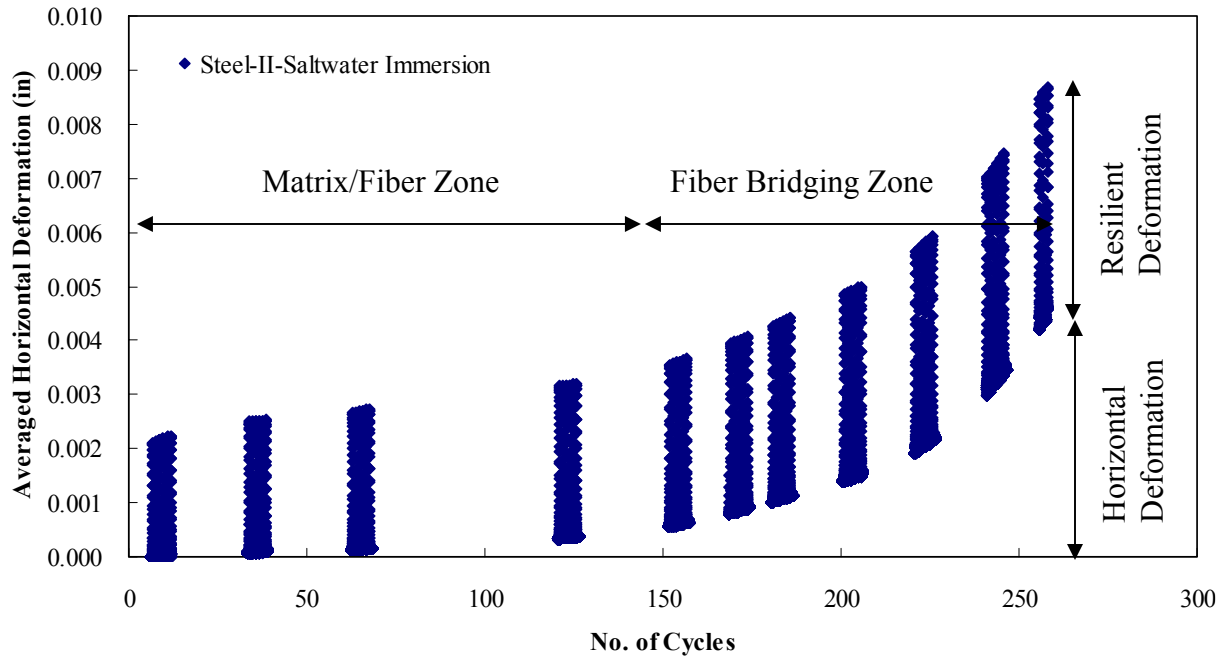
Figure 6-12. Comparison of strength test results at first cracking for steel-II mixes. A) IDT. B) Beam test.

#### **6.4.4.3 Examination of repeated load test results**

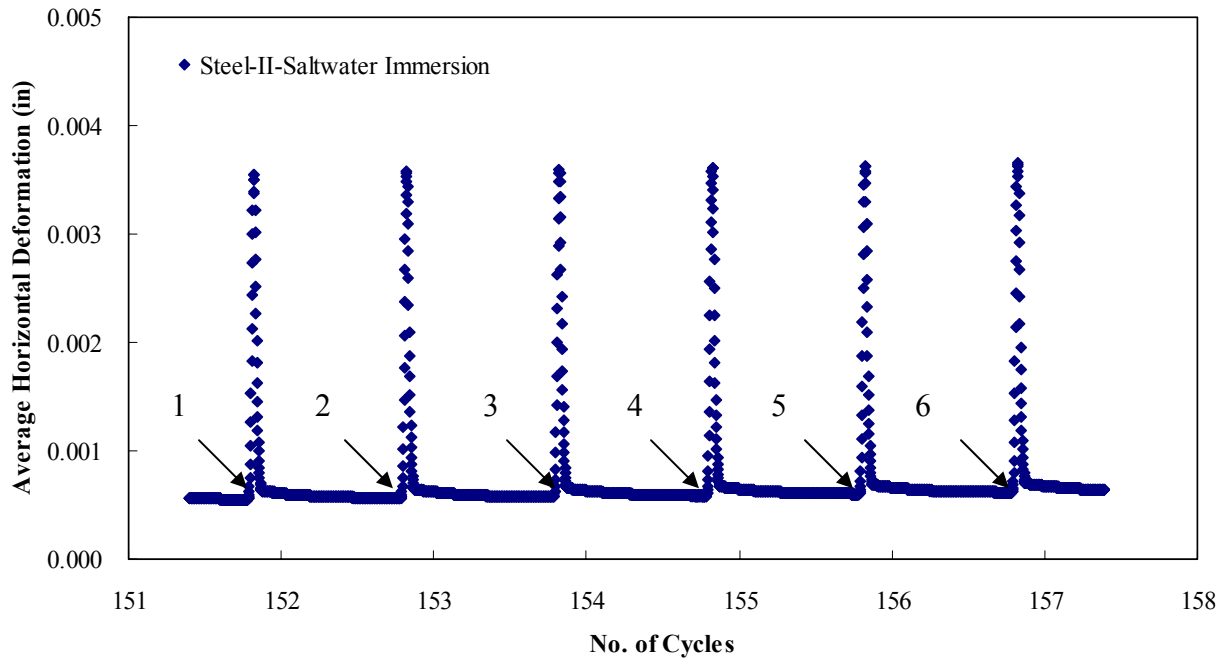
Bridging forces from the hardened cement paste matrix to the fiber resulting from shear deformation at the fiber-matrix interface can be represented as fiber resistance to crack propagation or pullout from the matrix during post-cracking behavior. The mechanical bonding properties for degraded fibers at the interface govern the fracture toughness and durability of FRC and results in different fracture mechanisms during crack propagation (Beaudoin, 1990 and Bentur and Mindess, 1990).

Typical test results from repeated load testing in Figure 6-13a show that the matrix and the fiber simultaneously resist crack propagation and/or pull-out of fibers embedded in the matrix during the initial part of cyclic loading. The reason for this initial cracking behavior is that fibers in concrete immediately resist a crack propagation of the matrix subsequent to first cracking due to the effect of fairly uniform distribution of stresses around the fracture plane resulting from slow loading rate. Therefore, the instant when fiber resistance initiates and matrix effect is minimized needs to be clearly identified.

Horizontal deformations were averaged from six repeated cycles as shown in Figure 6-13b and were plotted again in Figure 6-14, 6-15, and 6-16 for each fiber type. Averaged horizontal deformation clearly shows the effects of matrix and fiber on post-cracking behavior and can be used to determine the point when the effect of the matrix minimizes.



A



B

Figure 6-13. Repeated loading test results for steel fiber mix for Class II concrete. A) Averaged horizontal deformation vs. number of cycles. B) Averaged horizontal deformation vs. number of cycles @150 cycles.

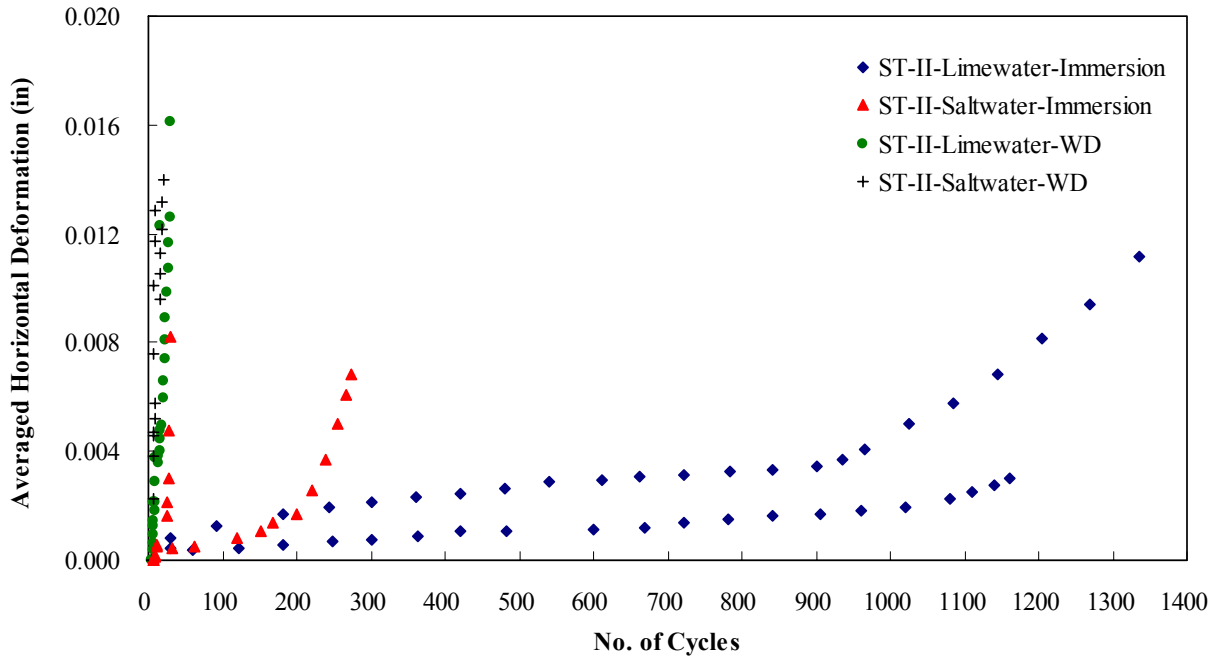


Figure 6-14. Averaged horizontal permanent deformation vs. number of cycles for steel fiber mix

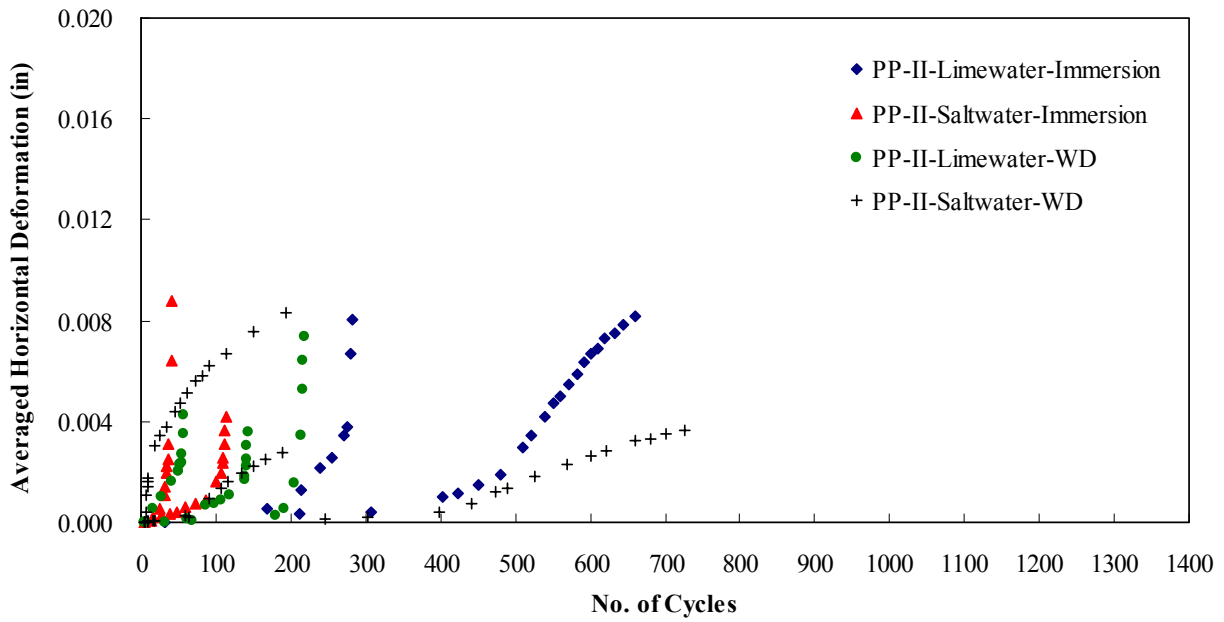


Figure 6-15. Averaged horizontal permanent deformation vs. number of cycles for PP fiber mix.

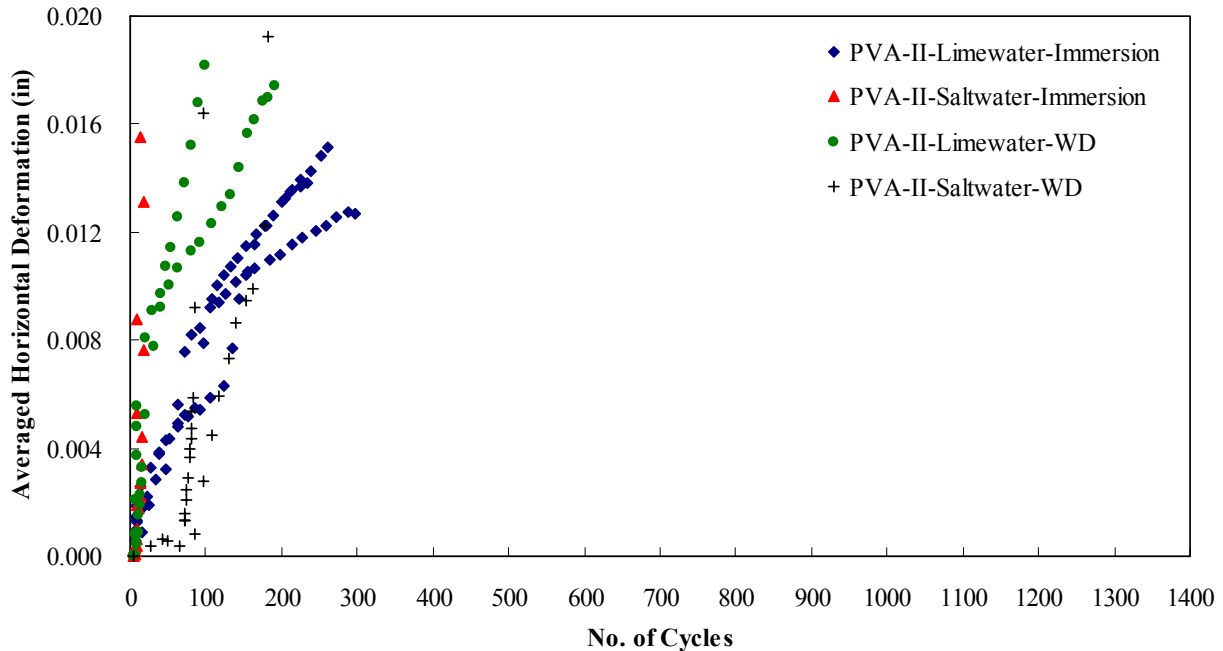


Figure 6-16. Averaged horizontal permanent deformation vs. number of cycles for PVA fiber mix

#### 6.4.4.4 Evaluation of failure mechanisms of fibers

Determination of Crack Stabilization of Fibers:

Wecharatana and Shah (1983) proposed the idealization of crack subsequent to matrix cracking as consisting of a traction free zone, a fiber bridging zone, and a matrix process zone as shown in Figure 2.4. Among the three zones, the fiber bridging zone showing crack closing pressure from frictional slip of the fibers should be determined to evaluate failure mechanisms of fibers degraded by environmental conditioning. The schematic diagram in Figure 6-17 describes the calculation procedure for determination of the point where fibers stabilize crack propagation and the evaluation of effects of degradation of fibers from resilient deformation ratio can begin.

Calculation procedure involves the following steps:

1. Determine the point when the matrix effect minimizes and only fibers resist crack propagation showing crack closing pressure from the plot of horizontal deformation ( $\delta$ ) vs. number of load repetitions (N) in Figure 6-17a. Draw linear regression line 1 corresponding to matrix/fiber zone and linear regression line 2 corresponding to fiber bridging zone.

- Determine point A, corresponding to the point where the two regression lines intersect. Find point B ( $N_B$ ), which is number of load repetitions to when the fiber bridging zone starts.
- Determine the resilient horizontal deformation ( $\delta_{H0}$ ) at point B ( $N_B$ ). Plot the resilient deformation ratio ( $\delta_H/\delta_{H0}$ ) for fiber bridging zone and plot the linear regression line 3 in Figure 6-17b. Gradients from fiber and fiber type degraded by conditioning represent rate of stiffness reduction and were used to evaluate resistance to degradation in the post-cracking phase.

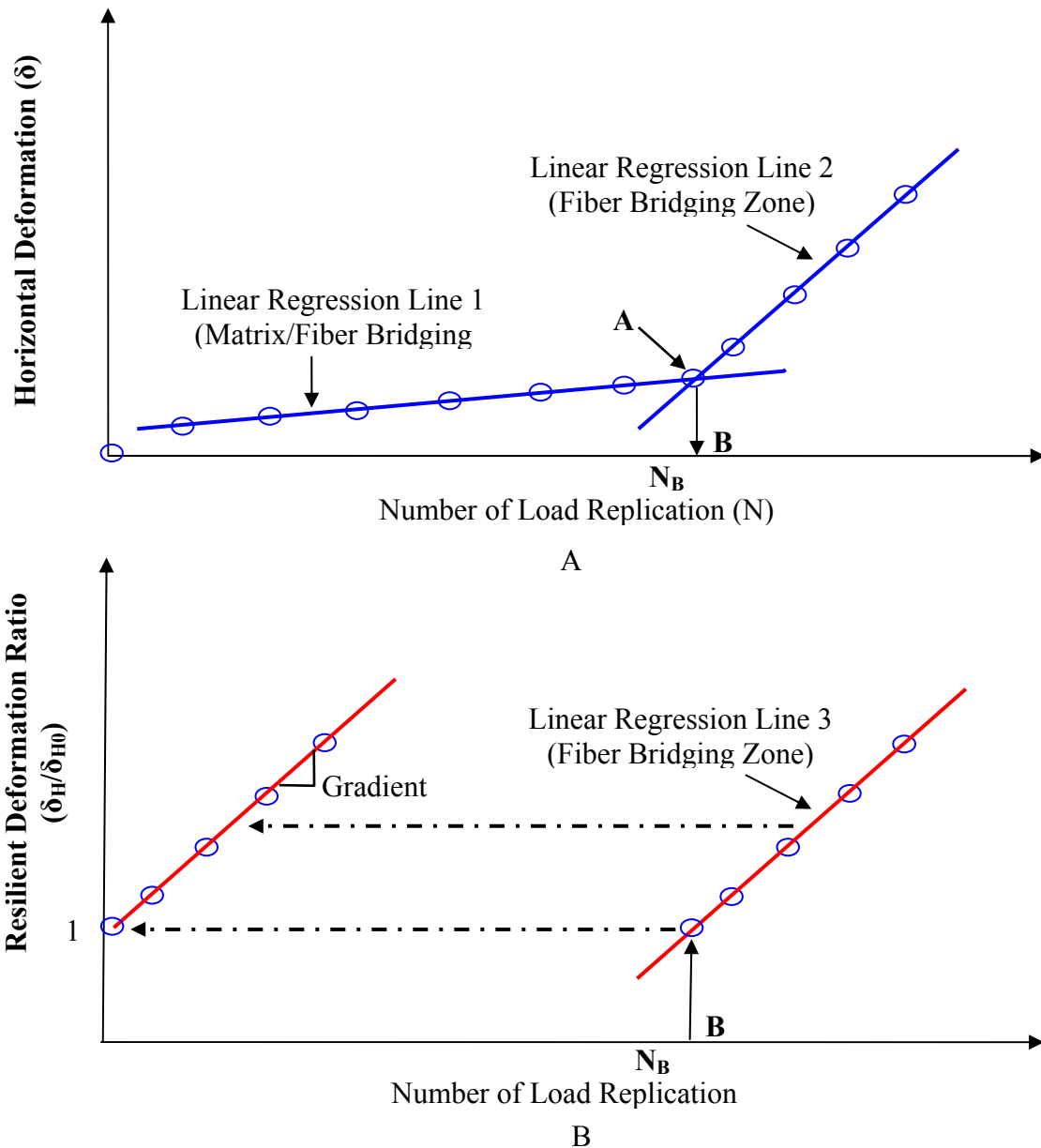


Figure 6-17. Schematic diagram explaining calculation procedure for resilient deformation ratio for fiber bridging zone

## Results and Evaluation:

Detailed test results from linear regression analysis for failure mechanisms of fibers to fiber bridging zone can be found in Appendix J. Summarized test results to fiber bridging zone for each fiber type subjected to different conditioning methods are shown in Figures 6-18, 6-19, and 6-20. Averaged rates of stiffness reduction, which are the gradients from the linear regression line for fiber bridging zone, are summarized in Figure 6-21. Evaluation for deterioration of fibers is summarized as follows:

- **Limewater/Saltwater Immersion:** the addition of PVA and steel fibers to limewater immersion showed good resistance to mechanical degradation compared to PP fibers. PVA and steel fibers have relatively rough surfaces, high modulus, and usually have good bonding in the hardened cement paste (steel fiber was the best). However, PVA and steel fibers are much more susceptible to degradation when subjected to saltwater immersion (PVA fiber was the worst). This is the reason why PVA and steel fibers in saltwater immersion showed much lower resistance to crack propagation than limewater immersion. On the other hand, PP fibers have a naturally smooth surface, are hydrophobic in nature, do not have good bonding in the hardened cement paste, and have low modulus. Consequently, PP fibers had the highest absorption rate and permeable pore space among all control and fiber mixes. This implies that mass transport of deleterious materials into concrete with PP fibers is greater than that of PVA and steel fibers. However, the degradation process of PP fibers themselves, which have naturally strong resistance to acid, salt and alkali solutions, was much slower in saltwater than either PVA or steel fibers. Saltwater solutions in PP fibers contributed to pores being filled without degradation of fibers, which appeared to increase the density of PP fiber mix, thereby improving mechanical properties. This is the reason why PP fibers in saltwater showed higher resistance to crack propagation than PVA and steel fibers.
- **Limewater/Saltwater W/D:** the addition of PVA and steel fibers to limewater w/d cycles showed good resistance to mechanical degradation compared to PP fibers. PVA and steel fibers have better bonding in the hardened cement paste and maintain enough resistance to micro damage induced by cyclic wetting and drying. For saltwater w/d cycles PVA fiber was significantly degraded and showed low resistance to crack propagation. PVA fiber degraded in saltwater solution and could not resist stresses resulting from salt crystallization in the interfacial zone. This is the reason why steel fibers having high modulus relative to PVA fiber showed better resistance to stresses as a result of salt crystallization in pores. It is interesting to note that steel fibers exposed to saltwater w/d cycles showed better resistance than those exposed to limewater w/d cycles. The increased volume from steel corrosion on the surface appeared to considerably contribute to resistance of stresses from repeated shrinkage effect (micro-damage). The resistance of PP fibers to cyclic w/d in limewater was relatively weak compared to saltwater w/d because

the effect of w/d condition in limewater without various chemical ions simply causes repeated stresses and micro-damage in the interfacial zone. Therefore, PP fibers, which are not structural, could not resist the stresses from cyclic w/d. However, salt crystallization in saltwater w/d cycles filled the relatively high pore content in the PP fiber mixes without fiber damage, which contributed to increased resistance to repeated stresses.

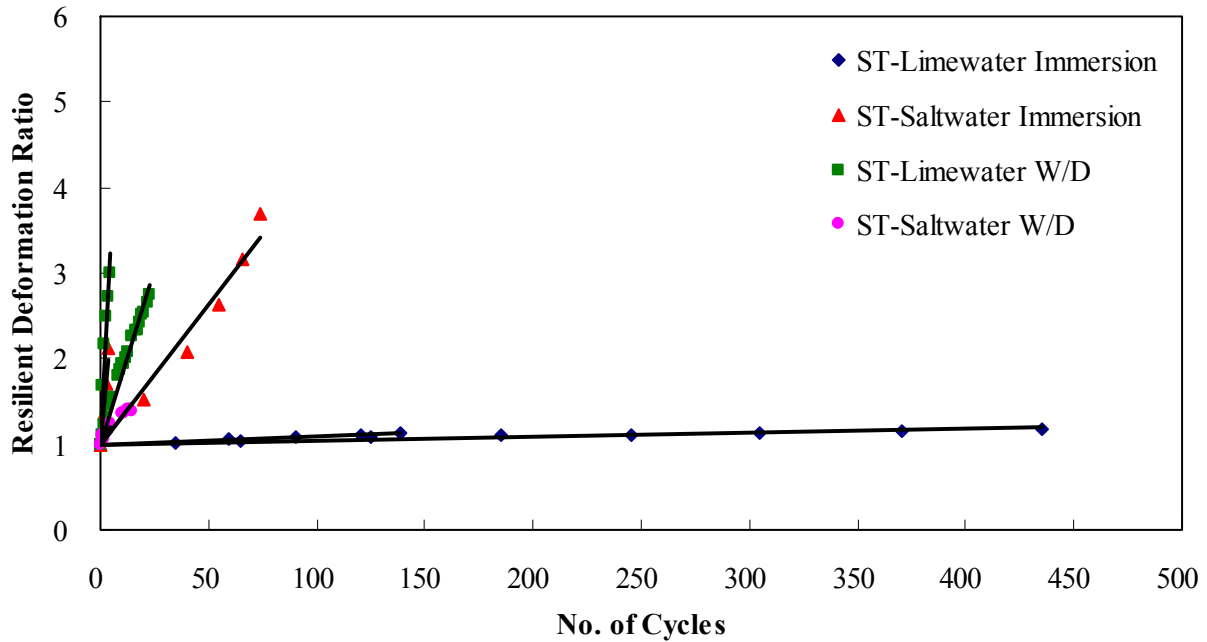


Figure 6-18. Resilient deformation ratio vs. no. of cycles for fiber bridging zone (steel fibers)

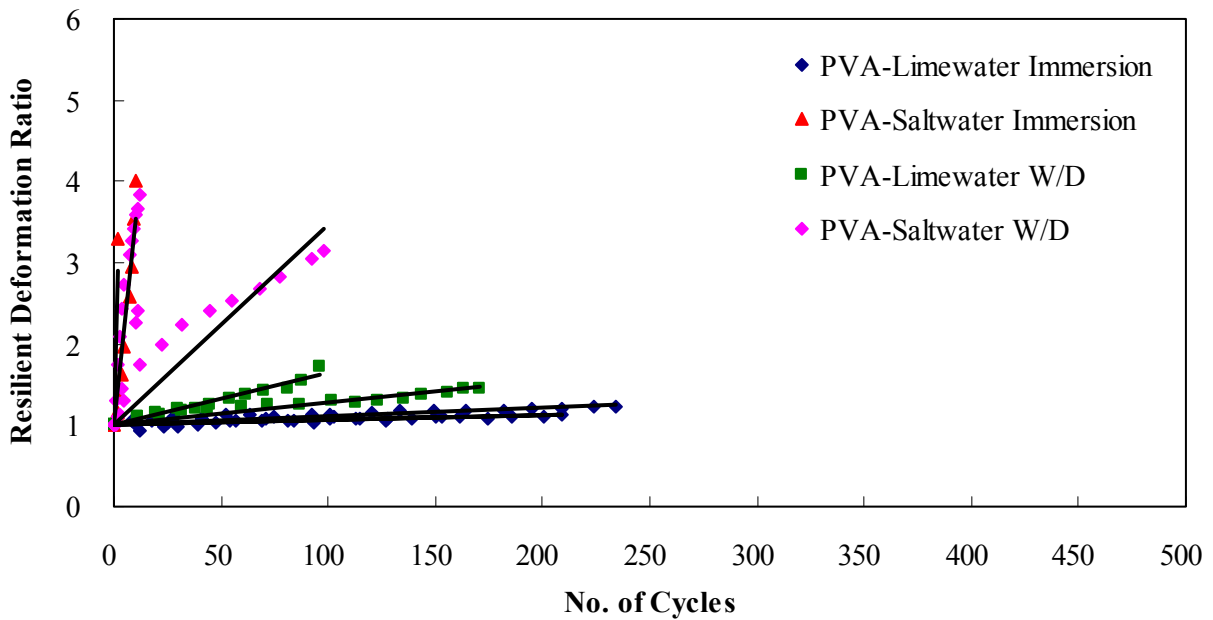


Figure 6-19. Resilient deformation ratio vs. no. of cycles for fiber bridging zone (PP fibers)

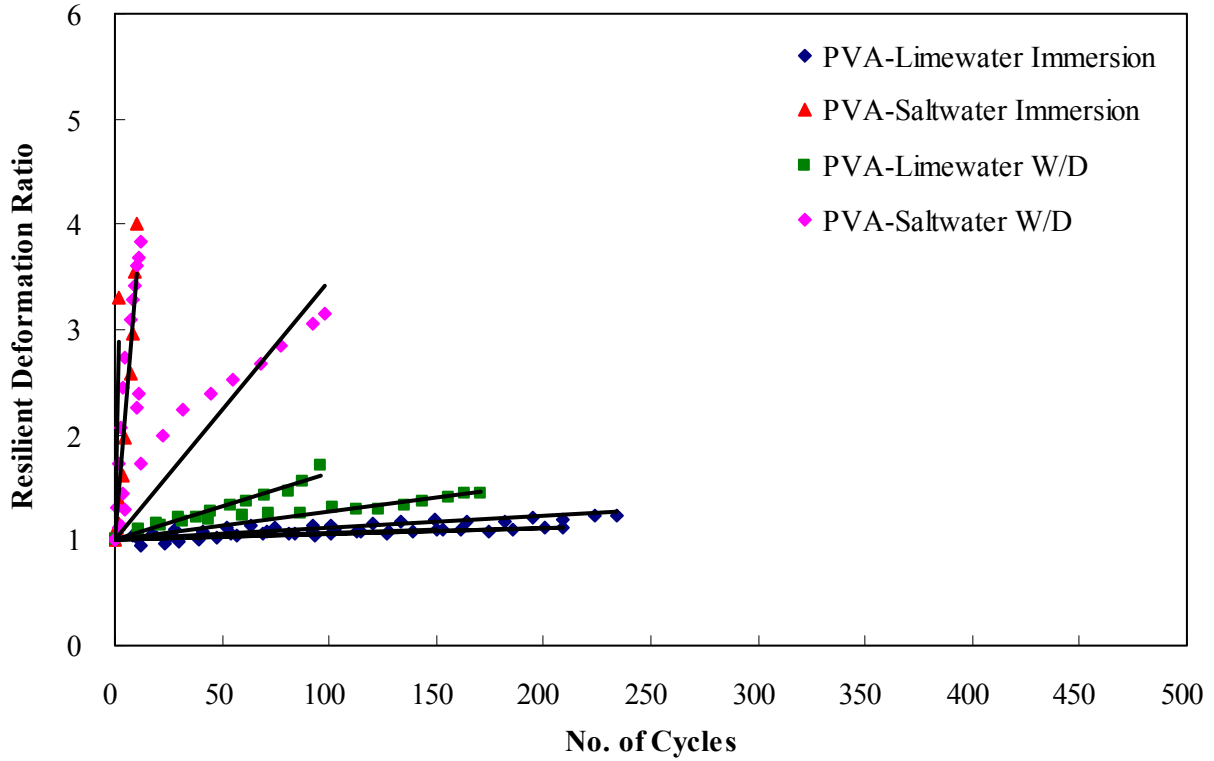


Figure 6-20 Resilient deformation ratio vs. no of cycles for fiber bridging zone (PVA fibers)

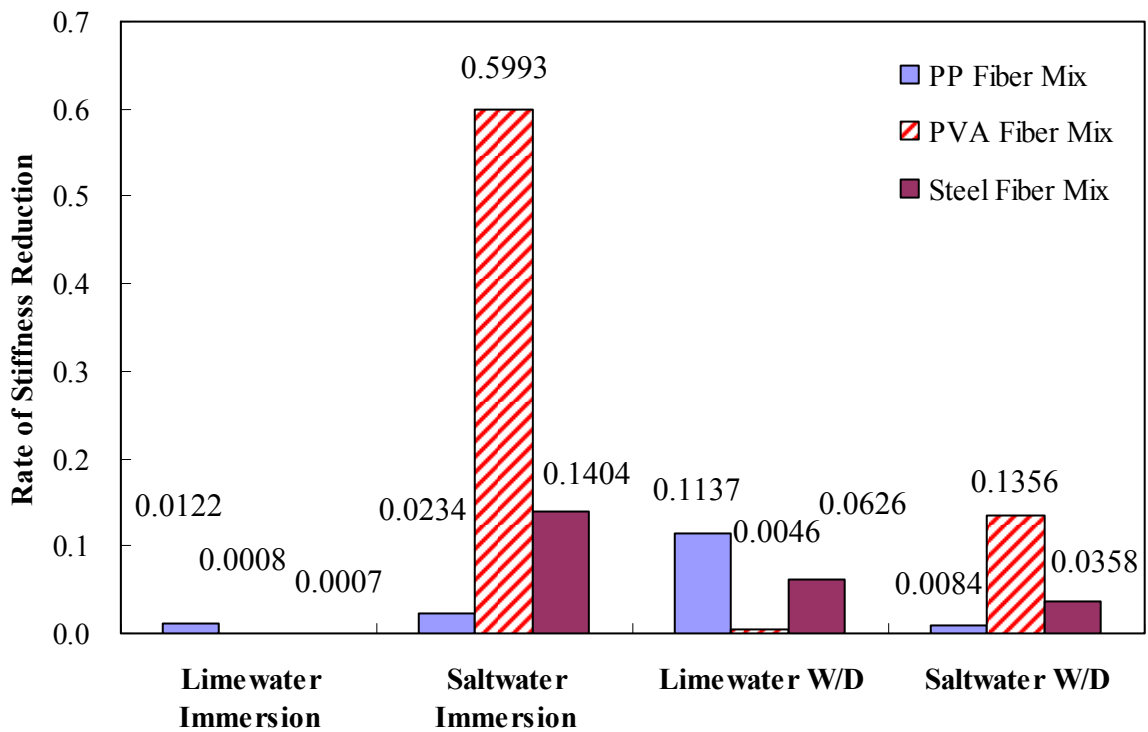


Figure 6-21. Rate of stiffness reduction from linear regression analysis of resilient deformation ratio

## 6.5 Summary of Findings

Findings from this portion of the study may be summarized as follows:

- Moisture movement by capillary action was a much faster transport mechanism than that of permeation and diffusion processes through concrete matrix and is therefore most effective to accelerate mass transport of deleterious materials and the deterioration mechanism.
- Absorption test was identified as the most critical transport mechanism for determining damage conditioning method and specimen thickness required to implement the indirect tensile test mode. A 14-day wetting and drying cyclic conditioning procedure was determined to result in uniform damage throughout the specimen based on absorption test results.
- A circular hole in the center of the specimen was identified to accelerate transport mechanisms and concentrate stress around the hole.
- FEM analysis indicated the same stress distribution in circular and square shaped specimens subjected to indirect tension testing. This finding allowed for testing of 25.4 mm thick square specimens sliced from cast beam or slabs.
- The use of thin IDT specimen has unique advantages for transporting deleterious materials and obtaining uniformly deteriorated stress distribution at the failure surface compared with conventional beam specimen.
- A 100 × 100 mm square specimen with a 25.4 mm thickness with a hole cored at its center was recommended to most effectively assess the effect of fibers on deterioration of FRC.
- Strength testing with indirect tension mode by low loading rate significantly reduced the high energy dissipation and high rate of deflection subsequent to the hardened cement paste cracking, which is a common problem associated with the conventional flexural beam approach.
- Steel fiber mix had the strongest resistance to crack propagation in limewater immersion due to excellent bonding in the matrix. In addition, steel corrosion reaction during cyclic wetting and drying in saltwater contributed to increased resistance of fiber pull-out from embedded matrix.
- PVA fiber mix had the weakest resistance to saltwater immersion and cyclic wetting and drying. PVA fibers, which have poor environmental resistance to saltwater, was significantly degraded and good bonding effect in the matrix disappeared.
- PP fiber mix exhibited good performance to saltwater immersion and cyclic wetting and drying. PP fibers, which have relatively good resistance to aggressive environments, was not degraded in saltwater immersion or from repeated shrinkage effect. The increased

density in pores from continuous immersion and salt crystallization from cyclic wetting and drying both contributed to improve resistance of PP fiber to cracking.

- The repeated loading approach with thin indirect tension mode significantly reduced the conditioning time and also more clearly identified the failure mechanism of fibers subjected to conditioning than the conventional beam approach because of a more uniformly damaged specimen and uniform stress distribution on the fracture plane. The indirect tensile mode may provide a reasonable solution to replace the conventional beam approach for evaluation of failure mechanisms associated with durability issue.

CHAPTER 7  
FINDINGS, CONCLUSIONS, AND RECOMMENDATIONS

**7.1 Summary of Findings**

An experimental program was performed to examine the effects of fiber type on concrete durability from measurements of both the fresh and hardened concrete properties. The fresh fibrous concrete was characterized by its slump, inverted slump time, Vebe time, and air content. Mechanical properties included compressive, splitting tensile, pressure tension, beam, and indirect tension testing. In addition, volume of voids, water permeability, absorption, chloride diffusion, surface resistivity, and steel bar corrosion tests were performed to evaluate transport properties of deleterious materials into concrete. Finally, an energy dispersive X-ray spectrometer, operating in tandem with scanning electron microscopy (SEM) was used to allow elemental and chemical analysis of deteriorated specimens.

Significant reduction in workability resulting from the addition of PP, PVA, and steel fibers to concrete can be clearly measured. Both inverted slump cone and Vebe time test methods were more accurate and sensitive to presence of fibers than conventional slump test. However, the inverted slump cone test had the greatest sensitivity to distinguish between workability of different fiber types and involved less expensive equipment than the Vebe test.

Tests results from the experimental investigation of transport properties indicated that the addition of fibers improved resistance of mass transport of deleterious materials. However, among the fiber types, the addition of steel fibers had the best ability to resist mass transport of deleterious materials in concrete. Mass transport by capillary action in FRC was much faster than that either permeation or diffusion processes. It is evident that absorption can be a critical transport mechanism in terms of accelerating the ingress of deleterious materials into concrete. Therefore, it appears that the most effective approach for achieving uniformly damaged

specimens for evaluation is through the use of repeated absorption by wetting and drying combined with a specimen geometry that ensures uniformity of absorption within a reasonable amount of time.

Peak strengths were affected mainly by the matrix not the fibers. Only the addition of hooked-end steel fibers with high modulus and high tensile strength resulted in a slight improvement in peak strengths.

A large number of pre-cracked and un-cracked beams consisting of different fiber types and two Classes of concrete were exposed to simulated Florida environments for 27 months. Conventional flexural beam testing was performed to assess the effect of fibers on deterioration of FRC. Unfortunately, serious problems were identified regarding the effectiveness of both the conditioning and test methods used. Effect of fibers on cracking resistance could not be assessed based on test results from either average residual strength (ASTM C 1399) or flexural performance (ASTM C 1609) tests. It was determined that the conventional flexural beam approach resulted in non-uniform degradation and stress/strain distributions through the cross-section. Also, beam tests generally resulted in multiple cracks initiating at the bottom of the specimen and instability subsequent to matrix cracking. These critical factors significantly affected the pull-out mechanism of fibers and disturbed the evaluation of failure during post-cracking. Observations and test results from SEM and EDS analysis were probably also affected by problems associated with the flexural beam approach. Beam specimens also can be problems in terms of achieving proper conditioning using cyclic wetting and drying. It was found that cyclic wetting and drying only degrades the outer half-inch shell of beams, which results in non-uniformly damaged cross-sections.

These results clearly indicated the need to develop more effective conditioning methods to achieve uniformly damaged specimens. In addition, more effective test methods were required to clearly evaluate the effects of fibers on resistance to chemical deterioration. Based on findings and observations, the indirect tensile test mode was introduced, which allowed for accelerated transport of deleterious materials and resulted in a uniformly degraded cross-section and uniform stress/strain distributions. Absorption by capillary suction was identified as the most critical transport mechanism for determining an effective damage conditioning method and specimen thickness. A 14-day wetting and drying cyclic conditioning procedure was determined to result in uniform damage throughout the specimen based on absorption test results. A 4×4 inch square specimen one inch thick, which was sliced from beam specimens exposed to lime water immersion, with a hole cored at its center was proposed to most effectively assess the effect of fibers on deterioration of FRC.

The effects of fiber type on resistance to chemical degradation were clearly observed from the SuperPave™ IDT test methods. In addition, the approach resulted in a great reduction of specimen volume, labor, and cost. IDT strength test performed at a slow loading rate was determined to minimize the high energy dissipation and the high rate of deflection subsequent to matrix cracking. Additionally, repeated loading test showed superior advantages to assess deterioration of FRC by evaluating averaged horizontal deformation and increase in horizontal resilient deformation ratio.

It was determined that the following issues should be considered to properly evaluate the effect of fiber type on durability of FRC:

- Determination of fresh properties to evaluate workability related to fiber distribution in fresh mixes.

- Determination of transport properties to evaluate mass transport of deleterious materials and to identify conditioning methods and specimen thickness.
- Use of effective accelerated conditioning methods that results in uniformly degraded specimen
- Use of appropriate tensile testing systems that result in uniform stress/strain distributions at the failure surface.
- Use of slower loading rates to minimize problems associated with conventional IDT strength tests, which cause excessively high energy dissipation and rate of deflection at first cracking.
- Use of repeated loading testing after first cracking to evaluate rate of damage accumulation during post-cracking.

The major findings regarding test methods and interpretation may be summarized as follows:

- Transport properties alone are not necessarily a good indicator of the effects of fibers on resistance to degradation. For example, the addition of PP fibers showing a high absorption rate had good resistance to saltwater immersion and cyclic wetting and drying.
- Transport properties can be used to identify appropriate conditioning and specimen thickness.
- Conventional beam test and interpretation were not suitable for evaluation of damage accumulation in FRC.
- The use of a heater/blower system and a reduced volume tank was effective in accelerating W/D conditioning.

The major findings regarding effectiveness of different fibers may be summarized as follows:

- The addition of PP fibers at  $V_f = 0.5\%$  exhibited excellent resistance to degradation in saltwater environments: little or no degradation effects were observed for polypropylene fiber reinforced concrete (PFRC) subjected to continuous saltwater immersion, while an improvement in properties was observed for PFRC subjected to saltwater wet/dry cycling.
- The addition of PVA fibers at  $V_f = 0.75\%$  exhibited poor resistance to degradation in saltwater environments, particularly when subjected to continuous saltwater immersion and to a lesser extent, when subjected to saltwater wet/dry cycling.

- The addition of steel fibers at  $V_f = 1\%$  to degradation in saltwater environments exhibited resistance somewhere between PFRC and PVAFRC. Considerable degradation effects were observed for steel fiber reinforced concrete (SFRC) subjected to continuous saltwater immersion, while no degradation and even a modest improvement in properties was observed for SFRC subjected to saltwater wet/dry cycling.
- SFRC accelerated the degradation of steel reinforcement in saltwater wet/dry cycling.
- The detrimental effect of acetic acid on aggregate and cement overwhelmed the degradation mechanism in swamp water environments. Therefore, the effect of fibers could not be distinguished for these environments.
- The effect of cellulose fibers at  $V_f = 0.1\%$  could not be evaluated because good fiber distribution was not achieved in laboratory mixing.

## 7.2 Conclusions

Based on various experimental investigations, conclusions are as follows:

- Inverted slump cone provides the most cost effective of the test methods evaluated to appropriately assess workability of FRC.
- Uniformly damaged specimens and tension tests are needed for proper assessment of resistance to degradation of fibers.
- IDT should be further developed by considering use of fiber in cement paste only in order to achieve better fiber distribution.
- PFRC provides the best resistance to degradation (best durability) for non-structural application in saltwater environment subjected to submerged and tidal zones.
- SFRC may be suitable in saltwater environment subjected to tidal zones, but should not be used if it will be in contact with reinforcing bars.
- PVAFRC should not be used in saltwater environment subjected to submerged and tidal zones.

## 7.3 Recommendations

The recommendations are proposed as follows:

- IDT should be further developed to establish IDT application to FRC by evaluating the effects of multiple fiber types, fiber volume fractions, fiber aspect ratios, and fiber configurations.
- The procedures developed should be used to optimize performance and durability of FRC.

## LIST OF REFERENCES

- ACI Committee 544 (1999), "Measurement of Properties of Fiber-Reinforced Concrete," ACI 544.2R-99.
- ACI Committee 544 (1996), "State-of-the-Art Report on Fiber-Reinforced Concrete," ACI 544.1R-96.
- ASHTO-AGC-ARTBA Joint Committee (2001), "The Use and State-of-the-Practice of Fiber Reinforced Concrete," American Concrete Pavement Association.
- ASTM C 39/C 39M-01 (2004), "Standard Test Method for Compressive Strength of Cylindrical Concrete Specimen," Annual Book of ASTM Standards.
- ASTM C 78 (2004), "Standard Test Method for Flexural Strength of Concrete (Using Simple Beam with Third-Point Loading)," Annual Book of ASTM Standards.
- ASTM C 94/C 94M (2004), "Standard Specification for Ready-Mixed Concrete" Annual Book of ASTM Standards.
- ASTM C 143/C 143M-00 (2004), "Standard Test Method for Slump of Hydraulic-Cement Concrete," Annual Book of ASTM Standards.
- ASTM C 192/C 192 M-02 (2004), "Standard Practice for Making and Curing Concrete Test Specimens in the Laboratory," Annual Book of ASTM Standards.
- ASTM C 231-97 (2004), "Standard Test Method for Air Content of Freshly Mixed Concrete by the Pressure Method," Annual Book of ASTM Standards.
- ASTM C 496-01 (2004), "Standard Test Method for Splitting Tensile Strength of Cylindrical Concrete Specimen," Annual Book of ASTM Standards, 2004.
- ASTM C 597-02 (2004), "Standard Test Method for Pulse Velocity Through Concrete," Annual Book of ASTM Standards.
- ASTM C 642-97 (2004), "Standard Test Method for Density, Absorption, and Voids in Hardened Concrete," Annual Book of ASTM Standards.
- ASTM C 995-94 (2004), "Standard Test Method for Time of Flow of Fiber-Reinforced Concrete through Inverted Slump Cone," Annual Book of ASTM Standards.
- ASTM C 1116-03 (2004), "Standard Specification for Fiber-Reinforced Concrete and Shotcrete," Annual Book of ASTM Standards.
- ASTM C 1018-97 (2004), "Standard Test Method for Flexural Toughness and First-Crack Strength of Fiber-Reinforced Concrete (Using Beam with Third-Point Loading)," Annual Book of ASTM Standards.

- ASTM C1170-91 (2004), "Standard Test Method for Determining Consistency and Density of Roller-Compacted Concrete Using a Vibrating Table," Annual Book of ASTM Standards.
- ASTM C 1399-07a (2008), "Standard Test Method for Obtaining Average Residual-Strength of Fiber-Reinforced Concrete," Annual Book of ASTM Standards.
- ASTM C 1585-04e1 (2004), "Standard Test Method for Measurement of Rate of Absorption of Water by Hydraulic-Cement Concretes." Annual Book of ASTM Standards.
- ASTM C 1609-06 (2008), "Standard Test Method for Flexural Performance of Fiber-Reinforced Concrete (Using Beam with Third-Point Loading)," Annual Book of ASTM Standards.
- ASTM G109-99a (2004), "Standard Test Method for Determination the Effects of Chemical Admixtures on the Corrosion of Embedded Steel Reinforcement in Concrete Exposed to Chloride Environments," Annual Book of ASTM Standards.
- Al-Tayyib, A.J., Al-Zahrani, M.M., Rasheeduzzafar and Al-Suaimani, G.J. (1988), "Effect of Polypropylene Fiber Reinforcement on the Properties of Fresh and Harden Concrete in the Arabian Gulf Environment," Cement and Concrete Research, Vol. 18, pp. 561-570.
- Al-Khalaf, M.N. and Page, C.L. (1979), "Steel Mortar Interfaces: Microstructural Features and Mode of Failure," Cement and Concrete Research, Vol. 9, pp. 197-208.
- Balaguru PN, Ramakrishnan V. (1986), "Freeze-Thaw Durability of Fiber Reinforced Concrete," ACI Journal (May-June), Vol. 83, pp. 374-382.
- Banthia, N. & Trottier, J.F. (Jan.-Feb. 1995), "Test Methods for Flexural Toughness Characterization of Fiber Reinforced Concrete: Some Concerns and a Proposition," ACI Materials Journal, Vol 92, pp. 48-57.
- Beaudoin, J.J. (1990), Handbook of Fiber-Reinforced Concrete: Principles, Properties, Developments and Applications, Noyes Publications, Inc., New Jersey.
- Bentur, A. & Mindess, S. (1990), Fibre Reinforced Cementitious Composites, Elsevier Applied Science, London and New York.
- Bentur, A, Mindess, S, Vondran, G. (1989), "Bonding in Polypropylene Fibre Reinforced Concretes," The International Journal of Cement Composite and Lightweight Concrete, Vol 11, No. 3.
- Bertolini, L., Elsener, B., Pedferri, and Polder, R.B. (2004), Corrosion of Steel in Concrete, WILEY-VCH Verlag GmbH & Co. KGaA, Weinheim.
- Buckeye UltraFiber500™ Fiber A/E Manual (2006), Buckeye Technologies Inc.
- Bungey, J. H. (1989), Testing of Concrete in Structures, 2<sup>nd</sup> edition, Chapman and Hall, p.52.

- Boyd, A. J. and Mindess, S. (2001), "The Effect of Concrete Sulfate Attack on the Tensile to Compressive Strength Ratio of Concrete," Proceedings Third International Conference on Concrete Under Severe Conditions, Edited by N. Banthia, K. Sakai and O. E. Gjorv, Vol. 1, pp. 789-796, The University of British Columbia, Vancouver, Canada.
- Choi, Y., and Yuan, R.L. (2005), "Experimental Relationship between Splitting Tensile Strength and Compressive Strength of GFRC and PFRC," Cement and Concrete Research, Vol. 35, pp. 1587-1591.
- Cohen, M. D., Shah, S. P., and Young, J. F. (1993), "Teaching the Materials Science, Engineering, and Field Aspects of Concrete," NCS-ACBM Center, Northwestern University.
- Clayton, N. and Grimer, F. J. (1979), "The Diphase Concept, with Particular Reference to Concrete," in "Developments in Concrete Technology-1", edited by Lydon, F. D., Applied Science Publisher LTD, pp. 283-318, UK.
- Clayton, N. (March 1978), "Fluid-Pressure Testing of Concrete Cylinders," Magazine of Concrete Research, Vol. 30, No. 102, pp. 26-30.
- Cox, H.L. (1952), "The Elasticity and Strength of Paper and Other Fibrous Materials", British Journal of Applied Physics, pp.72-79.
- Dhir, R. K., Hewlett, P. C. and Chan, Y. N. (1987), "Near-Surface Characteristics of Concrete: Assessment and Development of In Situ Test Methods," Magazine of Concrete Research, Vol. 39, No. 141, December, pp. 183-195.
- Fanella, D. A., and Naaman, A. E. (1985), "Stress-Strain Properties of Fiber Reinforced Concrete in Compression," ACI Journal, Vol. 82, No. 4, pp. 475-483.
- FDOT (2004), "Standard Specification for Road and Bridge Construction," Florida Department of Transportation (FDOT).
- FM5-578 (2004), "Florida Method of Test for Concrete Resistivity an Electrical Indicator of its Permeability," Florida Sampling and Testing Method (FSTM).
- FM1-T027 (2004), "Florida Method of Sieve Analysis of Fine and Coarse Aggregate," Florida Sampling and Testing Method (FSTM).
- Greszczuk, L.B. (1969), "Theoretical Studies of the Mechanics of the Fiber-Matrix Interface in Composites," In interfaces in Composites, American Society of Testing and Materials, ASTM STP 452, Philadelphia, pp. 42-58.
- Hall, C. (June 1989), "Water Sorptivity of Mortars and Concretes: A Review," Magazine of Concrete Research, Vol. 41, No. 147.
- Haque, M. N. (February 1990), "Some Concretes Need 7 Days Initial Curing," Concrete International.

- Hikasa, J. Genba, T. Mizobe, A. and Okazaki, M. (1986), "Replacement for Asbestos in Reinforced Cement Products-"Kuralon" PVA fibres, Properties and Structure," International Man-Made Fibres Congress, The Austrian Chemical Society, Dornbirm.
- Hong, K. and Hooton, R.D. (1999), "Effects of Cyclic Chloride Exposure on Penetration of Concrete Cover," *Cement and Concrete Research*, Vol. 29, pp.1379-1386.
- Kosa, K., Naaman, A.E., and Hansen, W. (May-June 1991), "Durability of Fiber Reinforced Mortar," *ACI Materials Journal*, Vol.88, No. 3.
- Kropp, J. Hilsdorf H. K., Grube, H. Andrade C., Nilsson, L. (1995), "Transport Mechanisms and Definitions," in *Performance Criteria for Concrete Durability*, edited by Kropp, J. & Hilsdorf, H.K, Taylor & Francis, New York.
- Krenchel, H. (1975), "Fibre Spacing and Specific Fibre Surface," In *Fibre Reinforced Cement and Concrete*, edited by A. Neville, Proc. RILEM Conf., The Construction Press, UK, pp. 69-79.
- Leung, C. K. Y., Lai, R., and Lee, A. Y. F. (2005), "Properties of Wet-Mixed Fiber Reinforced Shotcrete and Fiber Reinforced Concrete with Similar Composition," *Cement and Concrete Research*, Vol. 35, pp. 788-795, 2005.
- Malhotra, V. M., Carrette, G. G., and Bilodeau, A. (Set-Oct 1994), "Mechanical Properties and Durability of Polypropylene Fiber Reinforced High-Volume Fly Ash Concrete for Shotcrete Application," *ACI Materials Journal*, Vol. 91, No. 5, pp. 478-486.
- Mangat, P.S. and Gurusamy, K. (1985), "Steel Fibre Reinforced Concrete for Marine Applications," 4<sup>th</sup> International Conference on Behaviour of Offshore Structures, Delft, The Netherlands, pp. 867-879.
- Martys, M. S and Ferraris, C. F. (1997), "Capillary Transport in Mortars and Concrete," *Cement and Concrete Research*, Vol. 27, No. 5, pp. 747-760.
- Mehta, P. K. (1980), "Performance of Concrete in Marine Environment," *ACI SP-65*, pp. 1-20.
- Mehta, P. K. and Monteiro, Paulo. J. M. (2005), *Concrete Microstructure, Properties, and Materials*, McGraw-Hill Professional, Third Edition, New Jersey.
- Mier, J. G. M van (1997), *Fracture Processes of Concrete*. CRC Press, Inc., Florida.
- Mindess, S., Young, J. F., and Darwin, D. (2003), *Concrete*, Pearson Education, Inc. New Jersey.
- Mindess, S., Fujikake, K., Xu, H., and Uno, T. (2005), "The Nitrogen Gas Tension Test of Concrete," *Concrete Materials (Symposium in honor of Prof. Mindess)*, The University of British Columbia, Vancouver, Canada.

- Morse, D.C. and Williamson, G.R. (May 1977), "Corrosion Behavior of Steel Fibrous Concrete," Technical Report M-217, U.S. Army Corps of Engineers Construction Engineering Research Laboratory, Champaign, Illinois, pp. 36.
- Morrison, J. K., Shah, S. P, & Jenq, Y. S (1988), "Analysis of Fiber Debonding and Pull-out in Composites," *Journal of Engineering Mechanics*, ASCE, Vol. 114, No. 2, pp. 277-294.
- Naaman, A. E., Al-khairi, F. M., and Hammoud, H. (1993), "High Early Strength Fiber Reinforced Concrete (HESFRC)," in *Mechanical Behavior of High Performance Concrete*, Vol. 6, Strategic Highway Research Program, Nation Research Council, Washington, D.C., SHRP-C-366.
- Neville, A. M. (1971), "Hardened Concrete: Physical and Mechanical Aspects," American Concrete Institute, Detroit, MI and the Iowa State University Press, Ames, Iowa, 1971.
- Neville, A. M. (1981), *Properties of Concrete*, 3<sup>rd</sup> Edition, Pitman Publishing, London.
- NT BUILD 443 (1995), "Concrete, Hardened: Accelerated Chloride Penetration," Nordtest Method.
- Outwater, J.O. & Murphy, M.H. (1969), "On the Fracture Energy of Unidirectional Laminates," In Proc. 26th Annual Conf. on Reinforced Plastics, Composite Division of Society of Plastics Industry, paper 11-C-1, pp. 1-8.
- Pinchin, D.J. and Tabor, D. (1978), "Interfacial Phenomena in Steel Fiber Reinforced Cement I. Structure and Strength of the Interfacial Region," *Cement and Concrete Research*, Vol. 8, pp. 15-24.
- Powers, T. C., Copeland, L. E., Hayes, J. C., and Mann, H. M. (1954), "Permeability of Portland Cement Paste," *ACI Journal*, Vol. 50, pp. 285-298.
- Roque, R. and Buttlar, W.G. (1992), "The Development of a Measurement and Analysis System to Accurately Determine Asphalt Concrete Properties Using the Indirect Tensile mode," *Asphalt Association of Paving Technologist (AAPT)*, Vol 61, pp 304-332.
- Romualdi, J.P. & Batson, G.B. (1963), "Mechanics of Crack Arrest in Concrete," *Journal of Engineering Mechanics*, ASCE, vol.89, pp. 147-168.
- Romualdi, J.P. & Batson, G.B. (1963), "Behaviour of Reinforced Concrete Beams with Closely Spaced Reinforcement," *Journal of American Concrete Institute*, Vol.60, pp775-789.
- Romualdi, J.P. & Mandel, J. A. (1964), "Tensile Strength of Concrete Affected by Uniformly Dispersed and Closely Spaced Short Lengths of Wire Reinforcement," *Journal of American Concrete Institute*, Vol.61, pp. 657-672.
- Regourd, M. (1980), "Physico-Chemical Studies of Cement Pastes, Mortars, and Concretes Exposed to Sea Water," *Performance of Concrete in Marine Environment*, SP-65, American Concrete Institute, Detroit, pp.63-82.

- Rice, E.K, Vondon, G.L. and Kunbargi, H.O. (1988), "Bonding of Filbrillated Polypropylene Fiber to Cementitious Mateirals," Bonding in Cementitious Composites, (edited by S. Mindess and S.P. Shah), Materials Research Society, Proceedings, Vol. 114, pp. 145-152.
- Romualdi, J. P., and Batson, G. B. (June 1963), "Mechanics of Crack Arrest in Concrete," Proceedings, ASCE, Vol. 89, EM3, pp. 147-168.
- Romualdi, J. P., and Mandel J. A. (June 1964), "Tensile Strength of Concrete Affected by Uniformly Distributed Closely Spaced Short Lengths of Wire Reinforcement," ACI Journal, Proceedings Vol. 61, No. 6, pp. 657-671.
- Stang, H. & Shah, S.P. (1986), "Failure of Fibre Reinforced Composites by pull-out Fracture," Journal of Material Science, Vol 21, pp. 953-957.
- Swamy, R.N. (1983), "Linear Elastic Fracture Mechanics Parameter of Concrete", In Fracture Mechanics of Concrete, ed. F.H. Wittmann, Elsevier Applied Science, Amsterdam, pp. 411-461.
- Schwartzentruber, A., Philipe, M., and Marchese, G. (2004), "Effet of PVA, glass and metallic fibers, and of an expansive admixture on the cracking tendency of ultrahigh strength mortar," Cement & Concrete Composites, Vol. 24, pp. 573-580.
- Schonlin, K. and Hisdorf, H. K. (June 1989), "The Potential Durability of Concrete, ERMCO 89," The Norway to Concrete, Staanger, Oslo, Fabeko.
- Song, H.W., Lee, C.H., and Ann, K.Y. (2008), "Factors Influencing Chloride Transport in Concrete Structures Exposed to Marine Environments," Cement and Concrete Composites, Vol.30, pp. 113-121.
- Shaaban, A. M., and Gesund, H. (1993), " Splitting Tensile Strength of Steel Fiber Reinforced Concrete Cylinders Consolidated by Rodding or Vibrating," ACI Materials Journal, Vol. 90, No. 4, pp.366-369.
- Soongwang, P., Tia, M., Blomquist, D., Meletiou, C., and Sessions, L. (1998), "Efficient Test Setup for Determining the Water-Permeability of Concrete," Transportation Research Record, Vol. 1204, pp. 77-82.
- Stella L. M. (1995), "Sample Preparation- the Key to SEM Studied of Failed Concrete," Cement and Concrete Composites, Vol. 17, pp. 311-318.
- Tian, B. (1998), " Microanalytical and Microstructural Studies on the Mechanism of Sulfate Attack," Ph.D Dissertation, Purdue University.
- Timoshenko, S. P. and Goodier J. N. (2004), Theory of Elasticity, Third Edition, McGraw-Hill, Singapore.

Tyler, I. L., and Erlin, B. (1961), "A Proposed Simple Test Method for Determining the Permeability of Concrete," *Journal of the PCA Research and Development Laboratories*, Vol. 3, No. 3, pp. 2-7.

Wecharatana, M. & Shah, S.P. (1983), "A Model for Predicting Fracture Resistance of Fibre Reinforced Concrete," *Cement and Concrete Research*, Vol.13, pp. 819-829.

Zagar, L. (1955), "Die Grundlagen zur Ermittlung der Gasdurchlässigkeit von feuerfesten Baustoffen", *Deutscher Ausschub für Stahlbeton*, Heft 258.

Yao, W., Li, J., and W, K. (2003), "Mechanical Properties of Hybrid Fiber-Reinforced Concrete at Low Fiber Volume Fraction," *Cement and Concrete Research*, Vol. 33, pp. 27-30.

APPENDIX A  
FRESH PROPERTY TEST RESULTS

Table A-1. Fresh properties for Class II concrete

Mix Types	Slump (in)		I.S.C (sec)	Vebe (sec)	Air Content (%)		Air/Mix temp (°F)	Unit weight (lb/ft <sup>3</sup> )	Mix
	Without	With			Without	With			
PC	5.75	.	15	2	5.1	.	68/73	3679.56	Mix 1
PP	8.50	1.50	.	.	.	3.1	75/76	3781.44	Mix 1
	6.50	1.00	99	7	4.7	3.2			Mix 2
PVA	6.50	1.50	.	.	.	4.2	77/75	3771.36	Mix 1
	6.50	1.50	85	6	4.2	4.2			Mix 2
Cell	5.00	3.75	.	.	.	4.9	68/75	3761.28	Mix 1
	7.50	5.75	10	1	3.7	3.9			Mix 2
Steel	3.25	0.75	.	.	.	3.1	72/79	3859.92	Mix 1
	3.25	0.75	87	9	4.0	2.8			Mix 2

Table A-2. Fresh properties for Class V concrete

Mix Types	Slump (in)		I.S.C (sec)	Vebe (sec)	Air Content (%)		Air/Mix temp (°F)	Unit weight (lb/ft <sup>3</sup> )	Mix
	Without	With			Without	With			
PC	3.25	.	32	4	3.4	.	70/73	3853.44	Mix 1
PP	7.75	2.00	.	.	.	2.8	68/75	3870.45	Mix 1
	6.25	1.75	78	6	3.0	2.9			Mix 2
PVA	8.50	4.25	.	.	.	2.5	68/73	3870.99	Mix 1
	8.00	2.75	67	4	2.7	2.0			Mix 2
Cell	7.50	4.00	.	.	.	3.4	68/73	3813.84	Mix 1
	7.75	4.50	16	2	2.7	3.4			Mix 2
Steel	7.00	2.50	.	.	.	2.7	75/76	3907.44	Mix 1
	6.50	1.75	59	5	2.8	2.4			Mix 2

APPENDIX B  
DENSITY, ABSORPTION, VOLUME OF VOIDS TEST RESULTS

Table B-1. Summary of the values of density, absorption, and voids obtained (Class II concrete)

Mix Type	Specimen ID	Control Specimens			Fiber Specimens		
		Absorption (%)	Apparent Density (Mg/m <sup>3</sup> )	Voids (%)	Absorption (%)	Apparent Density (Mg/m <sup>3</sup> )	Voids (%)
PC	Control A	6.07	2.47	13.03			
	Control B	6.01	2.46	12.88			
	Control C	6.02	2.48	13.00			
	Average	6.03	2.47	12.97		N/A	
	S.D	0.03	0.01	0.08			
	C.O.V (%)	0.53	0.40	0.61			
PP	PP_0.5%_A	6.40	2.51	13.83	6.61	2.51	14.23
	PP_0.5%_B	6.37	2.50	13.72	6.58	2.54	14.31
	PP_0.5%_C	6.44	2.50	13.85	6.57	2.53	14.23
	Average	6.40	2.50	13.80	6.59	2.53	14.26
	S.D	0.04	0.01	0.07	0.02	0.02	0.05
	C.O.V (%)	0.55	0.23	0.51	0.32	0.60	0.32
PVA	PVA_0.75%_A	6.16	2.49	13.29	6.31	2.48	13.50
	PVA_0.75%_B	6.04	2.50	13.11	6.25	2.52	13.59
	PVA_0.75%_C	6.04	2.48	13.03	6.31	2.49	13.55
	Average	6.08	2.49	13.14	6.29	2.50	13.55
	S.D	0.07	0.01	0.13	0.03	0.02	0.05
	C.O.V (%)	1.14	0.40	1.01	0.55	0.83	0.33
Cell	CELL_0.1%_A	6.40	2.50	13.80	6.24	2.48	13.41
	CELL_0.1%_B	6.09	2.49	13.15	6.31	2.51	13.67
	CELL_0.1%_C	6.25	2.48	13.42	6.34	2.48	13.61
	Average	6.25	2.49	13.46	6.30	2.49	13.56
	S.D	0.16	0.01	0.33	0.05	0.02	0.14
	C.O.V (%)	2.52	0.40	2.43	0.81	0.70	1.00
Steel	ST_1%_A	5.99	2.47	12.90	5.47	2.54	12.19
	ST_1%_B	6.06	2.47	13.01	5.46	2.54	12.18
	ST_1%_C	6.00	2.48	12.98	5.34	2.55	11.98
	Average	6.02	2.47	12.96	5.42	2.54	12.12
	S.D	0.04	0.01	0.06	0.07	0.01	0.12
	C.O.V (%)	0.63	0.23	0.44	1.33	0.23	0.98

Table B-2. Summary of the values of density, absorption, and voids obtained (Class V concrete)

Mix Type	Specimen ID	Control Specimens			Fiber Specimens		
		Absorption (%)	Apparent Density (Mg/m <sup>3</sup> )	Voids (%)	Absorption (%)	Apparent Density (Mg/m <sup>3</sup> )	Voids (%)
PC	Control A	5.61	2.47	12.16			
	Control B	5.67	2.49	12.37			
	Control C	5.50	2.49	12.05			
	Average	5.59	2.48	12.19		N/A	
	S.D	0.09	0.01	0.16			
	C.O.V (%)	1.54	0.46	1.33			
PP	PP_0.5%_A	5.65	2.48	12.28	5.86	2.51	12.81
	PP_0.5%_B	5.68	2.50	12.42	5.78	2.53	12.77
	PP_0.5%_C	5.63	2.48	12.27	5.82	2.51	12.74
	Average	5.65	2.49	12.32	5.82	2.52	12.77
	S.D	0.03	0.01	0.06	0.04	0.01	0.04
	C.O.V (%)	0.45	0.46	0.68	0.69	0.46	0.27
PVA	PVA_0.75%_A	5.97	2.50	12.97	6.16	2.53	13.48
	PVA_0.75%_B	5.91	2.50	12.87	6.24	2.54	13.68
	PVA_0.75%_C	5.90	2.50	12.85	6.20	2.55	13.63
	Average	5.93	2.50	12.90	6.20	2.54	13.60
	S.D (%)	0.04	0.00	0.06	0.04	0.01	0.10
	C.O.V (%)	0.64	0.00	0.50	0.65	0.39	0.77
Cell	CELL_0.1%_A	5.76	2.53	12.69	5.47	2.52	12.11
	CELL_0.1%_B	5.73	2.49	12.47	5.68	2.49	12.38
	CELL_0.1%_C	5.73	2.49	12.48	5.57	2.49	12.17
	Average	5.74	2.50	12.55	5.57	2.50	12.22
	S.D	0.02	0.02	0.12	0.11	0.02	0.14
	C.O.V (%)	0.30	0.99	0.99	1.88	0.69	1.16
Steel	ST_1%_A	6.02	2.51	13.14	5.88	2.56	13.10
	ST_1%_B	6.07	2.52	13.25	5.80	2.58	13.01
	ST_1%_C	6.03	2.51	13.15	5.62	2.56	13.01
	Average	6.04	2.51	13.18	5.77	2.57	13.04
	S.D	0.03	0.01	0.06	0.13	0.01	0.05
	C.O.V (%)	0.44	0.23	0.46	2.31	0.45	0.40

APPENDIX C  
SURFACE RESISTIVITY TEST RESULTS

Table C-1. Summary of the values of surface resistivity (kΩ.cm) for Class II concrete: PC

Specimen ID	Test Day	Reading Locations (Degree)								Ave	Ave	S.D	C.O.V (%)
		0	90	180	270	0	90	180	270				
Control A	28	7.3	6.7	6.8	6.8	7.4	6.6	6.8	6.8	6.9	6.9	0.02	0.3
Control B		6.9	6.9	6.3	7.0	7.0	6.9	6.7	7.2	6.9			
Control C		6.9	6.8	6.8	7.0	6.8	7	6.7	6.9	6.9			
Control A	56	8	7.4	7.1	7.2	7.8	7.3	7.0	7.2	7.4	7.4	0.04	0.5
Control B		7.5	7.5	6.9	7.5	7.7	7.6	7.0	7.4	7.4			
Control C		7.2	7.2	7.4	7.3	7.2	7.6	7.3	7.3	7.3			
Control A	91	7.8	7.5	7.2	7.1	7.4	7.5	7.8	7.3	7.5	7.4	0.07	0.9
Control B		7.3	7.5	7.2	7.5	7.3	7.3	7.4	7.5	7.4			
Control C		7.3	7.7	7.2	7.5	7.7	7.9	7.3	7.5	7.5			
Control A	182	12.3	12.0	11.3	11.1	11.8	12.0	11.2	11.0	11.6	11.4	0.12	1.1
Control B		11.7	11.6	10.8	11.4	11.2	11.9	10.8	11.5	11.4			
Control C		11.4	11.9	11.1	11.1	11.4	11.7	11.1	11.4	11.4			
Control A	364	14.2	12.8	13.3	13.3	12.5	12.7	13.0	12.7	13.1	13.1	0.02	0.1
Control B		13.0	13.9	13.3	13.0	13	12.4	13.0	13.1	13.1			
Control C		13.1	13.2	13.5	13.0	12.8	12.9	13.1	12.8	13.1			
Control A	540	14.1	13.6	12.2	15.2	13.3	13.9	12.6	13.2	13.5	13.4	0.24	1.8
Control B		13.3	13.5	14.3	13.7	13.7	13.4	13.7	13.4	13.6			
Control C		13.5	13.5	12.8	12.6	13.6	13.6	12.3	13.4	13.2			
Control A	730	13.2	13.0	13.0	11.2	13.9	13.0	12.6	10.8	12.6	13.2	0.56	4.2
Control B		14.1	13.1	13.4	12.6	15	13.5	13.3	13.2	13.5			
Control C		14.0	14.2	13.2	13.6	13.6	13.5	13.5	13.0	13.6			

Table C-2. Summary of the values of surface resistivity (kΩ.cm) for Class II concrete: PP

Specimen ID	Test Day	Reading Locations (Degree)								Ave
		0	90	180	270	0	90	180	270	
PP (Block)	28	4.2	4.1	3.9	4.2	4.0	4.2	4.0	4.3	4.1
	56	4.5	4.3	3.9	4.2	3.8	4.3	3.9	3.8	4.1
	91	3.8	4.2	4.1	4.3	4.2	4.4	3.9	4.2	4.1
	182	6.7	6.5	8.0	5.7	6.8	5.9	7.9	6.2	6.7
	364	10.5	7.5	8.4	7.5	9.3	7.3	8.9	7.3	8.3
	540	7.5	6.0	5.4	6.8	8.1	5.6	5.4	5.4	6.3
	730	5.5	6.1	6.1	6.4	5.6	6.1	5.9	6.0	6.0

Table C-3. Summary of the values of surface resistivity (kΩ.cm) for Class II concrete: PVA

Specimen ID	Test Day	Reading Locations (Degree)								Ave
		0	90	180	270	0	90	180	270	
PVA (Block)	28	4.1	4.9	5.0	4.6	4.4	4.9	5.0	4.8	4.7
	56	4.8	5.3	4.8	4.9	5.0	5.3	5.2	5.1	5.1
	91	4.8	5.5	5.7	5.4	4.8	5.2	5.9	6.0	5.4
	182	8.5	8.0	7.1	7.6	8.2	7.8	7.1	7.5	7.5
	364	11.0	10.9	9.6	9.1	11.5	9.5	9.5	9.9	10.1
	540	8.1	6.5	5.5	6.4	7.1	6.1	5.6	6.2	6.4
	730	6.2	5.5	6.0	6.0	5.6	5.7	6.1	6.0	5.9

Table C-4. Summary of the values of surface resistivity (kΩ.cm) for Class II concrete: cellulose fiber mixture (Cell)

Specimen ID	Test Day	Reading Locations (Degree)								Ave
		0	90	180	270	0	90	180	270	
Cell (Block)	28	6.0	6.2	5.5	6.1	5.9	5.7	5.7	6.2	5.9
	56	6.5	6.2	6.3	6.5	6.4	6.5	6.3	6.4	6.4
	91	6.8	6.8	6.4	6.5	7.0	6.7	6.6	6.7	6.7
	182	10.5	10.6	10	10.2	10.8	10.8	9.8	10.0	10.3
	364	10.5	11.6	11.5	10.5	11.3	10.5	10.8	10.6	10.9
	540	8.5	7.4	8.7	7.9	7.5	8.6	7.4	6.9	7.9
	730	7.5	8.5	7.3	7.2	8.7	7.2	8.8	6.8	7.8

Table C-5. Summary of the values of surface resistivity (kΩ.cm) for Class II concrete: steel fiber mixture (St)

Specimen ID	Test Day	Reading Locations (Degree)								Ave
		0	90	180	270	0	90	180	270	
St (Block)	28	1.4	1.5	1.6	1.4	1.3	1.7	1.6	1.5	1.5
	56	1.5	2.4	1.5	1.7	1.5	2.4	1.7	1.7	1.8
	91	2.5	1.4	2.1	1.7	2.4	1.6	1.4	1.5	1.8
	182	3.5	2.0	2.5	2.4	2.8	2.1	2.6	2.4	2.5
	364	5.0	3.1	3.4	2.9	5.0	5.0	3.3	2.9	3.8
	540	3.0	3.7	2.3	2.1	5.4	5.2	2.2	2.0	3.2
	730	3.1	2.8	2.8	2.4	3.3	2.9	2.9	2.3	2.8

Table C-6. Summary of the values of surface resistivity (kΩ.cm) for Class V concrete: plain concrete (PC)

Specimen ID	Test Day	Reading Locations (Degree)								Ave	Ave	S.D	C.O.V (%)	
		0	90	180	270	0	90	180	270					
Control A	28	9.4	8.6	9.3	8.6	9.4	8.8	9.3	8.3	9.0	9.0	9.0	0.07	0.8
Control B		9.2	9.0	9.0	8.8	9.4	9.0	9.2	9.2	9.1				
Control C		9.4	9	9.2	8.7	9.2	9	9.2	8.8	9.1				
Control A	56	9.8	9.4	9.6	10.3	9.9	9.5	9.7	10.1	9.8	9.8	9.8	0.01	0.1
Control B		9.9	9.8	9.6	9.7	9.9	9.7	10.1	9.6	9.9				
Control C		10.2	9.4	10.2	9.3	10.4	9.5	10.2	9.2	10.2				
Control A	91	10.4	10.1	9.6	9.8	9.8	9.6	9.9	10.1	9.9	10.1	10.1	0.15	1.5
Control B		9.8	9.9	10.2	10.5	10.5	10	10.2	10.6	10.2				
Control C		10.5	10	10	9.5	10.6	10.1	10.4	9.3	10.1				
Control A	182	9.7	10.4	10.4	10.8	9.6	10.6	10.1	10.6	10.3	10.4	10.4	0.11	1.0
Control B		10.7	10.5	10.2	10.3	10.5	10.6	10.1	10.4	10.4				
Control C		11.1	10.2	10.6	9.8	11.3	10.2	10.7	10	10.5				
Control A	364	13.3	13.1	14.7	13.4	13	13	13.3	13.9	13.5	13.4	13.4	0.10	0.7
Control B		13.5	13.4	13.6	13.1	13.3	13.4	13.1	13.3	13.3				
Control C		13.3	13.1	13.3	13	13.5	13.4	13.2	13.4	13.3				
Control A	540	14.1	13.6	12.2	15.2	15.2	13.9	12.6	13.2	13.8	14.0	14.0	0.29	2.1
Control B		13.3	15.4	14.3	13.7	13.7	13.4	13.7	13.4	13.9				
Control C		13.5	15.4	12.8	12.6	15.2	15.2	12.3	17.4	14.3				
Control A	730	13.9	13.0	16.0	11.2	13.9	15.2	12.6	10.8	13.3	13.7	13.7	0.42	3.0
Control B		14.1	13.1	13.4	12.6	15	13.5	13.3	13.2	13.5				
Control C		14	14.2	14.9	13.6	13.6	13.5	16.2	13.0	14.1				

Table C-7. Summary of the values of surface resistivity (k $\Omega$ .cm) for Class V concrete: polypropylene fiber mixture (PP)

Specimen ID	Test Day	Reading Locations (Degree)								Ave
		0	90	180	270	0	90	180	270	
PP (Block)	28	5.2	5.3	4.9	5.0	5.3	5.0	5.1	5.1	5.1
	56	6.5	5.3	5.4	5.7	6.0	5.6	5.5	6.1	5.8
	91	6.4	5.4	5.8	5.7	5.9	5.9	6.0	5.8	5.9
	182	6.5	6.2	6.1	6.3	6.7	6.3	6.6	6.9	6.5
	364	6.7	7.5	7.8	7.1	6.9	7.6	7.3	7.3	7.3
	540	8.7	6.8	7.5	7.2	8.2	6.5	7.5	7.5	7.5
	730	6.9	8.3	7.5	7.2	7.1	7.6	7.8	7.5	7.5

Table C-8. Summary of the values of surface resistivity (k $\Omega$ .cm) for Class V concrete: polyvinyl alcohol fiber mixture (PVA)

Specimen ID	Test Day	Reading Locations (Degree)								Ave
		0	90	180	270	0	90	180	270	
PVA (Block)	28	4.9	5.1	5.3	5.3	4.8	5.2	5.4	5.3	5.2
	56	5.2	5.6	5.6	5.6	5.5	5.6	5.8	5.6	5.6
	91	6.3	5.7	6.2	5.5	6.3	5.9	6.4	5.9	6.0
	182	7.0	6.3	6.4	6.1	6.4	6.0	6.1	6.2	6.3
	364	7.9	7.7	8.2	7.9	8.4	7.7	8.4	7.6	8.0
	540	7.2	6.7	7.7	6.9	7.1	6.7	8	7.4	7.2
	730	8.4	7.3	8.9	8.7	8.2	7.2	8.2	8.6	8.2

Table C-9. Summary of the values of surface resistivity (k $\Omega$ .cm) for Class V concrete: cellulose fiber mixture (Cell)

Specimen ID	Test Day	Reading Locations (Degree)								Ave
		0	90	180	270	0	90	180	270	
Cell (Block)	28	6.1	5.8	6.4	6.1	6.3	6.0	6.4	6.2	6.2
	56	6.0	5.9	5.7	5.8	5.8	5.9	5.9	5.6	5.8
	91	6.2	5.4	5.5	6.3	5.9	5.4	5.6	5.9	5.8
	182	8.4	8.6	8.4	8.8	8.5	8.5	8.5	8.4	8.5
	364	13.2	11.4	10.8	11.5	11.1	12.3	10.0	11.1	11.4
	540	6.3	6.5	7.2	7.9	6.6	7.3	7.4	6.9	7.0
	730	7	7.2	7.3	7.2	7.1	7.2	7.2	6.8	7.1

Table C-10. Summary of the values of surface resistivity (k $\Omega$ .cm) for Class V concrete: steel fiber mixture (St)

Specimen ID	Test Day	Reading Locations (Degree)								Ave
		0	90	180	270	0	90	180	270	
St (Block)	28	2.4	2.0	3.6	1.9	2.5	2.6	3.1	1.8	2.5
	56	3.1	4.0	2.4	2.2	2.5	3.0	2.5	2.3	2.8
	91	2.7	3.0	3.7	2.3	3.0	2.6	4.0	2.9	3.0
	182	3.7	4.3	4.5	5.3	3.4	4.2	4.6	4.7	4.3
	364	6.8	5.8	5.3	4.1	5.8	4.6	4.8	5.3	5.3
	540	4.6	5.5	4.4	6.1	5.6	4.5	3.5	5.6	5.0
	730	3.4	4.4	3.5	6.8	3.4	3.5	2.5	5.6	4.1

APPENDIX D  
WATER PERMEABILITY TEST RESULTS

Table D-1. Summary of the values of water permeability coefficient obtained for Classes II/V concrete

Mix Type	Specimen ID	Class II Concrete		Class V Concrete	
		Control (x10 <sup>-13</sup> m/s)	Fiber (x10 <sup>-13</sup> m/s)	Control (x10 <sup>-13</sup> m/s)	Fiber (x10 <sup>-13</sup> m/s)
PC	Control A	2.83		2.34	
	Control B	-		2.17	
	Control C	3.19		-	
	Average	3.01	N/A	2.26	N/A
	S.D	0.25		0.12	
	C.O.V (%)	8.46		5.33	
PP	PP_0.5%_A	3.37	3.12	2.48	2.02
	PP_0.5%_B	3.46	2.90	2.92	2.37
	PP_0.5%_C	2.96	3.25	-	-
	Average	3.26	3.09	2.70	2.20
	S.D	0.27	0.18	0.31	0.25
	C.O.V (%)	8.17	5.73	11.52	11.28
PVA	PVA_0.75%_A	2.50	2.97	2.15	1.80
	PVA_0.75%_B	2.41	3.05	1.90	2.09
	PVA_0.75%_C	2.69	2.92	1.92	1.88
	Average	2.53	2.98	1.99	1.92
	S.D	0.14	0.07	0.14	0.15
	C.O.V	5.64	2.20	6.98	7.79
Cell	CELL_0.1%_A	4.31	3.32	2.24	2.55
	CELL_0.1%_B	4.31	3.58	2.53	2.25
	CELL_0.1%_C	4.41	3.37	-	2.35
	Average	4.34	3.42	2.39	2.38
	S.D	0.06	0.14	0.21	0.15
	C.O.V (%)	1.33	4.03	8.60	6.41
Steel	ST_1%_A	-	2.62	2.02	1.73
	ST_1%_B	3.92	2.28	1.84	1.78
	ST_1%_C	-	2.28	1.71	1.72
	Average	3.92	2.39	1.86	1.74
	S.D	-	0.20	0.16	0.03
	C.O.V (%)	-	8.20	8.38	1.84

APPENDIX E  
ABSORPTION TEST RESULTS

Table E-1. Summary of the values of absorption rate obtained for Class II concrete

Mix Type	Specimen ID	Control Specimens		Fiber Specimens	
		Initial (x10 <sup>-2</sup> mm/s <sup>0.5</sup> )	Second (x10 <sup>-2</sup> mm/s <sup>0.5</sup> )	Initial (x10 <sup>-2</sup> mm/s <sup>0.5</sup> )	Second (x10 <sup>-2</sup> mm/s <sup>0.5</sup> )
PC	Control A	2.48	1.34		
	Control B	2.45	1.48		
	Control C	2.43	1.53	N/A	N/A
	Average	2.45	1.45		
	S.D	0.0002	0.001		
	C.O.V (%)	0.93	6.82		
PP	PP_0.5%_A	2.44	1.48	2.48	1.76
	PP_0.5%_B	2.15	1.43	2.59	1.86
	PP_0.5%_C	-	-	-	-
	Average	2.29	1.45	2.54	1.81
	S.D	0.0021	0.0003	0.0008	0.0007
	C.O.V (%)	9.18	2.14	3.04	3.87
PVA	PVA_0.75%_A	1.79	1.02	1.75	1.22
	PVA_0.75%_B	1.82	1.03	1.79	1.29
	PVA_0.75%_C	-	-	-	-
	Average	1.81	1.03	1.77	1.26
	S.D	0.0002	0.0001	0.0003	0.0005
	C.O.V (%)	1.33	0.62	1.76	4.28
Cell	CELL_0.1%_A	2.19	1.59	2.40	1.63
	CELL_0.1%_B	2.38	1.60	2.37	1.68
	CELL_0.1%_C	2.15	1.55	-	-
	Average	2.24	1.58	2.39	1.65
	S.D	0.0012	0.0003	0.0002	0.0004
	C.O.V (%)	5.42	1.73	0.83	2.22
Steel	ST_1%_A	-	-	1.90	1.34
	ST_1%_B	2.09	1.27	1.98	1.43
	ST_1%_C	2.30	1.44	-	-
	Average	2.20	1.36	1.94	1.39
	S.D	0.0015	0.0012	0.0006	0.0006
	C.O.V (%)	6.73	8.87	2.91	4.59

Table E-2. Summary of the values of absorption rate obtained for Class V concrete

Mix Type	Specimen ID	Control Specimens		Fiber Specimens	
		Initial (x10 <sup>-2</sup> mm/s <sup>0.5</sup> )	Second (x10 <sup>-2</sup> mm/s <sup>0.5</sup> )	Initial (x10 <sup>-2</sup> mm/s <sup>0.5</sup> )	Second (x10 <sup>-2</sup> mm/s <sup>0.5</sup> )
PC	Control A	1.71	0.98		
	Control B	1.69	0.96		
	Control C	1.75	0.94		
	Average	1.72	0.96	N/A	N/A
	S.D	0.0003	0.0002		
	C.O.V (%)	1.65	2.35		
PP	PP_0.5%_A	1.02	0.46	1.92	1.05
	PP_0.5%_B	1.14	0.51	-	-
	PP_0.5%_C	-	-	2.14	1.16
	Average	1.08	0.48	2.03	1.10
	S.D	0.0009	0.0003	0.0015	0.0008
	C.O.V (%)	8.05	6.90	7.62	7.06
PVA	PVA_0.75%_A	-	-	-	-
	PVA_0.75%_B	1.17	0.97	1.26	0.91
	PVA_0.75%_C	1.38	1.06	1.44	0.95
	Average	1.27	1.02	1.35	0.93
	S.D	0.0015	0.0006	0.0012	0.0003
	C.O.V (%)	11.48	5.85	9.06	3.50
Cell	CELL_0.1%_A	1.17	0.65	1.38	0.81
	CELL_0.1%_B	1.22	0.67	-	-
	CELL_0.1%_C	-	-	1.38	0.85
	Average	1.20	0.66	1.38	0.83
	S.D	0.0003	0.0002	0.00002	0.0003
	C.O.V (%)	2.78	2.67	0.15	4.18
Steel	ST_1%_A	-	-	1.46	0.93
	ST_1%_B	1.22	0.64	-	-
	ST_1%_C	1.31	0.72	1.63	0.96
	Average	1.26	0.68	1.55	0.95
	S.D	0.0007	0.0005	0.0012	0.0002
	C.O.V (%)	5.16	8.00	7.95	2.02

APPENDIX F  
BULK DIFFUSION TEST RESULTS

Table F-1. Summary of the values of coefficient of chloride diffusion obtained for Class II concrete

Mix Type	Specimen ID	Class II Concrete	Class V Concrete
		Diffusion Coefficient (x10-12 m <sup>2</sup> /s)	Diffusion Coefficient (x10-12 m <sup>2</sup> /s)
PC	Control A	-	7.28
	Control B	16.10	7.92
	Control C	17.55	8.08
	Average	16.83	7.76
	S.D	1.028	0.42
	C.O.V (%)	6.11	5.42
PP	PP_0.5%_A	-	5.87
	PP_0.5%_B	17.17	6.28
	PP_0.5%_C	17.96	6.86
	Average	17.57	6.33
	S.D	0.559	0.50
	C.O.V (%)	3.18	7.83
PVA	PVA_0.75%_A	-	-
	PVA_0.75%_B	11.37	7.35
	PVA_0.75%_C	12.23	6.64
	Average	11.80	6.99
	S.D	0.61	0.50
	C.O.V (%)	5.13	7.20
Cell	CELL_0.1%_A	-	11.32
	CELL_0.1%_B	14.84	11.87
	CELL_0.1%_C	17.29	-
	Average	16.07	11.60
	S.D	1.73	0.39
	C.O.V (%)	10.78	3.37
Steel	ST_1%_A	6.47	5.27
	ST_1%_B	-	-
	ST_1%_C	6.04	5.91
	Average	6.26	5.59
	S.D	0.30	0.45
	C.O.V (%)	4.86	8.11

Table F-2. Summary of the values of 1-year bulk diffusion chloride profile for Class II concrete

Mix Type	Specimen ID	Depth (in)	NaCl (lb/yd <sup>3</sup> )			
			A	B	C	AVG
PC	Control B	0.0" - 0.5"	30.708	30.709	30.764	30.727
		0.5" - 1.0"	18.086	18.537	18.227	18.284
		1.0" - 1.5"	11.174	10.885	11.194	11.085
		1.5" - 2.0"	7.258	7.359	7.225	7.281
		2.0" - 2.5"	3.385	3.296	3.376	3.352
		2.5" - 3.0"	0.660	0.709	0.711	0.693
		3.0" - 3.5"	0.194	0.184	0.174	0.184
	Control C	0.0" - 0.5"	34.833	34.388	34.162	34.461
		0.5" - 1.0"	22.254	22.971	22.597	22.607
		1.0" - 1.5"	13.189	12.686	13.185	13.120
		1.5" - 2.0"	8.118	7.992	7.911	8.007
		2.0" - 2.5"	4.335	4.412	4.624	4.457
		2.5" - 3.0"	1.316	1.305	1.336	1.319
		3.0" - 3.5"	0.298	0.319	0.289	0.302
PP	PP_0.5%_B	0.0" - 0.5"	30.195	30.525	30.116	30.279
		0.5" - 1.0"	18.472	18.442	18.802	18.572
		1.0" - 1.5"	11.416	11.031	11.177	11.208
		1.5" - 2.0"	7.427	7.439	7.309	7.392
		2.0" - 2.5"	4.005	4.057	4.048	4.037
		2.5" - 3.0"	1.062	1.043	1.073	1.059
		3.0" - 3.5"	0.332	0.335	0.338	0.335
	PP_0.5%_C	0.0" - 0.5"	25.992	26.675	26.286	26.318
		0.5" - 1.0"	16.283	16.446	16.446	16.392
		1.0" - 1.5"	10.746	10.584	10.621	10.650
		1.5" - 2.0"	6.555	6.625	6.796	6.659
		2.0" - 2.5"	3.385	3.188	3.207	3.260
		2.5" - 3.0"	0.959	0.911	0.969	0.946
		3.0" - 3.5"	0.283	0.317	0.301	0.300
PVA	PVA_0.75%_B	0.0" - 0.5"	34.945	34.261	34.668	34.625
		0.5" - 1.0"	18.620	18.972	18.908	18.833
		1.0" - 1.5"	10.280	10.178	10.379	10.279
		1.5" - 2.0"	5.485	5.205	5.476	5.389
		2.0" - 2.5"	1.387	1.393	1.393	1.391
		2.5" - 3.0"	0.289	0.293	0.304	0.295
		3.0" - 3.5"	0.268	0.272	0.276	0.272
	PVA_0.75%_C	0.0" - 0.5"	33.392	32.979	33.661	33.344
		0.5" - 1.0"	19.730	18.958	19.660	19.449
		1.0" - 1.5"	10.399	10.199	10.227	10.275
		1.5" - 2.0"	5.577	5.756	5.510	5.614
		2.0" - 2.5"	1.402	1.339	1.351	1.364
		2.5" - 3.0"	0.307	0.300	0.286	0.298
		3.0" - 3.5"	0.284	0.296	0.295	0.292

Table F-2. Continued

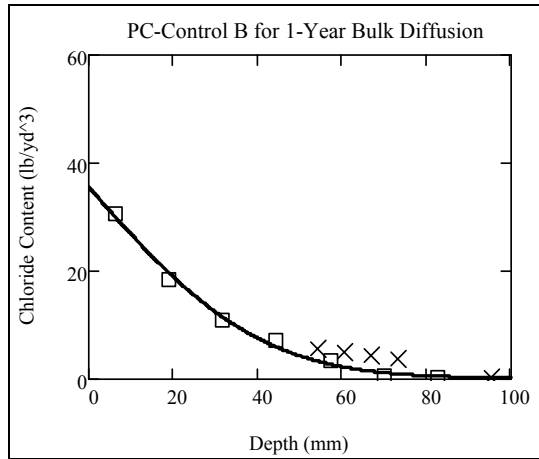
Mix Type	Specimen ID	Depth (in)	NaCl (lb/yd <sup>3</sup> )			
			A	B	C	AVG
Cell	Cell_0.1%_B	0.0" - 0.5"	34.636	34.642	34.251	34.510
		0.5" - 1.0"	19.787	20.326	19.743	19.952
		1.0" - 1.5"	11.728	11.752	11.738	11.739
		1.5" - 2.0"	7.206	6.600	7.116	6.974
		2.0" - 2.5"	3.854	4.096	4.453	4.134
		2.5" - 3.0"	1.120	1.150	1.129	1.133
		3.0" - 3.5"	0.369	0.371	0.389	0.376
	Cell_0.1%_C	0.0" - 0.5"	25.261	24.939	24.149	25.116
		0.5" - 1.0"	16.976	16.189	16.845	16.670
		1.0" - 1.5"	10.044	10.308	10.459	10.270
		1.5" - 2.0"	5.885	5.944	6.091	5.973
		2.0" - 2.5"	2.534	2.503	2.543	2.527
		2.5" - 3.0"	0.434	0.501	0.479	0.471
		3.0" - 3.5"	0.259	0.270	0.253	0.261
Steel	St_1%_A	0" - 0.125"	44.404	44.725	44.555	44.561
		0.125" - 0.25"	37.053	36.870	36.784	36.903
		0.25" - 0.375"	28.695	28.810	28.619	28.708
		0.375" - 0.5"	23.639	23.371	23.090	23.367
		0.5" - 1"	14.343	14.792	14.686	14.607
		1" - 1.5"	7.159	7.575	7.384	7.373
		1.5" - 2"	1.403	1.407	1.427	1.413
	St_1%_C	0.0" - 0.5"	38.218	37.589	38.039	37.949
		0.5" - 1.0"	15.412	15.271	15.087	15.257
		1.0" - 1.5"	7.127	7.291	7.268	7.229
		1.5" - 2.0"	1.539	1.567	1.562	1.556
		2.0" - 2.5"	0.285	0.267	0.288	0.280
		2.5" - 3.0"	0.247	0.243	0.244	0.245
		3.0" - 3.5"	0.296	0.242	0.225	0.254

Table F-3. Summary of the values of 1-year bulk diffusion chloride profile for Class V concrete

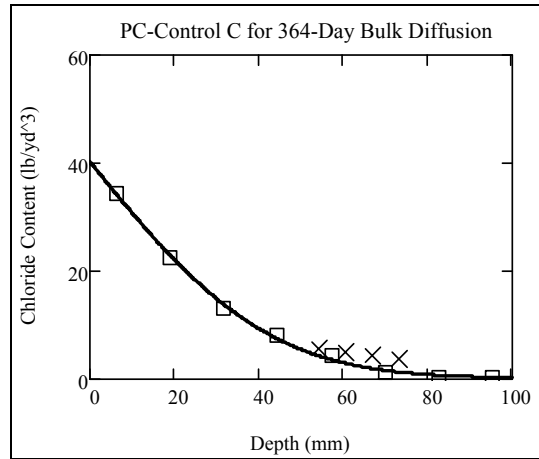
Mix Type	Specimen ID	Depth (in)	NaCl (lb/yd <sup>3</sup> )			
			A	B	C	AVG
PC	Control A	0" – 0.125"	43.960	43.960	43.858	43.993
		0.125" – 0.25"	34.481	34.481	34.774	34.597
		0.25" – 0.375"	28.458	28.458	28.696	28.577
		0.375" – 0.5"	24.725	24.725	24.751	24.742
		0.5" - 1"	16.290	16.290	16.377	16.335
		1" – 1.5"	6.067	6.067	6.106	6.001
		1.5" - 2"	0.770	0.770	0.784	0.772
	Control B	0.0" - 0.5"	35.306	34.848	34.519	34.891
		0.5" - 1.0"	18.311	18.509	18.352	18.391
		1.0" - 1.5"	7.346	7.490	7.489	7.442
		1.5" - 2.0"	1.177	1.202	1.126	1.168
		2.0" - 2.5"	0.371	0.353	0.332	0.352
		2.5" - 3.0"	0.468	0.452	0.470	0.463
		3.0" - 3.5"	0.399	0.393	0.385	0.392
	Control C	0.0" - 0.5"	37.365	37.808	37.515	37.563
		0.5" - 1.0"	19.823	19.535	19.421	19.593
		1.0" - 1.5"	8.164	8.387	8.429	8.327
		1.5" - 2.0"	1.561	1.576	1.558	1.565
		2.0" - 2.5"	0.490	0.488	0.459	0.479
		2.5" - 3.0"	0.441	0.505	0.489	0.478
		3.0" - 3.5"	0.388	0.441	0.406	0.412
PP	PP_0.5%_A	0" – 0.125"	38.179	38.179	38.169	38.078
		0.125" – 0.25"	30.835	30.835	31.206	31.024
		0.25" – 0.375"	25.536	25.536	25.799	25.688
		0.375" – 0.5"	21.937	21.937	22.132	22.133
		0.5" - 1"	13.427	13.427	13.420	13.440
		1" – 1.5"	3.079	3.079	3.172	3.093
		1.5" - 2"	0.283	0.283	0.290	0.283
	PP_0.5%_B	0.0" - 0.5"	34.341	34.988	34.697	34.675
		0.5" - 1.0"	16.263	16.189	16.385	16.279
		1.0" - 1.5"	5.298	5.185	5.176	5.220
		1.5" - 2.0"	0.466	0.459	0.469	0.465
		2.0" - 2.5"	0.193	0.198	0.212	0.201
		2.5" - 3.0"	0.213	0.201	0.203	0.206
		3.0" - 3.5"	0.216	0.208	0.225	0.216
	PP_0.5%_C	0.0" - 0.5"	34.840	34.410	34.548	34.599
		0.5" - 1.0"	17.112	17.200	17.307	17.206
		1.0" - 1.5"	5.863	5.912	5.905	5.893
		1.5" - 2.0"	0.536	0.548	0.524	0.536
		2.0" - 2.5"	0.255	0.267	0.205	0.242
		2.5" - 3.0"	0.441	0.432	0.471	0.448
		3.0" - 3.5"	0.204	0.258	0.209	0.224

Table F-3. Continued

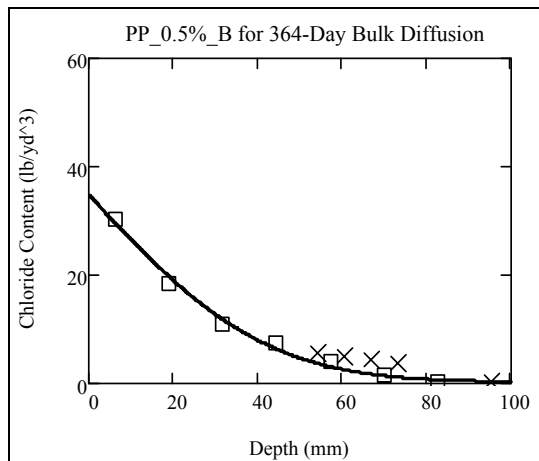
Mix Type	Specimen ID	Depth (in)	NaCl (lb/yd <sup>3</sup> )			
			A	B	C	AVG
PVA	PVA_0.75%_B	0.0" - 0.5"	31.916	31.643	31.366	31.642
		0.5" - 1.0"	15.327	15.327	15.276	15.310
		1.0" - 1.5"	6.423	6.642	6.624	6.563
		1.5" - 2.0"	1.117	1.095	1.092	1.101
		2.0" - 2.5"	0.306	0.302	0.301	0.303
		2.5" - 3.0"	0.313	0.283	0.288	0.295
		3.0" - 3.5"	0.453	0.485	0.488	0.475
	PVA_0.75%_C	0.0" - 0.5"	34.975	34.409	35.139	34.841
		0.5" - 1.0"	16.489	16.255	16.725	16.490
		1.0" - 1.5"	6.194	6.241	5.543	5.993
		1.5" - 2.0"	0.581	0.574	0.577	0.577
		2.0" - 2.5"	0.364	0.350	0.352	0.355
		2.5" - 3.0"	0.588	0.618	0.590	0.599
		3.0" - 3.5"	0.315	0.313	0.310	0.313
Cell	Cell_0.1%_A	0" - 0.125"	40.091	40.091	40.173	40.264
		0.125" - 0.25"	34.985	34.985	35.033	35.101
		0.25" - 0.375"	28.380	28.380	28.103	28.183
		0.375" - 0.5"	21.742	21.742	22.041	22.033
		0.5" - 1"	17.539	17.539	17.484	17.496
		1" - 1.5"	9.974	9.974	9.952	9.931
		1.5" - 2"	5.029	5.029	5.198	5.086
	Cell_0.1%_B	0.0" - 0.5"	30.138	30.290	29.596	30.008
		0.5" - 1.0"	28.970	29.548	29.728	29.415
		1.0" - 1.5"	16.220	16.383	16.171	16.258
		1.5" - 2.0"	6.767	6.208	6.549	6.508
		2.0" - 2.5"	1.024	0.978	1.050	1.017
		2.5" - 3.0"	0.217	0.220	0.239	0.225
		3.0" - 3.5"	0.266	0.251	0.238	0.252
Steel	St_1%_A	0" - 0.125"	45.617	45.617	46.154	46.040
		0.125" - 0.25"	38.458	38.458	37.903	38.123
		0.25" - 0.375"	30.001	30.001	29.868	29.869
		0.375" - 0.5"	23.177	23.177	23.193	23.095
		0.5" - 1"	15.487	15.487	15.372	15.439
		1" - 1.5"	4.207	4.207	3.972	4.135
		1.5" - 2"	0.325	0.325	0.275	0.312
	St_1%_C	0.0" - 0.5"	28.131	27.972	28.048	28.050
		0.5" - 1.0"	13.016	12.966	12.827	12.936
		1.0" - 1.5"	3.638	3.617	3.557	3.604
		1.5" - 2.0"	0.471	0.432	0.419	0.441
		2.0" - 2.5"	0.326	0.295	0.305	0.309
		2.5" - 3.0"	0.306	0.305	0.290	0.300
		3.0" - 3.5"	0.252	0.279	0.260	0.264



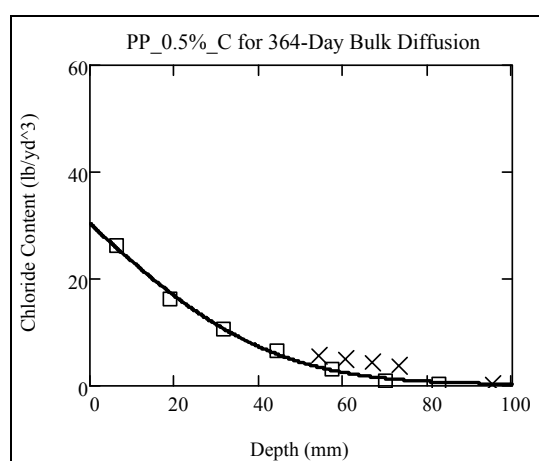
<b>Diffusion(m<sup>2</sup>/sec)</b>	1.610E-11	<b>Background(lb/yd<sup>3</sup>)</b>	0.213
<b>Surface(lb/yd<sup>3</sup>)</b>	35.570	<b>R<sup>2</sup> Value</b>	0.9966



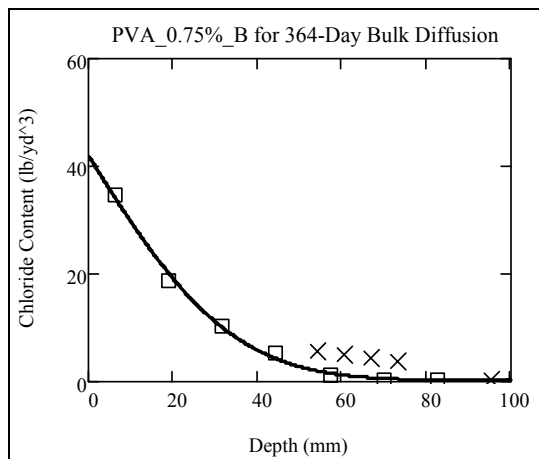
<b>Diffusion(m<sup>2</sup>/sec)</b>	1.755E-11	<b>Background(lb/yd<sup>3</sup>)</b>	0.213
<b>Surface(lb/yd<sup>3</sup>)</b>	40.247	<b>R<sup>2</sup> Value</b>	0.9991



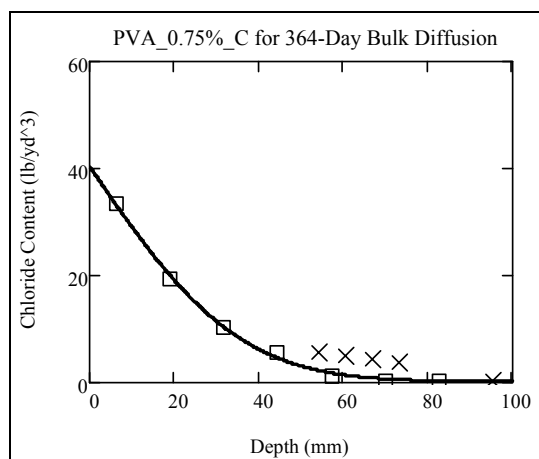
<b>Diffusion(m<sup>2</sup>/sec)</b>	1.717E-11	<b>Background(lb/yd<sup>3</sup>)</b>	0.285
<b>Surface(lb/yd<sup>3</sup>)</b>	34.814	<b>R<sup>2</sup> Value</b>	0.9968



<b>Diffusion(m<sup>2</sup>/sec)</b>	1.796E-11	<b>Background(lb/yd<sup>3</sup>)</b>	0.285
<b>Surface(lb/yd<sup>3</sup>)</b>	30.307	<b>R<sup>2</sup> Value</b>	0.9978

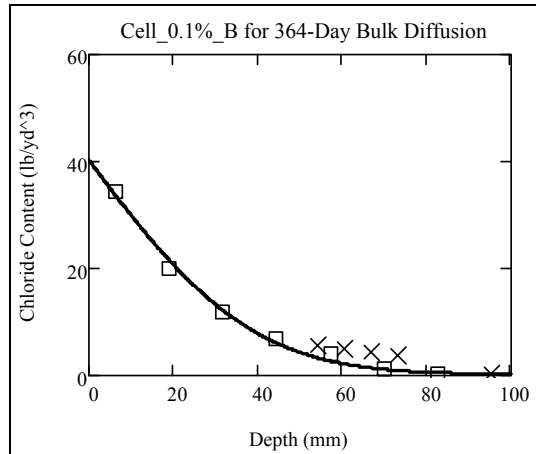


<b>Diffusion(m<sup>2</sup>/sec)</b>	1.137E-11	<b>Background(lb/yd<sup>3</sup>)</b>	0.216
<b>Surface(lb/yd<sup>3</sup>)</b>	41.926	<b>R<sup>2</sup> Value</b>	0.9983

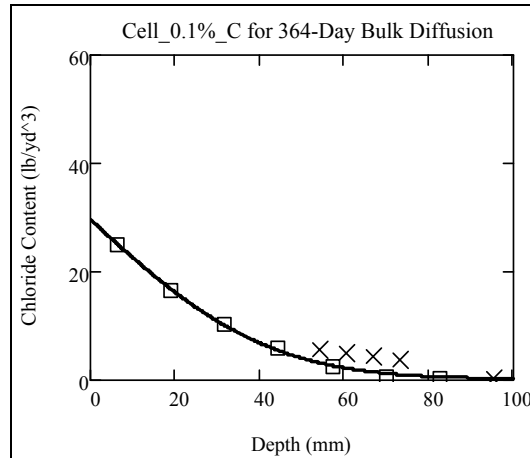


<b>Diffusion(m<sup>2</sup>/sec)</b>	1.226E-11	<b>Background(lb/yd<sup>3</sup>)</b>	0.216
<b>Surface(lb/yd<sup>3</sup>)</b>	40.356	<b>R<sup>2</sup> Value</b>	0.9991

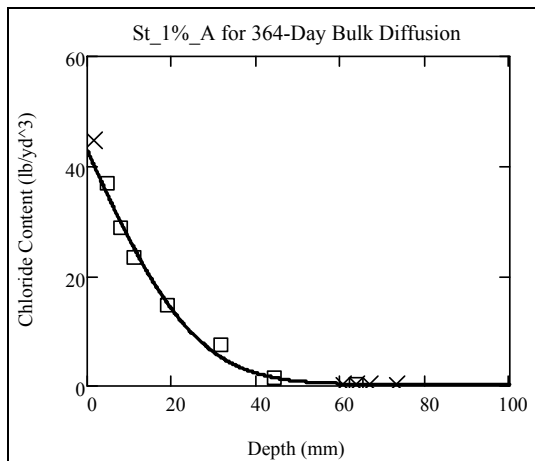
Figure F-1. Regression analysis of bulk diffusion for Class II concrete



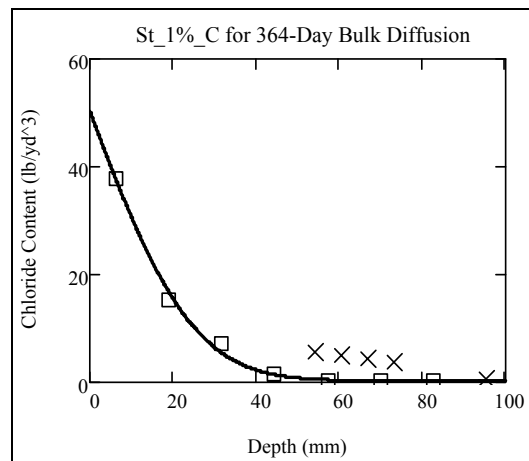
<b>Diffusion(m<sup>2</sup>/sec)</b>	1.484E-11	<b>Background(lb/yd<sup>3</sup>)</b>	0.268
<b>Surface(lb/yd<sup>3</sup>)</b>	40.171	<b>R<sup>2</sup> Value</b>	0.9966



<b>Diffusion(m<sup>2</sup>/sec)</b>	1.729E-11	<b>Background(lb/yd<sup>3</sup>)</b>	0.268
<b>Surface(lb/yd<sup>3</sup>)</b>	29.615	<b>R<sup>2</sup> Value</b>	0.9992

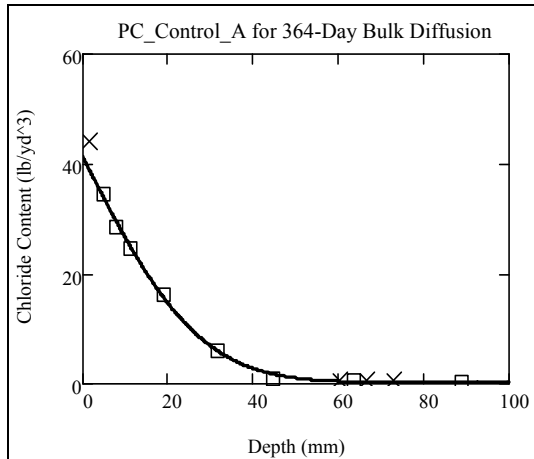


<b>Diffusion(m<sup>2</sup>/sec)</b>	6.474E-12	<b>Background(lb/yd<sup>3</sup>)</b>	0.304
<b>Surface(lb/yd<sup>3</sup>)</b>	42.831	<b>R<sup>2</sup> Value</b>	0.9947

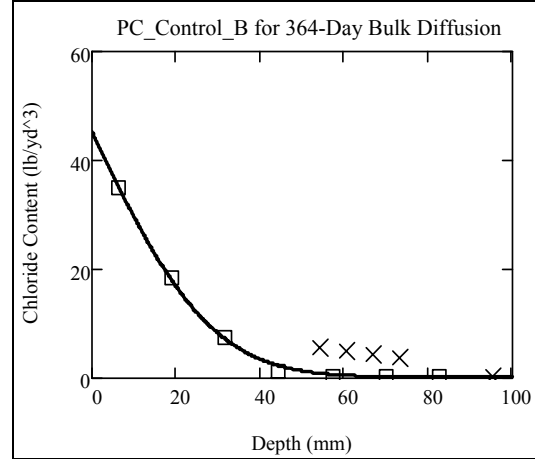


<b>Diffusion(m<sup>2</sup>/sec)</b>	6.044E-12	<b>Background(lb/yd<sup>3</sup>)</b>	0.304
<b>Surface(lb/yd<sup>3</sup>)</b>	50.313	<b>R<sup>2</sup> Value</b>	0.9977

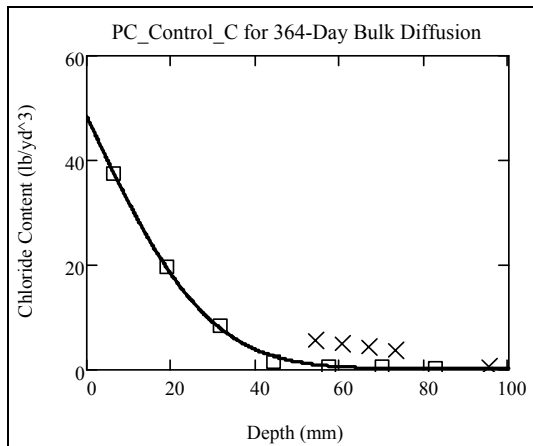
Figure F-1. Continued



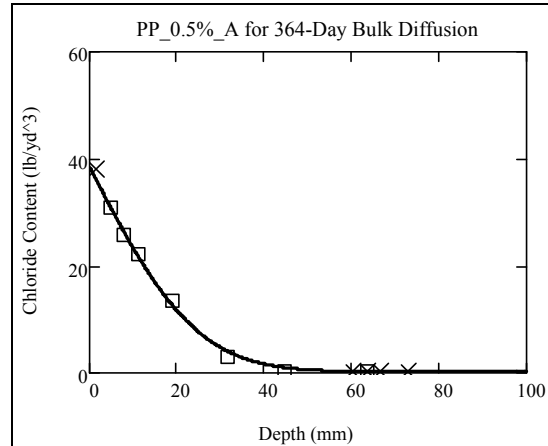
<b>Diffusion(m<sup>2</sup>/sec)</b>	7.282E-12	<b>Background(lb/yd<sup>3</sup>)</b>	0.243
<b>Surface(lb/yd<sup>3</sup>)</b>	41.254	<b>R<sup>2</sup> Value</b>	0.9990



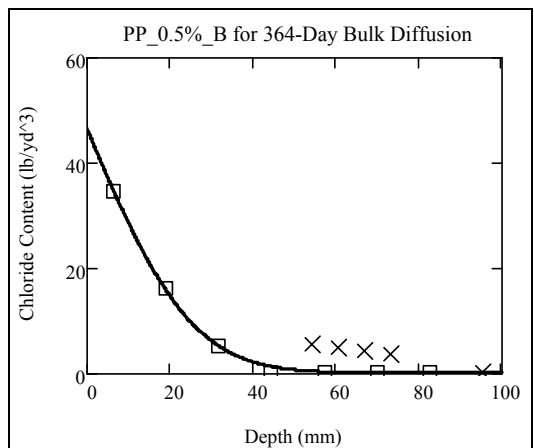
<b>Diffusion(m<sup>2</sup>/sec)</b>	7.919E-12	<b>Background(lb/yd<sup>3</sup>)</b>	0.243
<b>Surface(lb/yd<sup>3</sup>)</b>	45.170	<b>R<sup>2</sup> Value</b>	0.9992



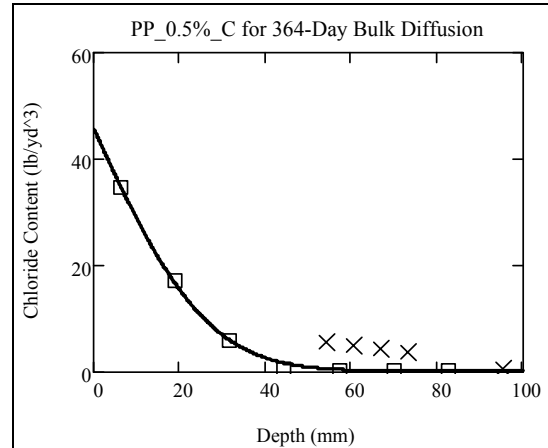
<b>Diffusion(m<sup>2</sup>/sec)</b>	8.075E-12	<b>Background(lb/yd<sup>3</sup>)</b>	0.243
<b>Surface(lb/yd<sup>3</sup>)</b>	48.364	<b>R<sup>2</sup> Value</b>	0.9994



<b>Diffusion(m<sup>2</sup>/sec)</b>	5.868E-12	<b>Background(lb/yd<sup>3</sup>)</b>	0.236
<b>Surface(lb/yd<sup>3</sup>)</b>	38.517	<b>R<sup>2</sup> Value</b>	0.9988

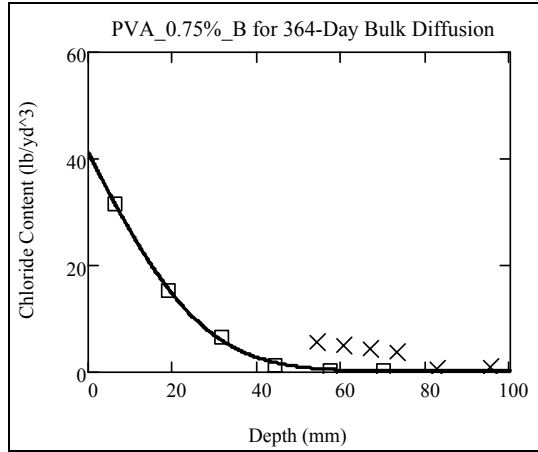


<b>Diffusion(m<sup>2</sup>/sec)</b>	6.277E-12	<b>Background(lb/yd<sup>3</sup>)</b>	0.236
<b>Surface(lb/yd<sup>3</sup>)</b>	46.407	<b>R<sup>2</sup> Value</b>	0.9995

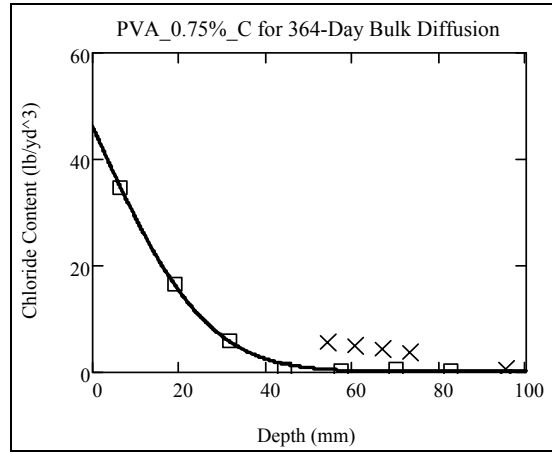


<b>Diffusion(m<sup>2</sup>/sec)</b>	6.855E-12	<b>Background(lb/yd<sup>3</sup>)</b>	0.236
<b>Surface(lb/yd<sup>3</sup>)</b>	45.768	<b>R<sup>2</sup> Value</b>	0.9992

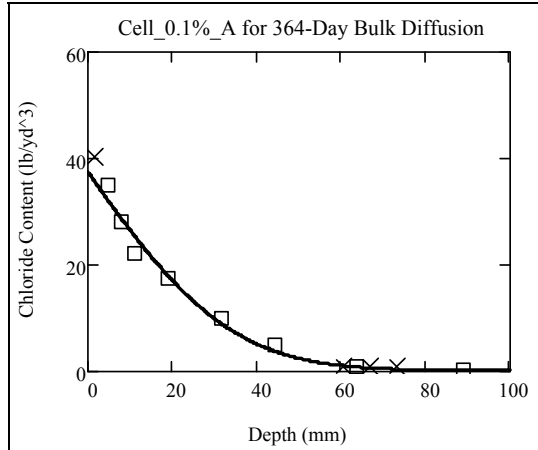
Figure F-2. Regression analysis of bulk diffusion for Class V concrete



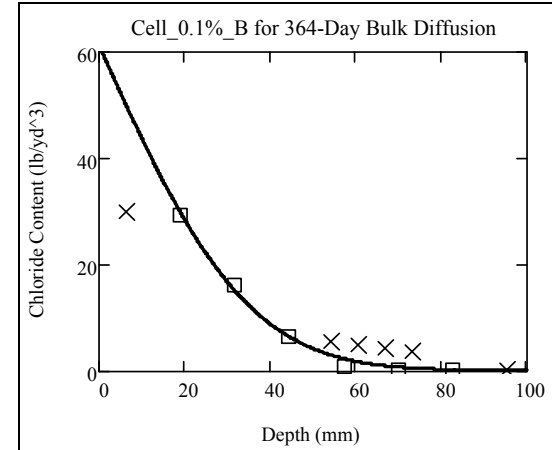
<b>Diffusion(m<sup>2</sup>/sec)</b>	7.347E-12	<b>Background(lb/yd<sup>3</sup>)</b>	0.202
<b>Surface(lb/yd<sup>3</sup>)</b>	41.101	<b>R<sup>2</sup> Value</b>	0.9994



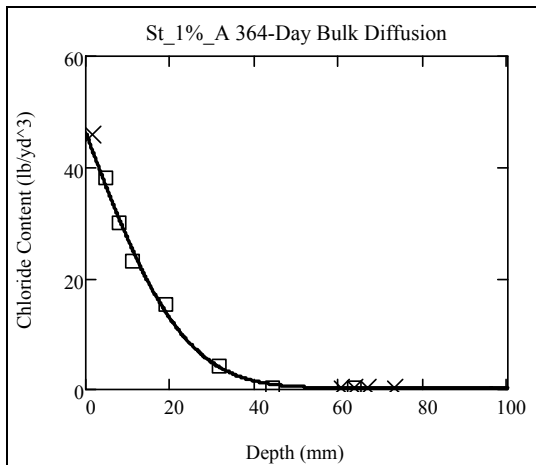
<b>Diffusion(m<sup>2</sup>/sec)</b>	6.635E-12	<b>Background(lb/yd<sup>3</sup>)</b>	0.202
<b>Surface(lb/yd<sup>3</sup>)</b>	46.132	<b>R<sup>2</sup> Value</b>	0.9994



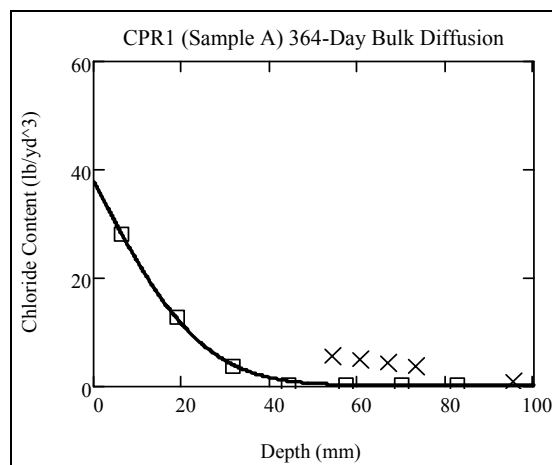
<b>Diffusion(m<sup>2</sup>/sec)</b>	1.132E-11	<b>Background(lb/yd<sup>3</sup>)</b>	0.211
<b>Surface(lb/yd<sup>3</sup>)</b>	37.428	<b>R<sup>2</sup> Value</b>	0.9902



<b>Diffusion(m<sup>2</sup>/sec)</b>	1.187E-11	<b>Background(lb/yd<sup>3</sup>)</b>	0.211
<b>Surface(lb/yd<sup>3</sup>)</b>	61.204	<b>R<sup>2</sup> Value</b>	0.9978



<b>Diffusion(m<sup>2</sup>/sec)</b>	5.267E-12	<b>Background(lb/yd<sup>3</sup>)</b>	0.243
<b>Surface(lb/yd<sup>3</sup>)</b>	46.164	<b>R<sup>2</sup> Value</b>	0.9964



<b>Diffusion(m<sup>2</sup>/sec)</b>	5.909E-12	<b>Background(lb/yd<sup>3</sup>)</b>	0.243
<b>Surface(lb/yd<sup>3</sup>)</b>	37.934	<b>R<sup>2</sup> Value</b>	0.9995

Figure F-2. Continued

APPENDIX G  
MECHANICAL PROPERTIES TEST RESULTS

Table G-1. Summary of the values of  $f_c$ ,  $f_{st}$ , and  $f_{pt}$  obtained for Class II concrete

Mix Type	Specimen ID	Compressive Strength (ksi)		Splitting Tensile Strength (psi)		Pressure Tension (psi)
		Control	Fiber	Control	Fiber	
PC	Control A	8.12		722.00		817.22
	Control B	7.98		737.39		834.85
	Control C	8.51	N/A	706.10	N/A	851.47
	Average	8.20		721.83		834.51
	S.D	0.22		15.65		17.13
	C.O.V (%)	2.74		2.17		2.05
PP	PP_0.5%_A	8.32	7.87	659.30	725.84	732.15
	PP_0.5%_B	8.20	8.42	653.78	608.26	756.57
	PP_0.5%_C	8.60	8.20	590.59	626.28	725.36
	Average	8.37	8.09	634.56	653.46	738.03
	S.D	0.21	0.27	38.18	63.33	16.41
	C.O.V (%)	2.49	3.34	6.02	9.69	2.22
PVA	PVA_0.75%_A	8.25	8.25	604.50	655.44	734.58
	PVA_0.75%_B	8.51	8.95	633.24	697.41	721.65
	PVA_0.75%_C	8.26	8.02	670.90	620.89	743.25
	Average	8.34	8.41	636.21	657.91	733.16
	S.D	0.15	0.48	33.30	38.32	10.87
	C.O.V (%)	1.77	5.73	5.23	5.82	1.48
Cell	CELL_0.1%_A	7.55	8.18	645.97	696.18	624.25
	CELL_0.1%_B	7.43	7.90	617.56	666.46	635.23
	CELL_0.1%_C	7.93	7.46	684.55	637.77	601.75
	Average	7.64	7.70	649.36	666.80	620.41
	S.D	0.26	0.36	33.62	29.21	17.07
	C.O.V (%)	3.42	4.71	5.18	4.38	2.75
Steel	ST_1%_A	8.52	9.37	692.58	781.14	765.87
	ST_1%_B	8.49	9.30	681.88	804.21	781.35
	ST_1%_C	8.47	9.12	669.53	768.88	779.75
	Average	8.49	9.26	681.33	784.74	775.66
	S.D	0.03	0.13	11.53	17.94	8.51
	C.O.V (%)	0.34	1.39	1.69	2.29	1.10

Table G-2. Summary of the values of  $f_c$ ,  $f_{st}$ , and  $f_{pt}$  obtained for Class V concrete

Mix Type	Specimen ID	Compressive Strength (ksi)		Splitting Tensile Strength (psi)		Pressure Tension (psi)
		Control	Fiber	Control	Fiber	
PC	Control A	9.21		790.41		877.90
	Control B	9.88		765.11		938.07
	Control C	9.89		788.30		970.97
	Average	9.66	N/A	781.27	N/A	928.98
	S.D	0.32		14.04		47.20
	C.O.V (%)	3.29		1.80		5.08
PP	PP_0.5%_A	9.96	9.94	680.45	672.34	-
	PP_0.5%_B	9.73	10.50	656.34	648.51	697.21
	PP_0.5%_C	10.24	9.95	675.84	634.61	755.09
	Average	9.97	10.13	670.88	651.82	736.15
	S.D	0.26	0.32	12.80	19.08	55.07
	C.O.V (%)	2.56	3.16	1.91	2.93	7.48
PVA	PVA_0.75%_A	9.84	10.21	630.34	671.60	-
	PVA_0.75%_B	10.00	9.76	642.12	622.89	756.79
	PVA_0.75%_C	9.83	10.32	614.22	651.20	795.57
	Average	9.89	10.10	628.89	648.56	776.18
	S.D	0.09	0.30	14.01	24.46	27.42
	C.O.V (%)	0.93	2.93	2.23	3.77	3.53
Cell	CELL_0.1%_A	9.35	8.67	613.61	726.26	606.73
	CELL_0.1%_B	9.43	8.97	606.79	708.18	-
	CELL_0.1%_C	9.90	9.86	656.81	731.26	589.89
	Average	9.56	9.17	625.74	721.90	633.57
	S.D	0.30	0.62	27.13	12.14	11.91
	C.O.V (%)	3.10	6.71	4.33	1.68	1.99
Steel	ST_1%_A	9.61	10.48	636.54	845.43	757.72
	ST_1%_B	9.91	9.91	632.24	762.70	803.71
	ST_1%_C	9.77	10.19	593.02	818.31	846.93
	Average	9.76	10.19	620.60	808.81	802.79
	S.D	0.15	0.28	23.98	42.17	44.61
	C.O.V (%)	1.51	2.77	3.86	5.21	5.56



A



B



C



D



E

Figure G-1. Compression failures for FRC. A) PC. B) PP. C) PVA. D) Cell. E) Steel fiber mixtures.



Figure G-2. Splitting tensile failures for FRC. A) PC. B) PP. C) PVA. D) Cell. E) Steel fiber mixtures.



A



B



C



D



E

Figure G-3. Pressure tensile failures for FRC. A) PC. B) PP. C) PVA. C) Cell. D) Steel fiber mixtures.

APPENDIX H  
STEEL CORROSION TEST RESULTS

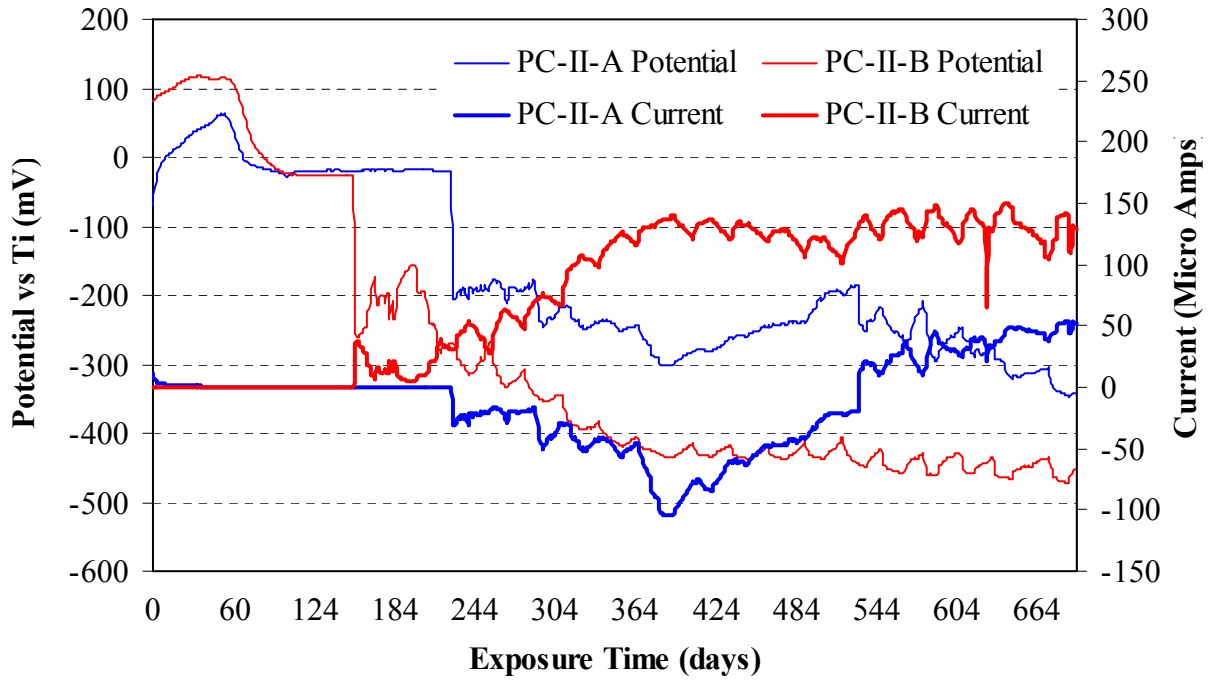


Figure H-1. Plain concrete for steel bar corrosion test

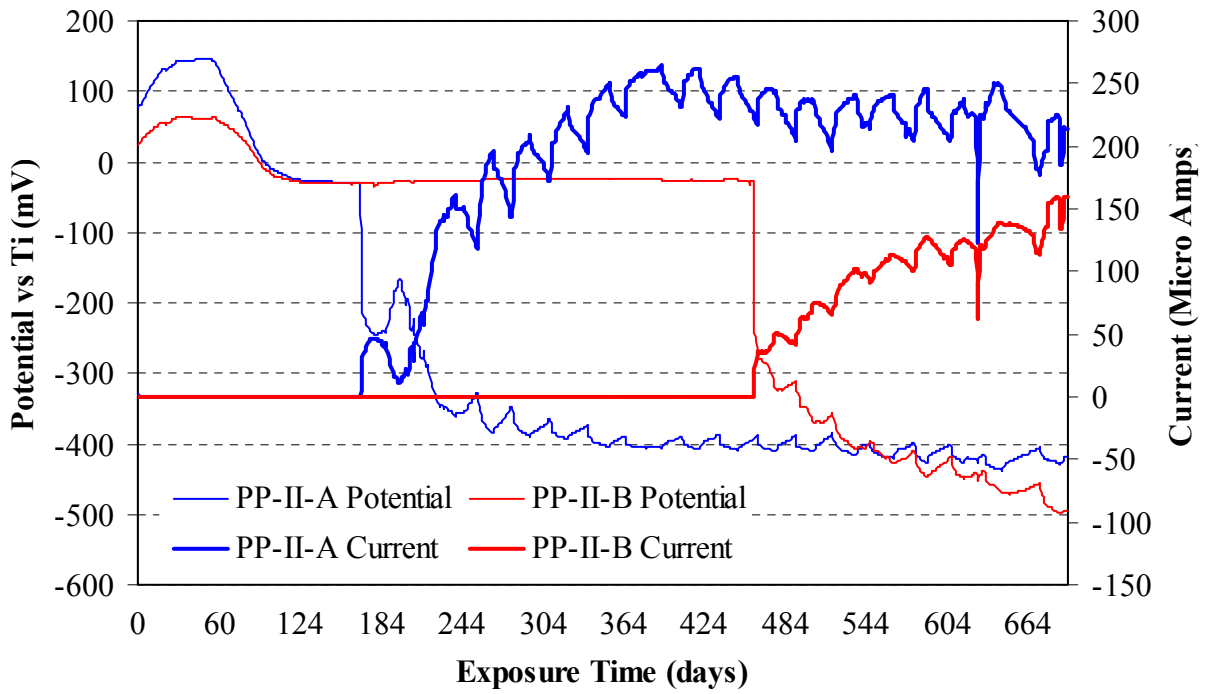


Figure H-2. Polypropylene fibers for steel bar corrosion test

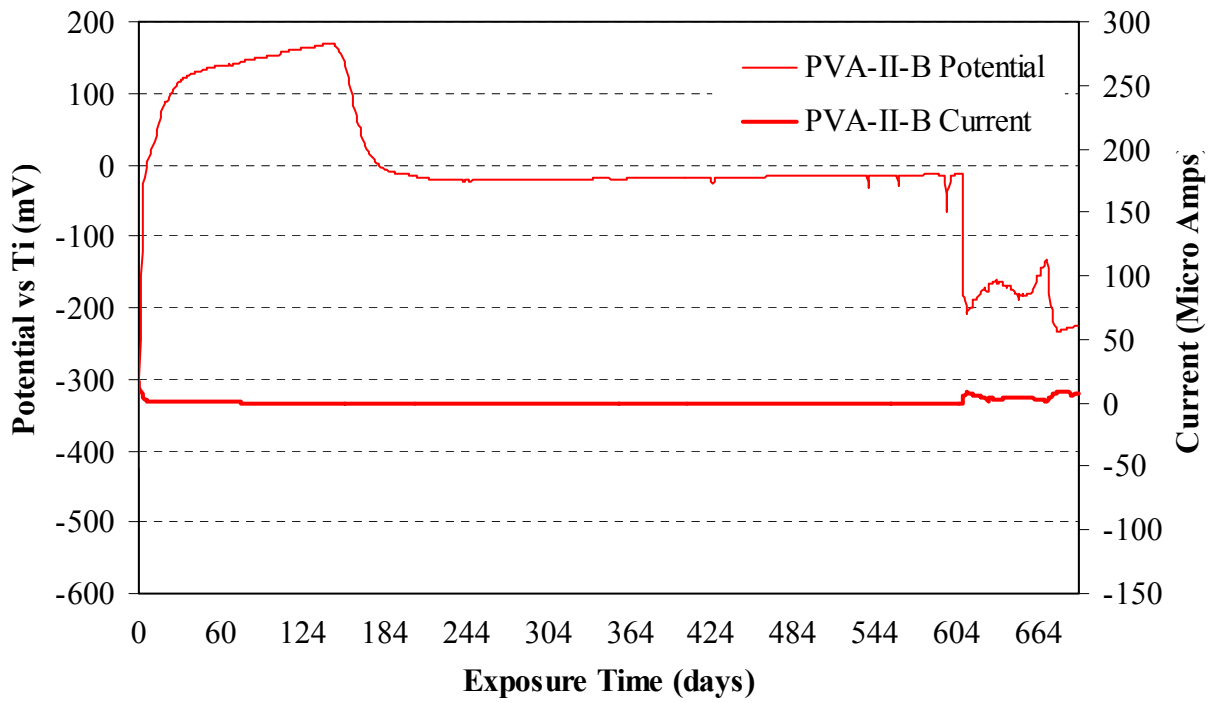


Figure H-3. Polyvinyl alcohol fibers for steel bar corrosion test

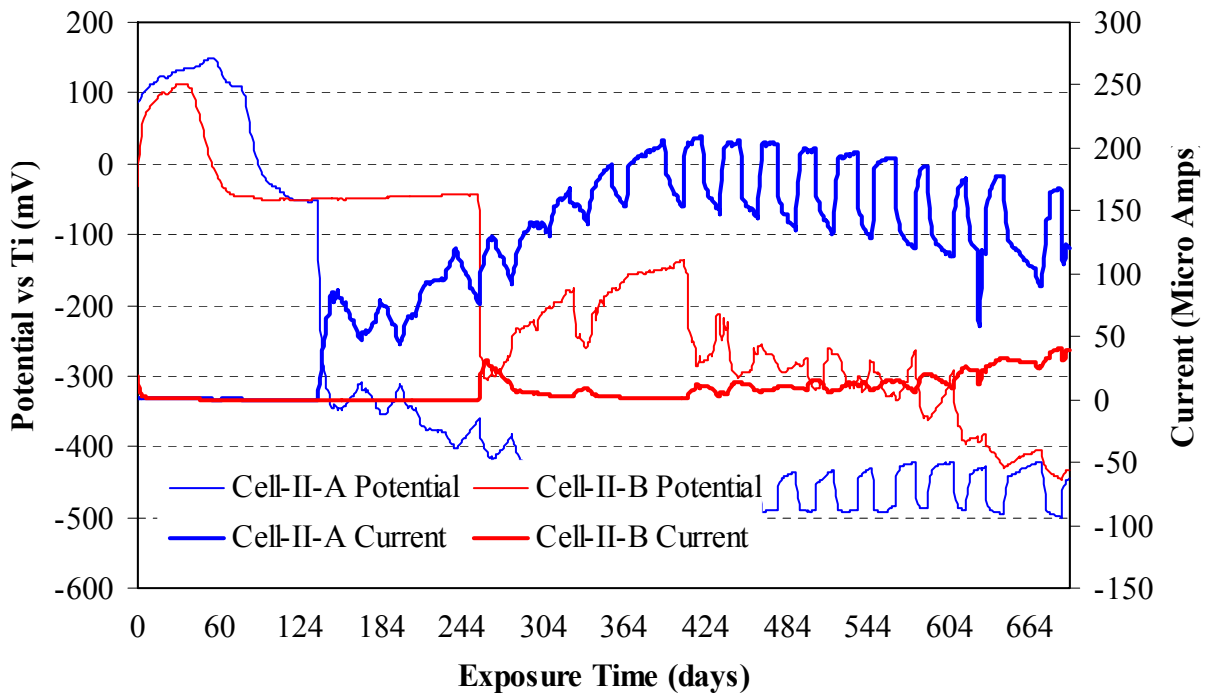


Figure H-4. Cellulose fibers for steel bar corrosion test

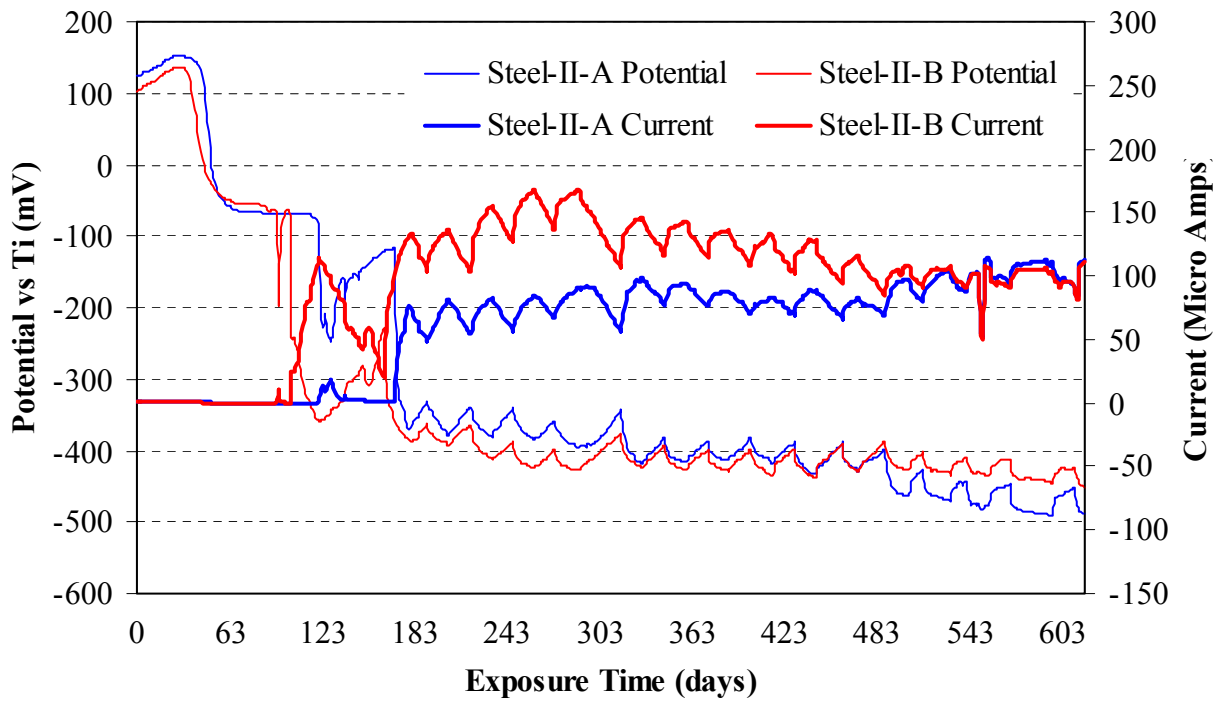


Figure H-5. Steel fibers for steel bar corrosion test

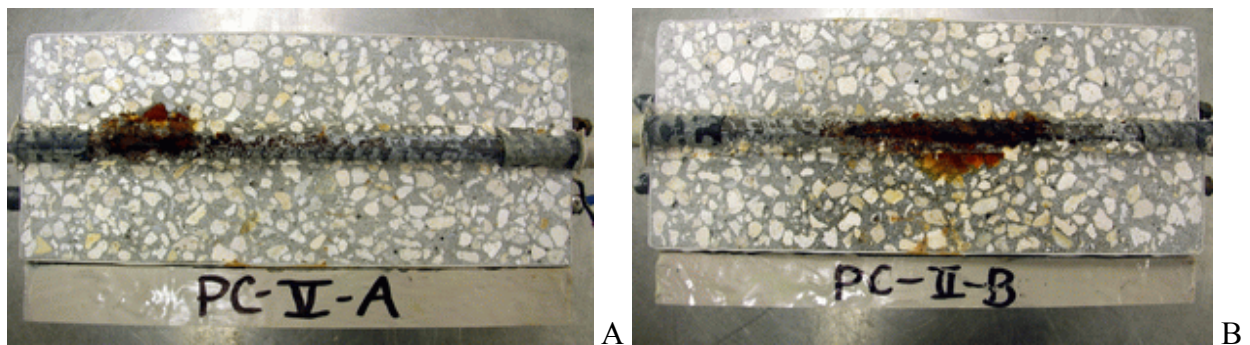


Figure H-6. Corroded steel bar for plain concrete mix. A) Specimen A. B) Specimen B.

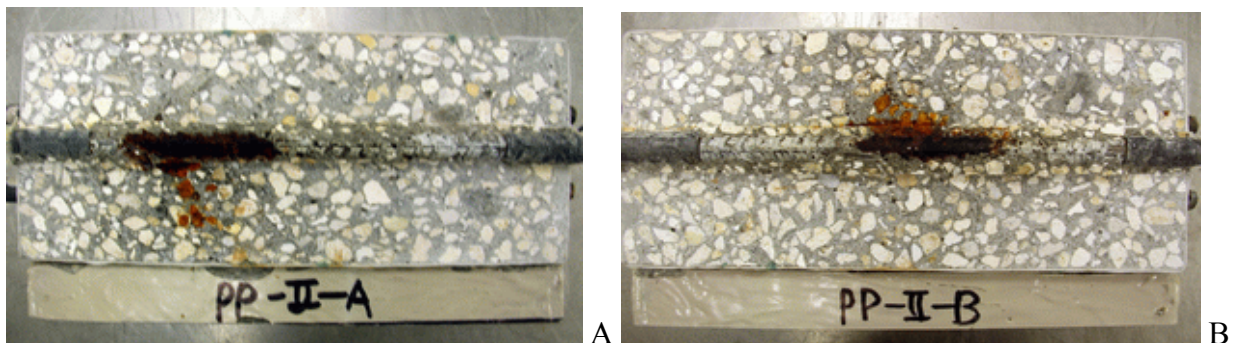


Figure H-7. Corroded steel bar for PP fiber mix . A) Specimen A. B) Specimen B.

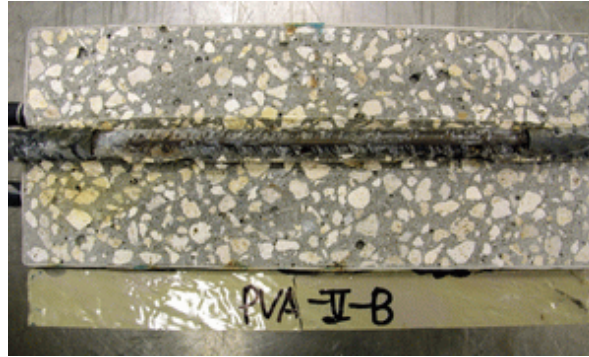


Figure H-8. Steel bar corrosion for PVA fiber mix. A) Specimen B.

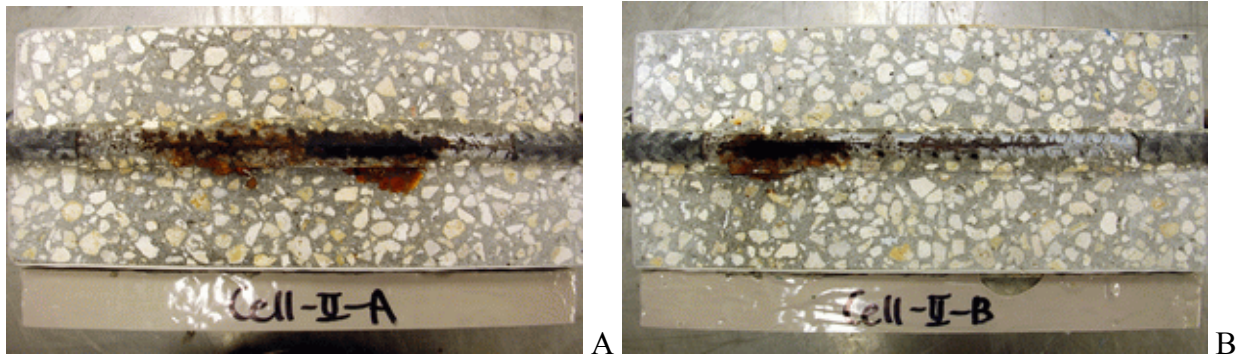


Figure H-9. Steel bar corrosion for cellulose fiber mix. A) Specimen A. B) Specimen B.

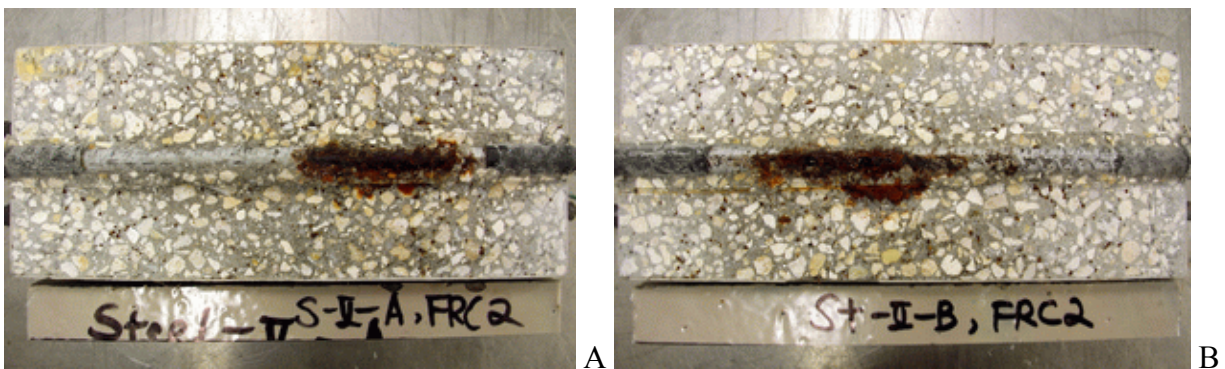


Figure H-10. Steel bar corrosion for steel fiber mix. A) Specimen A. B) Specimen B.

APPENDIX I  
DEGRADED BEAM TEST RESULTS

Table I-1. Averaged UPV test results for Class II concrete

UPV (m/s)	Exposure Tank #	Tank 1	Tank 6	Tank 9	Tank 3	Tank 7
	Environmental Exposure	Lime-Imm.	Salt-Imm.	Swamp-Imm.	Lime-W/D	Salt-W/D
ASTM C 1399 Specimen	PP-II-Precracked	4441	4157	3336	4268	4137
	PP-II-Uncracked	4458	4219	3359	4292	4156
	PVA-II-Precracked	4561	4306	3468	4355	4133
	PVA-II-Uncracked	4599	4357	3528	4355	4262
	Steel-II-Precracked	4563	4396	3697	4356	4331
	Steel-II-Uncracked	4639	4375	3715	4349	4344
ASTM C 1609 Specimen	PC-II-Uncracked	4639	4400	3624	4359	4214
	PP-II-Uncracked	4495	4221	3376	4302	4225
	PVA-II-Uncracked	4621	4372	3634	4407	4254
	Steel-II-Uncracked	4629	4414	3814	4385	4361

Table I-2. Averaged UPV test results for Class V concrete

UPV (m/s)	Exposure Tank #	Tank 2	Tank 5	Tank 10	Tank 4	Tank 8
	Environmental Exposure	Lime-Imm.	Salt-Imm.	Swamp-Imm.	Lime-W/D	Salt-W/D
ASTM C 1399 Specimen	PP-V-Precracked	4399	4330	3605	4338	4378
	PP-V-Uncracked	4572	4351	3676	4355	4457
	PVA-V-Precracked	4660	4343	3659	4405	4423
	PVA-V-Uncracked	4653	4424	3611	4479	4485
	Steel-V-Precracked	4710	4363	3887	4308	4350
	Steel-V-Uncracked	4723	4390	4148	4279	4351
ASTM C 1609 Specimen	PC-V-Uncracked	4423	4369	3859	4515	4616
	PP-V-Uncracked	4578	4316	3823	4449	4476
	PVA-V-Uncracked	4695	4426	3621	4562	4520
	Steel-V-Uncracked	4713	4445	4070	4476	4504

Table I-3. Summary of the values of residual load and average residual strength obtained for polypropylene fiber mixture for Class II concrete (pre-cracked beam)

Specimen ID	Residual Load (lbf)				Average Residual Strength (psi)
	0.02 in	0.03 in	0.04 in	0.05 in	
PP_II_T1_Lime_Con_Precracked_A	1568	1721	1775	1789	304.95
PP_II_T1_Lime_Con_Precracked_B	1869	2050	2130	2090	363.06
PP_II_T1_Lime_Con_Precracked_C	1357	1492	1527	1537	265.07
Average	1598	1754	1811	1805	311.03
S.D	257.31	280.49	303.08	276.86	49.28
C.O.V (%)	16.10	15.99	16.74	15.84	15.84
PP_II_T6_Salt_Con_Precracked_A	1558	1663	1740	1754	296.61
PP_II_T6_Salt_Con_Precracked_B	1552	1697	1763	1753	299.56
PP_II_T6_Salt_Con_Precracked_C	1322	1432	1495	1545	254.68
Average	1477	1597	1666	1684	283.62
S.D	134.56	144.19	148.54	120.38	25.10
C.O.V (%)	9.11	9.03	8.92	7.15	8.85
PP_II_T9_Swamp_Con_Precracked_A	677	746	789	811	143.49
PP_II_T9_Swamp_Con_Precracked_B	530	590	630	658	111.76
PP_II_T9_Swamp_Con_Precracked_C	649	714	750	772	136.26
Average	619	683	723	747	130.5
S.D	78.05	82.40	82.87	79.50	16.63
C.O.V (%)	12.62	12.06	11.46	10.64	12.74
PP_II_T3_Lime_WD_Precracked_A	1282	1397	1429	1433	250.25
PP_II_T3_Lime_WD_Precracked_B	1511	1654	1704	1682	298.05
PP_II_T3_Lime_WD_Precracked_C	1317	1459	1563	1565	271.32
Average	1370	1503	1565	1560	273.21
S.D	123.36	134.11	137.51	124.58	23.95
C.O.V (%)	9.00	8.92	8.79	7.99	8.77
PP_II_T7_Salt_WD_Precracked_A	1330	1425	1405	1390	249.41
PP_II_T7_Salt_WD_Precracked_B	1212	1294	1338	1341	231.86
PP_II_T7_Salt_WD_Precracked_C	1407	1488	1507	1468	263.14
Average	1316	1402	1416	1399	248.13
S.D	98.22	98.97	85.10	64.05	15.68
C.O.V (%)	7.46	7.06	6.01	4.58	6.32

Table I-4. Continued (un-cracked beam)

Specimen ID	Residual Load (lbf)				Average Residual Strength (psi)
	0.02 in	0.03 in	0.04 in	0.05 in	
PP_II_T1_Lime_Con_Uncracked_A	1113	1164	1201	1212	297.15
PP_II_T1_Lime_Con_Uncracked_B*	1227	1287	1331	1338	233.49
PP_II_T1_Lime_Con_Uncracked_C	1095	1174	1218	1246	212.69
Average	1145	1208	1250	1265	247.78
S.D	71.58	68.31	70.66	65.19	44.00
C.O.V (%)	6.25	5.65	5.65	5.15	17.76
PP_II_T6_Salt_Con_Uncracked_A	1153	1216	1252	1253	215.29
PP_II_T6_Salt_Con_Uncracked_B	1163	1209	1246	1260	216.53
PP_II_T6_Salt_Con_Uncracked_C	1074	1122	1148	1167	197.80
Average	1130	1182	1215	1227	209.87
S.D	48.75	52.37	58.39	51.79	10.47
C.O.V (%)	4.31	4.43	4.80	4.22	4.99
PP_II_T9_Swamp_Con_Uncracked_A	800	836	852	856	152.90
PP_II_T9_Swamp_Con_Uncracked_B	806	870	925	969	161.64
PP_II_T9_Swamp_Con_Uncracked_C	662	692	729	753	128.71
Average	756	799	835	859	147.75
S.D	81.46	94.50	99.06	108.04	17.06
C.O.V (%)	10.78	11.82	11.86	12.57	11.54
PP_II_T3_Lime_WD_Uncracked_A	1282	1397	1429	1433	250.25
PP_II_T3_Lime_WD_Uncracked_B*	1511	1654	1704	1682	298.05
PP_II_T3_Lime_WD_Uncracked_C	1317	1459	1563	1565	271.32
Average	1370	1503	1565	1560	273.21
S.D	123.36	134.11	137.51	124.58	23.95
C.O.V (%)	9.00	8.92	8.79	7.99	8.77
PP_II_T7_Salt_WD_Uncracked_A	1042	1078	1070	1084	189.72
PP_II_T7_Salt_WD_Uncracked_B	1387	1442	1466	1473	266.36
PP_II_T7_Salt_WD_Uncracked_C	1298	1397	1485	1522	258.17
Average	1242	1306	1340	1360	238.09
S.D	179.11	198.44	234.31	239.99	42.09
C.O.V (%)	14.42	15.20	17.48	17.65	17.68

\*: Cut beam (4 in × 3 in × 14 in) for IDT.

Table I-4. Summary of the values of residual load and average residual strength obtained for polyvinyl alcohol fiber mixture for Class II concrete (pre-cracked beam)

Specimen ID	Residual Load (lbf)				Average Residual Strength (psi)
	0.02 in	0.03 in	0.04 in	0.05 in	
PVA_II_T1_Lime_Con_Precracked_A	2440	2580	1906	1301	378.97
PVA_II_T1_Lime_Con_Precracked_B	2150	2340	2040	1463	360.09
PVA_II_T1_Lime_Con_Precracked_C	2160	2130	1933	1397	346.69
Average	2250	2350	1960	1387	361.92
S.D	164.62	225.17	70.87	81.46	16.22
C.O.V (%)	7.32	9.58	3.62	5.87	4.48
PVA_II_T6_Salt_Con_Precracked_A	1519	1644	1592	1241	266.81
PVA_II_T6_Salt_Con_Precracked_B	1646	1781	1794	1590	299.39
PVA_II_T6_Salt_Con_Precracked_C	1635	1614	1557	1157	263.40
Average	1600	1680	1648	1329	276.53
S.D	70.36	89.03	127.93	229.62	19.87
C.O.V (%)	4.40	5.30	7.76	17.27	7.18
PVA_II_T9_Swamp_Con_Precracked_A	546	607	633	654	112.40
PVA_II_T9_Swamp_Con_Precracked_B	478	523	550	574	95.97
PVA_II_T9_Swamp_Con_Precracked_C	540	604	657	704	112.02
Average	521	578	613	644	106.80
S.D	37.65	47.66	56.15	65.57	9.38
C.O.V (%)	7.22	8.24	9.15	10.18	8.78
PVA_II_T3_Lime_WD_Precracked_A	2620	2670	2670	2540	464.01
PVA_II_T3_Lime_WD_Precracked_B	2310	2370	2320	2040	392.63
PVA_II_T3_Lime_WD_Precracked_C	2190	2350	2270	2060	409.64
Average	2373	2463	2420	2213	422.09
S.D	221.89	179.26	217.94	283.08	37.28
C.O.V (%)	9.35	7.28	9.01	12.79	8.83
PVA_II_T7_Salt_WD_Precracked_A	2410	2590	2470	2050	429.96
PVA_II_T7_Salt_WD_Precracked_B	2020	2190	2080	1772	364.09
PVA_II_T7_Salt_WD_Precracked_C	2100	2140	2060	1890	368.96
Average	2177	2307	2203	1904	387.67
S.D	205.99	246.64	231.16	139.53	36.70
C.O.V (%)	9.46	10.69	10.49	7.33	9.47

Table I-4. Continued (un-cracked beam)

Specimen ID	Residual Load (lbf)				Average Residual Strength (psi)
	0.02 in	0.03 in	0.04 in	0.05 in	
PVA_II_T1_Lime_Con_Uncracked_A*	1270	1417	1497	1542	365.44
PVA_II_T1_Lime_Con_Uncracked_B	2480	2750	2580	2130	447.83
PVA_II_T1_Lime_Con_Uncracked_C	1782	2010	2210	2200	371.34
Average	1844	2059	2096	1957	394.87
S.D	607.38	667.85	550.48	361.39	45.96
C.O.V (%)	32.94	32.44	26.27	18.46	11.64
PVA_II_T6_Salt_Con_Uncracked_A	1720	1874	1833	1769	318.64
PVA_II_T6_Salt_Con_Uncracked_B	1609	1762	1924	1833	326.74
PVA_II_T6_Salt_Con_Uncracked_C	1663	1845	1953	1735	324.17
Average	1664	1827	1903	1779	323.19
S.D	55.51	58.13	62.61	49.76	4.14
C.O.V (%)	3.34	3.18	3.29	2.80	1.28
PVA_II_T9_Swamp_Con_Uncracked_A	647	742	730	670	123.19
PVA_II_T9_Swamp_Con_Uncracked_B	551	590	628	666	108.62
PVA_II_T9_Swamp_Con_Uncracked_C	588	642	698	750	123.06
Average	595	658	685	695	118.29
S.D	48.42	77.25	52.17	47.38	8.38
C.O.V (%)	8.13	11.74	7.61	6.81	7.08
PVA_II_T3_Lime_WD_Uncracked_A*	907	998	1064	1042	262.00
PVA_II_T3_Lime_WD_Uncracked_B*	959	995	1036	1074	262.87
PVA_II_T3_Lime_WD_Uncracked_C	1336	1434	1518	1554	265.14
Average	1067	1142	1206	1223	263.34
S.D	234.12	252.60	270.56	286.81	1.62
C.O.V (%)	21.94	22.11	22.43	23.45	0.61
PVA_II_T7_Salt_WD_Uncracked_A	1272	1363	1452	1394	243.91
PVA_II_T7_Salt_WD_Uncracked_B	1935	2110	2180	2240	376.67
PVA_II_T7_Salt_WD_Uncracked_C	1769	1889	1871	1838	331.10
Average	1659	1787	1834	1824	317.23
S.D	345.00	383.74	365.38	423.17	67.46
C.O.V (%)	20.80	21.47	19.92	23.20	21.27

\*: Cut beam (4 in × 3 in × 14 in) for IDT

Table I-5. Summary of the values of residual load and average residual strength obtained for steel fiber mixture for Class II concrete (pre-cracked beam)

Specimen ID	Residual Load (lbf)				Average Residual Strength (psi)
	0.02 in	0.03 in	0.04 in	0.05 in	
ST_II_T1_Lime_Con_Precracked_A	4890	4440	4100	3660	772.02
ST_II_T1_Lime_Con_Precracked_B	4730	4260	3960	3690	772.29
ST_II_T1_Lime_Con_Precracked_C	4430	4260	4010	3760	762.16
Average	4683	4320	4023	3703	768.82
S.D	233.52	103.92	70.95	51.32	5.77
C.O.V (%)	4.99	2.41	1.76	1.39	0.75
ST_II_T6_Salt_Con_Precracked_A	4600	4130	3710	3280	724.13
ST_II_T6_Salt_Con_Precracked_B	4950	4400	3960	3590	796.20
ST_II_T6_Salt_Con_Precracked_C	5250	4430	3880	3400	758.43
Average	4933	4320	3850	3423	759.59
S.D	325.32	165.23	127.67	156.31	36.05
C.O.V (%)	4600	4130	3710	3280	724.13
ST_II_T9_Swamp_Con_Precracked_A	1848	1864	1827	1789	339.24
ST_II_T9_Swamp_Con_Precracked_B	2300	2210	2120	2060	377.39
ST_II_T9_Swamp_Con_Precracked_C	1812	1698	1642	1571	308.95
Average	1987	1924	1863	1807	341.86
S.D	271.95	261.22	241.02	244.98	34.29
C.O.V (%)	13.69	13.58	12.94	13.56	10.03
ST_II_T3_Lime_WD_Precracked_A	5490	4740	4450	4170	857.86
ST_II_T3_Lime_WD_Precracked_B	3420	2980	2530	2230	515.44
ST_II_T3_Lime_WD_Precracked_C	3850	3410	3200	3030	638.71
Average	4253	3710	3393	3143	670.67
S.D	1092.35	917.55	974.49	974.95	173.43
C.O.V (%)	25.68	24.73	28.72	31.02	25.86
ST_II_T7_Salt_WD_Precracked_A	3380	3030	2790	2680	544.54
ST_II_T7_Salt_WD_Precracked_B	2560	2490	2220	2070	435.63
ST_II_T7_Salt_WD_Precracked_C	3880	3310	2870	2490	575.24
Average	3273	2943	2627	2413	518.47
S.D	666.43	416.81	354.45	312.14	73.36
C.O.V (%)	20.36	14.16	13.49	12.93	14.15

Table I-5. Continued (un-cracked beam)

Specimen ID	Residual Load (lbf)				Average Residual Strength (psi)
	0.02 in	0.03 in	0.04 in	0.05 in	
ST_II_T1_Lime_Con_Uncracked_A*	4360	4120	3670	3380	708.31
ST_II_T1_Lime_Con_Uncracked_B	3930	3790	3530	3210	657.88
ST_II_T1_Lime_Con_Uncracked_C	4100	3770	3450	3070	654.80
Average	4130	3893	3550	3220	673.66
S.D	216.56	196.55	111.36	155.24	30.05
C.O.V (%)	5.24	5.05	3.14	4.82	4.46
ST_II_T6_Salt_Con_Uncracked_A	4390	4040	3560	3290	679.94
ST_II_T6_Salt_Con_Uncracked_B	4650	4320	3940	3470	725.40
ST_II_T6_Salt_Con_Uncracked_C	4010	3700	3480	3090	630.81
Average	4350	4020	3660	3283	678.72
S.D	321.87	310.48	245.76	190.09	47.30
C.O.V (%)	7.40	7.72	6.71	5.79	6.97
ST_II_T9_Swamp_Con_Uncracked_A	2200	2220	2180	2040	394.06
ST_II_T9_Swamp_Con_Uncracked_B	2160	2180	2110	1936	383.43
ST_II_T9_Swamp_Con_Uncracked_C	2010	2000	1980	1949	366.64
Average	2123	2133	2090	1975	381.38
S.D	100.17	117.19	101.49	56.67	13.83
C.O.V (%)	4.72	5.49	4.86	2.87	3.63
ST_II_T3_Lime_WD_Uncracked_A	3590	3180	2640	2370	541.31
ST_II_T3_Lime_WD_Uncracked_B	4250	3360	3030	2720	621.62
ST_II_T3_Lime_WD_Uncracked_C	4590	3680	3290	3000	675.79
Average	4143	3407	2987	2697	612.91
S.D	508.46	253.25	327.16	315.65	67.66
C.O.V (%)	12.27	7.43	10.95	11.71	11.04
ST_II_T7_Salt_WD_Uncracked_A	4250	3260	2740	2440	566.08
ST_II_T7_Salt_WD_Uncracked_B	6320	5110	4000	3380	851.57
ST_II_T7_Salt_WD_Uncracked_C	6420	4420	3450	3110	778.12
Average	5663	4263	3397	2977	731.92
S.D	1225.00	934.90	631.69	483.98	148.24
C.O.V (%)	21.63	21.93	18.60	16.26	20.25

\*: Cut beam (4 in × 3 in × 14 in) for IDT

Table I-6. Summary of the values of residual load and average residual strength obtained for polypropylene fiber mixture for Class V concrete (pre-cracked beam)

Specimen ID	Residual Load (lbf)				Average Residual Strength (psi)
	0.02 in	0.03 in	0.04 in	0.05 in	
PP_V_T2_Lime_Con_Precracked_A	1652	1853	1947	1914	341.89
PP_VI_T2_Lime_Con_Precracked_B	1784	1980	2070	2070	351.72
PP_V_T2_Lime_Con_Precracked_C	-	-	-	-	-
Average	1718	1917	2009	1992	346.80
S.D	93.34	89.80	86.97	110.31	6.95
C.O.V (%)	5.43	4.69	4.33	5.54	2.00
PP_V_T5_Salt_Con_Precracked_A	2110	2290	2360	2320	409.04
PP_V_T5_Salt_Con_Precracked_B	2110	2300	2420	2440	417.601
PP_V_T5_Salt_Con_Precracked_C	2100	2280	2380	2410	407.05
Average	2107	2290	2387	2390	411.23
S.D	5.77	10.00	30.55	62.45	5.61
C.O.V (%)	0.27	0.44	1.28	2.61	1.36
PP_V_T10_Swamp_Con_Precracked_A	909	1019	1101	1154	189.84
PP_V_T10_Swamp_Con_Precracked_B	690	780	835	859	142.89
PP_V_T10_Swamp_Con_Precracked_C	761	840	895	921	158.59
Average	787	880	944	978	163.77
S.D	111.73	124.34	139.52	155.54	23.90
C.O.V (%)	14.20	14.13	14.78	15.90	14.60
PP_V_T4_Lime_WD_Precracked_A	939	1030	1085	1115	188.29
PP_V_T4_Lime_WD_Precracked_B	837	909	942	950	163.90
PP_V_T4_Lime_WD_Precracked_C	1293	1408	1422	1431	247.16
Average	1023	1116	1150	1165	199.78
S.D	239.32	260.30	246.45	244.42	42.80
C.O.V (%)	23.39	23.33	21.44	20.97	21.43
PP_V_T8_Salt_WD_Precracked_A	2240	2320	2410	2450	395.50
PP_V_T8_Salt_WD_Precracked_B	1812	1950	2010	2050	330.80
PP_V_T8_Salt_WD_Precracked_C	1895	2050	2140	2140	348.65
Average	1982	2107	2187	2213	358.32
S.D	226.97	191.40	204.04	209.84	33.42
C.O.V (%)	11.45	9.09	9.33	9.48	9.33

Table I-6. Continued (un-cracked beam)

Specimen ID	Residual Load (lbf)				Average Residual Strength (psi)
	0.02 in	0.03 in	0.04 in	0.05 in	
PP_V_T2_Lime_Con_Uncracked_A	1444	1510	1539	1551	274.30
PP_V_T2_Lime_Con_Uncracked_B	1232	1320	1361	1356	236.78
PP_V_T2_Lime_Con_Uncracked_C	1267	1350	1380	1368	241.69
Average	1314	1393	1427	1425	250.92
S.D	113.65	102.14	97.75	109.28	20.40
C.O.V (%)	8.65	7.33	6.85	7.67	8.13
PP_V_T5_Salt_Con_Uncracked_A	2190	2310	2360	2350	404.85
PP_V_T5_Salt_Con_Uncracked_B	1824	1958	2030	2050	350.70
PP_V_T5_Salt_Con_Uncracked_C	2090	2220	2270	2290	398.61
Average	2035	2163	2220	2230	384.72
S.D	189.17	182.87	170.59	158.75	29.63
C.O.V (%)	9.30	8.46	7.68	7.12	7.70
PP_V_T10_Swamp_Con_Uncracked_A	795	853	882	892	157.69
PP_V_T10_Swamp_Con_Uncracked_B	889	949	997	1036	180.57
PP_V_T10_Swamp_Con_Uncracked_C	807	868	918	969	162.47
Average	830.33	890.00	932.33	965.67	166.91
S.D	51.16	51.64	58.82	72.06	12.07
C.O.V (%)	6.16	5.80	6.31	7.46	7.23
PP_V_T4_Lime_WD_Uncracked_A	1160	1232	1284	1318	228.38
PP_V_T4_Lime_WD_Uncracked_B	997	1057	1088	1110	185.99
PP_V_T4_Lime_WD_Uncracked_C	1626	1656	1708	1743	301.83
Average	1261	1315	1360	1390	238.73
S.D	326.44	308.00	316.91	322.64	58.61
C.O.V (%)	25.89	23.42	23.30	23.21	24.55
PP_V_T8_Salt_WD_Uncracked_A	1954	1692	1742	1756	314.03
PP_V_T8_Salt_WD_Uncracked_B	1722	1801	1822	1831	309.34
PP_V_T8_Salt_WD_Uncracked_C	1653	1754	1791	1790	307.24
Average	1776	1749	1785	1792	310.20
S.D	157.68	54.67	40.34	37.55	3.48
C.O.V (%)	8.88	3.13	2.26	2.10	1.12

Table I-7. Summary of the values of residual load and average residual strength obtained for polyvinyl alcohol fiber mixture for Class V concrete (pre-cracked beam)

Specimen ID	Residual Load (lbf)				Average Residual Strength (psi)
	0.02 in	0.03 in	0.04 in	0.05 in	
PVA_V_T2_Lime_Con_Precracked_A	1630	1730	1523	1403	289.56
PVA_V_T2_Lime_Con_Precracked_B	1769	1921	1763	1255	306.72
PVA_V_T2_Lime_Con_Precracked_C	1985	2200	2220	1683	369.80
Average	1795	1950	1835	1447	322.03
S.D	178.89	236.37	354.09	217.37	42.26
C.O.V (%)	9.97	12.12	19.29	15.02	13.12
PVA_V_T5_Salt_Con_Precracked_A	1639	1760	1536	1321	279.76
PVA_V_T5_Salt_Con_Precracked_B	2310	2390	1960	1578	355.98
PVA_V_T5_Salt_Con_Precracked_C	2350	2660	2500	1694	391.97
Average	2100	2270	1999	1531	342.57
S.D	399.45	461.84	483.16	190.89	57.30
C.O.V (%)	19.02	20.35	24.17	12.47	16.73
PVA_V_T10_Swamp_Con_Precracked_A	1116	1258	1365	1452	233.86
PVA_V_T10_Swamp_Con_Precracked_B	1044	1154	1211	1131	207.07
PVA_V_T10_Swamp_Con_Precracked_C	1173	1293	1389	1439	243.26
Average	1111	1235	1322	1341	228.06
S.D	64.65	72.30	96.59	181.69	18.78
C.O.V (%)	5.82	5.85	7.31	13.55	8.23
PVA_V_T4_Lime_WD_Precracked_A	1760	1924	1990	1927	341.57
PVA_V_T4_Lime_WD_Precracked_B	1917	2080	2070	2080	370.66
PVA_V_T4_Lime_WD_Precracked_C	1682	1796	1851	1648	315.09
Average	1786	1933	1970	1885	342.44
S.D	119.69	142.23	110.82	219.04	27.80
C.O.V (%)	6.70	7.36	5.62	11.62	8.12
PVA_V_T8_Salt_WD_Precracked_A	1914	1995	1861	1594	336.73
PVA_V_T8_Salt_WD_Precracked_B	1938	2160	2090	1567	353.75
PVA_V_T8_Salt_WD_Precracked_C	2190	2310	2140	1949	382.19
Average	2014	2155	2030	1703	357.56
S.D	152.89	157.56	148.76	213.18	22.97
C.O.V (%)	7.59	7.31	7.33	12.52	6.42

Table I-7. Continued (un-cracked beam)

Specimen ID	Residual Load (lbf)				Average Residual Strength (psi)
	0.02 in	0.03 in	0.04 in	0.05 in	
PVA_V_T2_Lime_Con_Uncracked_A	1096	1212	1259	1216	224.22
PVA_V_T2_Lime_Con_Uncracked_B	1628	1739	1705	1355	300.52
PVA_V_T2_Lime_Con_Uncracked_C	1340	1423	1537	1491	273.50
Average	1355	1458	1500	1354	266.08
S.D	266.30	265.24	225.25	137.50	38.69
C.O.V (%)	19.66	18.19	15.01	10.16	14.54
PVA_V_T5_Salt_Con_Uncracked_A	1498	1694	1717	1752	300.83
PVA_V_T5_Salt_Con_Uncracked_B	1733	1906	1894	1813	335.91
PVA_V_T5_Salt_Con_Uncracked_C	1795	1977	2010	1927	348.20
Average	1675	1859	1874	1831	328.31
S.D	156.67	147.24	147.55	88.83	24.58
C.O.V (%)	9.35	7.92	7.88	4.85	7.49
PVA_V_T10_Swamp_Con_Uncracked_A	860	989	1093	1160	190.38
PVA_V_T10_Swamp_Con_Uncracked_B	828	913	989	1071	174.25
PVA_V_T10_Swamp_Con_Uncracked_C	923	997	1066	1124	193.63
Average	870.33	966.33	1049.33	1118.33	186.09
S.D	48.34	46.36	53.97	44.77	10.38
C.O.V (%)	5.55	4.80	5.14	4.00	5.58
PVA_V_T4_Lime_WD_Uncracked_A	1682	1746	1835	1761	328.50
PVA_V_T4_Lime_WD_Uncracked_B	1923	2040	2120	1994	384.35
PVA_V_T4_Lime_WD_Uncracked_C	1437	1518	1598	1567	289.06
Average	1681	1768	1851	1774	333.97
S.D	243.00	261.69	261.37	213.80	47.88
C.O.V (%)	14.46	14.80	14.12	12.05	14.34
PVA_V_T8_Salt_WD_Uncracked_A	1663	1781	1835	1746	323.63
PVA_V_T8_Salt_WD_Uncracked_B	1775	1958	2120	2140	363.71
PVA_V_T8_Salt_WD_Uncracked_C	1531	1618	1722	1585	298.14
Average	1656	1786	1892	1824	328.49
S.D	122.14	170.05	205.10	285.54	33.06
C.O.V (%)	7.37	9.52	10.84	15.66	10.06

Table I-8. Summary of the values of residual load and average residual strength obtained for steel fiber mixture for Class V concrete (pre-cracked beam)

Specimen ID	Residual Load (lbf)				Average Residual Strength (psi)
	0.02 in	0.03 in	0.04 in	0.05 in	
ST_V_T2_Lime_Con_Precracked_A	5660	5270	5010	4700	925.39
ST_V_T2_Lime_Con_Precracked_B	4740	4530	4290	4160	786.57
ST_V_T2_Lime_Con_Precracked_C	5300	4790	4400	4120	828.12
Average	5233	4863	4567	4327	846.69
S.D	463.61	375.41	387.86	323.93	71.25
C.O.V (%)	8.86	7.72	8.49	7.49	8.42
ST_V_T5_Salt_Con_Precracked_A	4730	4530	4120	3810	766.80
ST_V_T5_Salt_Con_Precracked_B	5220	4720	4380	4150	821.89
ST_V_T5_Salt_Con_Precracked_C	4960	4630	4130	3850	766.66
Average	4970	4627	4210	3937	785.12
S.D	245.15	95.04	147.31	185.83	31.84
C.O.V (%)	4.93	2.05	3.50	4.72	4.06
ST_V_T10_Swamp_Con_Precracked_A	2050	2050	2020	1961	376.92
ST_V_T10_Swamp_Con_Precracked_B	2450	2360	2250	2060	414.00
ST_V_T10_Swamp_Con_Precracked_C	1948	1866	1783	1662	331.90
Average	2149	2092	2018	1894	374.28
S.D	265.33	249.66	233.51	207.21	41.12
C.O.V (%)	12.34	11.93	11.57	10.94	10.99
ST_V_T4_Lime_WD_Precracked_A	4530	3970	3470	2960	692.91
ST_V_T4_Lime_WD_Precracked_B	4380	3470	3040	2590	613.30
ST_V_T4_Lime_WD_Precracked_C	4670	3900	3490	2980	689.39
Average	4527	3780	3333	2843	665.20
S.D	145.03	270.74	254.23	219.62	44.98
C.O.V (%)	3.20	7.16	7.63	7.72	6.76
ST_V_T8_Salt_WD_Precracked_A	4130	3850	3350	3130	641.94
ST_V_T8_Salt_WD_Precracked_B	4380	3720	3120	2830	636.09
ST_V_T8_Salt_WD_Precracked_C	4310	3470	3190	2850	628.77
Average	4273	3680	3220	2937	635.60
S.D	128.97	193.13	117.90	167.73	6.60
C.O.V (%)	3.02	5.25	3.66	5.71	1.04

Table I-8. Continued (un-cracked beam)

Specimen ID	Residual Load (lbf)				Average Residual Strength (psi)
	0.02 in	0.03 in	0.04 in	0.05 in	
ST_V_T2_Lime_Con_Uncracked_A	5050	4970	4770	4570	894.09
ST_V_T2_Lime_Con_Uncracked_B	5570	5180	4430	4130	891.86
ST_V_T2_Lime_Con_Uncracked_C	4010	3820	3720	3580	695.26
Average	4877	4657	4307	4093	827.07
S.D	794.31	732.14	535.75	496.02	114.16
C.O.V (%)	16.29	15.72	12.44	12.12	13.80
ST_V_T5_Salt_Con_Uncracked_A	4940	4780	4610	4360	839.90
ST_V_T5_Salt_Con_Uncracked_B	5450	5050	4450	4010	852.13
ST_V_T5_Salt_Con_Uncracked_C	4320	4080	3860	3640	725.19
Average	4903	4637	4307	4003	805.74
S.D	565.89	500.63	395.01	360.05	70.03
C.O.V (%)	11.54	10.80	9.17	8.99	8.69
ST_V_T10_Swamp_Con_Uncracked_A	3140	3130	3090	3050	556.35
ST_V_T10_Swamp_Con_Uncracked_B	3100	3080	3010	2950	540.20
ST_V_T10_Swamp_Con_Uncracked_C	3260	3280	3230	3080	586.08
Average	3167	3163	3110	3027	560.88
S.D	83.27	104.08	111.36	68.07	23.27
C.O.V (%)	2.63	3.29	3.58	2.25	4.15
ST_V_T4_Lime_WD_Uncracked_A	5210	4110	3380	2680	719.16
ST_V_T4_Lime_WD_Uncracked_B	4660	3930	3070	2760	651.22
ST_V_T4_Lime_WD_Uncracked_C	5170	3950	3100	2480	672.14
Average	5013	3997	3183	2640	680.84
S.D	306.65	98.66	170.98	144.22	34.80
C.O.V (%)	6.12	2.47	5.37	5.46	5.11
ST_V_T8_Salt_WD_Uncracked_A	5000	3230	2210	1672	552.42
ST_V_T8_Salt_WD_Uncracked_B	4920	3720	2620	1134	561.10
ST_V_T8_Salt_WD_Uncracked_C	4600	3820	3110	2630	650.74
Average	4840	3590	2647	1812	588.09
S.D	211.66	315.75	450.59	757.76	54.43
C.O.V (%)	4.37	8.80	17.02	41.82	9.26

Table I-9. Summary of the values of performance of FRC obtained for polypropylene fiber mixture for Class II concrete (un-cracked beam)

Specimen ID	Experimental Test Parameter Calculations for ASTM C 1609-06										
	P <sub>1</sub> (lbf)	P <sub>p</sub> (lbf)	f <sub>1</sub> (psi)	f <sub>p</sub> (psi)	δ <sub>1</sub> (in)	δ <sub>p</sub> (in)	P <sub>4,0.02</sub> (lbf)	f <sub>4,0.02</sub> (psi)	P <sub>4,0.08</sub> (lbf)	F <sub>4,0.08</sub> (psi)	T <sub>4,0.08</sub> (in-lbf)
PP_II_T1_Lime_Con_Uncracked_A	5260	5260	972	972	2.29E-03	2.29E-03	1953	361	2050	379	190
PP_II_T1_Lime_Con_Uncracked_B	5100	5100	947	947	2.26E-03	2.26E-03	2440	453	2480	460	221
PP_II_T1_Lime_Con_Uncracked_C	5190	5190	968	968	2.13E-03	2.13E-03	1683	314	1825	341	173
Average	5183	5183	962	962	2.23E-03	2.23E-03	2025	376	2118	393	195
S.D	80.21	80.21	13.43	13.43	8.79E-05	8.79E-05	383.65	70.74	332.80	61.28	24.50
C.O.V (%)	1.55	1.55	1.40	1.40	3.95	3.95	18.94	18.82	15.71	15.58	12.59
PP_II_T6_Salt_Con_Uncracked_A	5110	5110	923	923	2.49E-03	2.49E-03	1378	249	1378	249	145
PP_II_T6_Salt_Con_Uncracked_B	5100	5100	915	915	2.85E-03	2.85E-03	1178	211	1317	236	141
PP_II_T6_Salt_Con_Uncracked_C	4890	4890	881	881	2.67E-03	2.67E-03	1297	234	1350	243	143
Average	5033	5033	906	906	2.67E-03	2.67E-03	1284	231	1348	243	143
S.D	124.23	124.23	22.13	22.13	1.78E-04	1.78E-04	100.06	18.97	30.53	6.40	2.09
C.O.V (%)	2.47	2.47	2.44	2.44	6.66	6.66	7.83	8.20	2.26	2.64	1.46
PP_II_T9_Swamp_Con_Uncracked_A	1771	1771	331	331	2.39E-03	2.39E-03	764	143	904	169	75
PP_II_T9_Swamp_Con_Uncracked_B	2090	2090	388	388	2.80E-03	2.80E-03	749	139	836	155	75
PP_II_T9_Swamp_Con_Uncracked_C	1937	1937	356	356	2.64E-03	2.64E-03	766	141	845	155	73
Average	1933	1933	358	358	2.61E-03	2.61E-03	760	141	862	160	74
S.D	159.54	159.54	28.82	28.82	2.07E-04	2.07E-04	9.29	1.76	36.94	7.76	1.04
C.O.V (%)	8.26	8.26	8.04	8.04	7.93	7.93	1.22	1.25	4.29	4.86	1.39

Table I-9. Continued (un-cracked beam)

Experimental Test Parameter Calculations for ASTM C 1609-06

Specimen ID	$P_1$ (lbf)	$P_p$ (lbf)	$f_1$ (psi)	$f_p$ (psi)	$\delta_1$ (in)	$\delta_p$ (in)	$P_{4,0.02}$ (lbf)	$f_{4,0.02}$ (psi)	$P_{4,0.08}$ (lbf)	$F_{4,0.08}$ (psi)	$T_{4,0.08}$ (in-lbf)
PP_II_T3_Lime_WD_Uncracked_A	5240	5240	935	935	1.99E-03	1.99E-03	1520	271	1609	287	158
PP_II_T3_Lime_WD_Uncracked_B	5220	5220	913	913	2.15E-03	2.15E-03	1130	198	1301	228	133
PP_II_T3_Lime_WD_Uncracked_C	5450	5450	956	956	2.20E-03	2.20E-03	1376	241	1464	257	148
Average	5303	5303	935	935	2.11E-03	2.11E-03	1342	237	1458	257	147
S.D	127.41	127.41	21.35	21.35	1.07E-04	1.07E-04	197.21	36.97	154.09	29.73	12.59
C.O.V (%)	2.40	2.40	2.28	2.28	5.08	5.08	14.70	15.61	10.57	11.56	8.59
PP_II_T7_Salt_WD_Uncracked_A	5070	5070	944	944	1.76E-03	1.76E-03	1799	335	1950	363	179
PP_II_T7_Salt_WD_Uncracked_B	5440	5440	1010	1010	1.88E-03	1.88E-03	1837	341	1820	338	175
PP_II_T7_Salt_WD_Uncracked_C	5060	5060	949	949	2.08E-03	2.08E-03	1821	341	2080	390	183
Average	5190	5190	967	967	1.90E-03	1.90E-03	1819	339	1950	364	179
S.D	216.56	216.56	36.86	36.86	1.59E-04	1.59E-04	19.08	3.71	130.00	26.08	4.39
C.O.V (%)	4.17	4.17	3.81	3.81	8.35	8.35	1.05	1.09	6.67	7.17	2.45

Table I-10. Summary of the values of performance of FRC obtained for polyvinyl alcohol fiber mixture for Class II concrete (un-cracked beam)

Specimen ID	Experimental Test Parameter Calculations for ASTM C 1609-06										
	P <sub>1</sub> (lbf)	P <sub>p</sub> (lbf)	f <sub>1</sub> (psi)	f <sub>p</sub> (psi)	δ <sub>1</sub> (in)	δ <sub>p</sub> (in)	P <sub>4,0.02</sub> (lbf)	f <sub>4,0.02</sub> (psi)	P <sub>4,0.08</sub> (lbf)	F <sub>4,0.08</sub> (psi)	T <sub>4,0.08</sub> (in-lbf)
PVA_II_T1_Lime_Con_Uncracked_A	5360	5360	978	978	2.46E-03	2.46E-03	2100	383	1370	250	193
PVA_II_T1_Lime_Con_Uncracked_B	4850	4850	872	872	2.15E-03	2.15E-03	2150	387	1356	244	186
PVA_II_T1_Lime_Con_Uncracked_C	4870	4870	895	895	1.99E-03	1.99E-03	2130	391	1562	287	196
Average	5027	5027	915	915	2.20E-03	2.20E-03	2127	387	1429	260	192
S.D	288.85	288.85	55.79	55.79	2.38E-04	2.38E-04	25.17	4.17	115.11	23.41	5.32
C.O.V (%)	5.75	5.75	6.10	6.10	10.83	10.83	1.18	1.08	8.05	8.99	2.78
PVA_II_T6_Salt_Con_Uncracked_A	5210	5210	965	965	2.87E-03	2.87E-03	2200	407	912	169	178
PVA_II_T6_Salt_Con_Uncracked_B	5160	5160	934	934	2.70E-03	2.70E-03	2410	436	1764	319	203
PVA_II_T6_Salt_Con_Uncracked_C	5570	5570	994	994	2.84E-03	2.84E-03	1836	328	1052	188	172
Average	5313	5313	964	964	2.80E-03	2.80E-03	2149	390	1243	225	184
S.D	223.68	223.68	29.75	29.75	9.18E-05	9.18E-05	290.42	56.34	456.88	82.03	16.49
C.O.V (%)	4.21	4.21	3.09	3.09	3.28	3.28	13.52	14.43	36.77	36.40	8.95
PVA_II_T9_Swamp_Con_Uncracked_A	2200	2200	394	394	3.11E-03	3.11E-03	866	155	982	176	86
PVA_II_T9_Swamp_Con_Uncracked_B	2430	2430	441	441	5.13E-03	5.13E-03	899	163	899	163	92
PVA_II_T9_Swamp_Con_Uncracked_C	2050	2050	374	374	2.86E-03	2.86E-03	879	160	1031	188	88
Average	2227	2227	403	403	3.70E-03	3.70E-03	881	159	971	176	89
S.D	191.40	191.40	34.54	34.54	1.25E-03	1.25E-03	16.62	4.22	66.73	12.45	3.06
C.O.V (%)	8.60	8.60	8.57	8.57	33.69	33.69	1.89	2.65	6.87	7.09	3.43

Table I-10. Continued (un-cracked beam)

Experimental Test Parameter Calculations for ASTM C 1609-06

Specimen ID	$P_1$ (lbf)	$P_p$ (lbf)	$f_1$ (psi)	$f_p$ (psi)	$\delta_1$ (in)	$\delta_p$ (in)	$P_{4,0.02}$ (lbf)	$f_{4,0.02}$ (psi)	$P_{4,0.08}$ (lbf)	$F_{4,0.08}$ (psi)	$T_{4,0.08}$ (in-lbf)
PVA_II_T3_Lime_WD_Uncracked_A	5200	5200	985	985	1.92E-03	1.92E-03	1516	287	1673	317	164
PVA_II_T3_Lime_WD_Uncracked_B	5890	5890	1075	1075	1.90E-03	1.90E-03	1743	318	1559	284	184
PVA_II_T3_Lime_WD_Uncracked_C	5980	5980	1091	1091	1.95E-03	1.95E-03	1997	367	1515	276	197
Average	5690	5690	1050	1050	1.92E-03	1.92E-03	1752	324	1582	293	181
S.D	426.73	426.73	57.16	57.16	2.20E-05	2.05E-05	240.63	40.31	81.54	21.42	16.59
C.O.V (%)	7.50	7.50	5.44	5.44	1.14	1.07	13.73	12.44	5.15	7.32	9.14
PVA_II_T7_Salt_WD_Uncracked_A	6130	6130	1105	1105	1.98E-03	1.98E-03	1844	332	1090	196	177
PVA_II_T7_Salt_WD_Uncracked_B	6100	6100	1113	1113	2.05E-03	2.05E-03	1635	298	868	158	164
PVA_II_T7_Salt_WD_Uncracked_C	6040	6040	1097	1097	2.09E-03	2.09E-03	1956	355	1653	300	201
Average	6090	6090	1105	1105	2.04E-03	2.04E-03	1812	329	1204	218	181
S.D	45.83	45.83	8.18	8.18	5.94E-05	5.94E-05	162.92	28.59	404.66	73.35	18.56
C.O.V (%)	0.75	0.75	0.74	0.74	2.91	2.91	8.99	8.70	33.62	33.60	10.27

Table I-11. Summary of the values of performance of FRC obtained for steel fiber mixture for Class II concrete (un-cracked beam)

Specimen ID	Experimental Test Parameter Calculations for ASTM C 1609-06										
	P <sub>1</sub> (lbf)	P <sub>p</sub> (lbf)	f <sub>1</sub> (psi)	f <sub>p</sub> (psi)	δ <sub>1</sub> (in)	δ <sub>p</sub> (in)	P <sub>4,0.02</sub> (lbf)	f <sub>4,0.02</sub> (psi)	P <sub>4,0.08</sub> (lbf)	F <sub>4,0.08</sub> (psi)	T <sub>4,0.08</sub> (in-lbf)
ST_II_T1_Lime_Con_Uncracked_A	6490	6740	1187	1233	2.80E-03	1.08E-02	6330	1158	3980	728	426
ST_II_T1_Lime_Con_Uncracked_B	5600	5870	1024	1074	2.44E-03	7.46E-03	5220	955	3070	562	347
ST_II_T1_Lime_Con_Uncracked_C	5790	5790	1064	1064	2.34E-03	-	4860	893	2600	478	317
Average	5960	-	1092	1124	2.52E-03	-	5470	1002	3217	589	363
S.D	468.72	-	84.80	94.64	2.45E-04	-	766.22	138.35	701.59	127.26	56.46
C.O.V (%)	7.86	-	7.77	8.42	9.70	-	14.01	13.81	21.81	21.60	15.54
ST_II_T6_Salt_Con_Uncracked_A	5730	5730	1030	1030	2.80E-03	2.80E-03	3790	681	2480	446	263
ST_II_T6_Salt_Con_Uncracked_B	6070	6070	1099	1099	2.96E-03	2.96E-03	4530	820	2330	422	295
ST_II_T6_Salt_Con_Uncracked_C	5910	5910	1052	1052	2.97E-03	2.97E-03	3890	693	2070	375	263
Average	5903	5903	1061	1061	2.91E-03	2.91E-03	4070	731	2293	414	274
S.D	170.10	170.10	35.26	35.26	9.25E-05	9.25E-05	401.50	77.20	207.44	36.13	18.28
C.O.V (%)	2.88	2.88	3.32	3.32	3.18	3.18	9.86	10.55	9.05	8.72	6.68
ST_II_T9_Swamp_Con_Uncracked_A	2710	2710	501	501	3.77E-03	3.77E-03	2720	502	2289	423	181
ST_II_T9_Swamp_Con_Uncracked_B	2690	2690	487	487	3.31E-03	3.31E-03	2350	426	1797	325	174
ST_II_T9_Swamp_Con_Uncracked_C	2390	2390	443	443	3.64E-03	3.64E-03	2240	415	2050	380	172
Average	2597	2597	477	477	3.57E-03	3.57E-03	2437	448	2045	376	175
S.D	179.26	179.26	30.35	30.35	2.37E-04	2.37E-04	251.46	47.80	246.03	48.81	4.70
C.O.V (%)	6.90	6.90	6.37	6.37	6.64	6.64	10.32	10.68	12.03	12.98	2.68

Table I-11. Continued (un-cracked beam)

Experimental Test Parameter Calculations for ASTM C 1609-06

Specimen ID	$P_1$ (lbf)	$P_P$ (lbf)	$f_1$ (psi)	$f_P$ (psi)	$\delta_1$ (in)	$\delta_P$ (in)	$P_{4,0.02}$ (lbf)	$f_{4,0.02}$ (psi)	$P_{4,0.08}$ (lbf)	$F_{4,0.08}$ (psi)	$T_{4,0.08}$ (in-lbf)
ST_II_T3_Lime_WD_Uncracked_A	6450	6451	1177	1177	2.16E-03	2.16E-03	4100	748	1816	331	255
ST_II_T3_Lime_WD_Uncracked_B	6020	6020	1088	1088	2.18E-03	2.18E-03	4520	817	2190	396	282
ST_II_T3_Lime_WD_Uncracked_C	5890	5890	1064	1064	2.36E-03	2.36E-03	4670	854	1975	357	285
Average	6120	6120	1109	1110	2.23E-03	2.23E-03	4430	806	1994	361	274
S.D	293.09	293.65	59.53	59.63	1.07E-04	1.07E-04	295.47	53.88	187.70	32.37	16.47
C.O.V (%)	4.79	4.80	5.37	5.37	4.81	4.81	6.67	6.68	9.41	8.96	6.02
ST_II_T7_Salt_WD_Uncracked_A	6750	6750	1238	1238	2.28E-03	2.28E-03	4410	809	1599	293	251
ST_II_T7_Salt_WD_Uncracked_B	6750	6750	1244	1244	2.37E-03	2.37E-03	5210	960	2600	479	327
ST_II_T7_Salt_WD_Uncracked_C	6760	6760	1221	1221	2.21E-03	2.21E-03	4660	842	2640	477	317
Average	6753	6753	1234	1234	2.28E-03	2.28E-03	4760	870	2280	416	298
S.D	5.77	5.77	11.69	11.69	8.02E-05	8.02E-05	409.27	79.60	589.81	106.71	41.61
C.O.V (%)	0.09	0.09	0.95	0.95	3.52	3.52	8.60	9.15	25.87	25.63	13.94

Table I-12. Summary of the values of performance of FRC obtained for polypropylene fiber mixture for Class V concrete (un-cracked beam)

Specimen ID	Experimental Test Parameter Calculations for ASTM C 1609-06										
	P <sub>1</sub> (lbf)	P <sub>p</sub> (lbf)	f <sub>1</sub> (psi)	f <sub>p</sub> (psi)	δ <sub>1</sub> (in)	δ <sub>p</sub> (in)	P <sub>4,0.02</sub> (lbf)	f <sub>4,0.02</sub> (psi)	P <sub>4,0.08</sub> (lbf)	F <sub>4,0.08</sub> (psi)	T <sub>4,0.08</sub> (in-lbf)
PP_V_T2_Lime_Con_Uncracked_A	5840	5840	1065	1065	2.07E-03	2.07E-03	1675	306	1694	309	182
PP_V_T2_Lime_Con_Uncracked_B	5950	5950	1083	1083	1.99E-03	1.99E-03	1559	284	1635	298	175
PP_V_T2_Lime_Con_Uncracked_C	6020	6020	1090	1090	2.03E-03	2.03E-03	1735	314	1688	306	175
Average	5937	5937	1079	1079	2.03E-03	2.03E-03	1656	301	1672	304	177
S.D	90.74	90.74	12.69	12.69	3.98E-05	3.98E-05	89.47	15.71	32.47	5.91	3.82
C.O.V (%)	1.53	1.53	1.18	1.18	1.96	1.96	5.40	5.22	1.94	1.94	2.15
PP_V_T5_Salt_Con_Uncracked_A	7210	7210	1277	1277	2.84E-03	2.84E-03	1691	300	1852	328	202
PP_V_T5_Salt_Con_Uncracked_B	7300	7300	1303	1303	2.81E-03	2.81E-03	-	-	1853	331	223
PP_V_T5_Salt_Con_Uncracked_C	7150	7150	1251	1251	2.81E-03	2.81E-03	-	-	1413	247	204
Average	7220	7220	1277	1277	2.82E-03	2.82E-03	1691	300	1706	302	210
S.D	75.50	75.50	25.65	25.65	1.61E-05	1.61E-05	-	-	253.75	47.40	11.28
C.O.V (%)	1.05	1.05	2.01	2.01	0.57	0.57	-	-	14.87	15.69	5.38
PP_V_T10_Swamp_Con_Uncracked_A	2890	2890	538	538	2.97E-03	2.97E-03	885	165	1155	215	95
PP_V_T10_Swamp_Con_Uncracked_B	2860	2860	507	507	2.60E-03	2.30E-03	783	139	1012	179	93
PP_V_T10_Swamp_Con_Uncracked_C	2380	2380	440	440	2.79E-03	2.79E-03	951	176	1166	215	94
Average	2710	2710	495	495	2.79E-03	2.69E-03	873	160	1111	203	94
S.D	286.18	286.18	50.21	50.21	1.85E-04	3.47E-04	84.64	18.99	85.91	20.74	0.88
C.O.V (%)	10.56	10.56	10.15	10.15	6.64	12.91	9.70	11.89	7.73	10.21	0.94

Table I-12. Continued (un-cracked beam)

Experimental Test Parameter Calculations for ASTM C 1609-06

Specimen ID	P <sub>1</sub> (lbf)	P <sub>P</sub> (lbf)	f <sub>1</sub> (psi)	f <sub>P</sub> (psi)	δ <sub>1</sub> (in)	δ <sub>P</sub> (in)	P <sub>4,0.02</sub> (lbf)	f <sub>4,0.02</sub> (psi)	P <sub>4,0.08</sub> (lbf)	F <sub>4,0.08</sub> (psi)	T <sub>4,0.08</sub> (in-lbf)
PP_V_T4_Lime_WD_Uncracked_A	6450	6450	1222	1222	2.18E-03	2.18E-03	-	-	1776	336	198
PP_V_T4_Lime_WD_Uncracked_B	6290	6290	1177	1177	2.10E-03	2.10E-03	2090	391	2200	412	216
PP_V_T4_Lime_WD_Uncracked_C	6190	6190	1170	1170	2.09E-03	2.09E-03	2150	406	2320	438	217
Average	6310	6310	1189	1189	2.12E-03	2.12E-03	2120	399	2099	395	210
S.D	131.15	131.15	28.36	28.36	5.22E-05	5.22E-05	42.43	10.79	285.81	52.83	10.25
C.O.V (%)	2.08	2.08	2.38	2.38	2.46	2.46	2.00	2.71	13.62	13.36	4.87
PP_V_T8_Salt_WD_Uncracked_A	6880	6880	1216	1216	2.02E-03	2.02E-03	-	-	1597	282	196
PP_V_T8_Salt_WD_Uncracked_B	7370	7370	1302	1302	2.21E-03	2.21E-03	-	-	1494	264	192
PP_V_T8_Salt_WD_Uncracked_C	6830	6830	1222	1222	2.06E-03	2.06E-03	-	-	2080	372	222
Average	7027	7027	1247	1247	2.10E-03	2.10E-03	-	-	1724	306	203
S.D	298.38	298.38	48.21	48.21	1.00E-04	1.00E-04	-	-	312.86	57.90	16.56
C.O.V (%)	4.25	4.25	3.87	3.87	4.78	4.78	-	-	18.15	18.91	8.15

Table I-13. Summary of the values of performance of FRC obtained for polyvinyl alcohol fiber mixture for Class V concrete (uncracked beam)

Specimen ID	Experimental Test Parameter Calculations for ASTM C 1609-06										
	P <sub>1</sub> (lbf)	P <sub>p</sub> (lbf)	f <sub>1</sub> (psi)	f <sub>p</sub> (psi)	δ <sub>1</sub> (in)	δ <sub>p</sub> (in)	P <sub>4,0.02</sub> (lbf)	f <sub>4,0.02</sub> (psi)	P <sub>4,0.08</sub> (lbf)	F <sub>4,0.08</sub> (psi)	T <sub>4,0.08</sub> (in-lbf)
PVA_V_T2_Lime_Con_Uncracked_A	5610	5610	979	979	1.93E-03	1.93E-03	1199	209	977	171	151
PVA_V_T2_Lime_Con_Uncracked_B	5620	5620	971	971	1.86E-03	1.86E-03	1255	217	1028	178	150
PVA_V_T2_Lime_Con_Uncracked_C	5660	5660	978	978	2.18E-03	2.18E-03	1234	213	833	144	149
Average	5630	5630	976	976	1.99E-03	1.99E-03	1229	213	946	164	150
S.D	26.46	26.46	4.26	4.26	1.68E-04	1.68E-04	28.29	3.83	101.13	17.76	1.24
C.O.V (%)	0.47	0.47	0.44	0.44	8.46	8.46	2.30	1.80	10.69	10.82	0.82
PVA_V_T5_Salt_Con_Uncracked_A	7190	7190	1268	1268	2.82E-03	2.82E-03	1761	310	1283	226	214
PVA_V_T5_Salt_Con_Uncracked_B	7310	7310	1289	1289	2.65E-03	2.65E-03	1730	305	1323	233	207
PVA_V_T5_Salt_Con_Uncracked_C	7230	7230	1259	1259	2.68E-03	2.68E-03	1889	329	1370	239	212
Average	7243	7243	1272	1272	2.71E-03	2.71E-03	1793	315	1325	233	211
S.D	61.10	61.10	15.24	15.24	8.89E-05	8.89E-05	84.29	12.56	43.55	6.21	3.54
C.O.V (%)	0.84	0.84	1.20	1.20	3.28	3.28	4.70	3.99	3.29	2.67	1.68
PVA_V_T10_Swamp_Con_Uncracked_A	2450	2450	447	447	3.22E-03	3.22E-03	1054	192	1220	223	109
PVA_V_T10_Swamp_Con_Uncracked_B	2640	1640	480	298	2.74E-03	2.74E-03	1195	217	1336	243	119
PVA_V_T10_Swamp_Con_Uncracked_C	2450	2450	444	444	2.34E-03	2.34E-03	1031	185	1033	187	104
Average	2513	2180	457	396	2.77E-03	2.77E-03	1093	198	1196	218	111
S.D	109.70	467.65	20.36	84.80	4.41E-04	4.41E-04	88.79	17.10	152.88	28.37	7.48
C.O.V (%)	4.36	21.45	4.45	21.39	15.94	15.94	8.12	8.62	12.78	13.04	6.74

Table I-13. Continued (un-cracked beam)

Experimental Test Parameter Calculations for ASTM C 1609-06

Specimen ID	P <sub>1</sub> (lbf)	P <sub>p</sub> (lbf)	f <sub>1</sub> (psi)	f <sub>p</sub> (psi)	δ <sub>1</sub> (in)	δ <sub>p</sub> (in)	P <sub>4,0.02</sub> (lbf)	f <sub>4,0.02</sub> (psi)	P <sub>4,0.08</sub> (lbf)	F <sub>4,0.08</sub> (psi)	T <sub>4,0.08</sub> (in-lbf)
PVA_V_T4_Lime_WD_Uncracked_A	6690	6690	1233	1233	2.06E-03	2.06E-03	3400	627	1368	252	204
PVA_V_T4_Lime_WD_Uncracked_B	6690	6690	1221	1221	2.04E-03	2.40E-03	1552	283	1080	197	183
PVA_V_T4_Lime_WD_Uncracked_C	7190	7190	1302	1302	2.12E-03	2.12E-03	1568	282	1171	212	191
Average	6857	6857	1252	1252	2.07E-03	2.19E-03	2173	397	1206	220	193
S.D	288.68	288.68	44.05	44.05	3.86E-05	1.86E-04	1062.35	198.60	147.22	28.45	10.69
C.O.V (%)	4.21	4.21	3.52	3.52	1.86	8.49	48.88	50.00	12.20	12.91	5.55
PVA_V_T8_Salt_WD_Uncracked_A	7770	7770	1383	1383	2.33E-03	2.33E-03	-	-	1340	239	217
PVA_V_T8_Salt_WD_Uncracked_B	6960	6960	1279	1279	2.19E-03	2.19E-03	-	-	1519	279	196
PVA_V_T8_Salt_WD_Uncracked_C	7890	7890	1418	1418	2.45E-03	2.45E-03	2260	406	1875	337	251
Average	7540	7540	1360	1360	2.32E-03	2.32E-03	2260	406	1578	285	221
S.D	505.87	505.87	72.29	72.29	1.30E-04	1.30E-04	-	-	272.34	49.51	27.90
C.O.V (%)	6.71	6.71	5.31	5.31	5.60	5.60	-	-	17.26	17.38	12.61

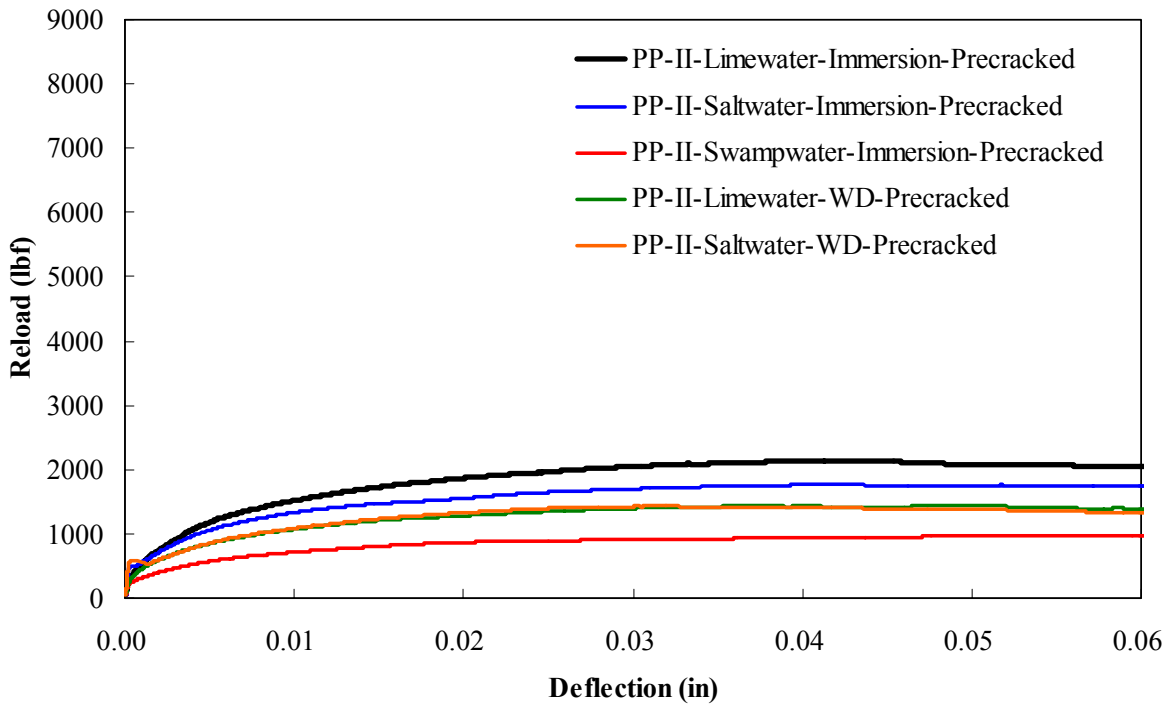
Table I-14. Summary of the values of performance of FRC obtained for steel fiber mixture for Class V concrete (un-cracked beam)

Specimen ID	Experimental Test Parameter Calculations for ASTM C 1609-06										
	P <sub>1</sub> (lbf)	P <sub>p</sub> (lbf)	f <sub>1</sub> (psi)	f <sub>p</sub> (psi)	δ <sub>1</sub> (in)	δ <sub>p</sub> (in)	P <sub>4,0.02</sub> (lbf)	f <sub>4,0.02</sub> (psi)	P <sub>4,0.08</sub> (lbf)	F <sub>4,0.08</sub> (psi)	T <sub>4,0.08</sub> (in-lbf)
ST_V_T2_Lime_Con_Uncracked_A	6320	6410	1114	1130	2.30E-03	1.08E-02	5730	1010	3900	687	402
ST_V_T2_Lime_Con_Uncracked_B	6690	6690	1145	1145	2.40E-03	2.40E-03	5880	1007	4440	760	427
ST_V_T2_Lime_Con_Uncracked_C	6340	6340	1148	1148	2.09E-03	2.09E-03	5020	927	3290	596	345
Average	6450	-	1136	1141	2.26E-03	-	5543	981	3877	681	392
S.D	208.09	-	18.96	9.86	1.60E-04	-	459.38	46.69	575.35	82.26	41.84
C.O.V (%)	3.23	-	1.67	0.86	7.10	-	8.29	4.76	14.84	12.08	10.69
ST_V_T5_Salt_Con_Uncracked_A	7260	7260	1289	1042	2.90E-03	2.90E-03	5470	971	3490	620	374
ST_V_T5_Salt_Con_Uncracked_B	7680	7680	1370	1126	2.88E-03	2.88E-03	6050	1079	3600	642	403
ST_V_T5_Salt_Con_Uncracked_C	7250	7250	1297	1023	3.00E-03	3.00E-03	5270	943	3700	662	377
Average	7397	7397	1319	1064	2.93E-03	2.93E-03	5597	998	3597	641	385
S.D	245.42	245.42	44.85	54.64	6.43E-05	6.43E-05	405.13	72.18	105.04	21.10	16.28
C.O.V (%)	3.32	3.32	3.40	5.14	2.20	2.20	7.24	7.23	2.92	3.29	4.23
ST_V_T10_Swamp_Con_Uncracked_A	2920	2920	550	499	2.61E-03	2.61E-03	2310	435	2310	435	199
ST_V_T10_Swamp_Con_Uncracked_B	3410	3410	619	481	3.20E-03	3.20E-03	2640	479	2220	403	197
ST_V_T10_Swamp_Con_Uncracked_C	3200	3200	597	565	2.94E-03	2.94E-03	3020	563	2480	463	219
Average	3177	3177	589	515	2.91E-03	2.91E-03	2657	493	2337	434	205
S.D	245.83	245.83	35.13	44.30	2.96E-04	2.96E-04	355.29	65.11	132.04	29.87	12.10
C.O.V (%)	7.74	7.74	5.97	8.60	10.16	10.16	13.37	13.22	5.65	6.89	5.89

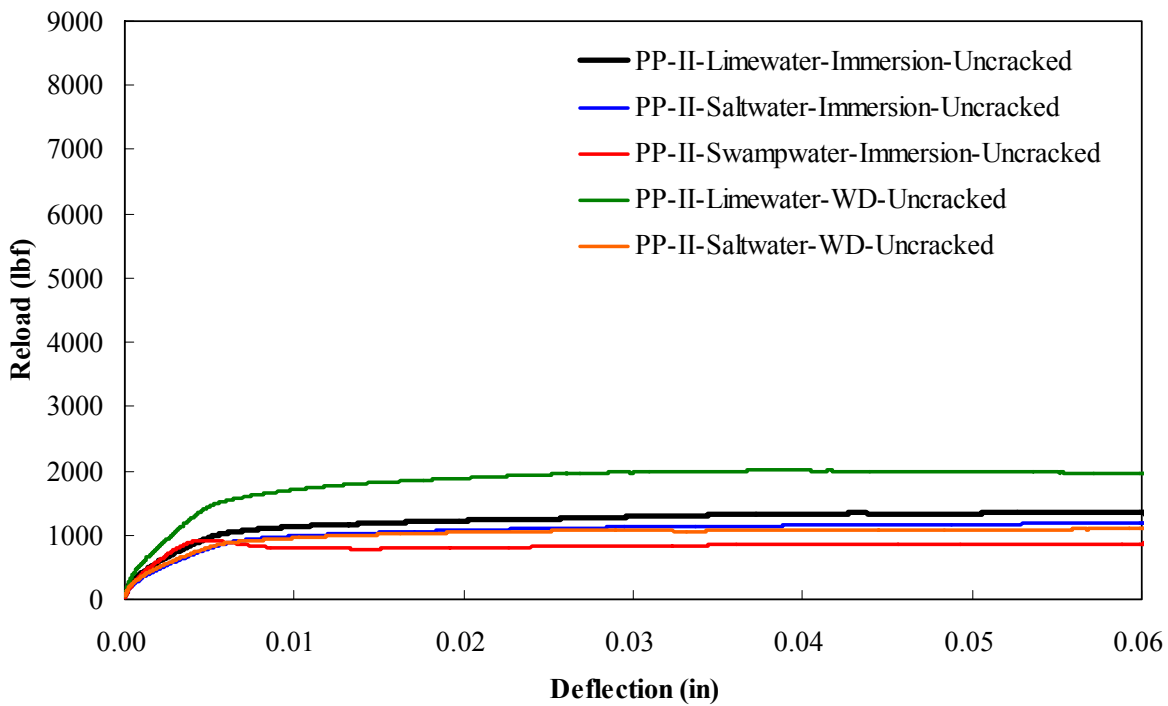
Table I-14. Continued (un-cracked beam)

Experimental Test Parameter Calculations for ASTM C 1609-06

Specimen ID	P <sub>1</sub> (lbf)	P <sub>p</sub> (lbf)	f <sub>1</sub> (psi)	f <sub>p</sub> (psi)	δ <sub>1</sub> (in)	δ <sub>p</sub> (in)	P <sub>4,0.02</sub> (lbf)	f <sub>4,0.02</sub> (psi)	P <sub>4,0.08</sub> (lbf)	F <sub>4,0.08</sub> (psi)	T <sub>4,0.08</sub> (in-lbf)
ST_V_T4_Lime_WD_Uncracked_A	6970	6970	1268	1196	2.05E-03	2.05E-03	4630	843	1516	276	265
ST_V_T4_Lime_WD_Uncracked_B	6830	6830	1237	1237	2.01E-03	2.01E-03	3630	657	1310	237	215
ST_V_T4_Lime_WD_Uncracked_C	6770	6770	1229	1187	2.21E-03	2.21E-03	4980	904	1281	233	263
Average	6857	6857	1245	1207	2.09E-03	2.09E-03	4413	801	1369	249	248
S.D	102.63	102.63	20.88	26.56	1.03E-04	1.03E-04	700.59	128.41	128.13	23.79	28.06
C.O.V (%)	1.50	1.50	1.68	2.20	4.92	4.92	15.87	16.02	9.36	9.57	11.32
ST_V_T8_Salt_WD_Uncracked_A	7470	7570	1307	1325	2.29E-03	1.10E-02	7360	1288	2870	502	403
ST_V_T8_Salt_WD_Uncracked_B	7570	8250	1341	1461	2.23E-03	9.15E-03	7660	1357	2850	505	426
ST_V_T8_Salt_WD_Uncracked_C	6860	7240	1274	1344	2.03E-03	1.04E-02	6720	1173	3390	629	430
Average	7300	7687	1307	1377	2.18E-03	1.02E-02	7247	1272	3037	545	419
S.D	384.32	515.01	33.64	73.93	1.37E-04	9.64E-04	480.14	92.87	306.16	72.67	14.75
C.O.V (%)	5.26	6.70	2.57	5.37	6.26	9.45	6.63	7.30	10.08	13.32	3.52

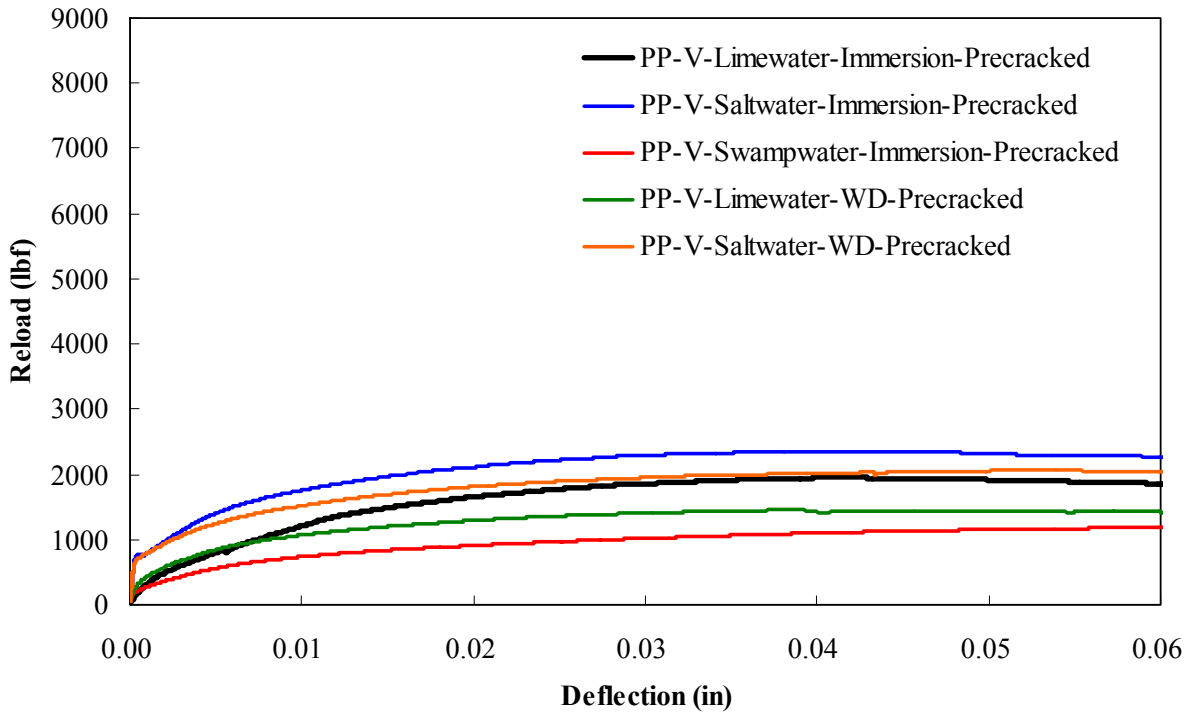


A

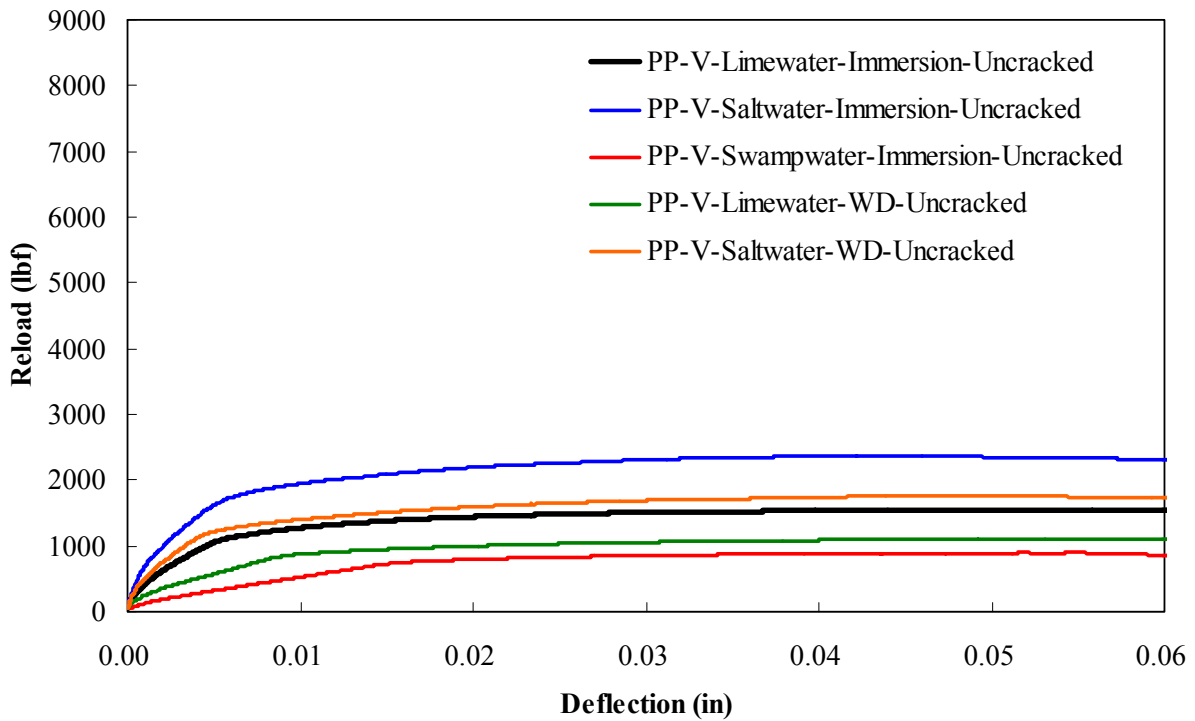


B

Figure I-1. Residual load vs. deflection curve for PP fiber mix for Class II concrete. A) Pre-cracked beams. B) Un-cracked beams.

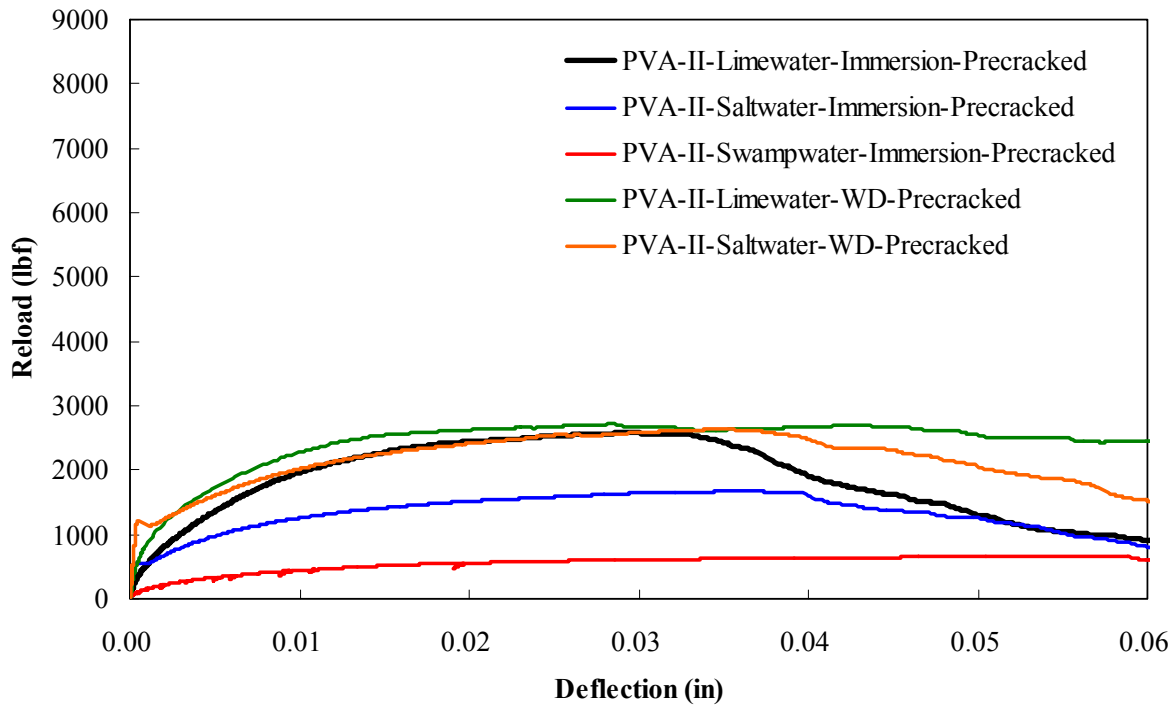


A

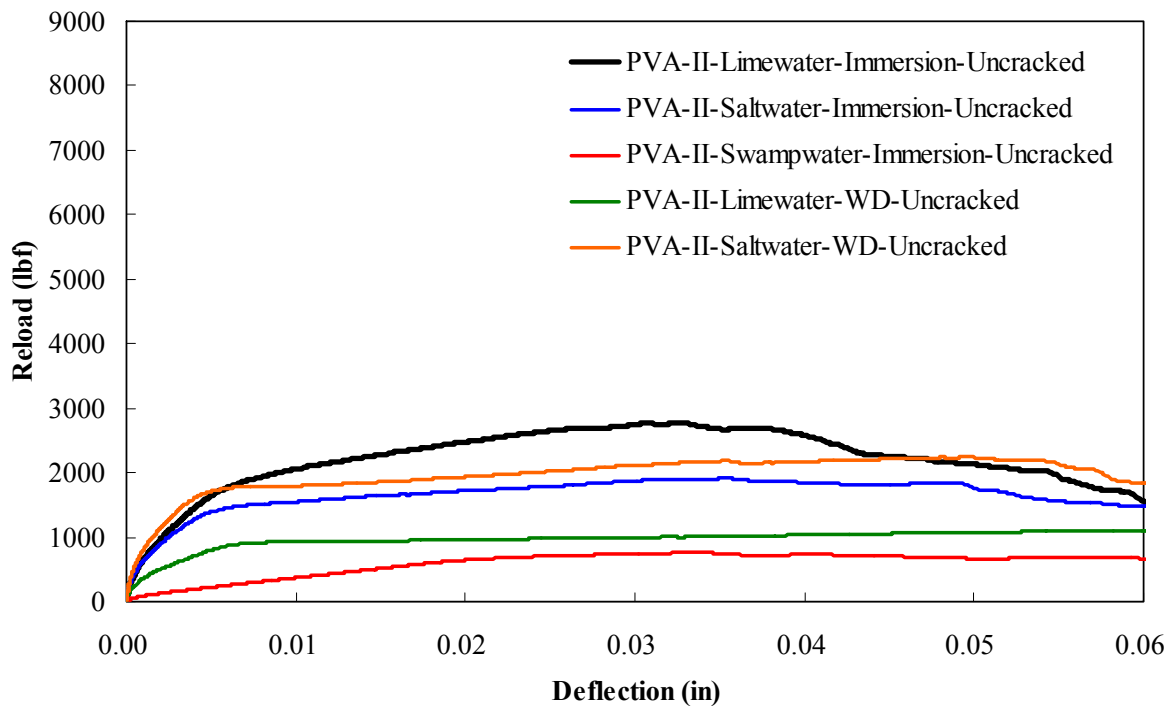


B

Figure I-2. Residual load vs. deflection curve for PP fiber mix for Class V concrete. A) Pre-cracked beams. B) Un-cracked beams.

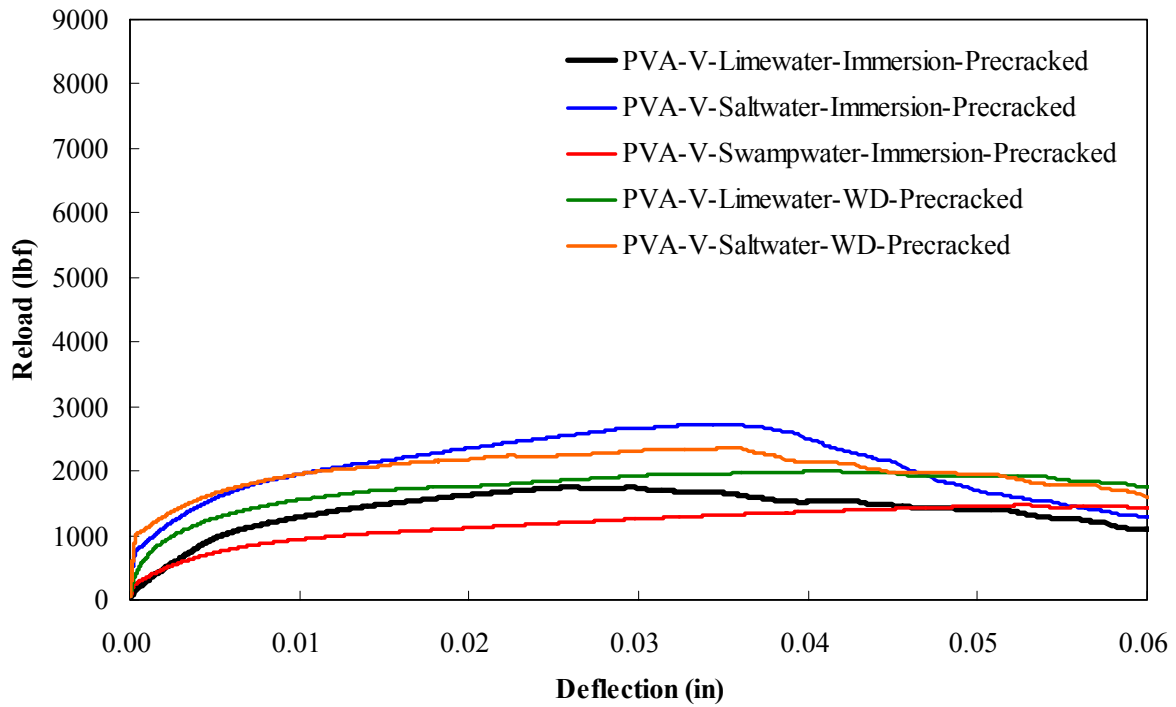


A

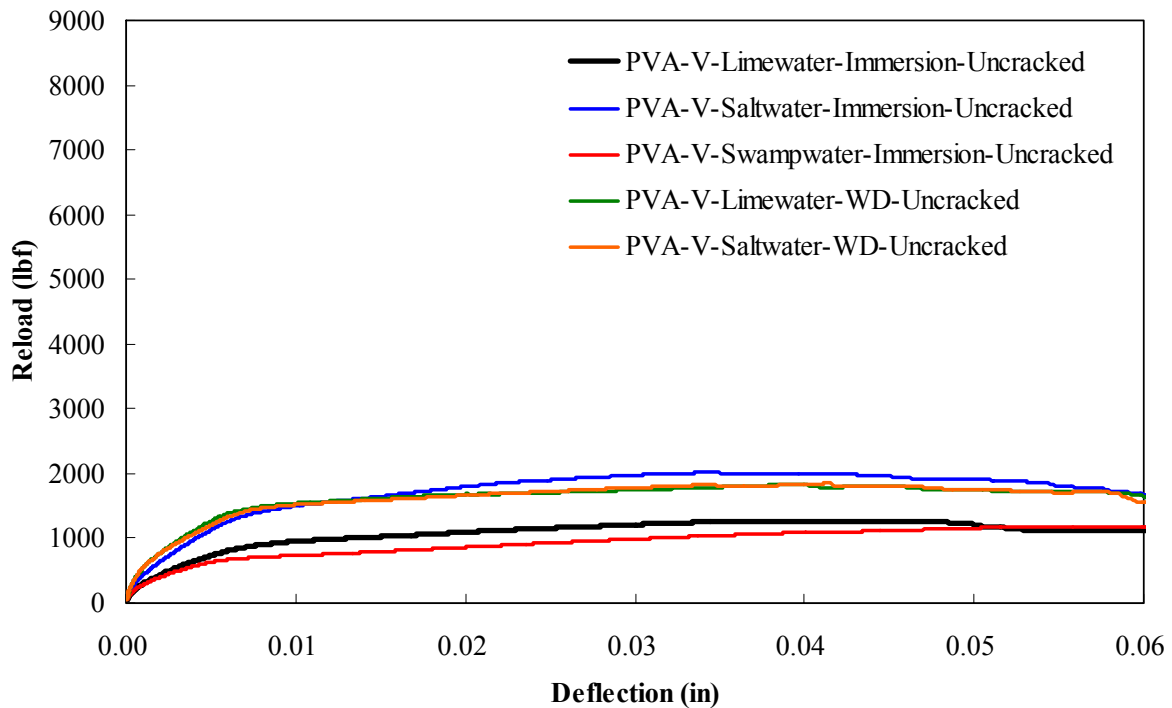


B

Figure I-3. Residual load vs. deflection curve for PVA fiber mix for Class II concrete. A) Pre-cracked beams. B) Un-cracked beams.

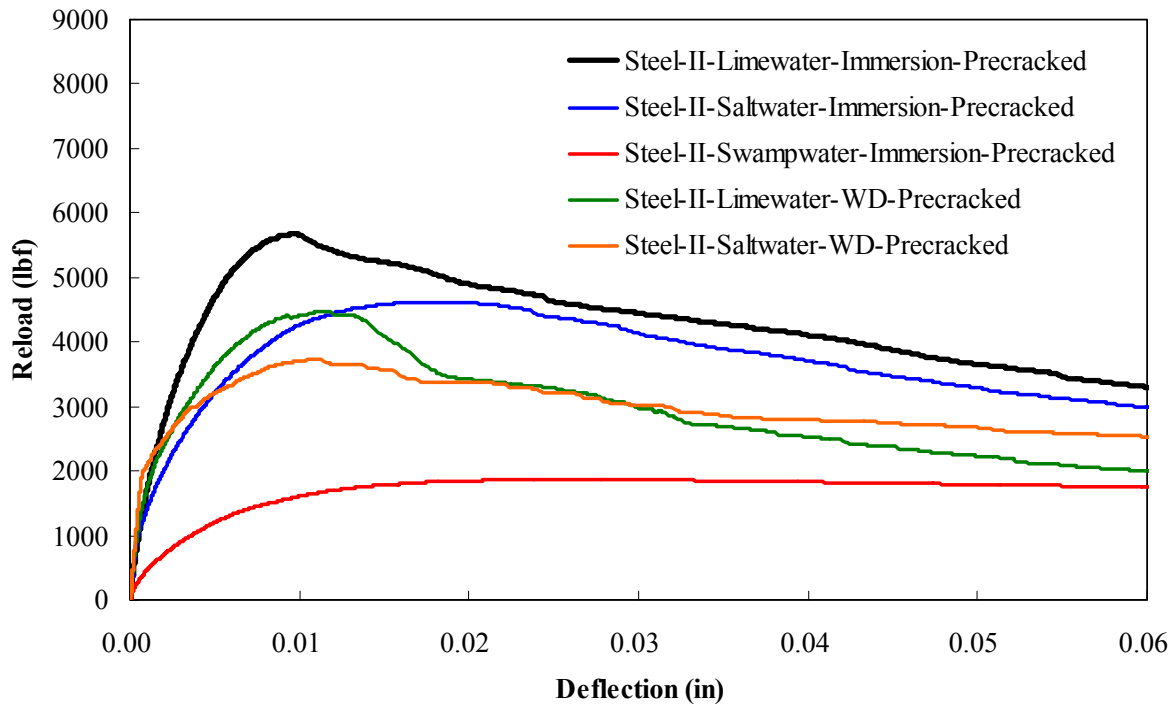


A

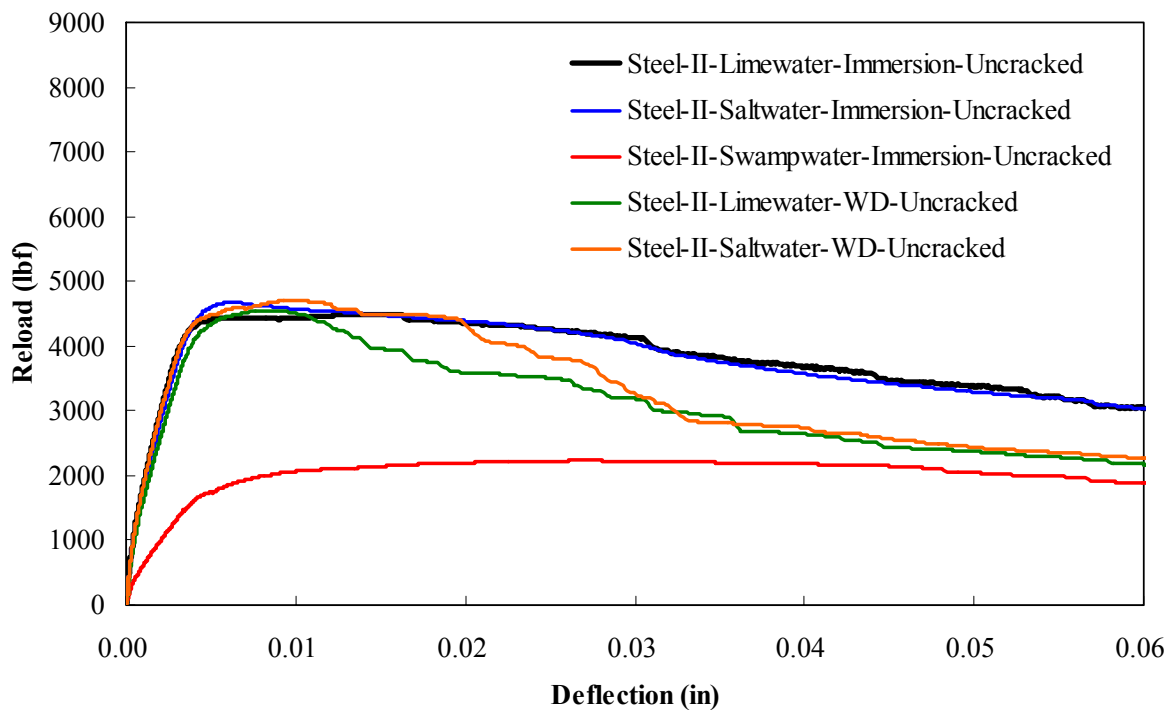


B

Figure I-4. Residual load vs. deflection curve for PVA fiber mix for Class V concrete. A) Pre-cracked beams. B) Un-cracked beams.

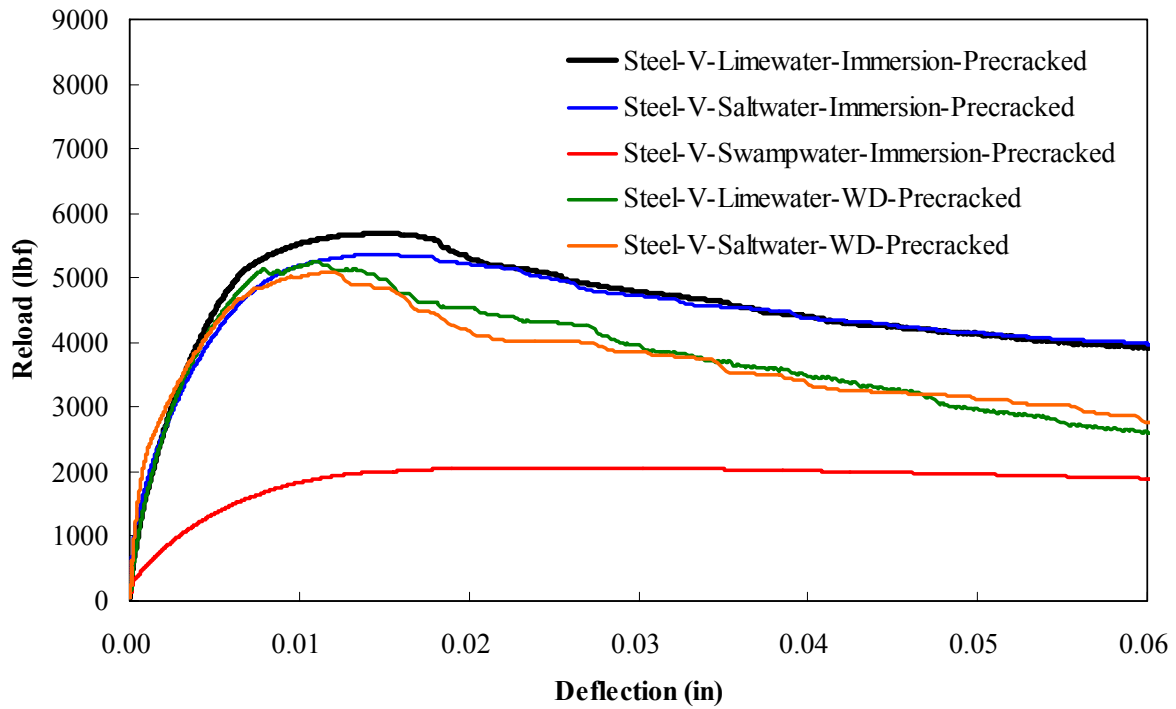


A

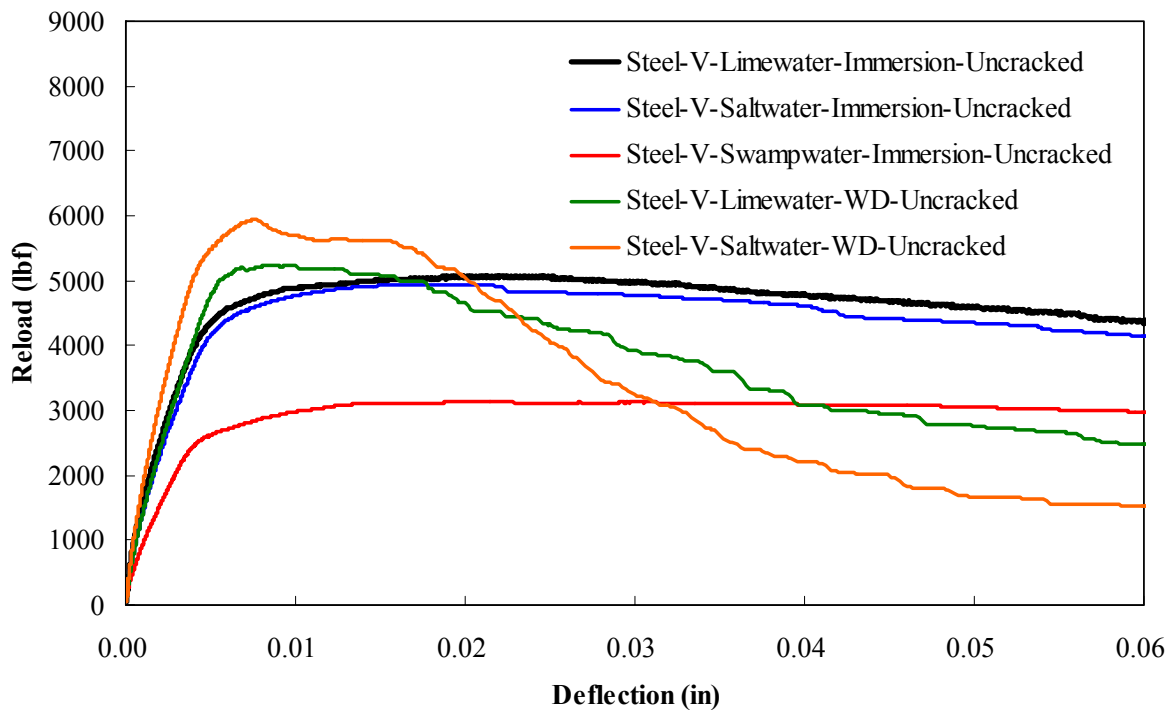


B

Figure I-5. Residual load vs. deflection curve for steel fiber mix for Class II concrete. A) Pre-cracked beams. B) Un-cracked beams.

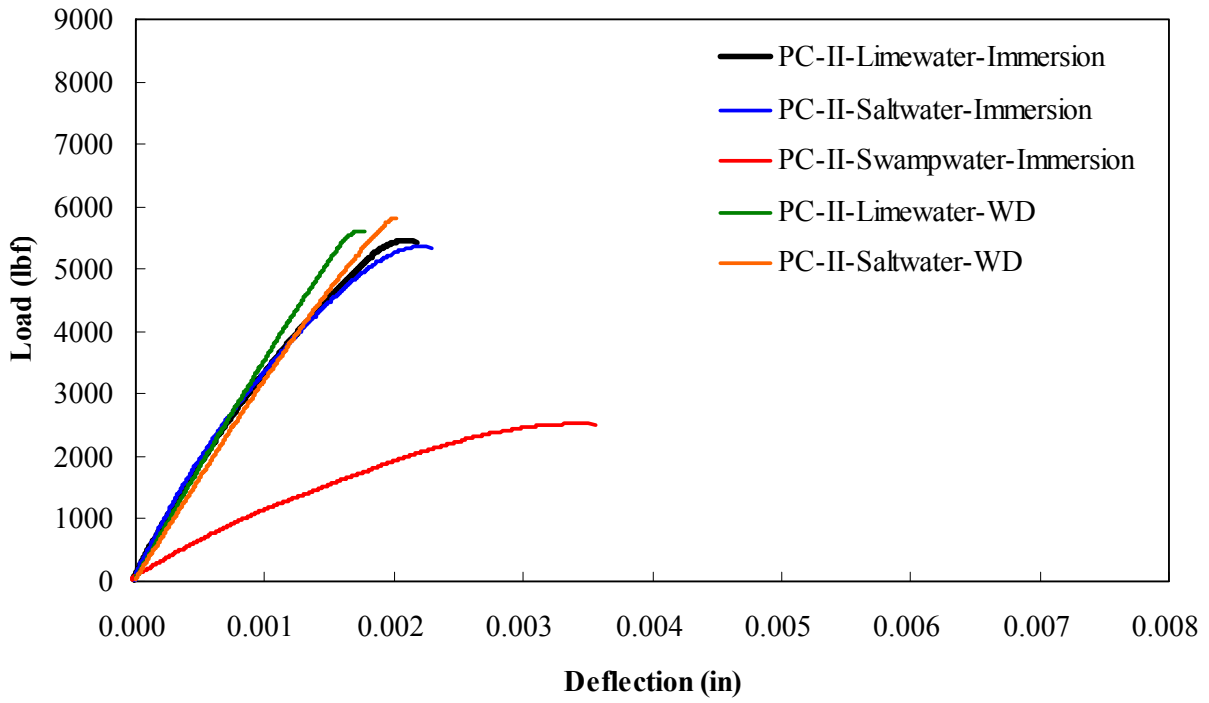


A

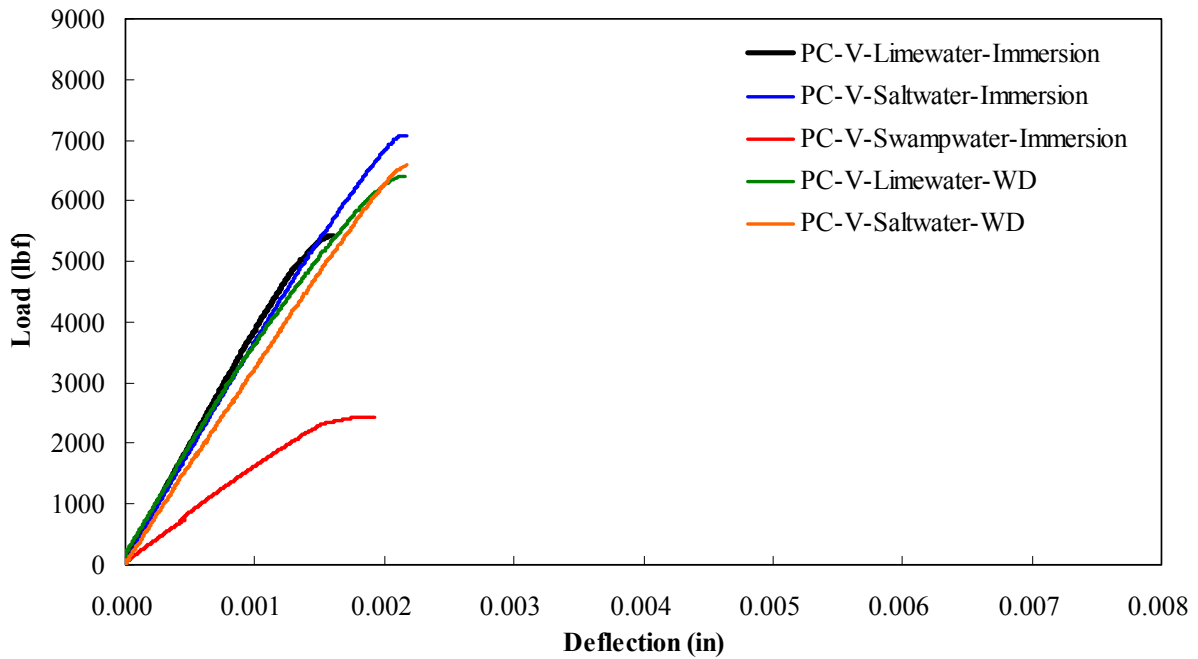


B

Figure I-6. Residual load vs. deflection curve for steel fiber mix for Class V concrete. A) Pre-cracked beams. B) Un-cracked beams.

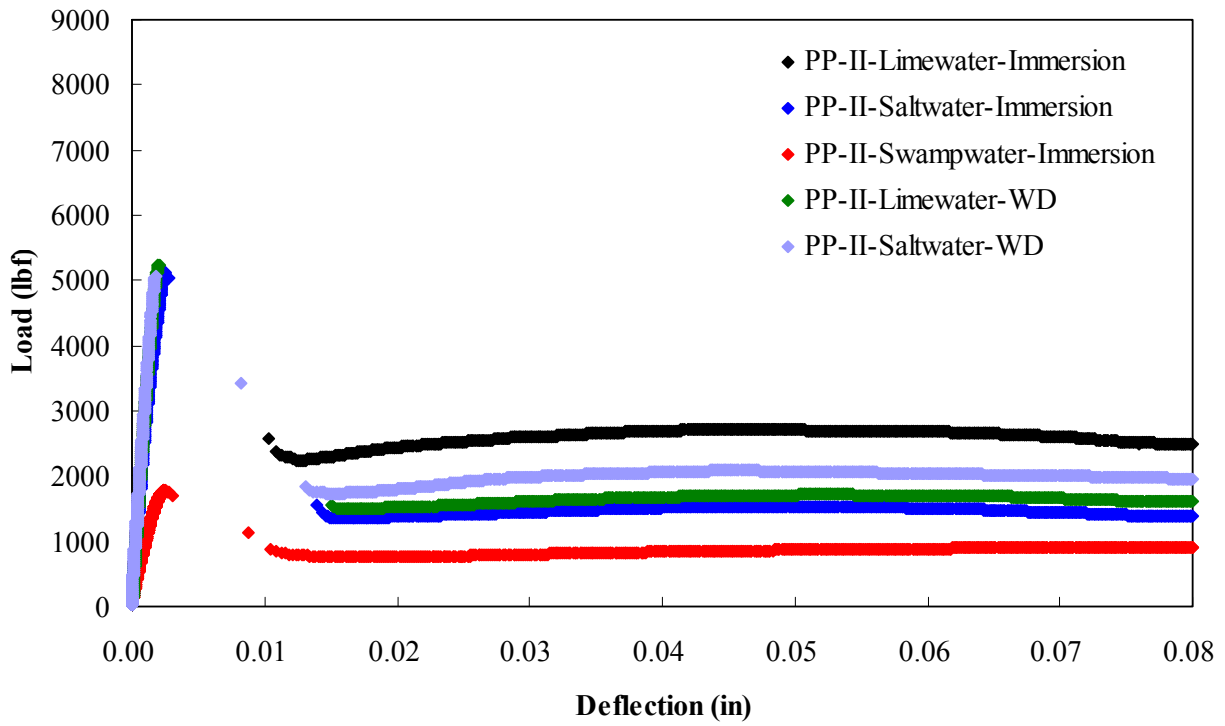


A

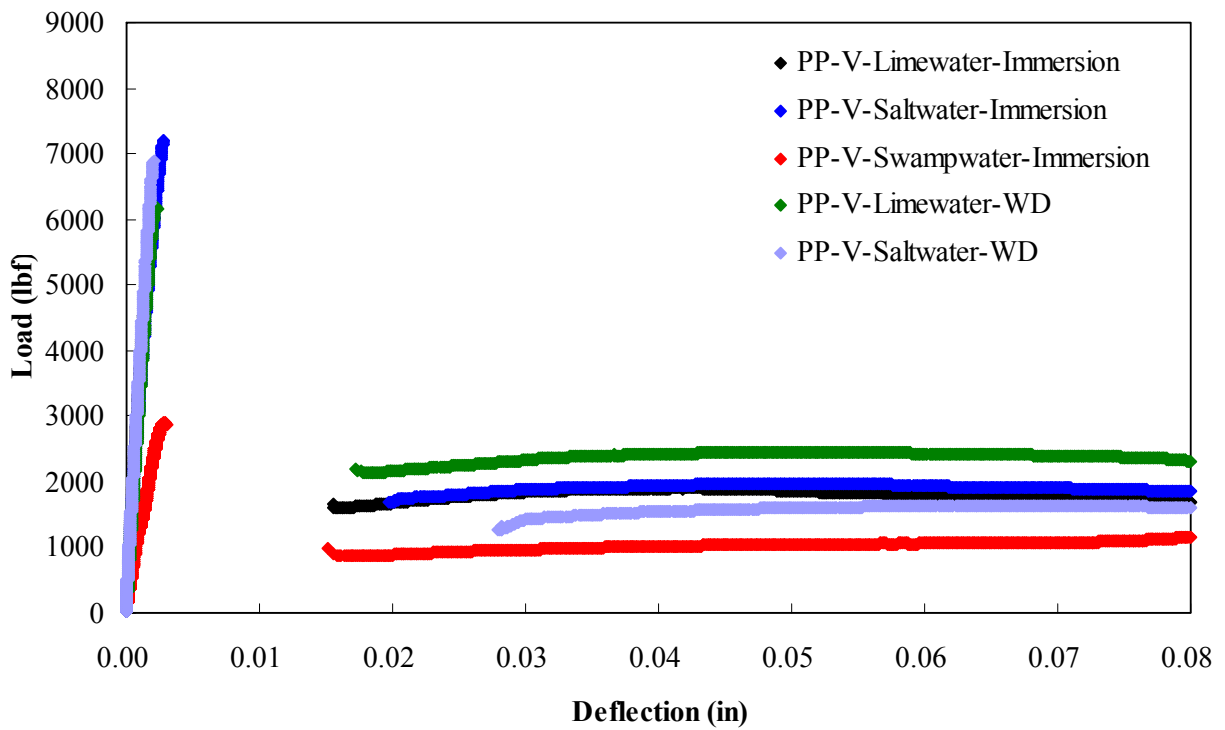


B

Figure I-7. Load vs. deflection curve for plain concrete mixes. A) Class II. B) Class V.

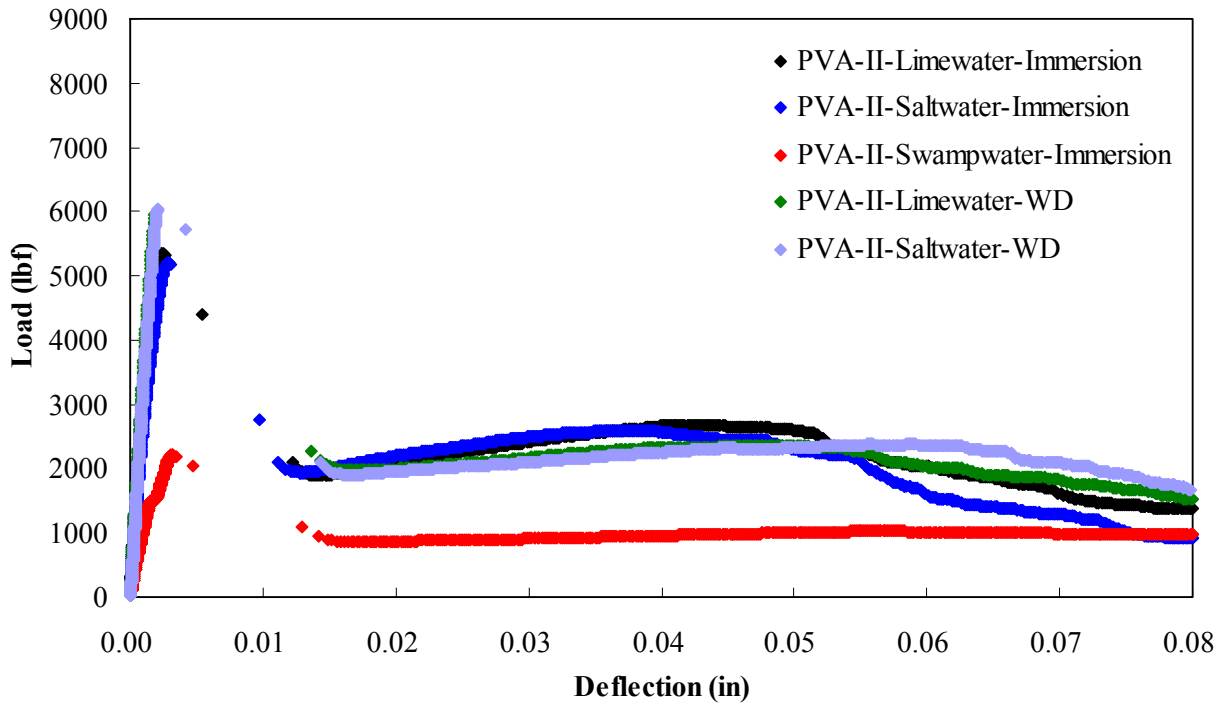


A

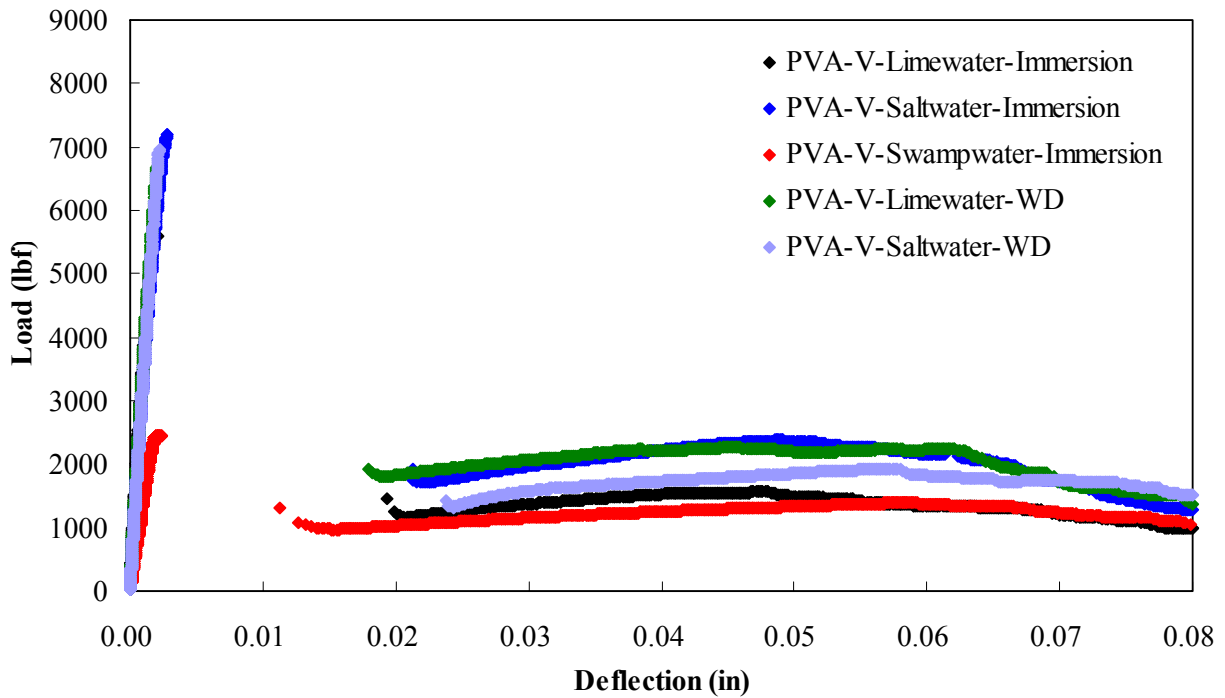


B

Figure I-8. Load vs. deflection curve for PP fiber mixes. A) Class II. B) Class V.

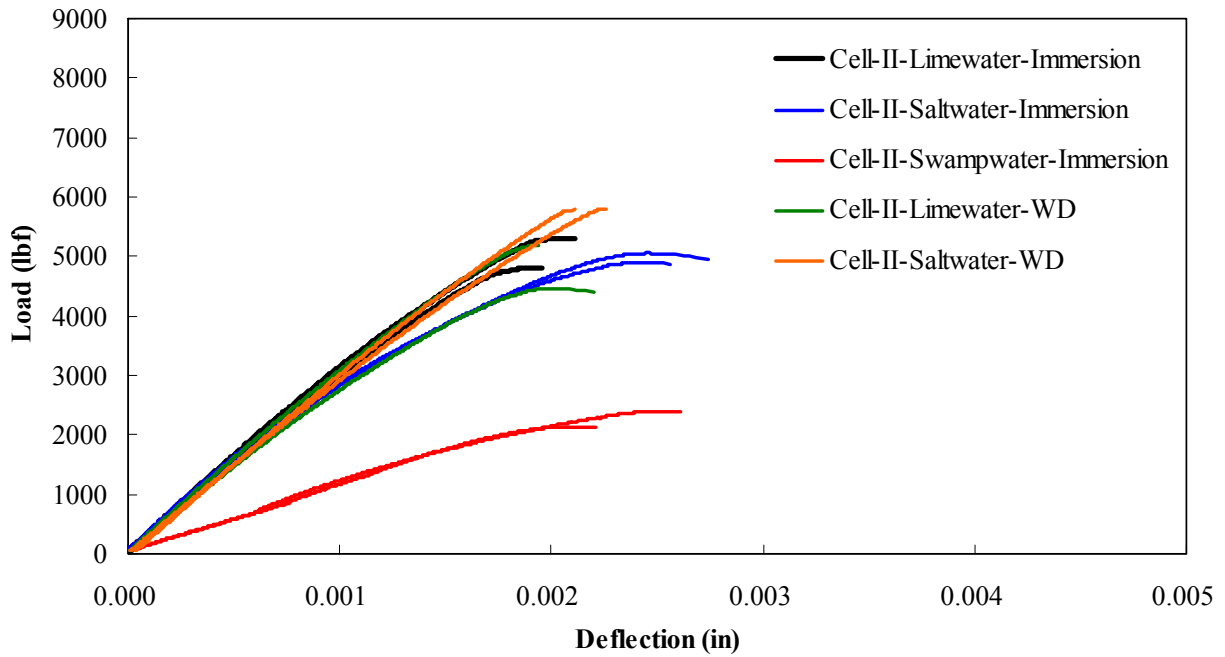


A

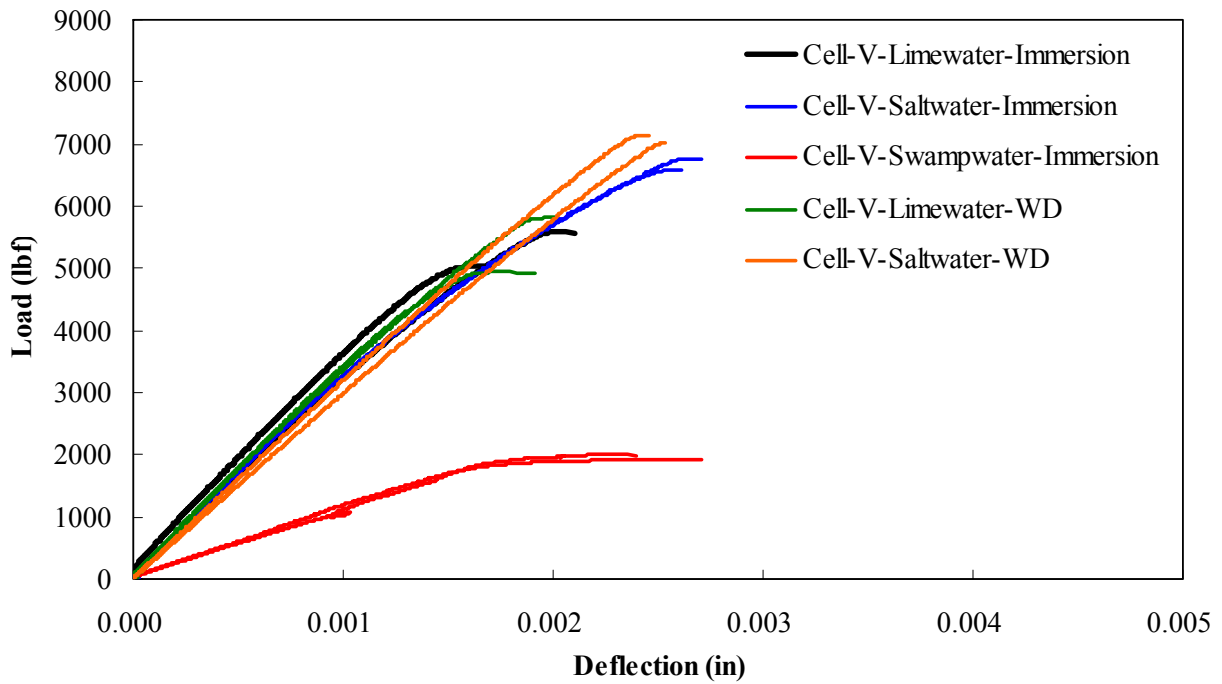


B

Figure I-9. Load vs. deflection curve for PVA fiber mixes. A) Class II. B) Class V

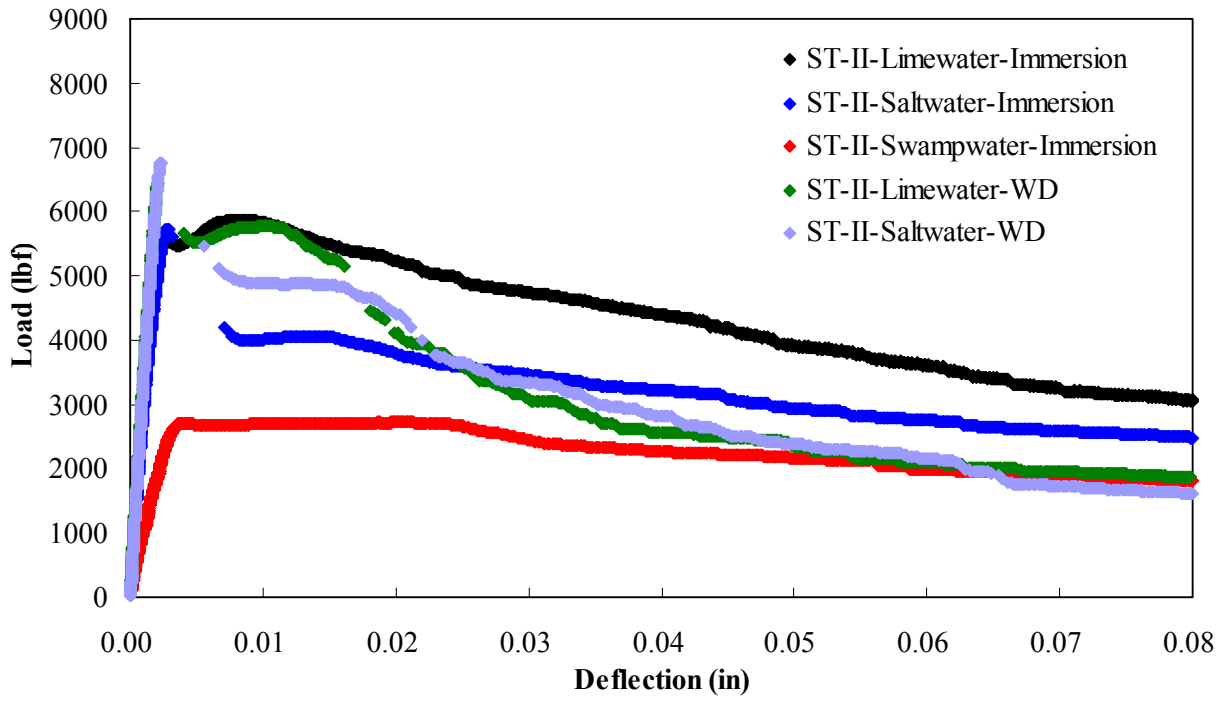


A

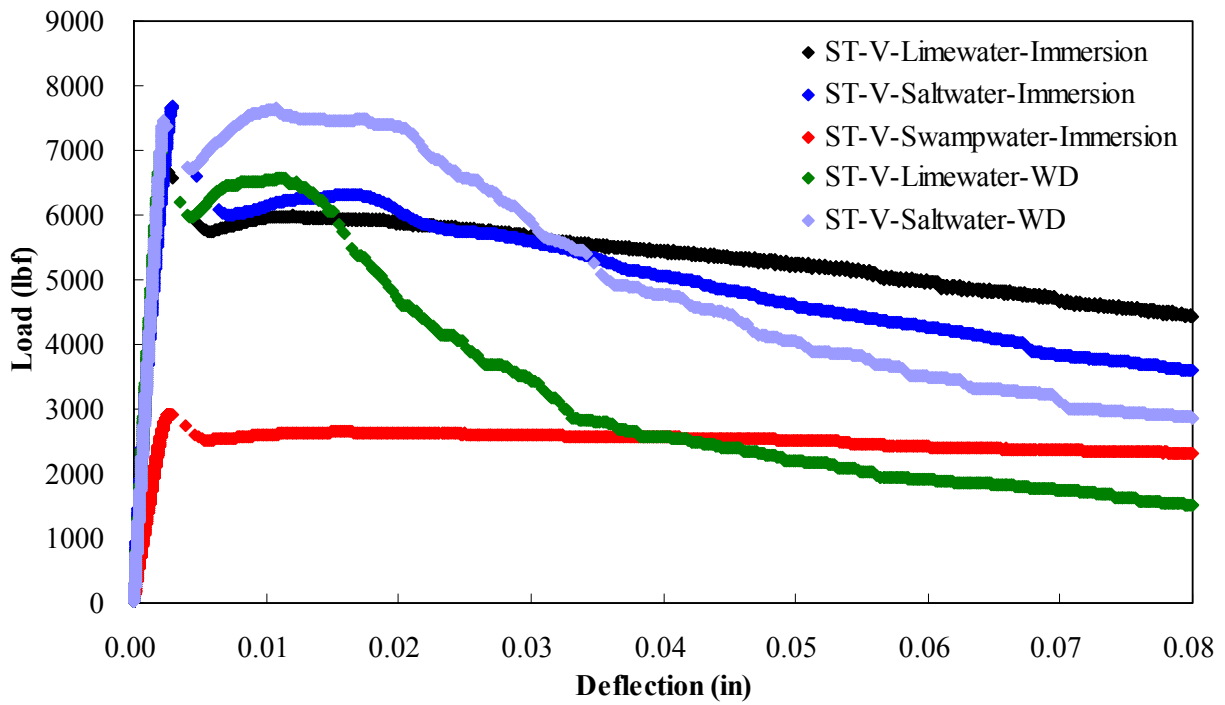


B

Figure I-10. Load vs. deflection curve for cellulose fiber mixes. A) Class II. B) Class V.



A



B

Figure I-11. Load vs. deflection curve for steel fiber mixes. A) Class II. B) Class V.

APPENDIX J  
INDIRECT TENSILE TEST RESULTS

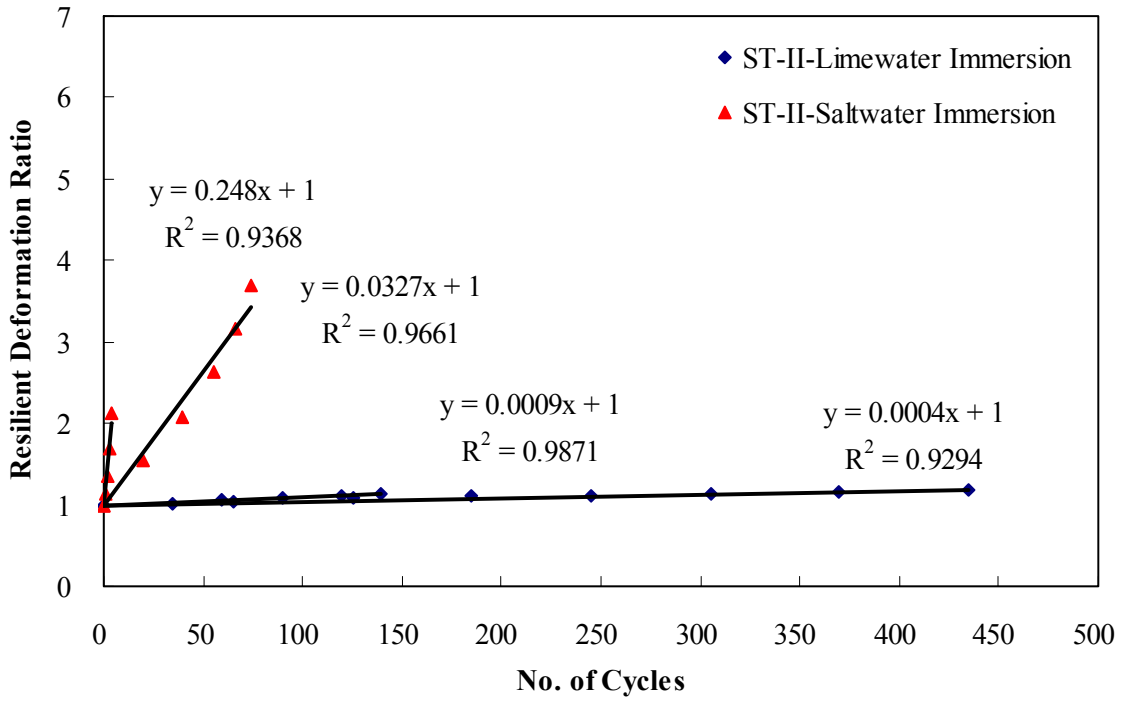


Figure J-1. Fiber bridging zone for steel fiber mix for Class II concrete

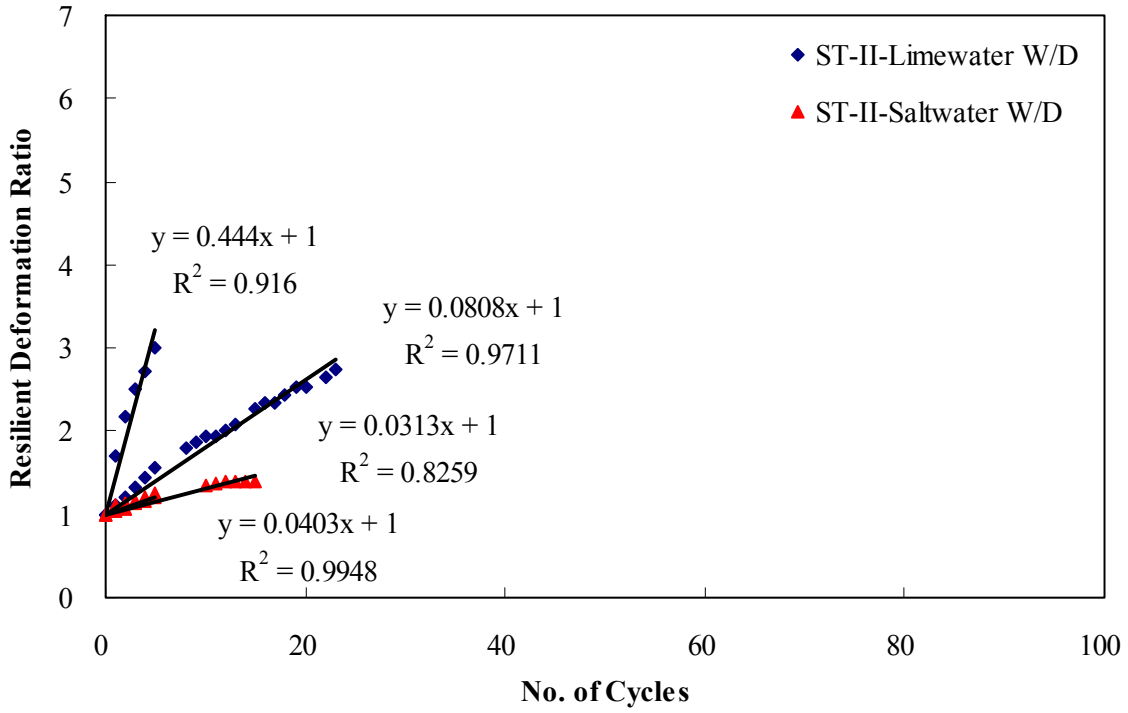


Figure J-1. Continued

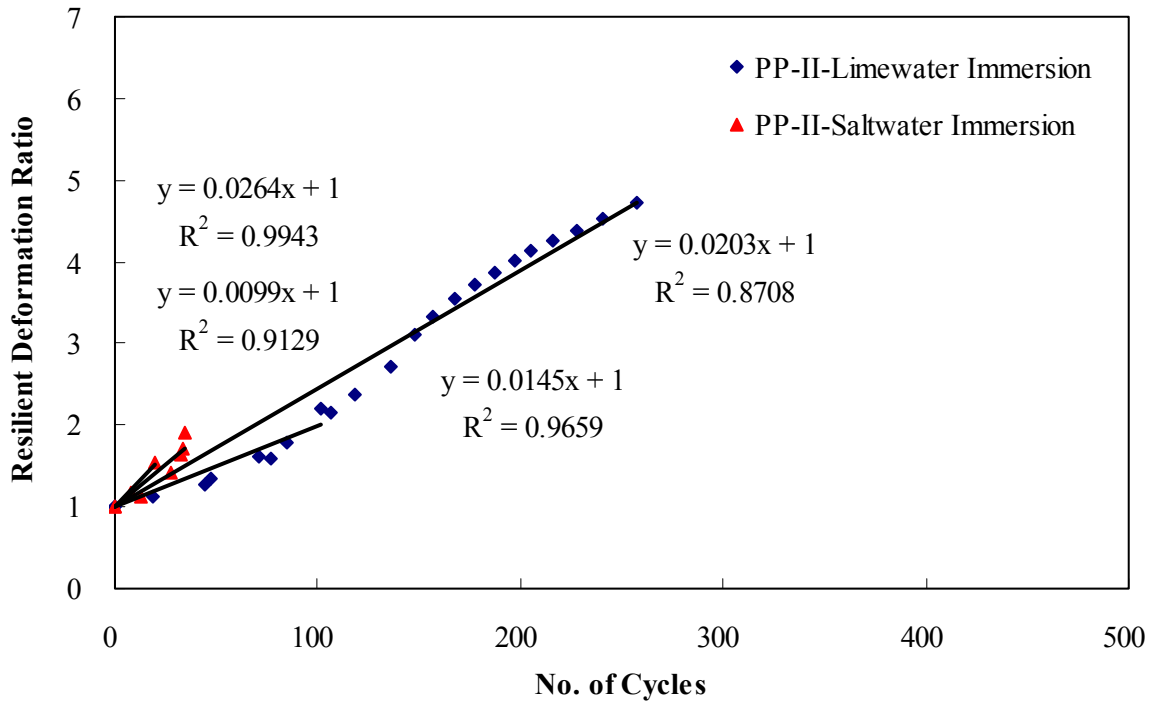


Figure J-2. Fiber bridging zone for PP fiber mix for Class II concrete

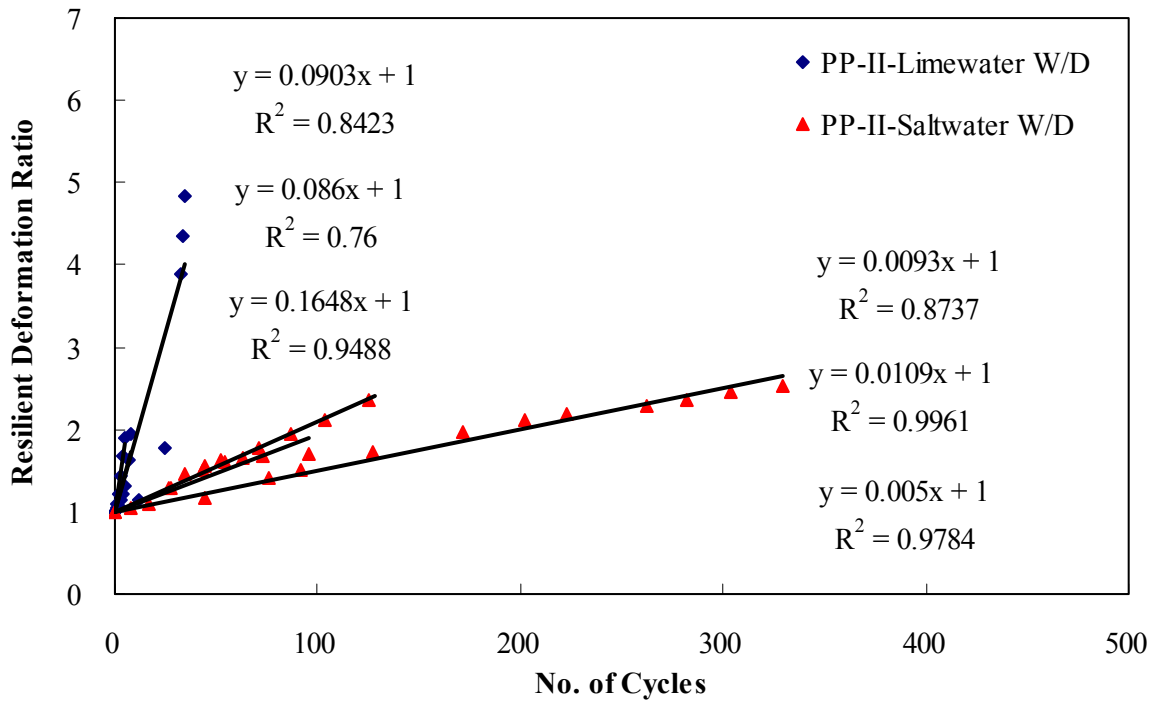


Figure J-2. Continued

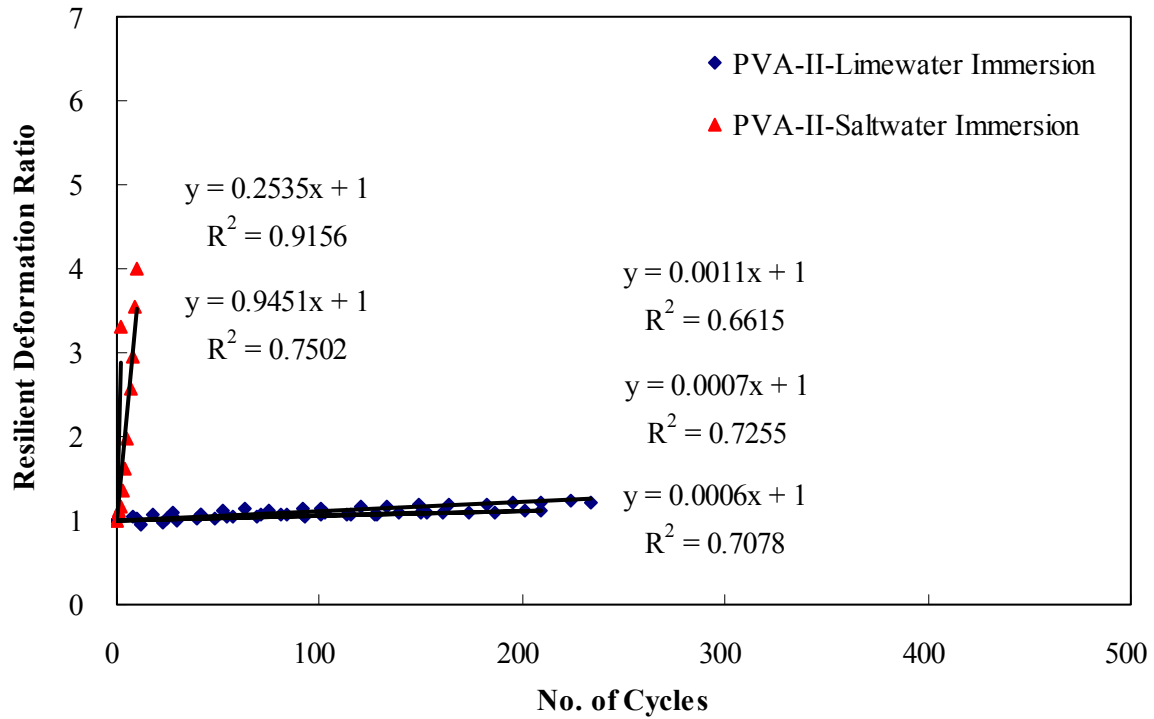


Figure J-3. Fiber bridging zone for PVA fiber mix for Class II concrete

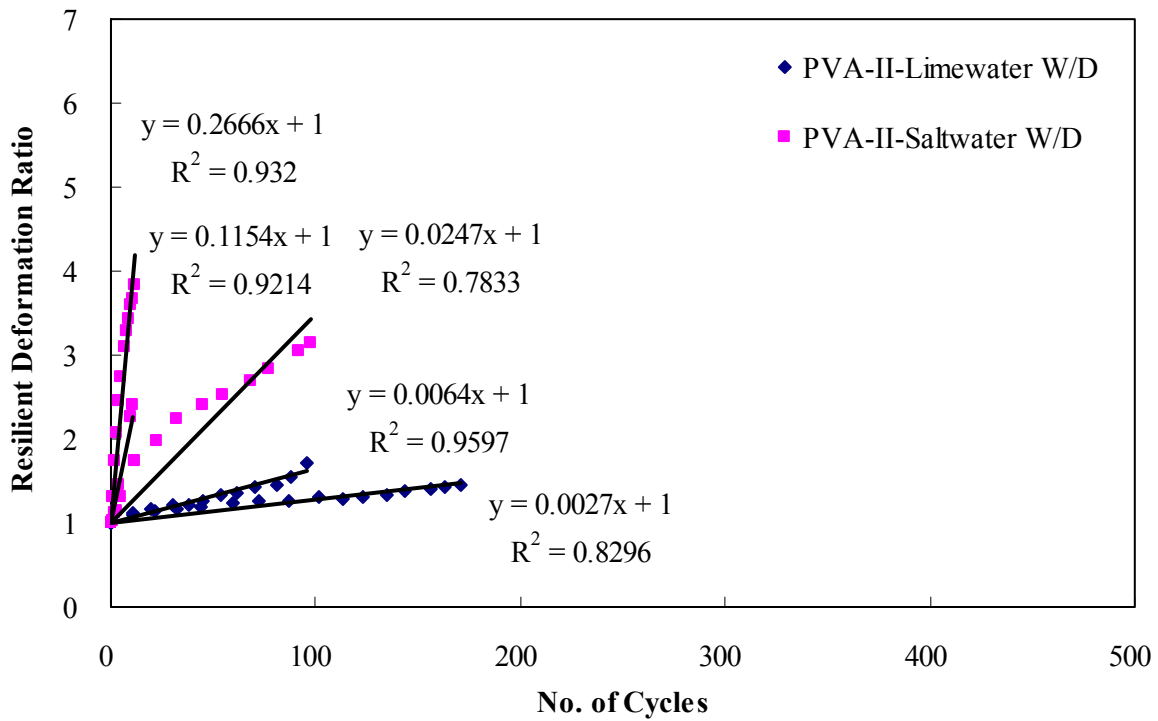


Figure J-3. Continued